NASA CONTRACTOR REPORT

NASA CR - 152131

NASA CR - 152131

STUDY OF AERODYNAMIC TECHNOLOGY FOR VSTOL FIGHTER/ATTACK AIRCRAFT – *VERTICAL ATTITUDE CONCEPT*

H. A. Gerhardt, W. S. Chen

Prepared by

NORTHROP CORPORATION, AIRCRAFT GROUP

Hawthorne, Ca.

for Ames Research Center

NATIONAL AERONAUTICS AND SPACE ADMINISTRATION • WASHINGTON, D. C. • MAY 1978

1. Report No.	2. Government Accession No.	3. Recipient's Catalog No.
NASA CR-152131		

4. Title and Subtitle	5. Report Date
STUDY OF AERODYNAMIC TECHNOLOGY FOR VSTOL FIGHTER/ATTACK AIRCRAFT- VERTICAL ATTITUDE CONCEPT	6. Performing Organization Code

7. Author(s)	8. Performing Organization Report No.
H. A. GERHARDT, W.S. CHEN	10. Work Unit No.

9. Performing Organization Name and Address	11. Contract or Grant No.
NORTHROP CORPORTION, AIRCRAFT GROUP HAWTHORNE, CAL.	NAS2-9771

12. Sponsoring Agency Name and Address	13. Type of Report and Period Covered
NASA, Ames Research Center, Moffett Field, Calif. 94035, David Taylor Naval Ship Research & Development Center, Bethesda, Md. 20084	Contractor Final Report Nov 1, '77 - May 31, '78
	14. Sponsoring Agency Code

15. Supplementary Notes

Ames Research Center Technical Monitor – W. P. Nelms (415) 965-5855
NSRDC Point of Contact – R. L. Schaeffer (202) 227-1180

16. Abstract

A study is made of the aerodynamic technology for a vertical attitude VSTOL (VATOL) supersonic fighter/attack aircraft. The selected configuration features a tailless clipped delta wing with leading-edge extension (LEX), maneuvering flaps, top-side inlet, twin dry engines and vectoring nozzles. A relaxed static stability is employed in conjunction with the maneuvering flaps to optimize transonic performance and minimize supersonic trim drag. Control for subaerodynamic flight is obtained by gimballing the nozzles in combination with wing tip jets.

Emphasis is placed on the development of aerodynamic characteristics and the identification of aerodynamic uncertainties. A wind tunnel test program is proposed to resolve these uncertainties and ascertain the feasibility of the conceptual design. Ship interface, flight control integration, crew station concepts, advanced weapons, avionics, and materials are discussed.

17. Key Words (Suggested by Author(s))	18. Distribution Statement

19. Security Classif. (of this report)	20. Security Classif. (of this page)	21. No. of Pages	22. Price*
Unclassified	Unclassified		

*For sale by the National Technical Information Service, Springfield, Virginia 22161

SUMMARY

A study is made of the aerodynamic technology for a vertical attitude VSTOL (VATOL) supersonic fighter/attack aircraft. The selected configuration features a tailless clipped delta wing with leading-edge extension (LEX), maneuvering flaps, top-side inlet, twin dry engines and vectoring nozzles. A relaxed static stability is employed in conjunction with the maneuvering flaps to optimize transonic performance and minimize supersonic trim drag. Control for subaerodynamic flight is obtained by gimballing the nozzles in combination with wing tip jets.

Emphasis is placed on the development of aerodynamic characteristics and the identification of aerodynamic uncertainties. A wind tunnel test program is proposed to resolve these uncertainties and ascertain the feasibility of the conceptual design. Ship interface, flight control integration, crew station concepts, advanced weapons, avionics, and materials are discussed.

Aerodynamic uncertainties which have been identified include LEX effects on lift and flow to the topside inlet, aerodynamics center shift, high angle-of-attack characteristics, supersonic wave drag estimation, supersonic maneuvering flaps, and jet spray effects on takeoff and landing.

SYMBOLS

a.c.	Aerodynamic Center
a_l	Aircraft Longitudinal Acceleration
a_n	Aircraft Normal Acceleration
AR	Aspect Ratio
a_x	Aircraft Longitudinal Acceleration
a_y	Aircraft Lateral Acceleration
a_z	Aircraft Vertical Acceleration
$\bar{c}$	Mean Aerodynamic Chord
c.g., C.G.	Center of Gravity
C_D	Drag Coefficient
C_{D_F}	Flat Plate Skin Friction Drag Coefficient
C_{D_L}	Drag-Due-to-Lift Coefficient
$C_{D_{min}}$	Minimum Drag Coefficient
$C_{D_{VISC}}$	Viscous Drag Coefficient
$\Delta C_{D_{RN}}$	Incremental Drag Due to Reynolds Number Variation
C_f	Flat Plate Skin Friction Coefficient
C_L	Lift Coefficient
C_{L_o}	Lift at Zero Angle-of-Attack
$C_{L_{BO}}$	Buffet Onset Lift Coefficient
$C_{L_{max}}$	Maximum Lift Coefficient
C_l	Rolling Moment Coefficient
C_m	Pitching Moment Coefficient
C_{m_o}	Pitching Moment at Zero Lift
C_n	Yawing Moment Coefficient
C_y	Side Force Coefficient
e	Oswald Spanload Efficiency Factor

F_N	Net thrust
g	Acceleration due to Gravity
h	Altitude
I_{XX}	Roll Moment of Inertia
I_{YY}	Pitch Moment of Inertia
I_{ZZ}	Yaw Moment of Inertia
L/D	Lift to Drag Ratio
l	Length
M	Mach Number
m.a.c.	Mean Aerodynamic Center
n_z	Normal Load Factor
O.P.R.	Overall Pressure Ratio
P_s	Specific Excess Power
p, q, r	Angular Rates About Aircraft's Y, X, and Z Axes
q	Dynamic Pressure
ΔP	Pilot's Pedal Displacement
R_N	Reynold's Number
R_L, R_R	Force at Left and Right Wingtip Reaction Jets
S	Area
S_{LEX}	Leading-Edge Extension Exposed Area
SM	Static Margin
ΔS_p, ΔS_R	Pilot's Fore-Aft and Lateral Stick Displacement
S_W, S_{ref}	Wing Reference Area
S_{wet}	Component Wetted Area
T	Thrust
T_{LC}, T_{RC}	Commanded Thrust from Left and Right Engines
ΔT_L, ΔT_R	Pilot's Throttle Levers – Left and Right Engines
T_{RL}, T_{RR}	Thrust from Rear Left and Right Nozzles
U, V, W	Aircraft Velocity Components Along X, Y, and Z Axes

W/S	Wing Loading
ΔU_c	Pilot's Vertical Speed Command Switch
X, Y, Z	Aircraft Position with Respect to an Earth Reference
V_S	Stall Speed
W	Weight
α	Angle-of-Attack
β	Angle-of-Sideslip
γ	Ratio of specific heats
δ_f	Trailing Edge Flap Deflection
δ_n	Leading Edge Flap Deflection
δ_E, δ_A, δ_R	Elevator, Aileron and Rudder Angles
δ_{EC}, δ_{AC}, δ_{RC}	Commanded Elevator, Aileron and Rudder Angles
δ_T	Thrust Deflection
$\ddot{\theta}$	Pitch Acceleration (rad/sec^2)
θ	Aircraft Pitch Attitude
Λ_{LE}	Leading Edge Sweep
λ_F	Fore-Aft Deflection Angle of Forward Nozzle
λ_R	Deflection Angle of Rear Nozzles
λ_Y	Lateral Deflection Angle of Forward Nozzle
λ_{FC}	Commanded Forward Nozzle Angle
λ_{RC}	Commanded Rear Nozzle Angle
ϕ	Aircraft Roll Attitude
$\ddot{\phi}$	Roll Acceleration (rad/sec^2)
ψ	Aircraft Heading

CONTENTS

CONTENTS (Continued)

LIST OF TABLES

LIST OF ILLUSTRATIONS

SECTION 1

INTRODUCTION

The study of aerodynamic technology of VSTOL fighter/attack class aircraft is being pursued by the NASA Ames Research Center and the David Taylor Naval Ship Research and Development Center. This document reports the work covered under the joint sponsorship of these organizations in Phase I of Contract NAS2-9771, "Study of Aerodynamic Technology for VSTOL Fighter/Attack Aircraft." This phase covered the period from 1 November 1977 to 31 May 1978. Phase I objectives were:

1. To identify and analyze two high performance VSTOL concepts having potential utility to fulfill the Navy fighter/attack role.
2. To estimate the aerodynamic, propulsion, and performance characteristics of these concepts and to assess technical uncertainties requiring additional research.
3. To outline a wind tunnel program in which these aerodynamic uncertainties would be investigated and which would provide a data base for future use.

The VSTOL fighter/attack concepts studied both employ the lift/cruise propulsive lift concept; one is a vertical attitude configuration termed VATOL, and the other is a horizontal attitude configuration and is termed HAVSTOL. This report deals with the VATOL concept. Results of the study of the HAVSTOL concept are presented in NASA CR 152130.

Satisfying the combined requirements of supersonic flight and vertical takeoff provides a significant design challenge. The severity of this challenge is increased by the need to deal with the fighter-related issues of agility and combat persistence while minimizing the problems associated with the presence of engine exhaust flow in proximity to the aircraft and ground surface.

A listing of the major problem areas and the conceptual solutions offered by horizontal and vertical attitude configurations is presented in Table 1-1. This table

TABLE 1-1. SUPERSONIC VSTOL CONCEPT DIFFERENCES

Supersonic VSTOL Problem Area	Comparison of Solutions	
	Horizontal Attitude VSTOL: L/C Concept; Twin, Variable Cycle, Turbofans	Vertical Attitude VSTOL: L/C Concept, Twin Variable Turbine, Dry Turbojets
Achievement of smooth, low cross-sectional area	Propulsive lift separation, wide-spaced afterbodies	Thrust always through C.G. – conventional rear engine configuration shaping
Suckdown	Minimize by configuration shaping, high attitude liftoff and touchdown	Inherently minimum base area
Fountain	Avoid by jet location and direction, high attitude liftoff and touchdown	Closely spaced nozzles; no fountain
Exhaust ingestion	Avoid fountains, inlet location, high attitude liftoff and touchdown	Launch and recovery outside deck edge to avoid wall jet formation
Ship interface	Normal VTOL operations, exceptional STO performance very low conventional approach/landing speeds	Vertical operations restricted to specialized gantry, pilot attitude maintained by rotating cockpit enclosure, STO by limited sink off bow (or skijump), conventional attitude approach/landing speed requires arresting hook

shows that, compared with the HAVSTOL, the VATOL is a simpler approach to achieving supersonic performance and a minimum level of propulsion-induced interferences, but that its short takeoff performance is inferior and the shipboard interface is more complex.

During this study, emphasis was placed on the aerodynamic and propulsion areas. Supporting work in structures, flight control, avionics, and components areas was completed only to the extent needed to assure that the concept was credible. Correspondingly, the cruise-combat regime was emphasized and the hover-transition regimes studied to the extent necessary to assure configuration credibility.

A number of individuals have made major contributions to this study. They are identified below. The work was performed under the general direction of Dr. P. T. Wooler.

S. H. Brown	Aerodynamic-Propulsion Integration
R. F. Smith	Aerodynamics
J. R. Stevens	Aerodynamics
R. Hoenig	Propulsion
T. J. Weir	Configuration Integration
R. English	Flight Performance
W. Darby	Takeoff Performance
R. Kostanty	Flight Controls

SECTION 2

AIRCRAFT DESCRIPTION

The configuration selected for the VATOL study features a tailless clipped delta wing with leading edge extension (LEX), maneuvering flaps, tilt cockpit, topside inlet, twin dry engines and vectoring nozzles. A relaxed static stability is employed in conjunction with the maneuvering flaps to optimize transonic performance and minimize trim drag. Control for subaerodynamic flight is obtained by gimballing the nozzles in combination with wing tip jets.

2.1 DESIGN PHILOSOPHY

The design philosophy for the Vertical Attitude Takeoff and Landing (VATOL) concept was to use an unconventional operational approach to minimize VTOL impact on the aircraft design while accepting some complication of ship interface. This approach yields the lightest weight, lowest cost aircraft solution to supersonic VSTOL capability.

The achievement of VSTOL capability in a supersonic aircraft by rotating the aircraft to the vertical is an effective means of reducing VTOL/combat configuration compromises. A vertical attitude takeoff and landing concept reduces thrust deflection requirements, inherently aligns weight and thrust vectors, eases control requirements, and minimizes propulsion-induced VTOL effect such as suckdown, fountains and exhaust ingestion.

Vertical attitude operation requires a specialized launch/retrieval system which restricts the number of potential VTOL operational sites. Also, since the VATOL concept does not inherently offer propulsive lift benefits at conventional attitudes, STO ground/deck run and landing speeds will be greater than on the horizontal attitude concept. For future naval applications, however, site restrictions on takeoff and landing operations will occur naturally as ship size decreases and the VATOL concept adds the potential to minimize aircraft/ship structure interference. Further, operations from carrier decks can take advantage of the aircraft's high thrust-to-weight combined with either a nominal sink off the bow to effect rotation or the use of a ramp at the end of the deck (ski jump) to impart an upward momentum.

The aircraft configuration determined for the VATOL concept emphasizes high-speed agility with little compromise to achieve VTOL capability. In addition to a favorable blend of transonic turn performance and low wave drag, the slender leading edge extension/wing/body arrangement offers potential for minimizing radar cross section (RCS) level over a wide frontal spectrum. The dominant frontal contribution to RCS for tactical aircraft is the inlet duct cavity and engine compressor face. The use of airframe shielding for the compressor, and the use of radar absorbing materials (RAM) inside the duct cavity, offer substantial survivability advantage, particularly during penetration and attack of enemy ground or sea-based defenses. Flow control from tailored vortex flow surfaces facilitates use of efficient top-mounted inlet configurations appropriate to transonic maneuvering requirements. In addition to its RCS advantages, the top-mounted inlet provides design and operational advantages by maintaining an unrestricted lower surface for efficient weapon/landing gear integration and aircraft equipment accessibility.

The use of twin, dry turbojets provides significant operational advantages as well as performance benefits. Twin-engine design coupled with the high thrust-to-weight and vectoring nozzles provides not only good single-engine performance but also additional engine-out safety in the vertical flight mode. This safety results from the ability to control the attitude of the aircraft by directing the remaining engine's thrust through the c.g., thus giving the pilot time and proper attitude to execute a safe ejection. The twin, dry turbojets offer the advantages of minimum propulsion system length, reduced IR signature during combat and a high level of combat persistence.

The unique operational concept for the VATOL requires special consideration of the aircraft crew station and launch/retrieval system. Candidate crew station design approaches vary from rotation of the pilot seat, in a manner similar to current high acceleration cockpit studies, to rotation of the entire nose of the aircraft. The launch/retrival system for the proposed concept employs a nose gear hook/arresting wire engagement similar to that used in the Ryan X-13 program.

2.2 DESIGN GUIDELINES

The initial design guidelines for the VSTOL aircraft configuration were a VTO weight of 13,608 kg (30,000 lb) and a STO weight of 18,144 kg (40,000 lb). Wing size and engine thrust were selected to meet the performance requirements of a 6.2 g sustained turn at M0.6 at 3048 m (10,000 ft) and a specific power (P_s) of 274,32 m/sec. (900 ft/sec) at M0.9 at 3048 m (10,000 ft). Engine thrust should not be less than the VTO weight times 1.15 to ensure sufficient hot-day thrust for vertical takeoff. The wing sweep should be enough to allow the leading edge to remain subsonic at the design Mach number of 1.2.

2.3 AIRCRAFT ARRANGEMENT DESCRIPTION

The VATOL concept is shown in the general arrangement drawing of Figure 2.1. This high performance filter/attack aircraft is designed for a VTO weight of 13,608 kg (30,000 lb) with a wing loading of 293 kg/m^2 (60 psf) and an installed thrust-to-weight ratio of 1.17 on a tropical day and a fuel fraction of 0.41.

Distinguishing features of the concept are:

1. An integrated leading edge extension (LEX) blended delta wing
2. Tilt cockpit module
3. Topside inlets
4. Twin non-afterburning (dry) engines with 2-axis gimballed nozzles
5. Clipped delta wing with maneuvering flaps

The aircraft is area-ruled to achieve a smooth overall area distribution that closely matches an ideal area distribution as shown in Figure 2-2. This is possible through proper placement of the LEX, wing, inlets, and canopy in the area distribution plot. By locating the LEX between the canopy and inlet, a gradual area buildup in the total area distribution is achieved while permitting the wing area distribution to determine the location of the maximum area. Also shown in Figure 2-2 are wetted area distribution, body fuel distribution, and in Figure 2-3, the engine duct area distribution.

Leading-edge and trailing-edge surfaces are used to vary the wing camber to attain maximum maneuvering performance. In addition, with the absence of a horizontal tail, the trailing-edge surfaces provide pitch and roll moments.

Reaction control jets are located in each wing tip to provide roll control in the vertical attitude. Translation, yaw, and pitch control are achieved through proper scheduling of the two-axis gimballed nozzles with additional roll control capability attained by the differential gimballing of the nozzles to ±30 degrees.

The location of the engine inlets above the wing permits a wide, flat, low fuselage for maximum flexibility for weapon mounting and minimum structural complications while engaging the landing platform. In addition, this location reduces radar cross-section and has potential for reducing exhaust gas reingestion.

Subsystems integration is achieved by the consideration of functional location, maintainability, and survivability. The functional location of systems is of primary importance in the reduction of weight and volume. As shown on the inboard profile, Figure 2-4, the location of the radar, avionics, and cockpit close together is functional in that they all require air-conditioning, and their close proximity to each other and the ECS minimizes ducting and temperature losses.

Fighter/attack aircraft have long been designed to meet a high level of performance, while configured with little or no weapons. When, in the real operational world, these aircraft are loaded with external bombs and tanks, their performance is degraded such that they become vulnerable to attack from lower-performance aircraft. It has been recognized that better aircraft/weapon integration is necessary to improve aircraft performance and weapon delivery.

A total of six weapon configurations are shown on the Conformal Stores Matrix, Figure 2-5. The first five are representative of advanced air-to-ground weapons concepts. The sixth represents state-of-the-art air-to-air guided weapons, with large-span fixed main lifting surfaces in a cruciform configuration. This type of weapon is carried on the fuselage corners either semi-submerged or tangent-mounted. Minimum aircraft performance degradation and low detection signature are primary factors that influenced the weapon configuration and carriage.

The operational concept for VATOL requires special consideration of the aircraft crew station and launch/retrieval system. Of the candidate crew station approaches, a representative tilt cockpit module is indicated in Figures 2-1, 2-4 or 2-6. This approach avoids potential gantry interference problems with the proposed launch/retrieval system. The cockpit module is designed to tilt upward during landing transition until the fuselage is vertical, and the pilot remains in a normal landing

attitude. Aircraft launch and recovery are normally made in the vertical mode from ship-mounted gantries. Normal landing gear is provided to permit overload takeoffs and landings in a horizontal attitude.

A diagram of the launch and retrieval concept is shown in Figure 2-6. The rotating platform system consists of three retractable cable tiers for aircraft arrestment. The capturing hook mechanism is integral with the nose gear. This system has been configured to accomodate the relatively rapid and appreciable heave and roll motions expected with smaller ships. The platform, which is inclined to aid wire engagement and match the aircraft's pendulum position, can be rotated to bring the aircraft weight vector ahead of the main gear. Mechanical latching of the main gear is employed as the vertical motion is arrested. A conventional hook arrangement is retained to permit emergency recovery on a conventional carrier.

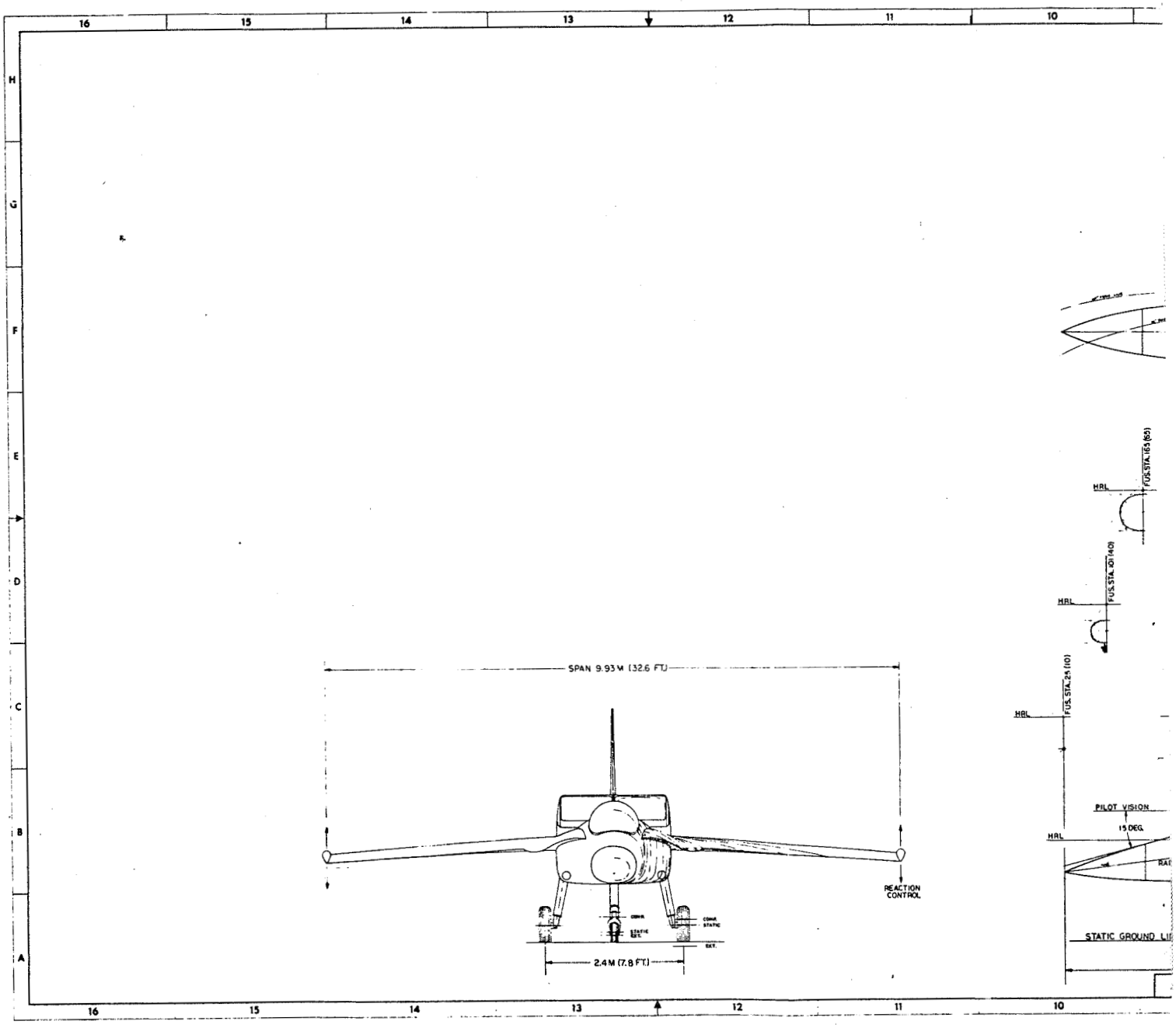

FIGURE 2-1. GENERAL ARRANGEMENT

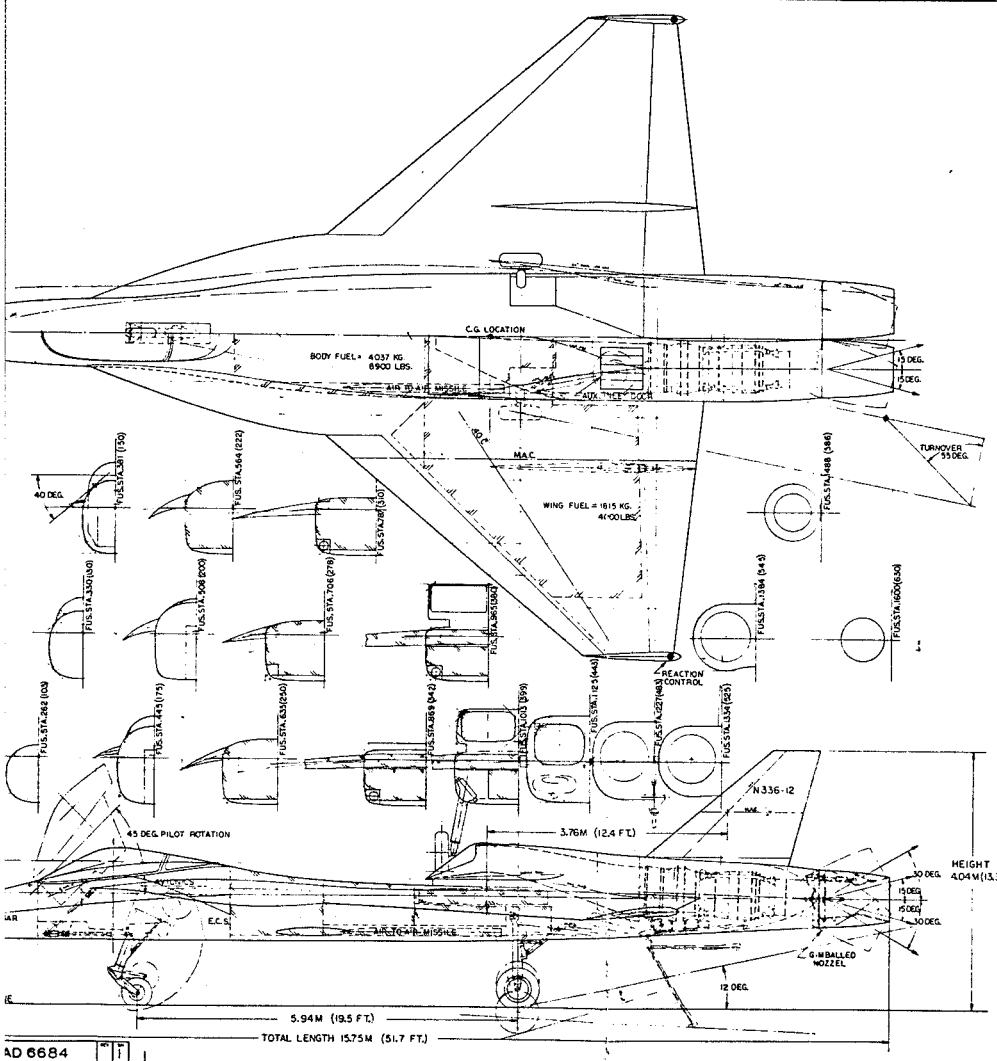

BASIC DIMENSIONAL DATA				
BASIC SURFACES	UNITS	WING	HORIZ TAIL	VERT TAIL
REFERENCE AREA	M^2 (FT²)	65.45 (700)	N/A	5.71 (59)
ASPECT RATIO	AR	2.12		1.10
TAPER RATIO	λ	0.18		.337
THICKNESS RATIO	t/c	0.04		0.04
L.E. SWEEP ANGLE	DEG	50		50
C/4 SWEEP ANGLE	DEG	40.8		44
DIHEDRAL/CANT ANGLE	DEG	-3		0
INCIDENCE ANGLE	DEG	0		—
TWIST ANGLE	DEG			—
AIRFOIL	—	65A004		—
PROJECTED SPAN	M (FT)	9.23 (30.29)		1.65 (5.36)
ROOT CHORD	(M) (IN)	1.83 (72.1)		.95 (38)
TIP CHORD	(M) (IN)	.18 (6.9)		.15 (6.0)
MEAN AERO CHORD	(M) (IN)	1.06 (42.0)		.33 (13.0)
TAIL ARM 0.40 $\bar{C}_w$ TO 0.25 $\bar{C}_t$	(M) (IN)	—		4.18 (164.8)
TAIL VOLUME COEFFICIENT	V	—		.020
CONTROL SURFACES				
TOTAL AREA	M^2	5.13 (55.2)		2.51
PERCENT SPAN	%b	65 70		ALL
PERCENT CHORD	%c	INBD .25 OUTBD .20		MOVING
DEFLECTION	DEG	INBD +20 -10 OUTBD +20 -10		15

WEIGHTS	KG.	LBS.	WETTED AREA M^2 (FT^2)	
STRUCTURE	3,201	7,055	NET BODY	71.9 (774)
POWER PLANT	2,715	5,985	WING	64.5 (694)
FIXED EQUIPMENT	1,634	3,614	HORIZ. TAIL	—
EMPTY WT.	7,550	16,654	VERT. TAIL	5.3 (57)
USEFUL LOAD	195	428	NACELLE	—
OPER.WT. EMPTY	7,745	17,082	L.E.X.	7.7 (83)
PAYLOAD	163	360		
FUEL	5,696	12,558		
TAKEOFF GROSS WT.	13,504	30,000	TOTAL	149.5(1608)

NOTES:

1. POWERPLANT: (2) P&W VARIABLE GEOM TURBOJET NON A/B THRUST: 19,400 LB/ENG S.L. STATIC T.I.T.: 3200° F O.P.R.: 20
2. NET DENSITY: $\rho = \frac{GW}{VOL} = \frac{13608}{227.8} = 59.7\ KG/M^3 (37.3\ LBS/FT^3)$

ADVANCED DESIGN

NORTHROP Northrop Corporation, Aircraft Division, 1001 East Broadway, Hawthorne, California 90250

Drawn	J. J. WEIR	4-2-73
DESIGN		4-12-73
APPROVAL		4-24-73
APPROVAL		

GENERAL ARRANGEMENT VSTOL-VERTICAL ATTITUDE

NORTHROP APPROVAL	MODEL	SIZE	CODE IDENT NO	AD 6684
OTHER APPROVAL	N 336-12	J	76823	
		SCALE 1/20		SHEET 1 OF 1

AD 6684

Page intentionally left blank

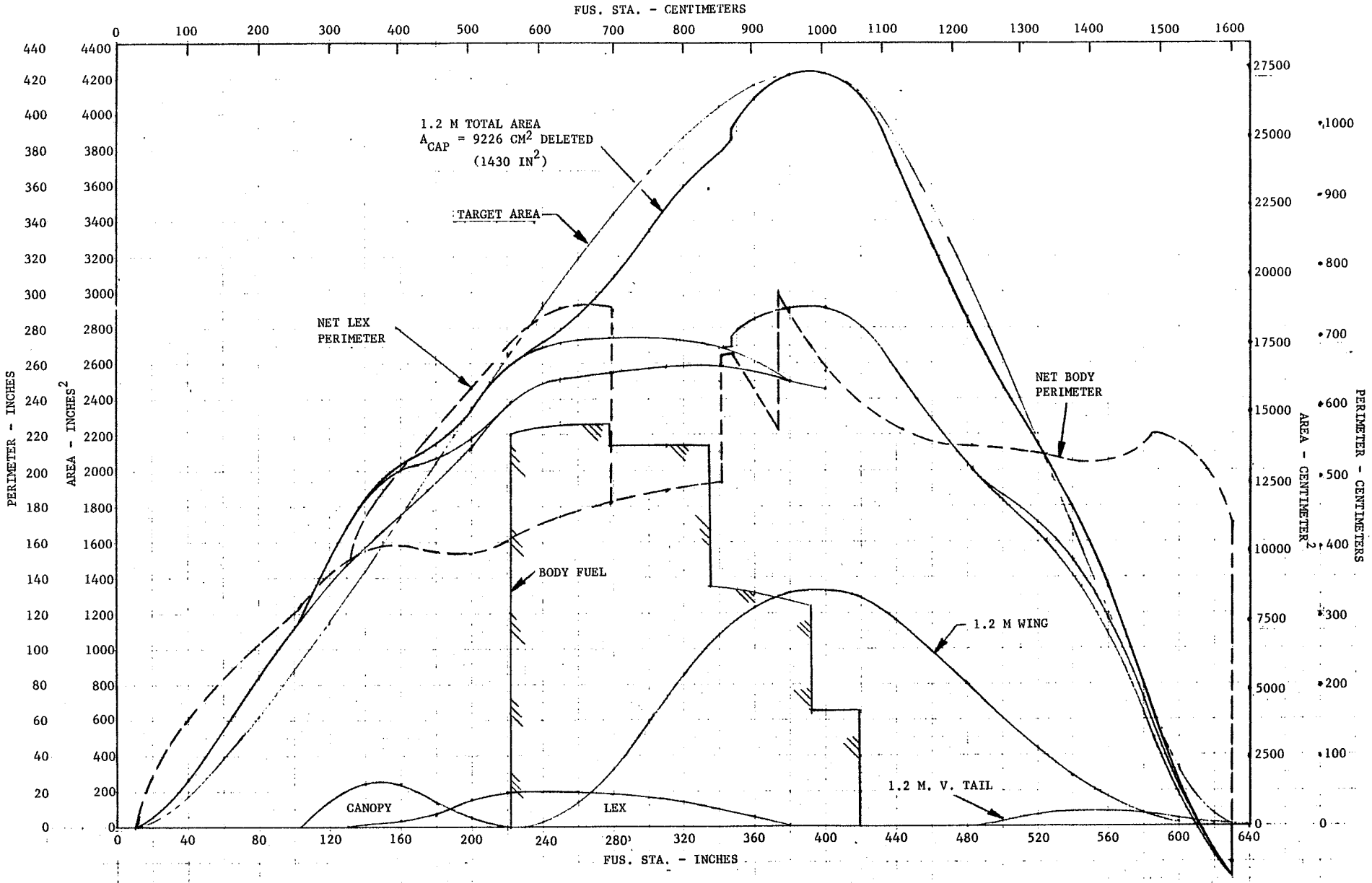

FIGURE 2-2. CROSS-SECTIONAL AREA AND WETTED AREA DISTRIBUTIONS

Page intentionally left blank

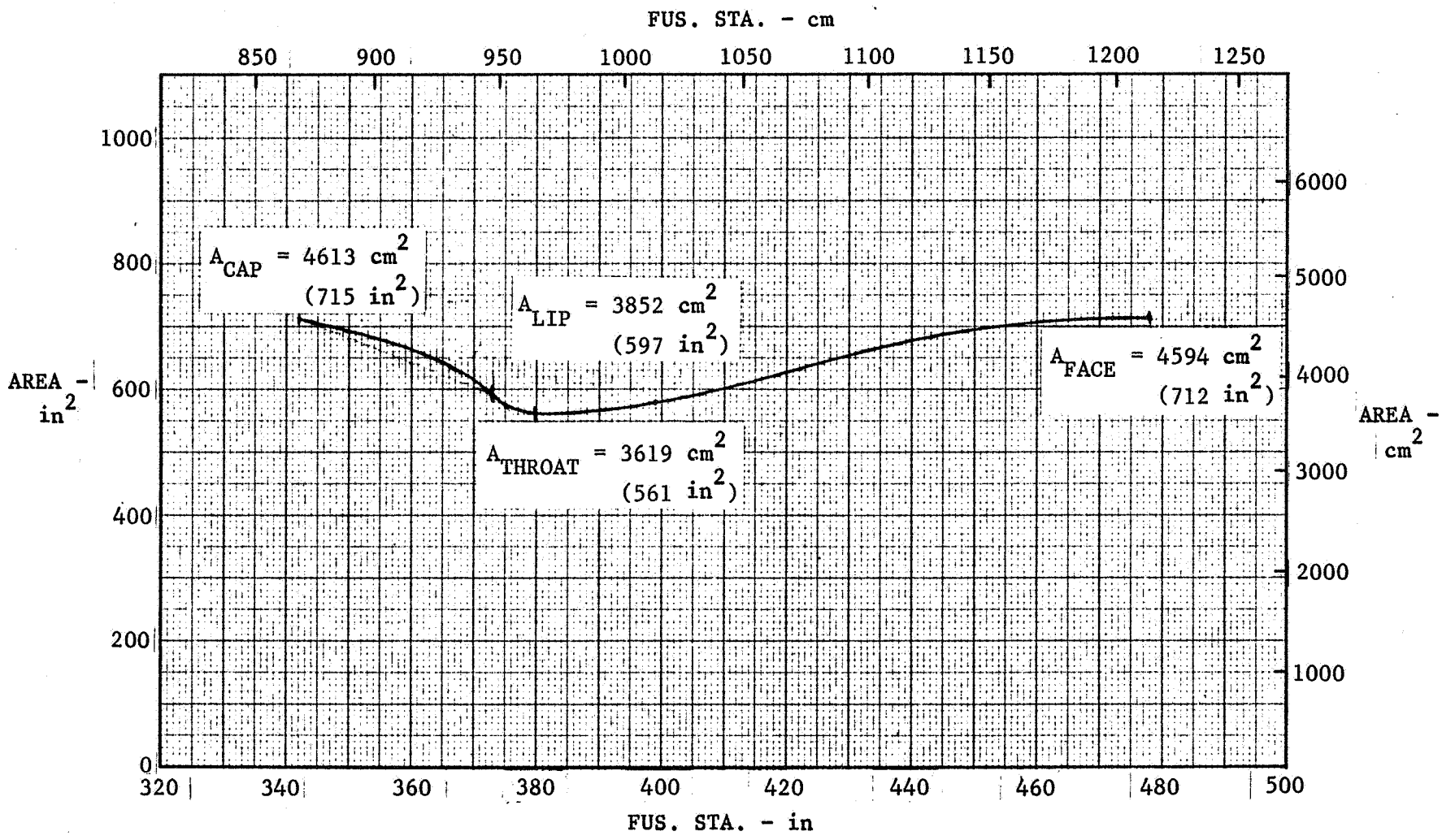

FIGURE 2-3. DUCT AREA DISTRIBUTION

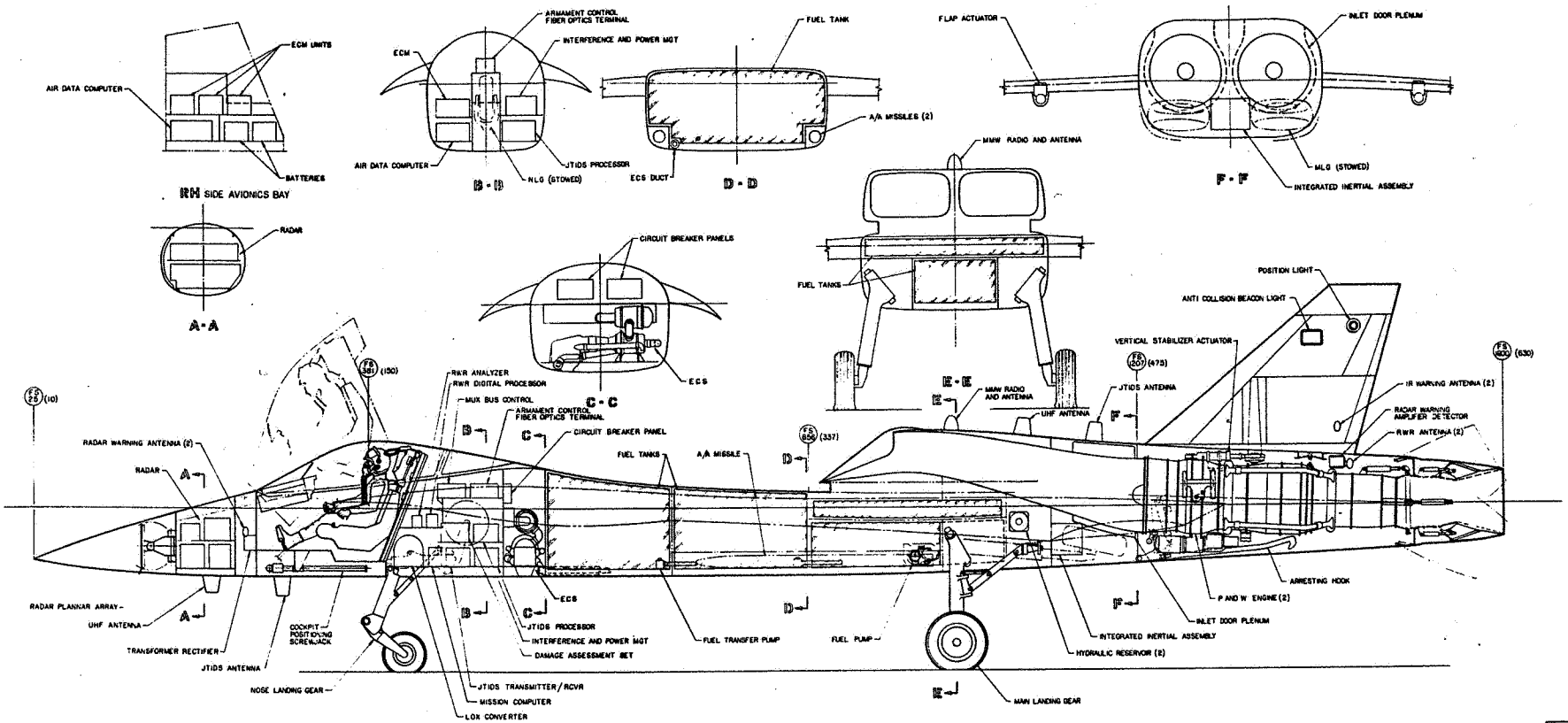

FIGURE 2-4.

ADVANCED DESIGN

GRUMMAN

SCALE	1/10
DWG.	1336-2
TITLE	INBOARD PROFILE, VATOL
FSCM No.	76823
SIZE	AD 668

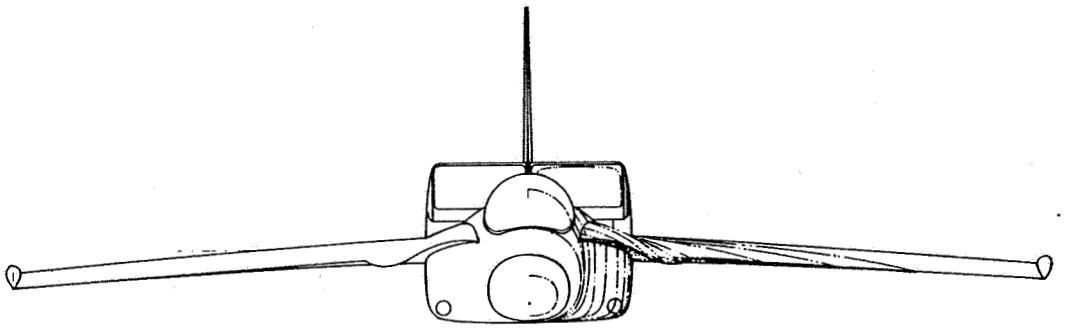

BOOSTERED MINI-MISSILE POD

OFF-BORESIGHT MISSILE POD

1250-LB CLASS GLIDE WEAPON

2500-LB CLASS GLIDE WEAPON

2500-LB CLASS POWERED WEAPON RAMJET

BODY CORNER SEMI-SUBMERGED FINNED WEAPON

BODY CORNER TANGENT FINNED WEAPON

FIGURE 2-5. CONFORMAL STORES MATRIX

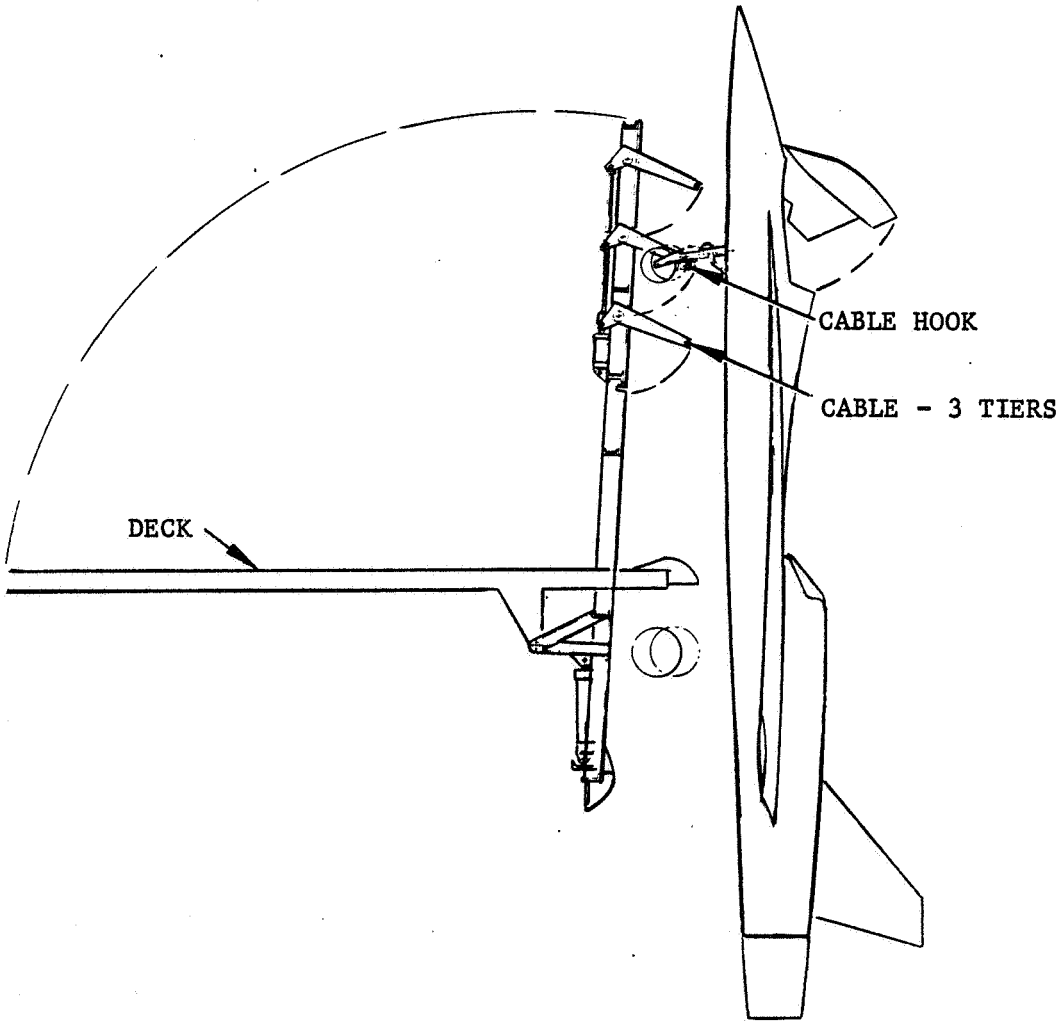

FIGURE 2-6. LAUNCH/RETRIEVAL CONCEPT

SECTION 3

AERODYNAMIC CHARACTERISTICS

Aerodynamic data for the selected VATOL configuration were generated based on a correlation of wind tunnel test results and computed results using the NASA-Ames Wing-Body Program. Stability, control, and trim to high angles-of-attack were determined for a c.g. location of $0.40\bar{c}$. The sea spray problem was analyzed through dimensional analysis of small-scale jet nozzle data.

3.1 WING SELECTION

The wing design incorporated in the VATOL concept was developed during an ongoing fighter technology IR&D program. The wing selection study examined a range of wing planforms to investigate impact on aircraft turn performance, acceleration capability, maximum speed and overall weight. The wings were configured with trailing edge flaps acting as pitch trim controls (applicable to both tailless or zero trim-load tailed designs) and automatic leading-edge flaps.

The use of negative static margin at subsonic speeds permits the aircraft to be balanced such that the trailing edge flap deflection for trim, at a given lift, matches the setting for minimum drag due to lift, so that the aircraft is trimmed for best L/D over a wide range of lift coefficients. At supersonic speeds, the shift in aerodynamic center results in near-neutral static stability, again yielding the least drag due to lift and trim. The synergism in this approach was found applicable over the full range of wings evaluated.

Three baseline configurations using a common, fixed engine were developed, including detailed area ruling and weight evaluation. Perturbations in aspect ratio, sweep, thickness, and wing camber were made to refine and optimize each baseline. Throughout, a fuel sizing mission, incorporating specific cruise, subsonic turn, supersonic turn and acceleration segments was used to establish the minimum weight/maximum performance geometry. Figure 3-1 summarizes some of the results of the study in the form of parameter ratios relative to the wing of this investigation. For the comparison shown, wing loadings were chosen to provide equal sustained turn rate

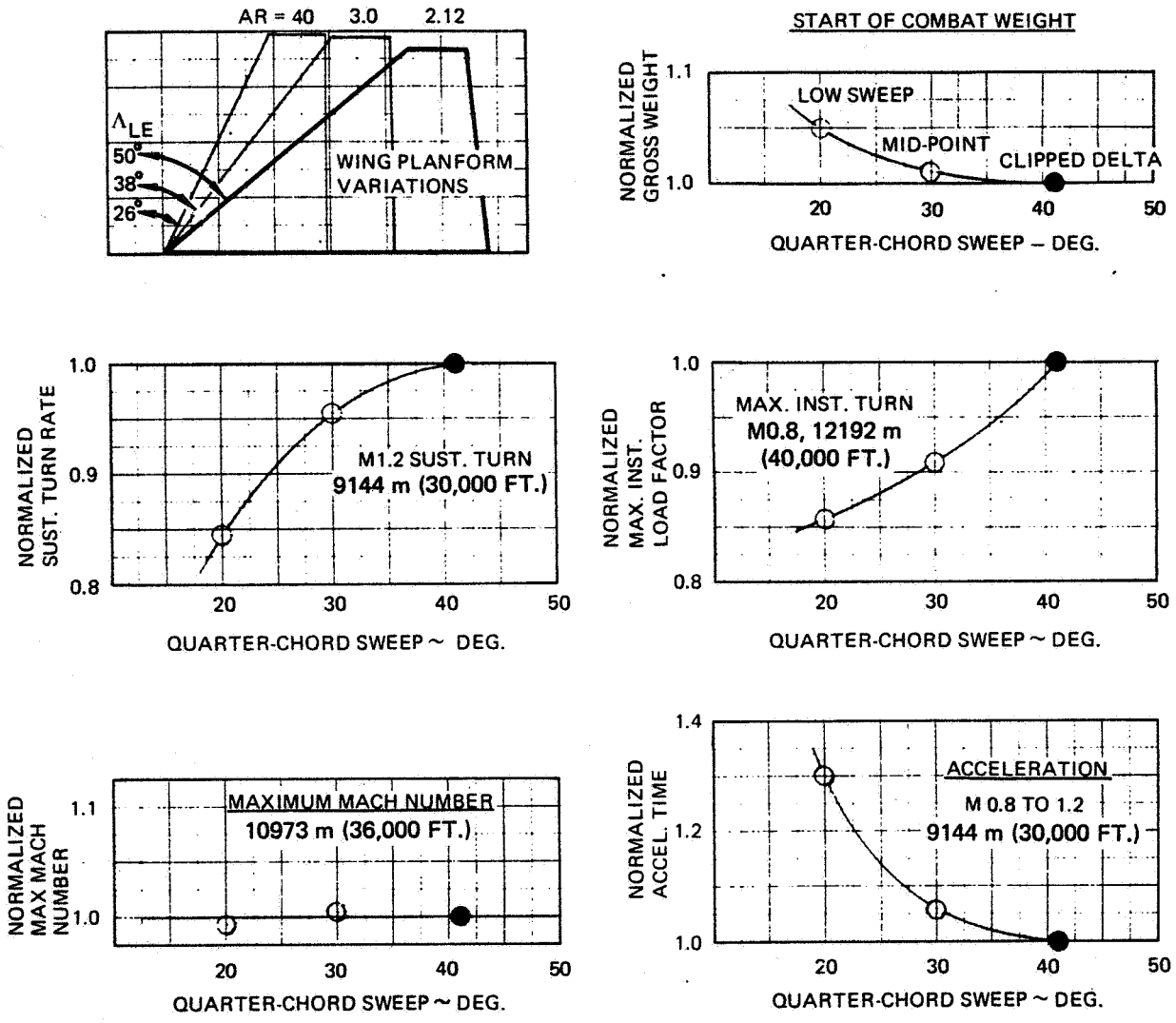

FIGURE 3-1. WING PLANFORM SELECTION

at M0.9 and 9144 meters (30,000 feet) altitude. This resulted in the wings having approximately the same span. The advantages evidenced by the baseline wing reflect a cross-sectional area distribution closer to ideal and a higher structural efficiency.

3.2 LONGITUDINAL

The aerodynamic analyses presented in Section 3 are for the clean configuration and do not include the effect of conformal or external stores.

3.2.1 Minimum Drag

The minimum drag includes all drag components that are independent of lift and engine throttle position. The reference conditions for thrust-drag bookkeeping purposes are as follows:

1. Maximum open nozzle position with nozzle static pressure ratio (P_9/P_{am}) equal to unity
2. Inlets operating at the supercritical mass flow point at each Mach number, (spillage drag for this condition is included in the aircraft drag)
3. Altitude of 9144 m (30,000 ft). Inlet bleed, ventilation, ram cooling drag increments and other components are included in the installed thrust data as listed in Table 4-2.

The minimum drag components are presented in Figure 3-2 as a function of Mach number at the reference altitude. Variation in minimum drag level with altitude is shown in Figure 3-3. The detailed drag buildup for the design is included as Table 3-1, showing the individual drag components for several Mach numbers at the reference altitude condition. The viscous drag component is further broken into its components in Table 3-2 for M 0.5 at the reference altitude.

Skin friction coefficients were obtained using charts contained in Reference 1. An equivalent roughness of 0.00127 cm (0.0005 in) was utilized to determine cut-off Reynold's number effects. Form factors were obtained from Reference 2 and an interference factor of 1.05 was applied to all planar surface components.

Wave drag was calculated using the Langley Wave Drag Program outlined in Reference 3. Two adjustments were made to the drag levels obtained from the program. The first adjustment, shown in Figure 3-4, adjusts the wave drag as a function of Mach number for he input option selected in this study. To facilitate input and area

ruling studies, the equivalent circular area input option was selected. Analysis of the YF-17, using both the equivalent circular area and the actual cross-section geometry inputs, agreed with previous NASA tests showing an increasingly optimistic drag level with Mach number when using the cirular input option. The adjustment in Figure 3-4 is based on the differences obtained in the YF-17 study. The second adjustment is a correction factor developed at Northrop, based on wind tunnel data, and applied to the wave drag of all wing and empennage surfaces. The adjustment is due to the fact that substituting three-dimensional bodies for wing surfaces generally results in underestimating the wing wave drag, especially for wings of low sweep having supersonic leading edges. The adjustment is a function of Mach number, sweep angle, and thickness ratio, and is shown in Figure 3-5. This adjustment is on the order of ±3 percent of the total wave drag estimate.

Subsonic canopy pressure drag was determined using data available in Reference 4 as a function of canopy frontal area. The supersonic drag increment is accounted for in the wave drag data. The reference spillage drag is included in the minimum drag. Subsonic afterbody-nozzle drag is based on scaled YF-17 afterbody wind tunnel test data. The supersonic afterbody-nozzle drag is included in the wave drag. The drag increment for boundary layer diverters was estimated using the data from Reference 5 as a function of frontal area and included wedge angle. The transonic drag levels between M 0.8 and M 1.2 were based on the drag rise characteristics of existing aircraft.

The remaining miscellaneous drag items include wing actuator fairings, wing tip pods, proturberance, gaps, vents, doors, etc., and are based on YF-17 analyses and data from References 4 and 6.

The final correction applied to the minimum drag buildup is the full scale adjustment which is based on a comparison of analytical results with flight test data of the YF-17 airplane. The adjustments for subsonic and supersonic flight are shown in Figure 3-6.

The final minimum drag for the complete airplane, given in Figure 3-2, shows a characteristic decrease at subsonic speeds before the drag rise; however, a rising trend in the minimum drag is indicated at supersonic speeds which contrasts with the constant level normally found in flight tests of high speed aircraft. This is an area of uncertainty needing test verification.

3.2.2 Basic Lift, Drag, and Pitching Moment

Basic subsonic aerodynamic data for the VATOL airplane have been generated at Mach numbers of 0.6 and 0.9 for four leading edge flap deflections and a range of trailing edge flap deflections. The data at M 0.6 are based on a correlation of wind tunnel test data at M 0.3 and 0.6 (References 7-10) and are, therefore, considered applicable to flight from M 0.6 down to low subsonic speeds. The wing-body configuration tested is essentially similar to the VATOL configuration with the exception of the smaller LEX which impacts primarily on the maximum lift and the maximum recovery moment. Methods of extrapolating the LEX size are explained in Section 3.2.5 on high angle-of-attack characteristics. However, the data at M 0.9 are presented without LEX size correction, which means a possible underestimation of nose up pitching moment at high angle of attack. Tests are desirable to ascertain these effects, since estimation methods are not available in the non-linear high angle-of-attack, transonic Mach number region.

Lift vs. angle-of-attack data at M0.6 are presented in Figures 3-7 to 3-10 for leading edge flap deflection of 0, 8, 16 and 24 degrees. Corresponding pitching moment data are presented in Figures 3-11 to 3-14, lift-drag data in Figures 3-15 to 3-18, and lift-drag ratios in Figures 3-19 to 3-22. Similar data for M0.9 are shown in Figures 3-23 to 3-38. Both sets of data were adjusted for effects of wing twist and camber which result in changes in C_{L_o} C_{m_o}, and location of the aerodynamic center. Values of these parameters were determined from the NASA-Ames Wing-Body Program (Carmichael-Woodward Program, Reference 11) and incorporated in the results shown.

Basic supersonic aerodynamic data have been generated at Mach numbers of 1.2 and 1.6 using the Carmichael-Woodward Program (Reference 11). Results are presented in Figures 3-39 to 3-46 for the case of undeflected leading-edge flaps. Computations with deflected leading edge flaps indicate some reduction in drag-due-to-lift, even at M 1.6 (cf. Section 3.2.4 on flap schedules and trim polars). Note the trim line on the pitching moment plot in Figure 3-40 showing neutral static stability at M 1.2 for a c.g. location of 0.40c. At M 1.6 (cf. Figure 3-44) a slightly positive static margin is shown for the 40 percent c.g. location. The rationale for establishing the c.g. location is given in the following section on stability analysis.

3.2.3 Longitudinal Stability Analysis

The effect of static margin on the VATOL longitudinal aerodynamics was determined with the aid of the Carmichael-Woodward program (Reference 11). The use of negative static margin at subsonic speeds was found to permit the aircraft to be balanced so that the trailing edge flap deflection for trim, at a given lift, is very nearly the deflection for minimum drag due to lift. At supersonic speeds, the aft shift in the aerodynamic center results in near-neutral static stability, again yielding the low drag due to lift and trim. This synergistic approach to unstable aircraft design was found to give optimum performance polars with minimum trim drag penalty over a wide range of lift coefficients for the Mach number range of interest.

Computations with the Carmichael-Woodward program were made showing the incremental effects for leading edge and trailing edge flaps, wing camber, and angle-of-attack. Minimum drag-due-to-lift was obtained as a function of lift and moment center for various control deflections.

Results at M 0.6 for various camber distributions are shown in Figure 3-47. Comparison of the polars for the flat wing and the design-camber wing (see Section 3.2.7 for details), with no flap deflections shows that there is a slight reduction in drag at a given lift due to wing camber. The polar which is obtained by deflecting the leading- and trailing-edge flaps to achieve least drag at a given lift without a pitching moment constraint (untrimmed) shows a large reduction in drag over the flat and design-camber wings. Also shown in Figure 3-47 are the optimum control surface deflection both untrimmed and trimmed. As expected, large deflections of the flaps occur at the higher lift coefficients. If a trim pitching moment constraint is imposed, the resulting polar is changed only slightly from the untrimmed polar illustrating the self-trimming property of the configuration. Note the comparison between test correlated data and theoretical polar for optimum trim. The lower drag in the test polar is attibuted to a significant amount of leading-edge suction which is not accounted for in the analytical calculations.

The effect of static stability on polar shape has been further studied and comparisons made with the HAVSTOL configuration (Reference 12) which is a canard configuration. The Oswald efficiency parameter "e" is shown plotted against static margin in Figure 3-48. For each of the configurations, as the static stability is

reduced, "e" increases and then levels off with the knee of the curve being at about $-0.15\bar{c}$ for the VATOL configuration, and a somewhat larger negative number for the HAVSTOL configuration. Current thinking is that a negative 15 percent static margin is about the maximum allowable from a controls point of view. Control system technology is expected to be developed for the 1990^{+} time period which will be capable of handling these levels of static instability.

Also shown on Figure 3-48 are test data for the VATOL configuration and for a configuration featuring a canard. The test data have a somewhat higher value of "e" because of the zero leading edge suction assumption of the theoretical method.

On an unstable airplane, the degree of negative longitudinal stability must be carefully chosen to achieve the associated performance benefits without creating conditions in which the capabilities of the control system are exceeded. As the center-of-gravity position also has to be fixed rather precisely because of thrust balancing conditions, the aerodynamic center position has to be carefully determined. Therefore, a considerable effort was undertaken to determine the a.c. position. A static instability limit of negative 15 percent was set for subsonic speeds, and the effort was made to achieve neutral or near neutral stability at supersonic speeds.

The basic tool for the a.c. calculations was the Carmichael-Woodward wing-body computer program used in conjunction with NASA and Northrop test data of similar configurations for a more accurate modeling of forebody effects. Previous experience with the wing-body program showed that the body contribution to stability is underestimated when compared to test results. The error in computed a.c. is less when the body is represented as a lifting surface rather than a body of revolution. For either representation it is necessary to establish a certain forebody geometry characteristic as a correlation parameter which most closely matches the test data incremental a.c. due to forebody.

For the case of bodies of revolution, the characteristic parameter appears to be the product of the maximum cross-sectional area forward of the wing panel and the distance from the theoretical center of pressure (on an isolated forebody from NACA TR 1307) to the intersection of the body and the leading edge of the exposed root chord of the forward wing panel.

The nose volume coefficient is not a good correlation parameter when the body is simulated by a low aspect ratio wing surface. A better parameter in this case is the product of the projected body planform area forward of the exposed forward wing panel and the distance to the nose center of pressure. As Figure 3-49 shows, in the range of interest in particular, good agreement of theory and test is indicated. In particular, the computed a.c. for the VATOL is estimated to be only $0.015\bar{c}$ ahead of the test a.c.

Results from the Carmichael-Woodward Program, corrected for forebody geometry, are shown in Figure 3-50 as a function of Mach number. The aerodynamic center location is $0.25\bar{c}$ at M 0.6 and $0.40\bar{c}$ at M 1.2. Thus with the CG at $0.40\bar{c}$ the limiting 15 percent negative static margin exists at low subsonic speeds.

3.2.4 Trim Analysis

The basic longitudinal data presented in Section 3.2.2 were trimmed to a c.g. location of $0.40\bar{c}$ by deflecting the trailing edge flaps. The leading edge flaps were varied in accordance with the deflection schedule shown in Figure 3-51, which resulted in conditions for minimum trimmed drag for a given lift, Mach number, and angle-of-attack. The corresponding trailing edge flap deflection for trim is shown in Figure 3-52. Maximum deflection limits are 30 degrees for the leading-edge flaps, and 40 degrees for the trailing-edge flaps.

These limits are reached only in subsonic flight, where the relatively large negative stability margins (-15 percent at M 0.6 and -12 percent at M 0.9, as shown in Figure 3-50) require full control deflections for aerodynamic trim at high angles of attack. At supersonic speeds, the Carmichael-Woodward program indicates some trim benefits to accrue from leading-edge flap deflection; the corresponding trailing-edge flap deflections are small, but negative.

For small angles of attack the optimum leading-edge flap deflections are small negative angles (leading edge up). This is due to the leading edge droop in the design camber. The benefits which could be derived from these small deflections are relatively small, and do not justify the structural and controls penalty. Thus, the leading edge flap remains undeflected until $\alpha = 4^{\circ}$ at M 1.2 and $\alpha = 9^{\circ}$ at M 1.6. At the higher angles of attack there are benefits to be obtained from deflecting the leading edge flap both at M 1.2 and M 1.6. This is not surprising at M 1.2, as the

leading edge of the wing is subsonic. At M 1.6, however, the wing leading edge is supersonic and the result was unexpected. The benefit is apparently due to a forward rotation of the local wing load. The corresponding trailing edge flap deflections are negative (trailing edge up) showing that the flaps are being unloaded with angle-of-attack for trim at supersonic speeds.

Optimum trim lift curves for the foregoing flap schedules are shown in Figure 3-53 for subsonic speeds, and Figure 3-54 for supersonic speeds. The corresponding trim polars are shown, respectively, in Figures 3-55 and 3-56. Based on previous experience with similar planforms, the maximum spanload efficiency factor, defined as $e = C_L^2 / (\pi AR C_{D_L})$, was limited to 0.95 at M 0.6, and to 0.80 at M 0.9. These conditions prevail only at the lower lift coefficients, since the spanload efficiency falls off naturally at the higher lift coefficients.

The supersonic polars at M 1.2 and 1.6 were obtained using the Carmichael-Woodward program and assuming neutral static stability; the polar at M 2.0 was estimated by methods presented in DATCOM. Note the trim drag penalty (18 to 19 counts at zero lift) resulting from the cambering effects which were built into the wing design.

The optimum trim lift-drag ratios for the full range of Mach numbers are summarized in Figure 3-57.

3.2.5 Longitudinal High α Aerodynamic Characteristics

High angle of attack characteristics are of critical importance in the design of the VATOL configuration, as they have a great impact on transition and STO performance, on angle of attack restrictions in maneuvering flight, and on the quality of the topside inlet flowfield. In that context, the size and shape of the leading edge extension (LEX) is of particular importance. Since the high attitude aerodynamics are not amenable to analytical prediction, they are determined by judicious extrapolation of wind tunnel test data of configurations featuring the same basic wing with a series of small LEX's.

The low speed longitudinal characteristics at high angles of attack as affected by LEX size are shown in Figures 3-58 and 3-59. The data used in the extrapolation procedure could not be used directly as a number of additional configuration

differences existed. Adjustments had to be made to account for differences in trailing edge flap span, the existence of chordwise wing root slots and saw teeth on the leading edges. The curves labeled test data in Figures 3-58 and 3-59 reflect these adjustments. A large amount of test data exist on tailed, but otherwise similar configurations, and attempts were also made to utilize these data. This effort was largely unsuccessful, as changes in downwash and resultant tail load changes due to LEX size variation tended to obscure the correlation trends.

It was observed that the rate of increase in $C_{L_{max}}$ with (exposed) LEX area was substantially higher on the proposed clipped delta wing than on the YF-17 wing of higher aspect ratio, higher taper ratio, and lower sweep. One reason is thought to be that the LEX vortex can influence the flow over a much larger part of the wing area for the delta wing which has a larger root chord. Another reason is that most high angle-of-attack test data were obtained on configurations with leading edge flaps deflected. The leading edge flap deflection tends to increase the effective exposed LEX area which, in the case of the relatively small LEX's tested on the delta wings, amounts to a rather large area increase.

In using the larger effective LEX areas with flaps deflected, on the present configuration, a smoother trend of $C_{L_{max}}$ with LEX area was established than had been the case when "flaps-up" LEX areas were used in the extrapolation of the earlier test data. This procedure has been used to determine the high angle-of-attack lift and moment characteristics in Figures 3-58 and 3-59. As compared to the earlier data, a slight reduction in $C_{L_{max}}$ and a substantial reduction in the nose-up pitching moment is indicated. Recent test data from a half-span model featuring the selected large LEX are in substantial agreement with the extrapolated data with the exception of pitching moment beyond the stall angle of attack which tended to be more positive. (It should be noted that the half-span model had only a rudimentary body, and therefore that test data, while tending to confirm, do not supersede the data determined through extrapolation.) The predicted decrease in nose-up pitching moment tends to ease the problems of angle-of-attack limitation in maneuvering flight.

Aerodynamic characteristics beyond the stall are presented to 90 degrees angle-of-attack in Figures 3-60 to 3-62. The results are based on low-speed high-attitude tests of the VATOL wing which have been run with smaller size LEX's. The lift curve (Figure 3-60) is shown to have a smooth and gradual fall-off past the stall. This is

believed the result of proper design of the LEX which governs the vortex-flow over the wing. Such post-stall lift behavior is important in alleviating transition difficulties during decelerating flight, where the aircraft is required to rotate through 90 degrees angle-of-attack range (Section 6.2).

$C_{L_{max}}$ Estimation. The estimate of usable $C_{L_{max}}$ as a function of Mach number is presented in Figure 3-63. Subsonic $C_{L_{max}}$ values represent trim limits achieved with maximum trailing edge flap deflection rather than aerodynamic limits. With the flap being at its maximum deflection, a nose-down recovery must be made using thrust vectoring. In maneuvering flight entailing high pitch rates, the maximum angle of attack may have to be limited to prevent an overshoot into an uncontrollable post-stall flight condition. This may result in a decrease in the usable $C_{L_{max}}$. On the other hand, at low speeds and certainly during transition flight, no angle-of-attack limits exist and the true aerodynamic $C_{L_{max}} = 1.64$ can be obtained when thrust vectoring is employed for trim.

At supersonic speeds, no trim limits exist as the airplane is essentially neutrally stable. Limitations arise from inlet operations on top of the wing. The inlet is designed for a maximum Mach number of 2.0, and the angle of attack at which the local Mach number is 2.0 was used to determine $C_{L_{max}}$ at the higher Mach numbers.

Buffet Onset. Buffet onset lift coefficients were estimated using wind tunnel test data from Reference 7. As previously noted, the wing which was tested had the same planform as the VATOL aircraft. The balance roll strain gauge dynamics output was recorded and the root mean square calculated. The angle of attack at which the root mean square of the rolling moment showed a significant increase was used to determine buffet onset. These data are shown in Figure 3-64 for various Mach numbers and leading and trailing edge flap deflections. Leading and trailing edge flaps, individually and in combination, are seen to increase the buffet onset boundary. The buffet onset curve is similar to the $C_{L_{max}}$ curve at subsonic Mach numbers as expected. At supersonic Mach numbers no buffet is expected to $C_{L_{max}}$.

3.2.6 Aerodynamic Control Effectiveness

Longitudinal control effectiveness for the VATOL airplane was determined using wind tunnel test data at subsonic speeds and Carmichael-Woodward Program calculations at supersonic speeds. Trailing-edge flap effectiveness data are presented for M0.6, 0.9, 1.2 and 1.6 in Section 3.2.2. At subsonic speeds, flap effectiveness is seen to decrease with angle-of-attack as full flap deflection is reached. Figures 3-7 and 3-10, for example, show the fall off in flap effectiveness at maximum lift conditions as the trailing-edge flaps are deflected from 0 to 40 degrees. Similarly, Figures 3-14 and 3-30 show the decrease in longitudinal control effectiveness as the flaps are deflected from 0 to 40 degrees. Some fall off in effectiveness is also expected at supersonic speeds, although linear variation in the computing method prevents its prediction. In any case, flap control requirements are less at supersonic speeds since the aerodynamic center is coincident with the c.g. at M 1.2, and only slightly behind the c.g. at M 1.6. Note that the maximum angle-of-attack for pitch recovery with fully deflected flaps is about 19 degrees at M 0.6 and 18 degrees at M 0.9, as indicated in Figures 3-14 and 3-30. Thrust vectoring would be required above these values to reach the maximum aerodynamic lift shown on the trim lift curves in Figure 3-53. At supersonic speeds of M 1.2 and above, the maximum angle-of-attack is limited only by the airflow requirements to the topside inlet.

3.2.7 Wing-Body Camber

The conventional approach to wing-body camber design has been to first determine the wing camber which minimizes drag for a specified lift and pitching moment coefficient at a given Mach number. The body area is then wrapped around the wing such that the body area growth is the same above and below the projected wing camber surface within the body. This approach is deficient in two important areas. First, the body is essentially uncambered in the spanwise direction so that the wing camber in this region is greatly modified by the presence of the body. Second, the optimum camber for the wing in the presence of the body is expected to be quite different from the wing-alone camber. Additionally, the use of pressure loadings in the optimization procedure precludes the imposition of geometric constraints such as a straight line for a control hinge.

An alternate approach has been developed which uses a selection of a number of component distributions of camber and twist. Each of the component shapes embodies desired geometric constraints so that any combination of the shapes will also satisfy the same constraints. The bodies are modeled as thin cambered surfaces based on previous comparisons with wind tunnel test data. The model configurations were divided into ten equal width chordwise strips (Figure 3-65). Appropriate element distributions were selected along each strip (not shown in Figure 3-65) such that a total of 115 elements were used.

The Carmichael-Woodward computer program was used for the calculations. The configuration was analyzed as a flat planform and with various combinations of control surface deflections at M1.2. The results of these calculations are tions are summarized in Table 3-3.

An optimum distribution of wing camber with limited twist was also calculated for the configuration. The design conditions were M 1.2, a lift coefficient of 0.2, and zero pitching moment coefficient. This design condition was selected from considerations of both maneuvering and cruise at M 1.2. It represents a lift coefficient which is approximately mid-way between cruise and sustained turn at 9,144 m (30,000 ft.). Geometry, rather than pressure control modes were selected for these calculations with constraints of straight flap hinge lines and single curvature body camber. Geometry modes also facilitate the optimization of control surface deflections at off-design conditions. The selected modes are listed in Table 3-4. The "root" designation means that the particular mode varies from a nominal value at the wing root to zero at the tip. For the "tip" designation, the variation is from a nominal value at the wing tip to zero at the root. The root is defined as the airplane center line, but the wing camber is only effective outboard of the body which is defined separately.

The Carmichael-Woodward program was used to calculate the aerodynamic load distribution for each mode. The interference drag terms between modes were then calculated. The optimum combination of modes was calculated to minimize the wave drag due to lift at the design conditions cited above. The VATOL design was optimized for body camber, leading edge extension (LEX) camber and twist, and wing camber and twist. The configuration was initially optimized with zero leading and trailing edge flap deflections at the design point. The resulting surfaces had unacceptably

high values of twist so that a limit was placed on the twist. Flap deflection modes were introduced to reoptimize. Again, the criterion was trim and minimum drag over the appropriate angle of attack range. These results are summarized in Table 3-5. The design mean lines along the center line of each chordwise strip are shown twice scale in Figure 3-65.

TABLE 3-1. MINIMUM DRAG BUILDUP BY COMPONENT

h = 9144 m(30,000 ft.) S_{REF} = 46.5 m^2 (500 $ft.^2$)

COMPONENT	M0.3	M0.6	M0.9	M1.2	M1.6
VISCOUS	.0090	.0081	.0073	.0066	.0059
WAVE/DRAG RISE	.0000	.0000	.0011	.0135	.0175
SUBSONIC CANOPY	.0002	.0002	.0002	(IN WAVE DRAG)	
SUBSONIC AFTERBODY NOZZLE	.0009	.0009	.0009	(IN WAVE DRAG)	
SPILLAGE	.0000	.0000	.0001	.0011	.0002
BOUNDARY LAYER DIVERTER	.0000	.0000	.0002	.0005	.0010
MISCELLANEOUS	.0009	.0009	.0012	.0026	.0025
FULL SCALE ADJUSTMENT	.0014	.0014	.0014	-.0010	.0015
TOTAL	.0124	.0115	.0124	.0233	.0286

TABLE 3-2. VISCOUS DRAG BUILDUP BY COMPONENT

M 0.50 h = 9144 m (30,000 ft) S_{REF} = 46.5 m^2 (500 ft^2)

COMPONENT	ℓ cm (in)	S_{WET}/S_{REF}	$R_{N/10^7}$	C_f	ΔC_{D_F}	FORM FACTOR	INTERF. FACTOR	$\Delta C_{D_{VISC.}}$
FUSELAGE	1570 (618)	1.660	7.35	.00212	.00352	1.081	1.00	.00381
WING (INB'D)	838 (330)	0.432	3.922	.00233	.00101	1.036	1.05	.00110
WING (OUTB'D)	411 (162)	1.072	1.925	.00259	.00278	1.048	1.05	.00306
VERTICAL	163 (64)	0.108	0.751	.00303	.00033	1.048	1.05	.00036
TOTAL		3.272			.00764			.00833

TABLE 3-3. DRAG DUE TO LIFT WITH NO CAMBER, M1.2

LIFT COEFFICIENT	0	0.2	0.4
UNTRIMMED	0	0.0111	0.0445
TRIMMED WITH:			
T.E. FLAPS	0	0.0114	0.0456
OPT L.E. AND T.E. FLAPS	0	0.0105	0.0419

TABLE 3-4 GEOMETRY DESIGN MODES

MODE NUMBER	MODE
1	FLAT ANGLE OF ATTACK
2	LINEAR TWIST
3	ROOT L.E. DROOP
4	TIP L.E. DROOP
5	ROOT CAMBER
6	TIP CAMBER
7	ROOT REFLEX
8	BODY BEND
9	BODY CAMBER
10	LEX ANGLE OF ATTACK
11	LEX LINEAR TWIST
12	LEX CAMBER (L.E. DROOP)
13	L.E. FLAP DEFLECTION
14	T.E. FLAP DEFLECTION

TABLE 3-5. DRAG DUE TO LIFT WITH DESIGN CAMBER, M1.2

LIFT COEFFICIENT	0	0.2	0.4
UNTRIMMED: UNCAMBERED (REF. TABLE 3-3)	0	0.0111	0.0445
TRIMMED			
T.E. FLAPS	0.0025	0.0088	0.0379
OPT. L.E. AND T.E. FLAPS	0.0019	0.0087	0.0366

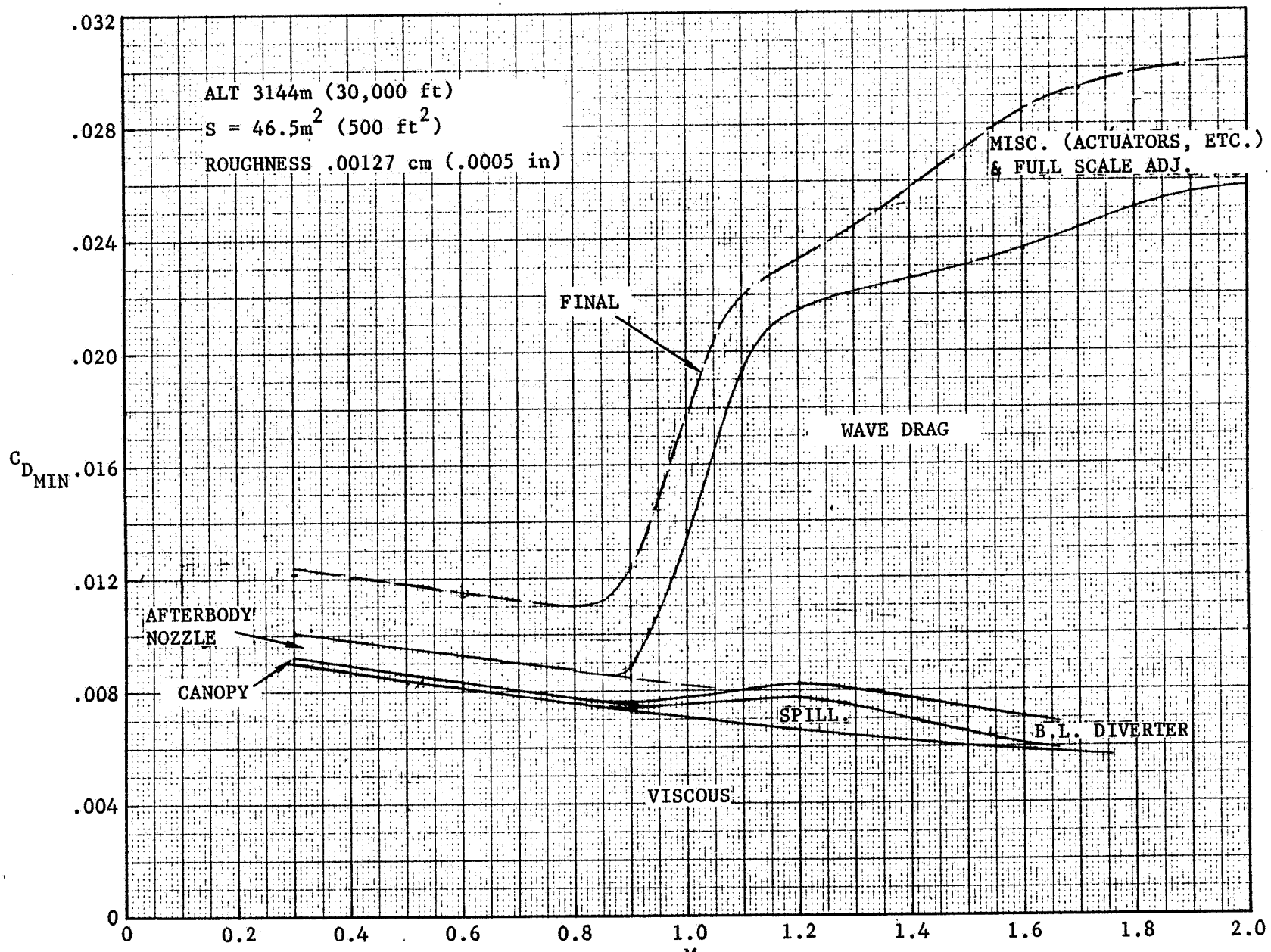

FIGURE 3-2. MINIMUM DRAG BUILDUP

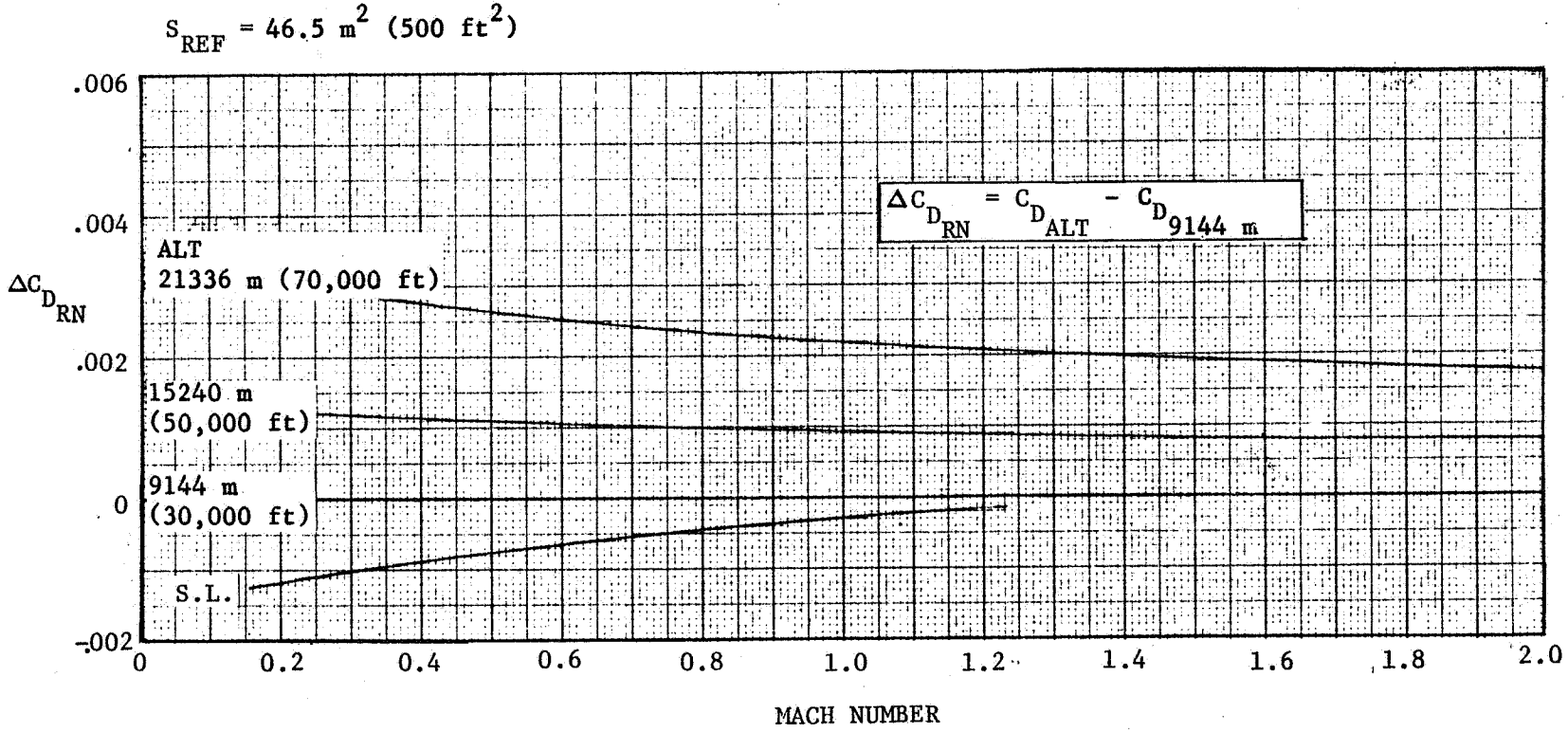

FIGURE 3-3. ALTITUDE EFFECTS ON MINIMUM DRAG

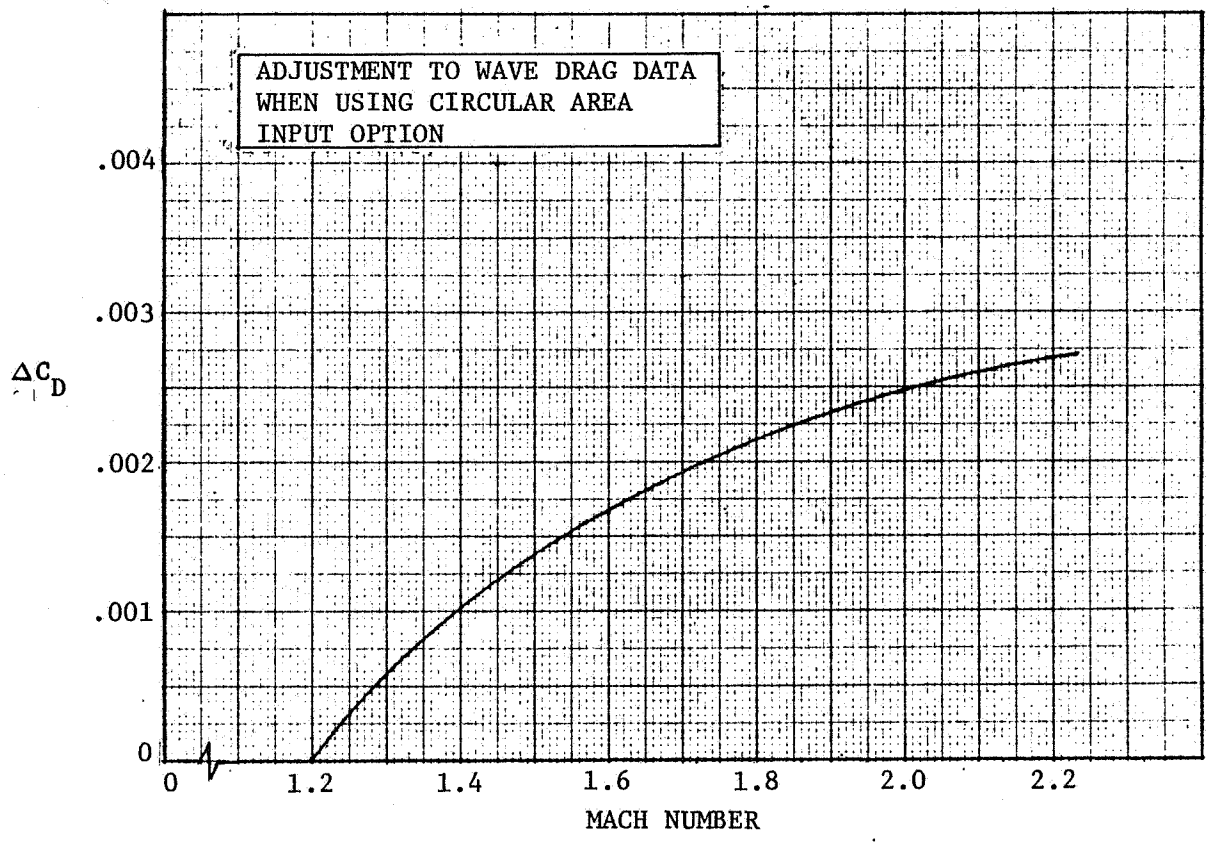

FIGURE 3-4. WAVE DRAG ADJUSTMENT VS MACH NUMBER

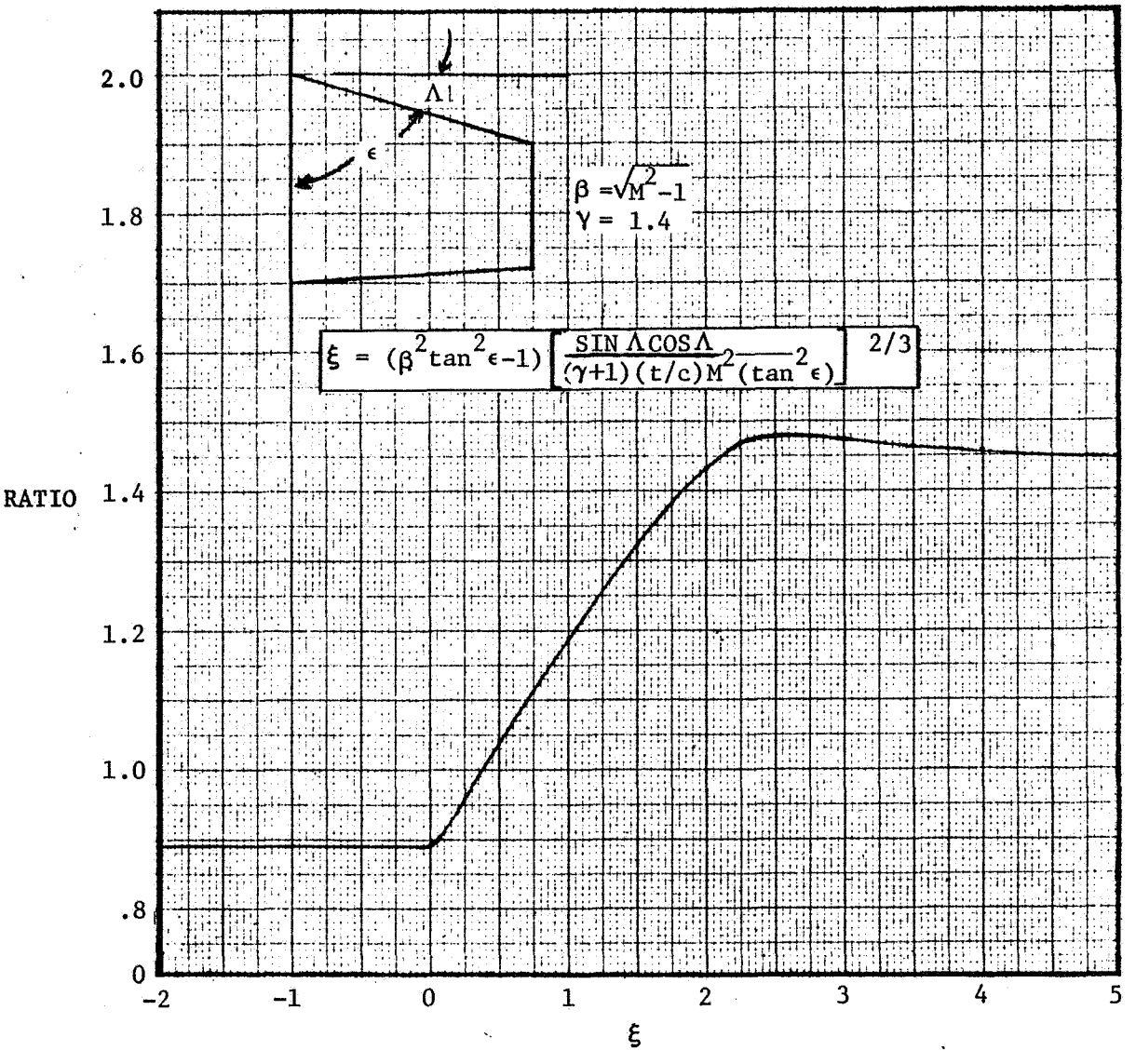

FIGURE 3-5. WAVE DRAG PLANAR SURFACE ADJUSTMENT

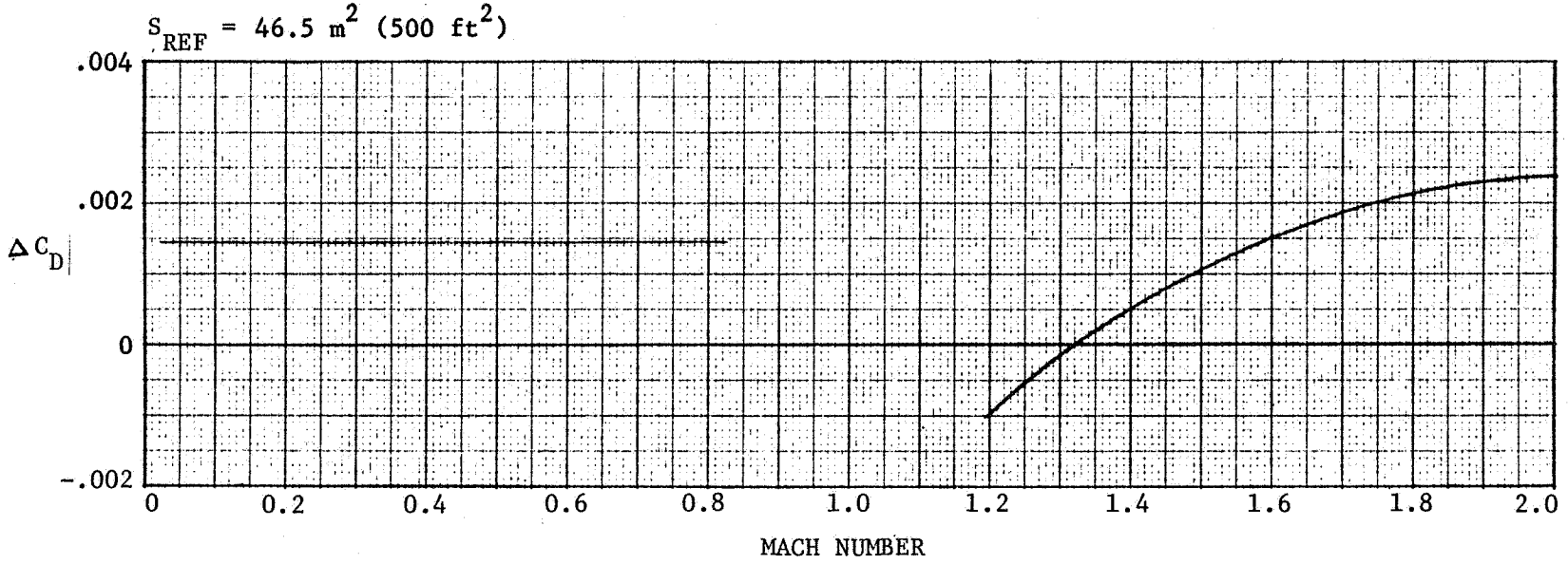

FIGURE 3-6. FLIGHT TEST ADJUSTMENT TO MINIMUM DRAG

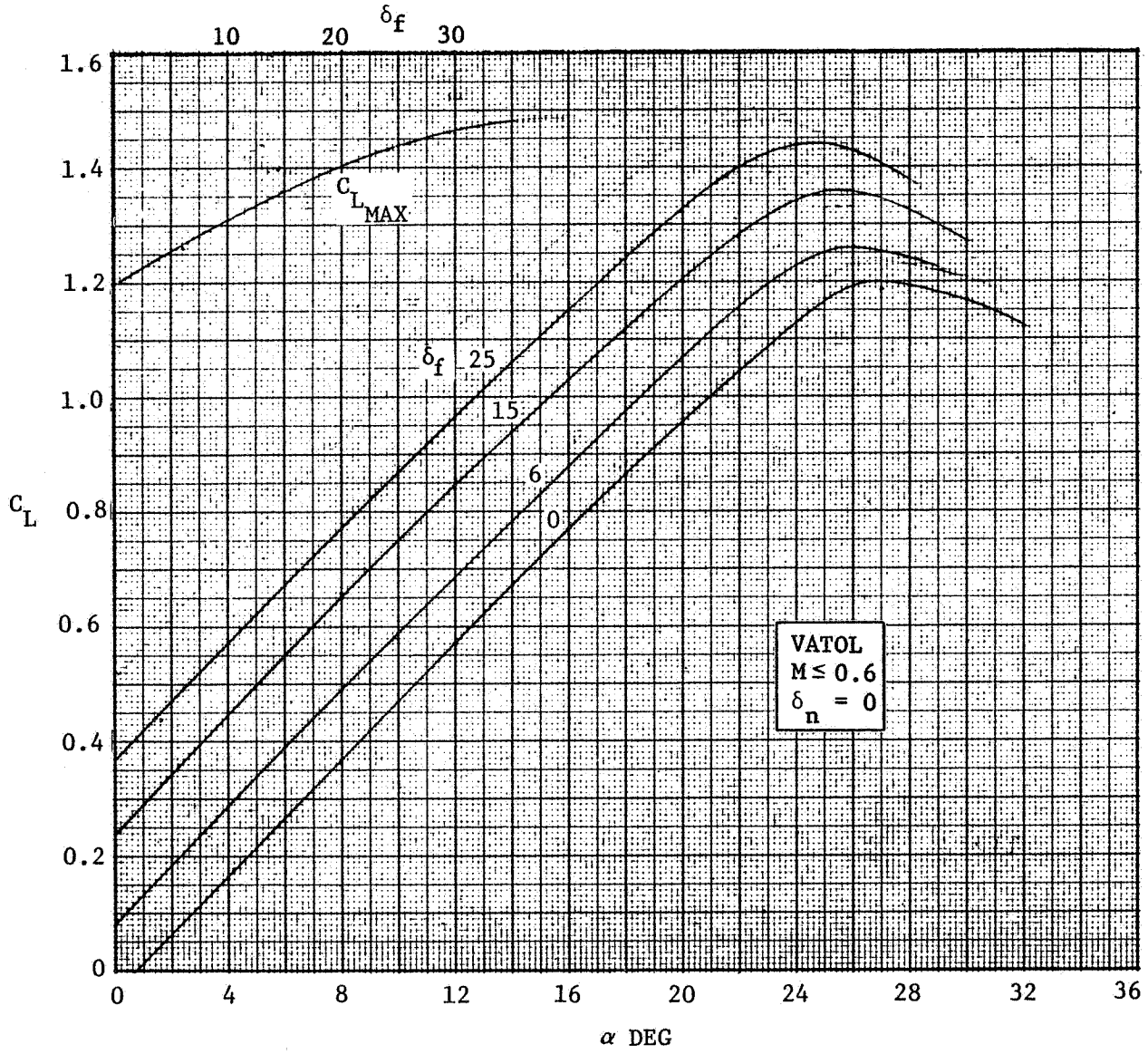

FIGURE 3-7. LIFT VS ANGLE OF ATTACK AT M≤0.6, δ_n=0

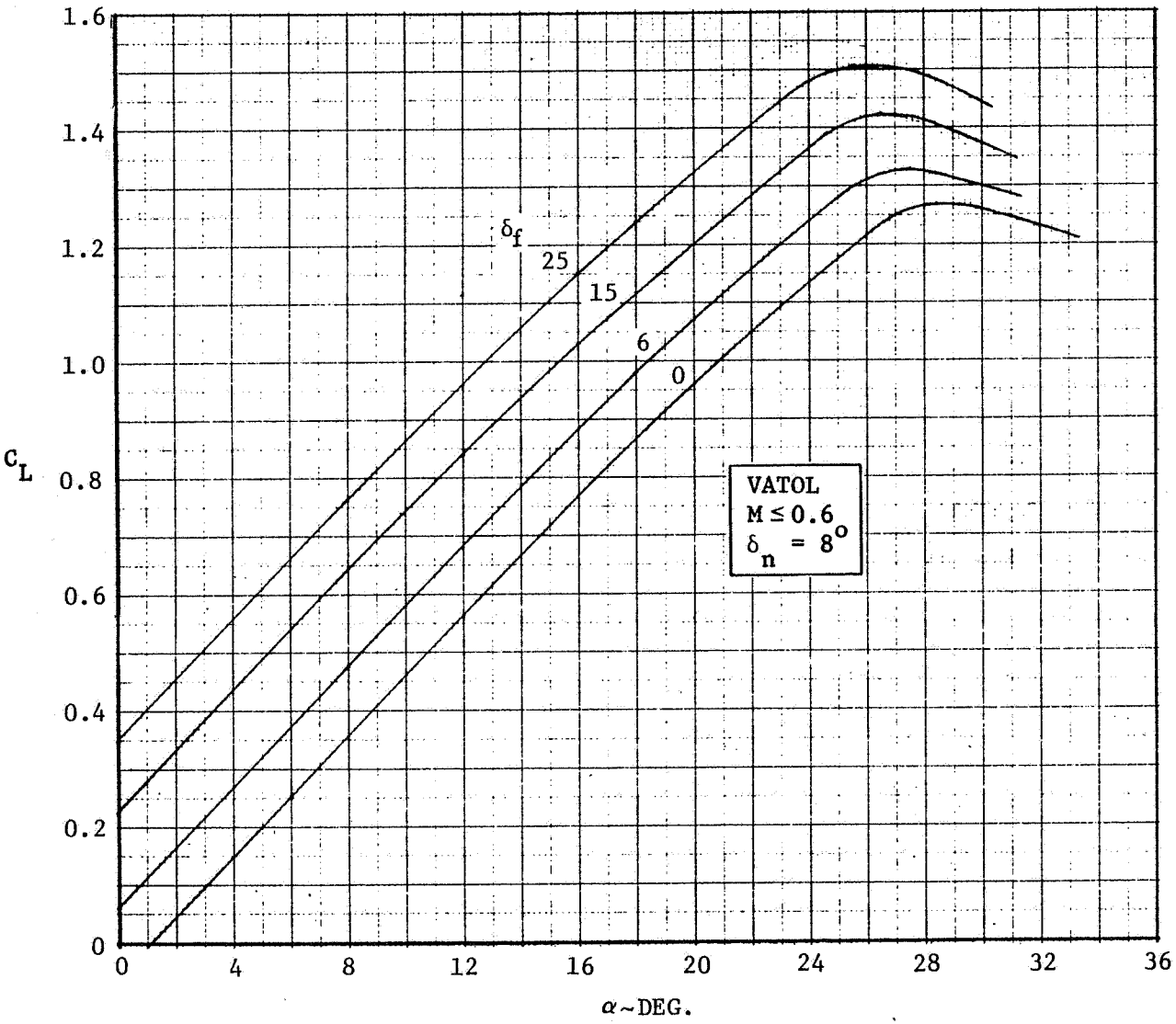

FIGURE 3-8. LIFT VS ANGLE OF ATTACK AT M≤0.6, δ_n=8°

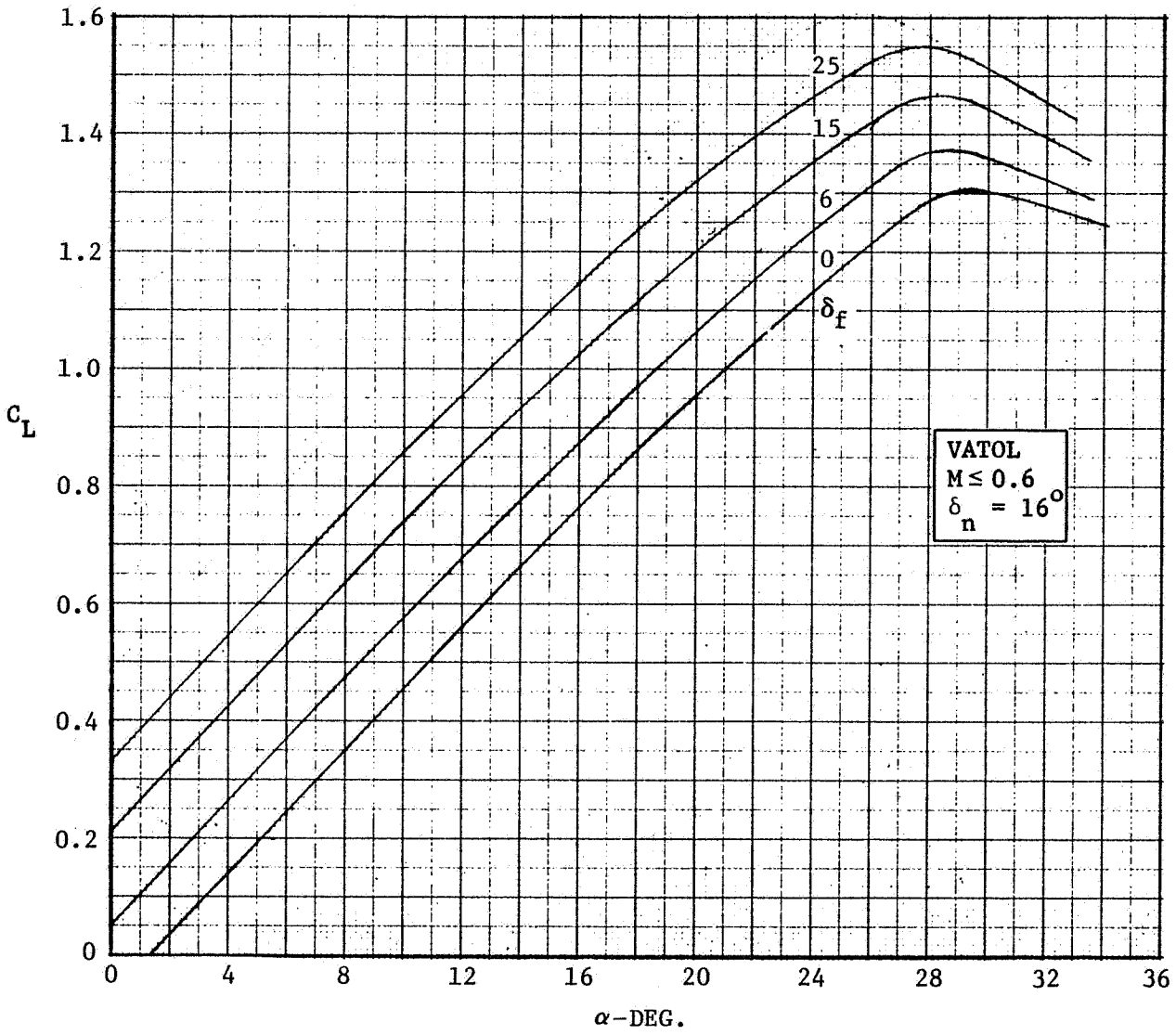

FIGURE 3-9. LIFT VS ANGLE OF ATTACK AT M≤0.6, δ_n=16°

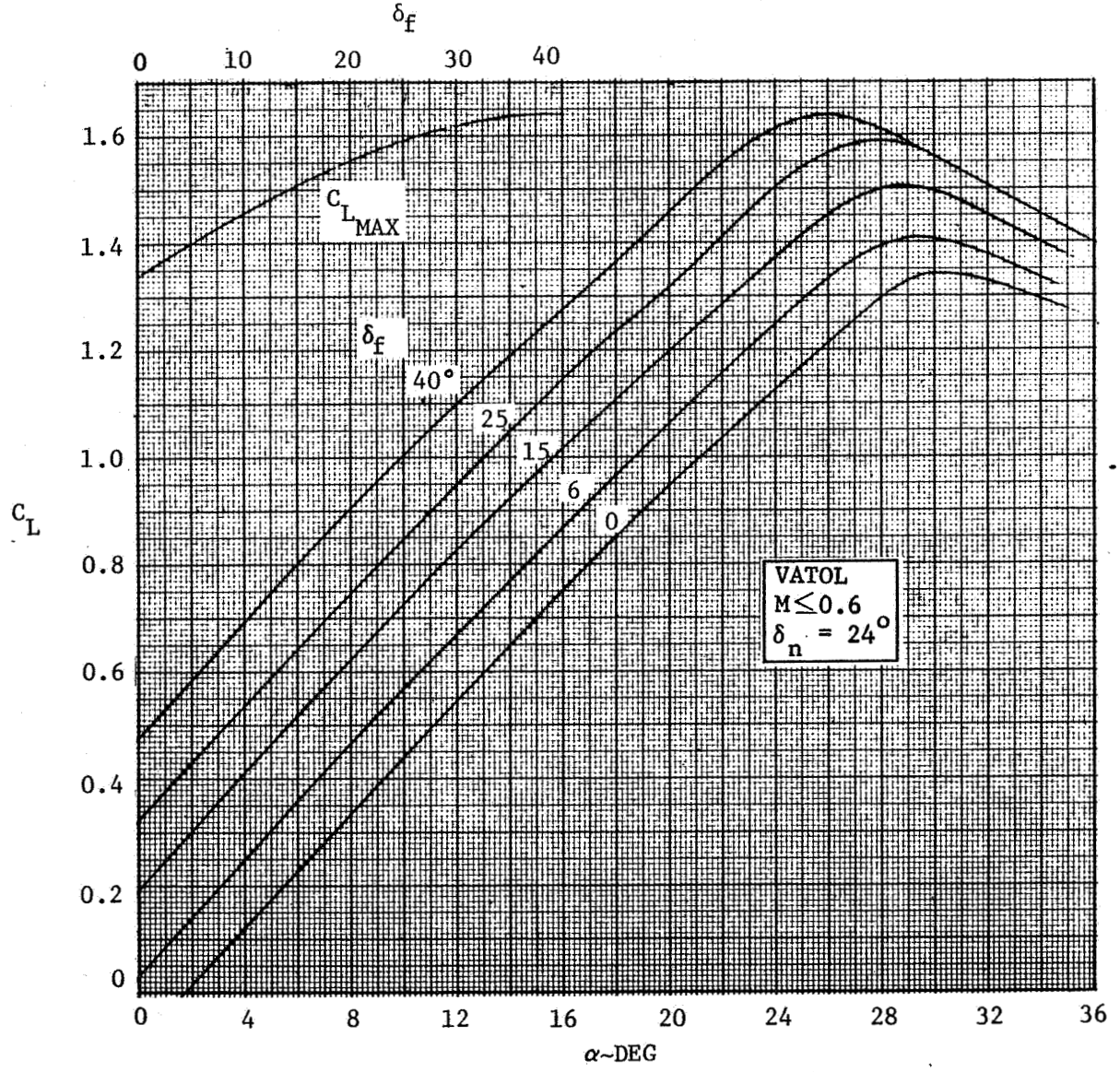

FIGURE 3-10. LIFT VS ANGLE OF ATTACK AT M≤0.6, δ_n = 24°

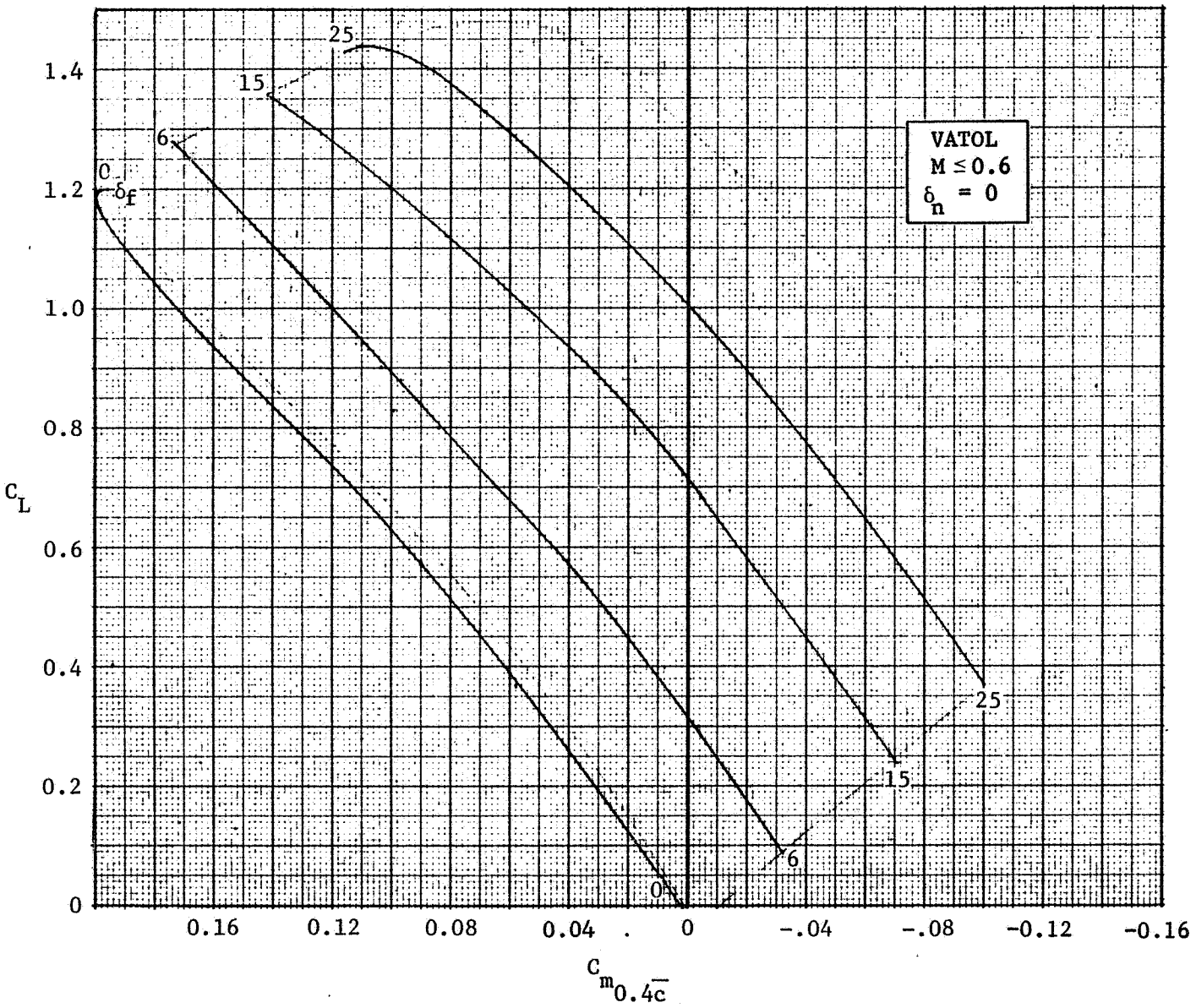

FIGURE 3-11. TRAILING-EDGE FLAP EFFECTIVENESS AT M≤0.6, δ_n=0

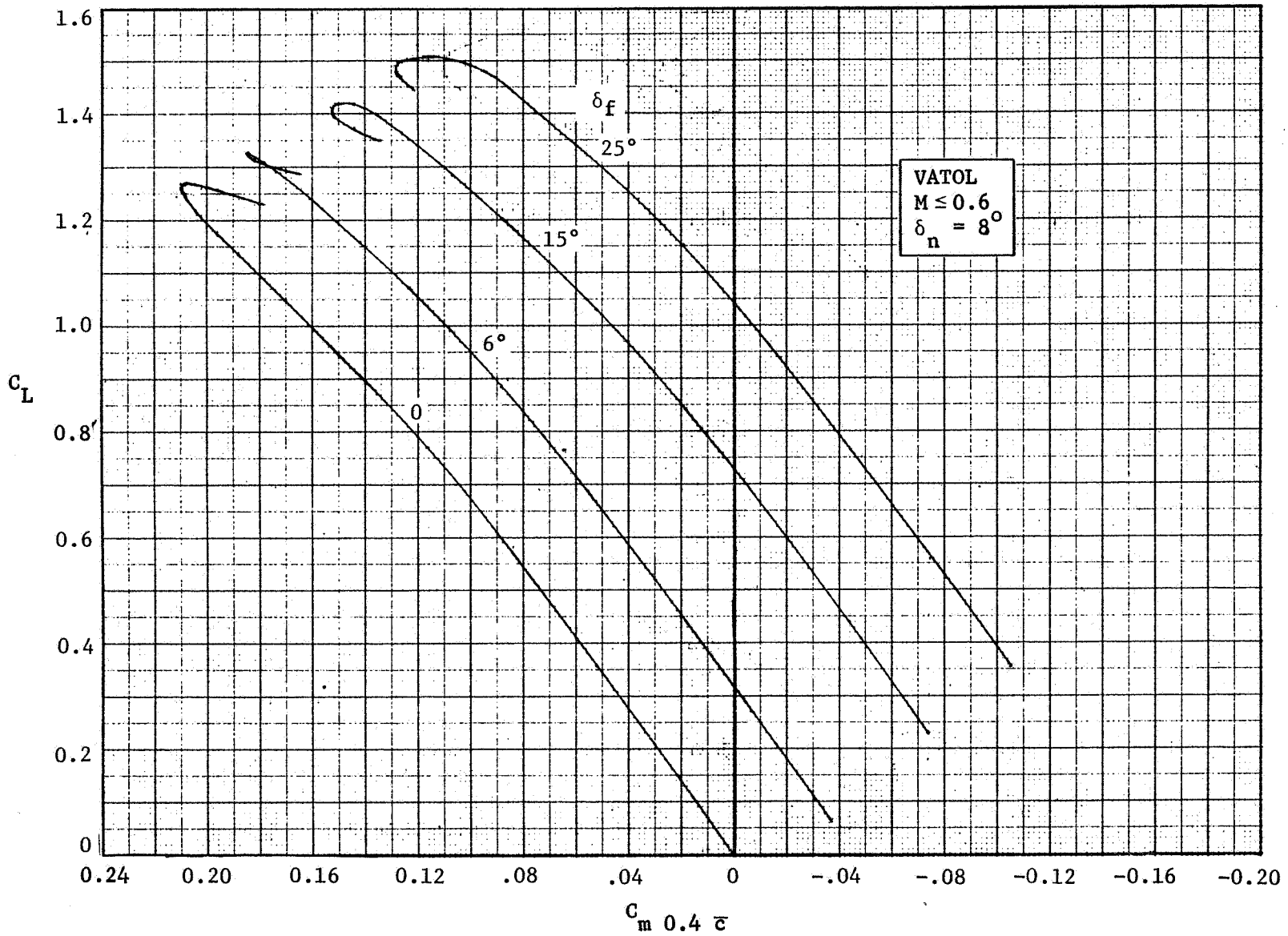

FIGURE 3-12. TRAILING-EDGE FLAP EFFECTIVENESS AT M≤0.6, δ_n=8°

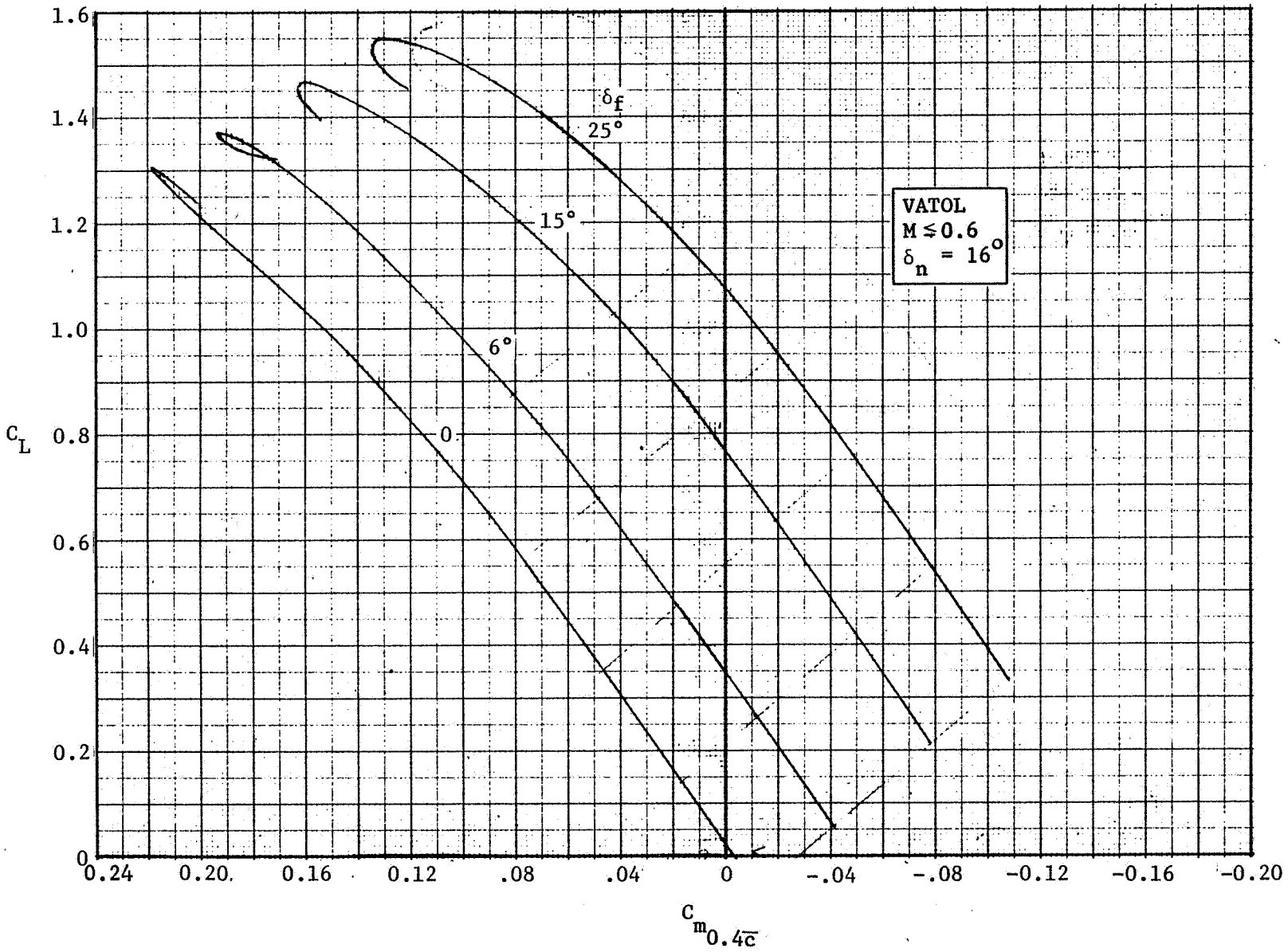

FIGURE 3-13. TRAILING-EDGE FLAP EFFECTIVENESS AT M≤0.6, δ_n=16°

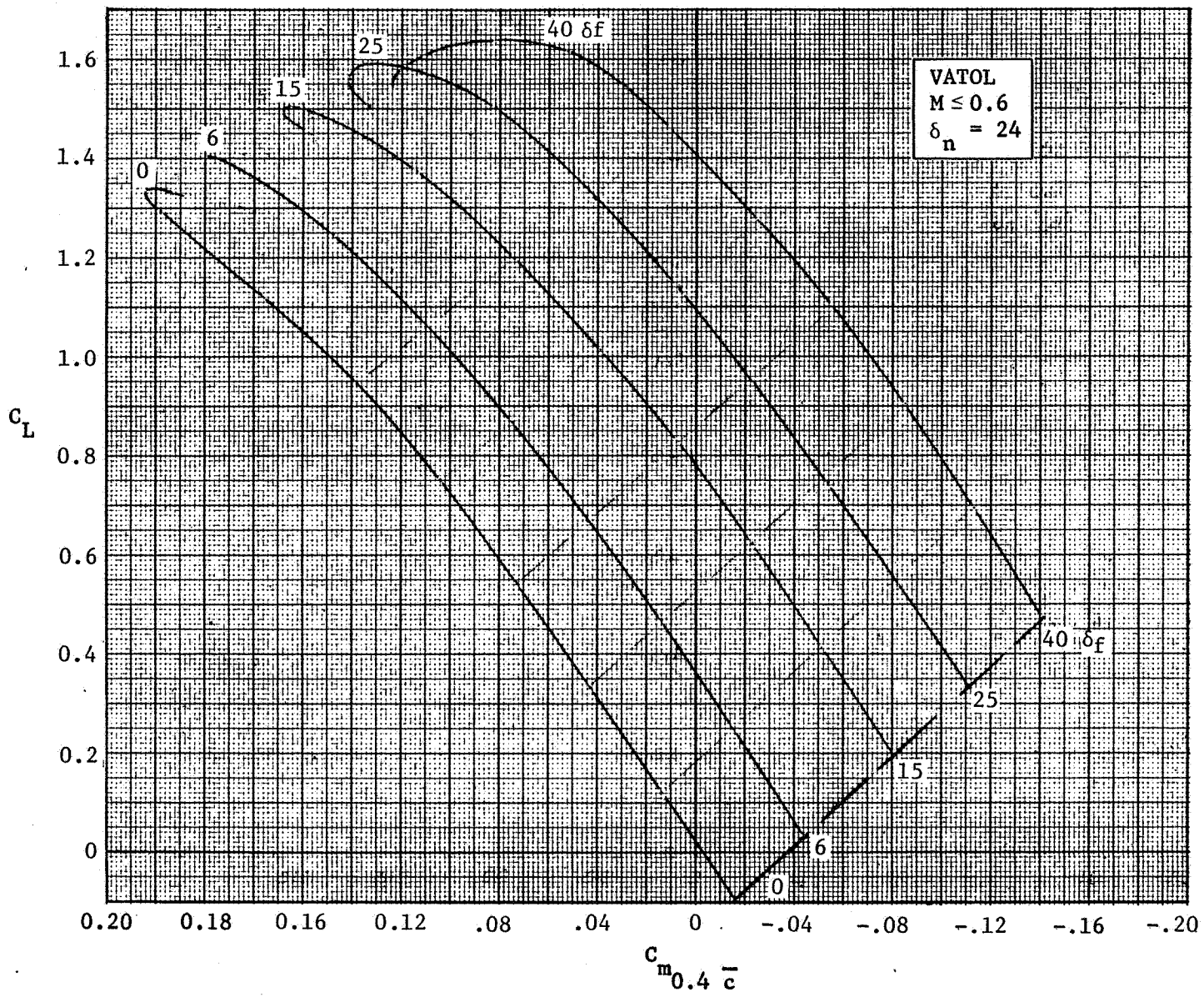

FIGURE 3-14. TRAILING-EDGE FLAP EFFECTIVENESS AT M≤0.6, δ=24°

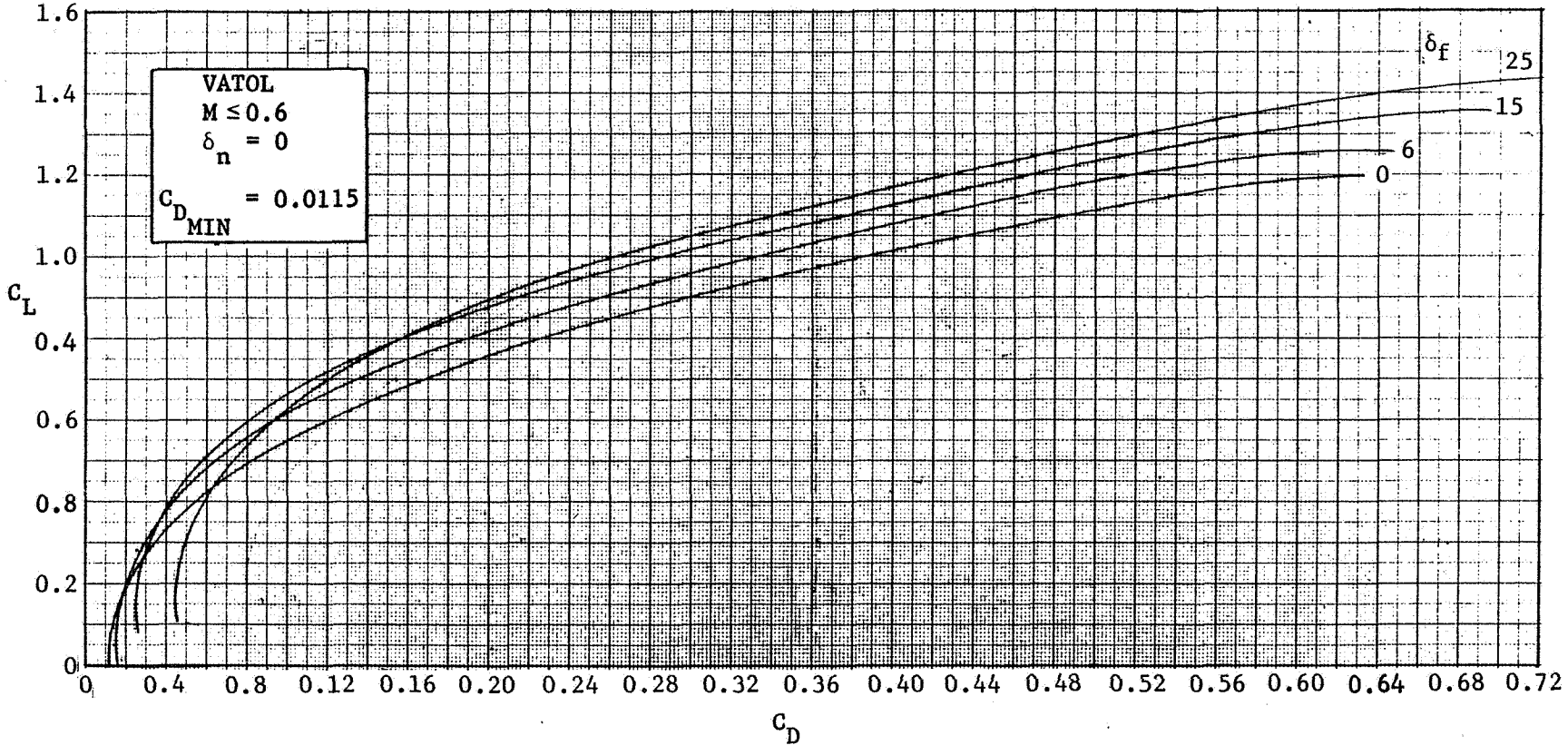

FIGURE 3-15. LIFT-DRAG POLAR AT M≤0.6, δ_n=0

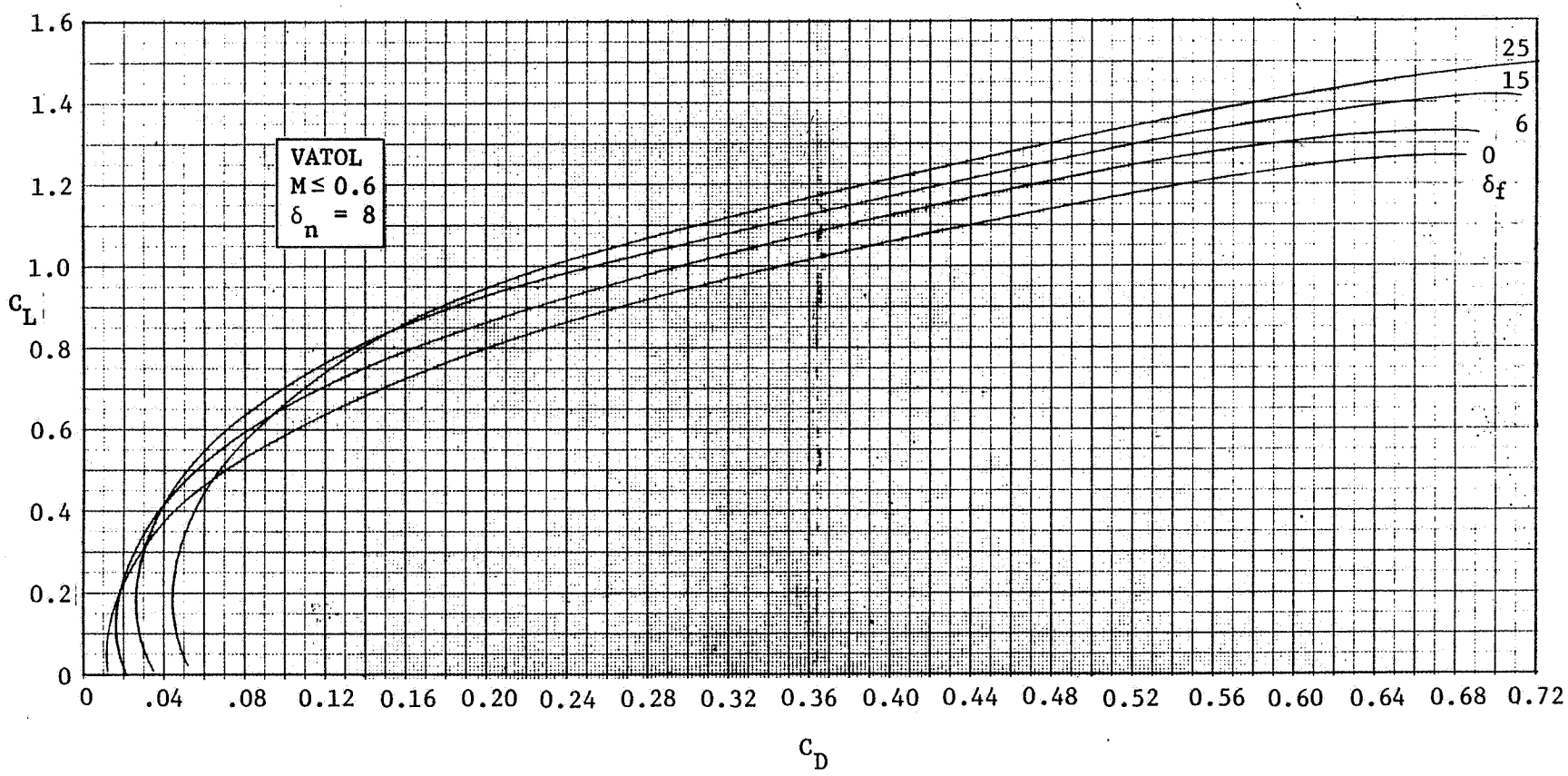

FIGURE 3-16. LIFT-DRAG POLAR AT M≤0.6, δ_n=8°

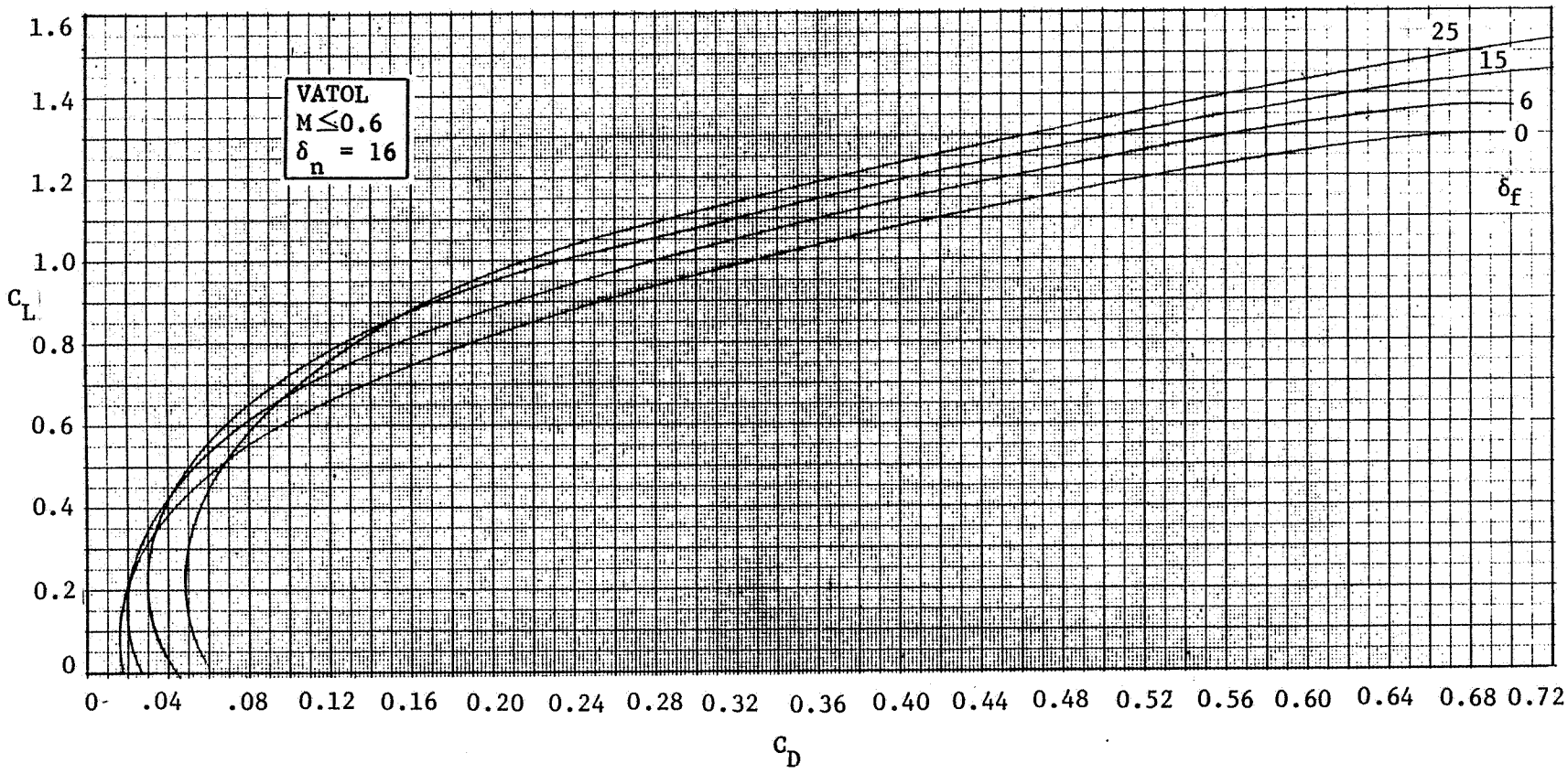

FIGURE 3-17. LIFT-DRAG POLAR AT M≤0.6, δ_n=16°

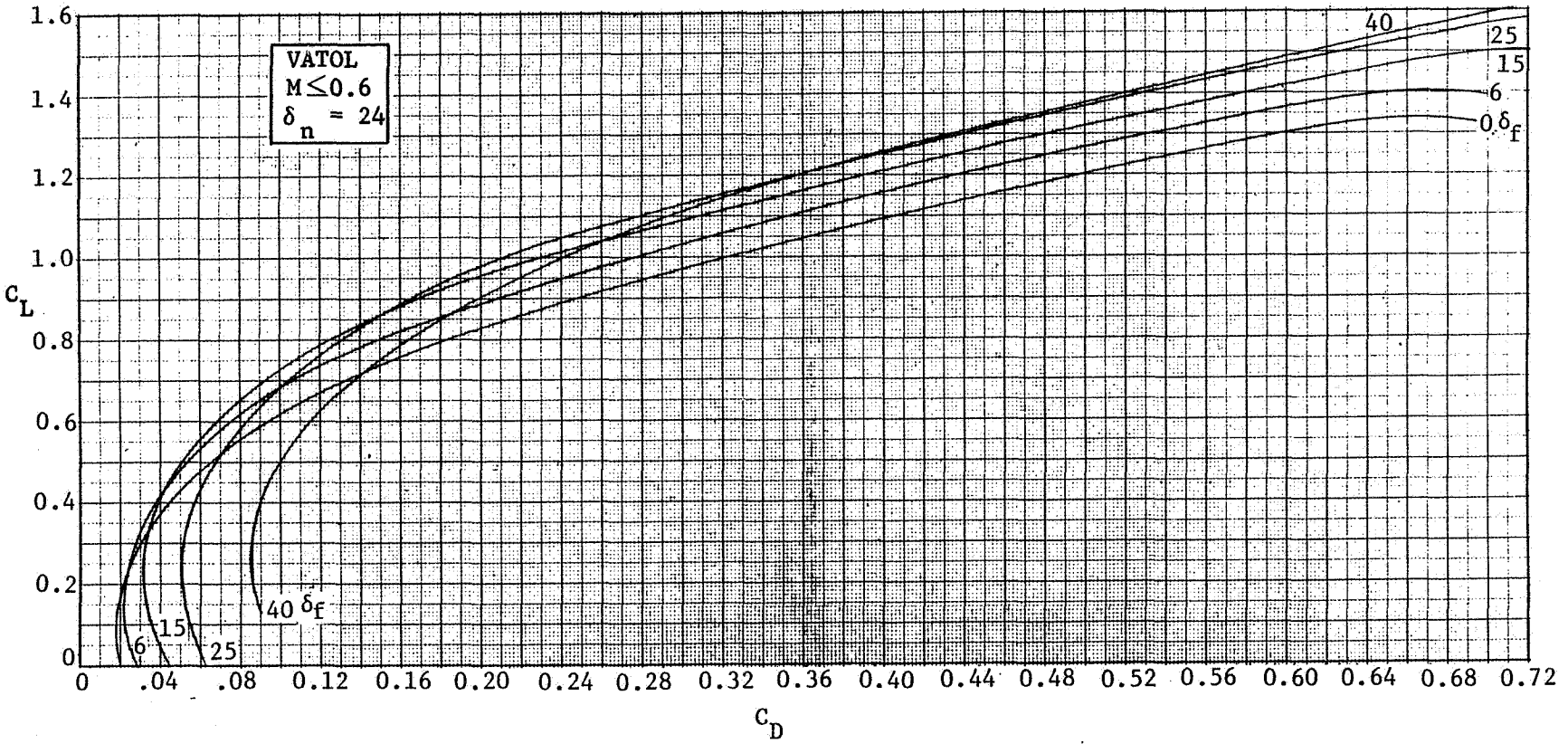

FIGURE 3-18. LIFT-DRAG POLAR AT M≤0.6, δ_n=24°

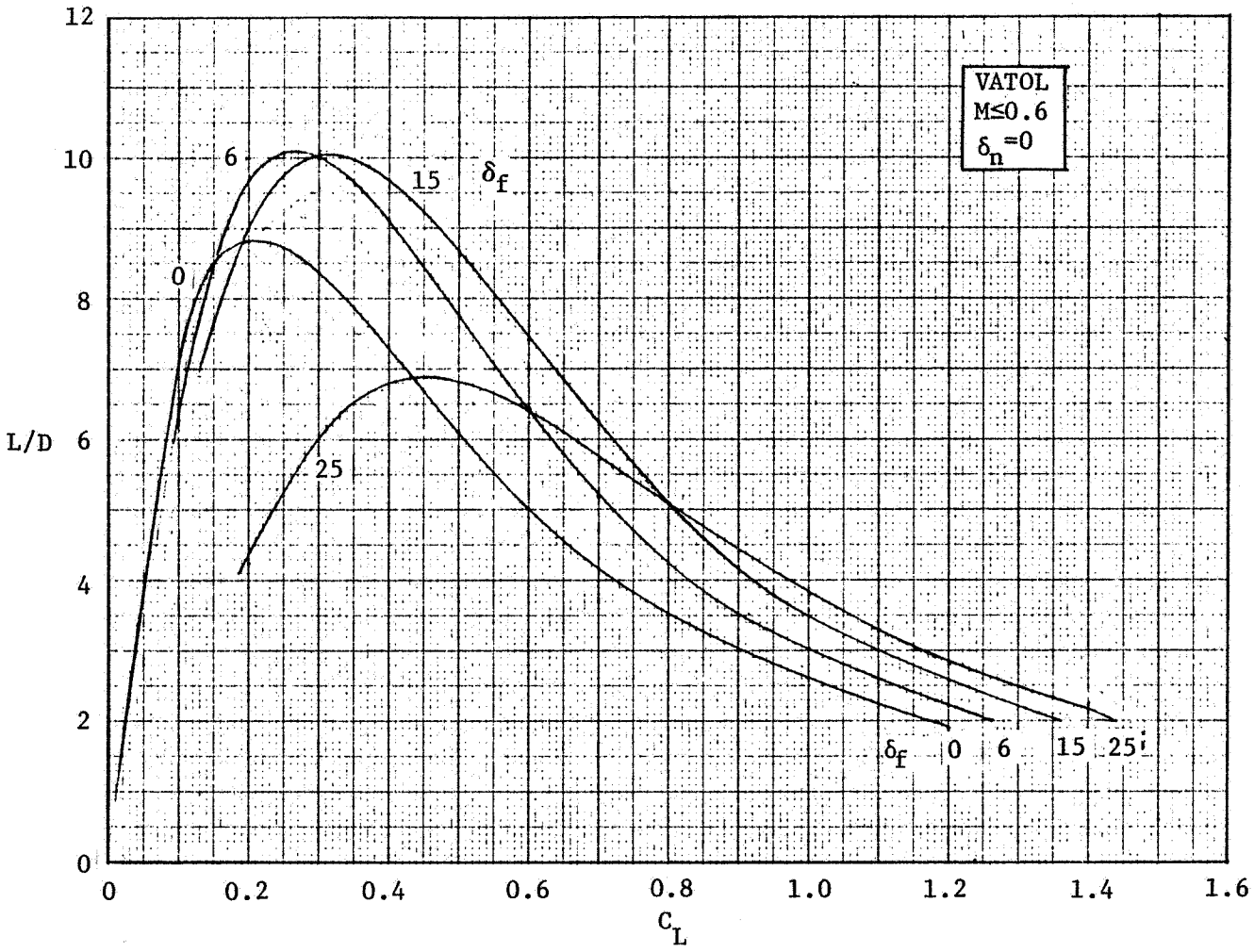

FIGURE 3-19. LIFT-DRAG RATIO AT M≤0.6, δ_n=0

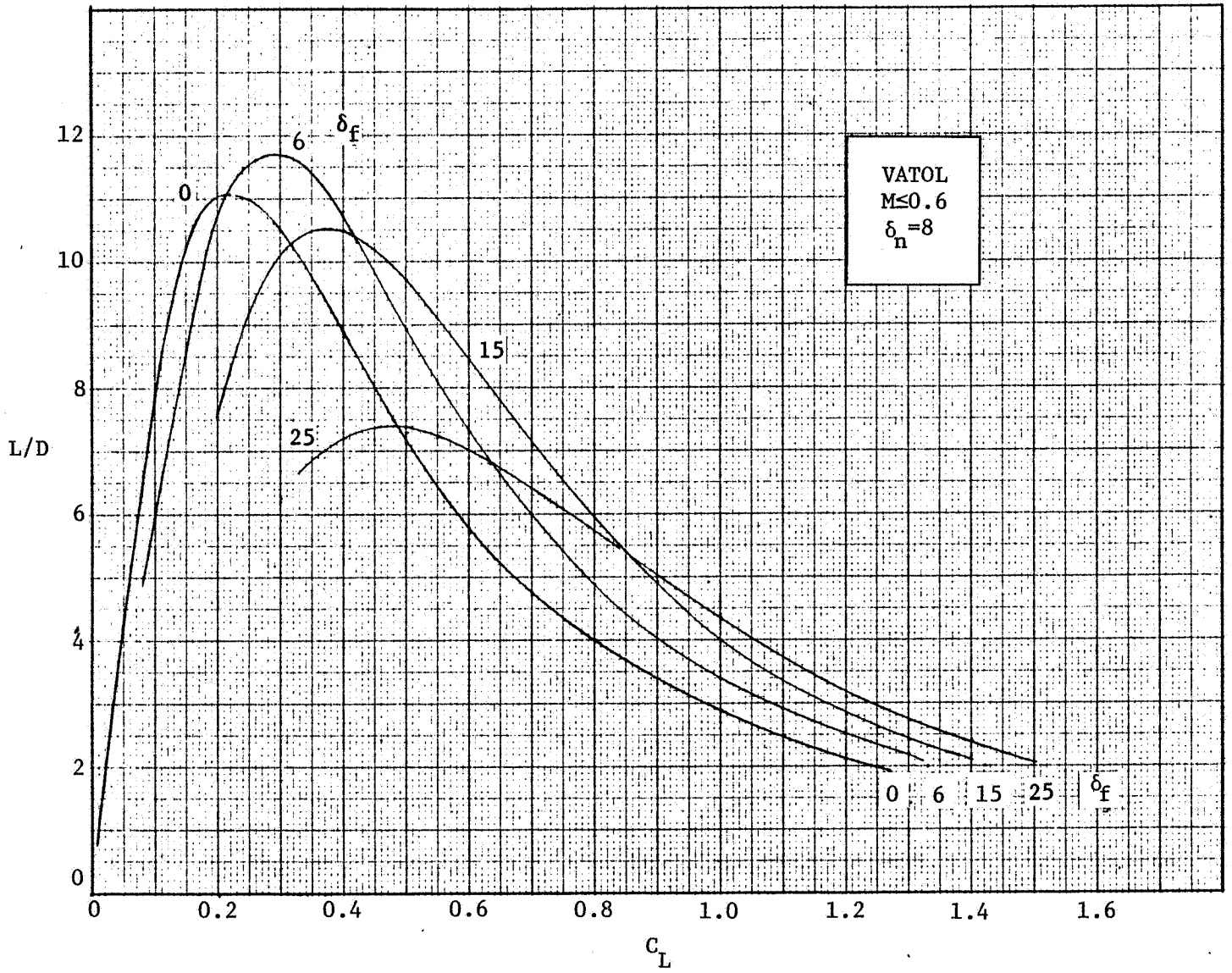

FIGURE 3-20. LIFT-DRAG RATIO AT M≤0.6, δ_n=8°

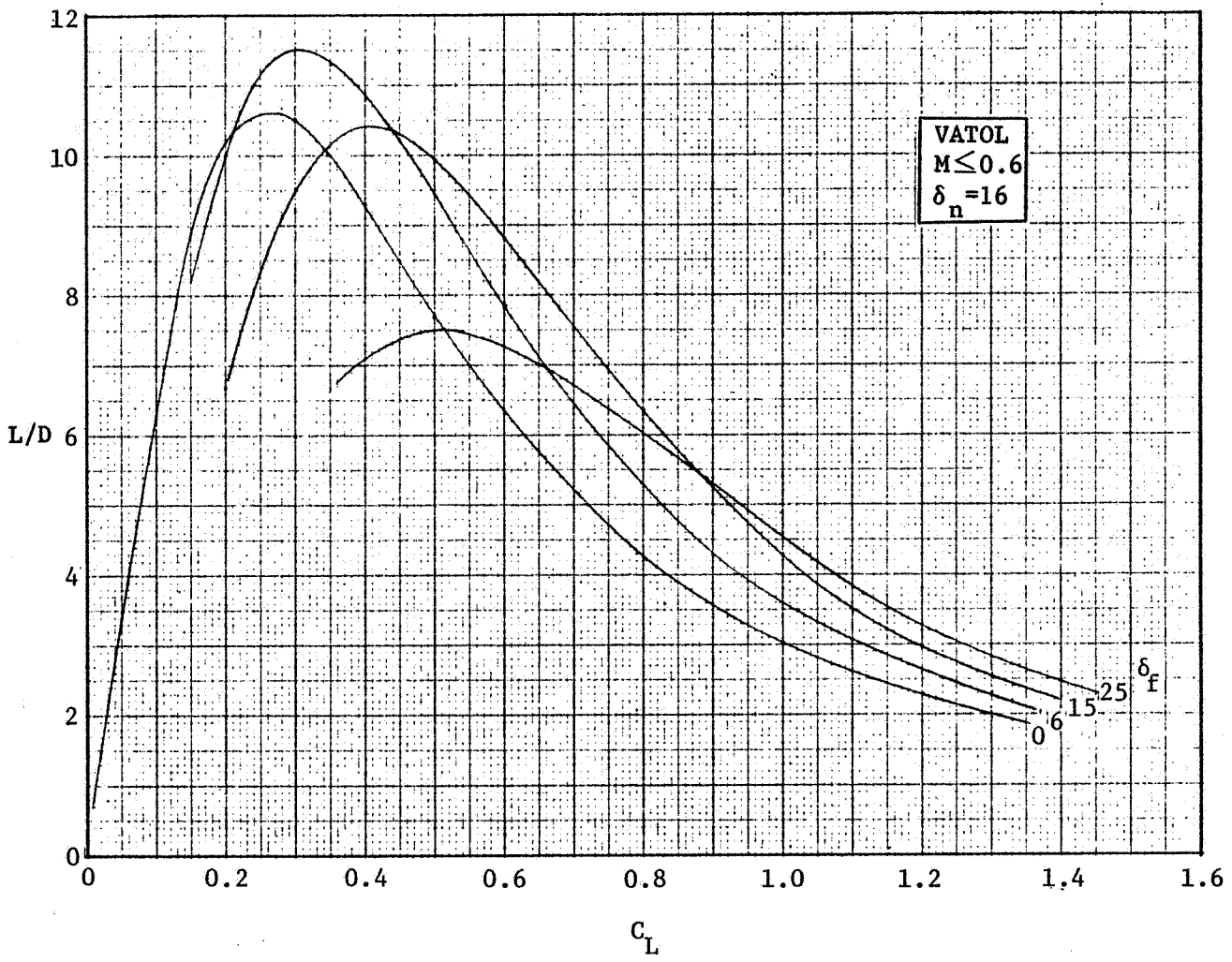

FIGURE 3-21. LIFT-DRAG RATIO AT M≤0.6, δ_n=16°

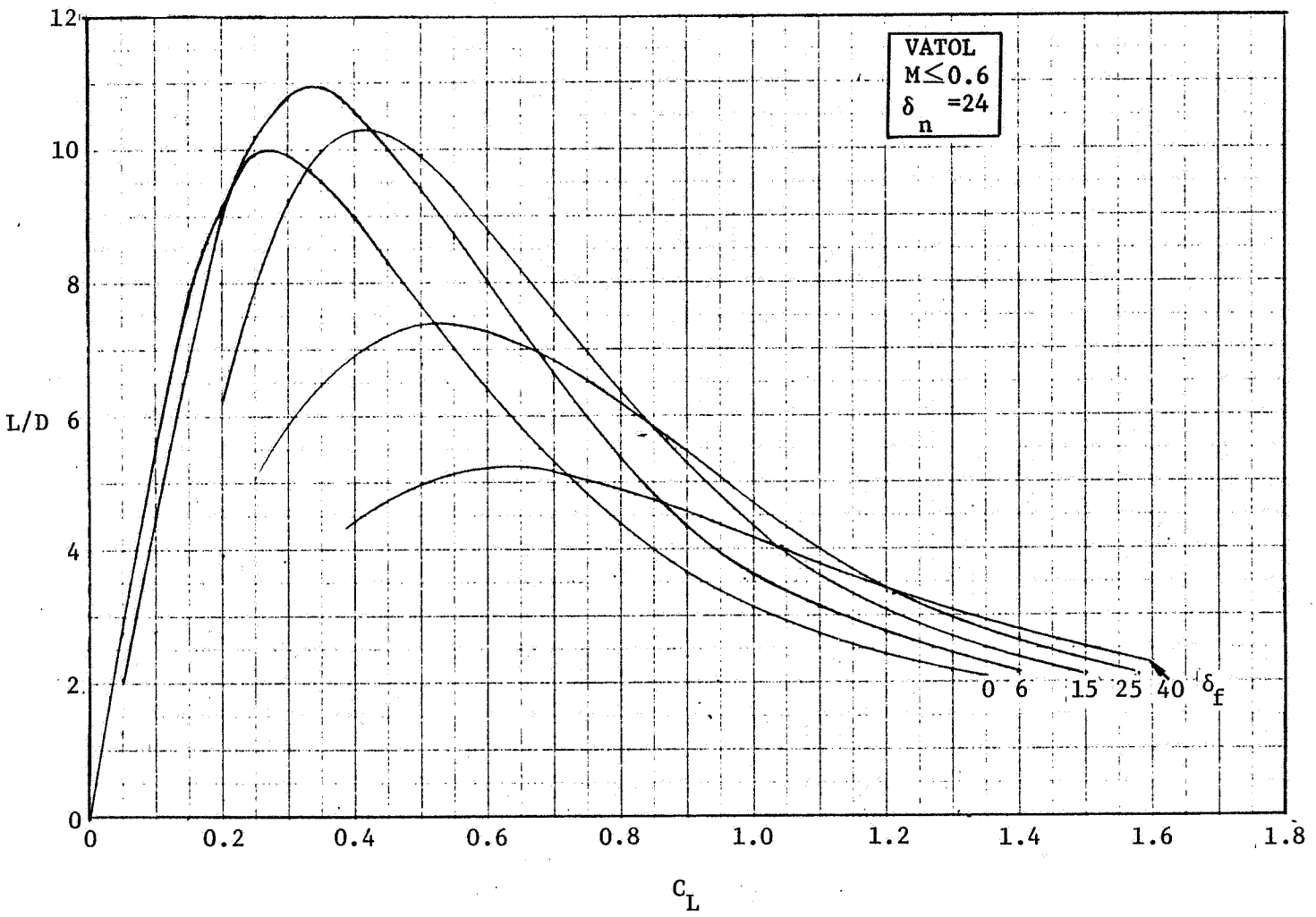

FIGURE 3-22. LIFT-DRAG RATIO AT M≤0.6, δ_n=24

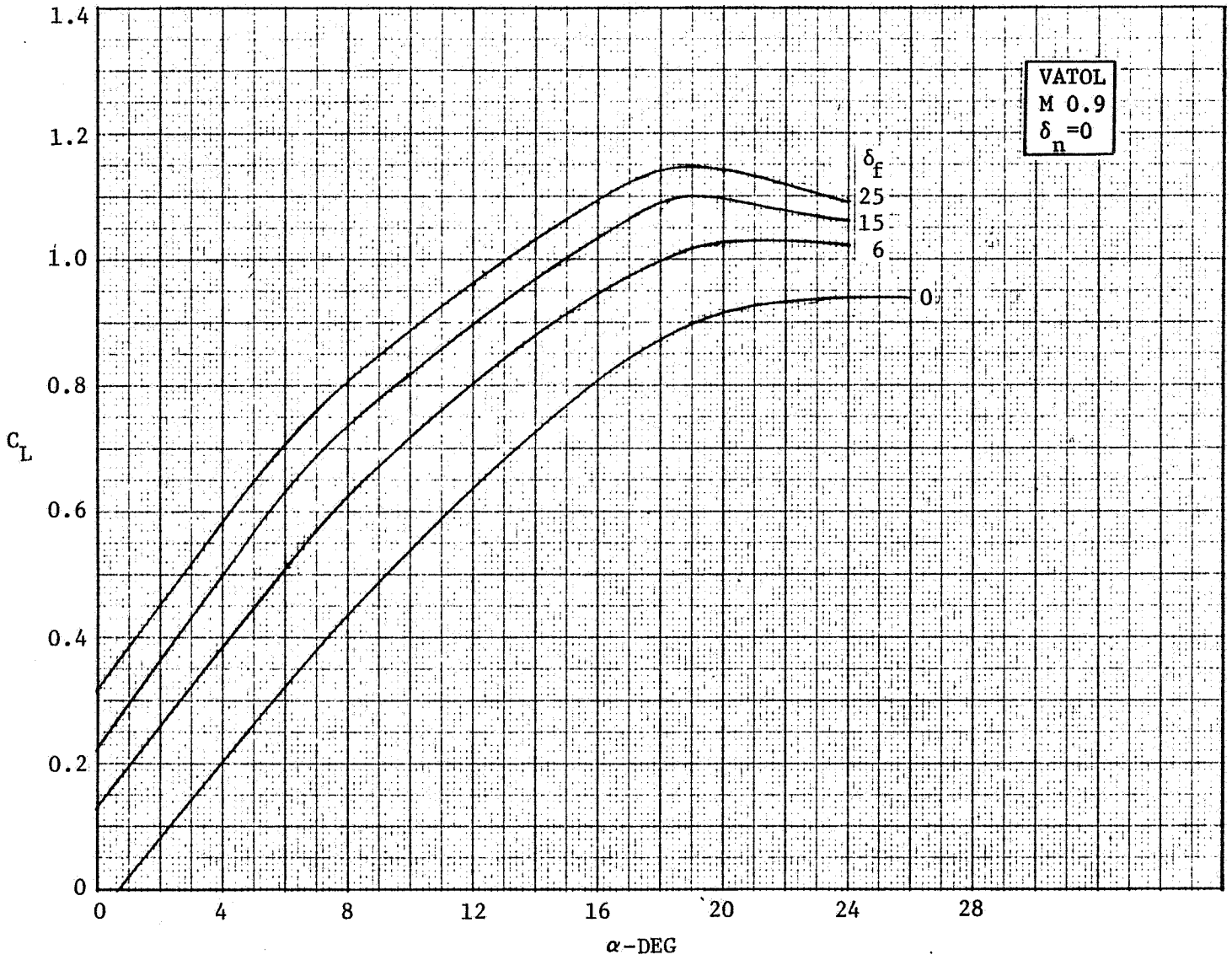

FIGURE 3-23. LIFT VS ANGLE OF ATTACK AT M 0.9, δ_n=0

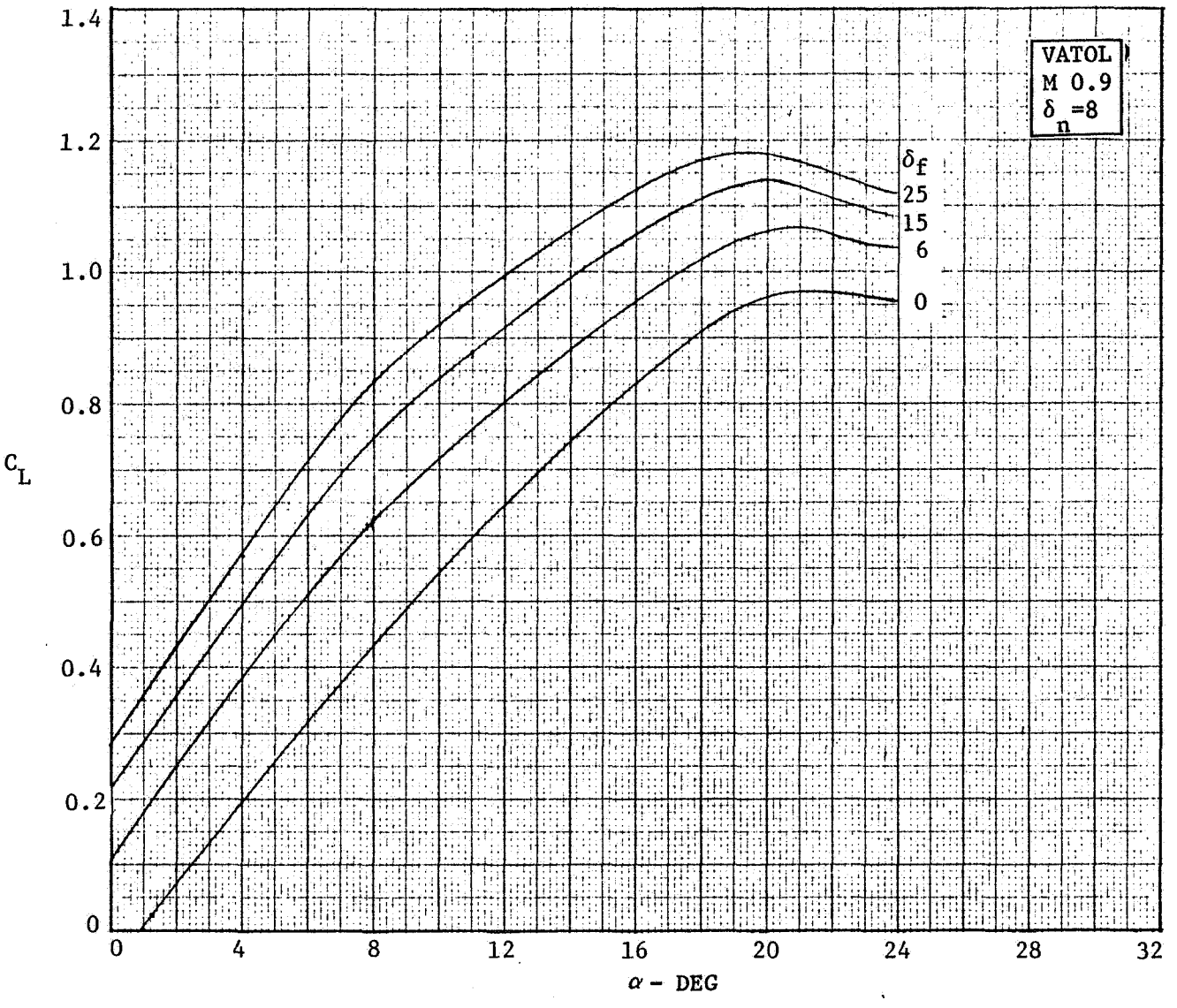

FIGURE 3-24. LIFT VS ANGLE OF ATTACK AT M 0.9, δ_n=8°

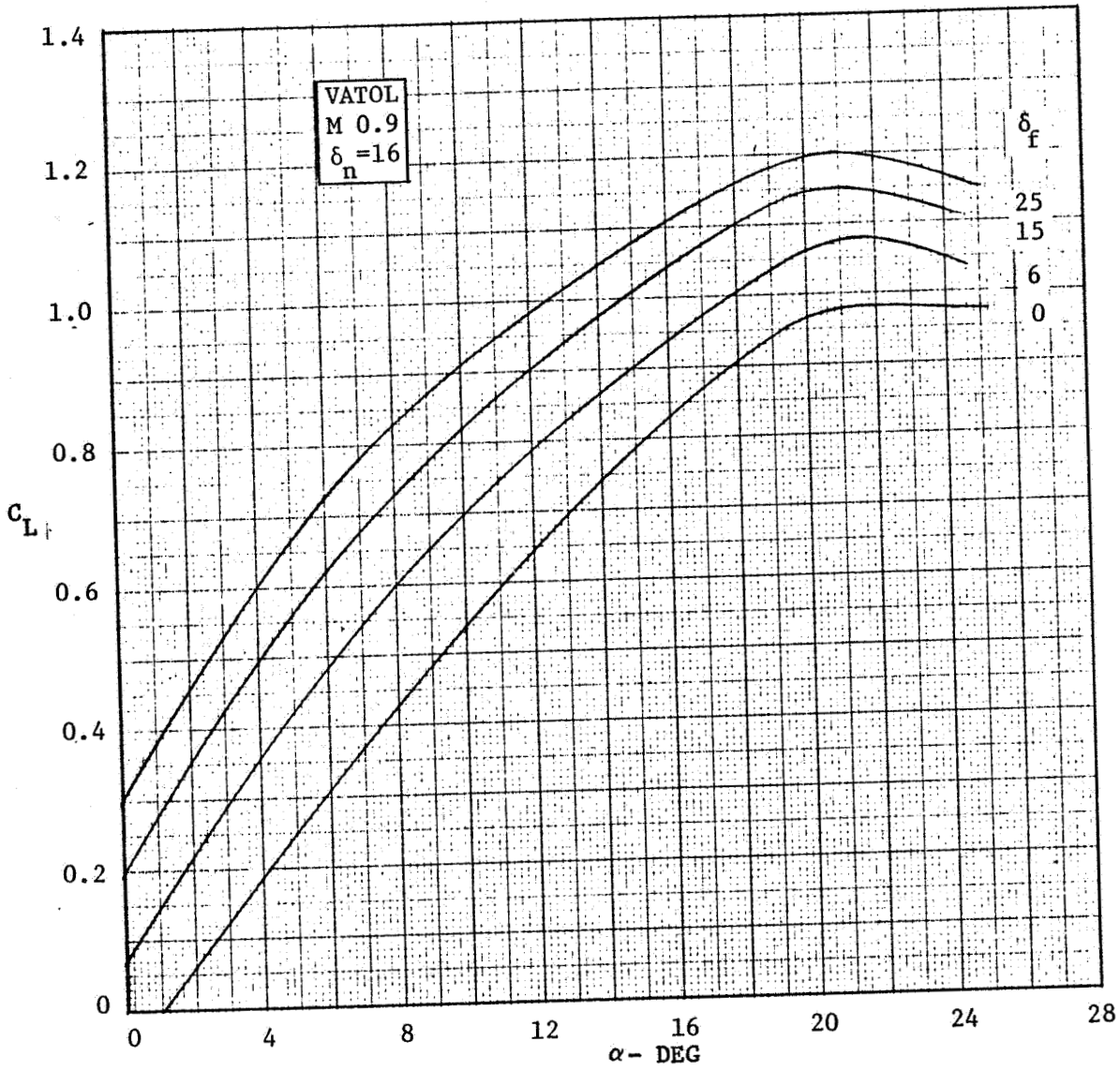

FIGURE 3-25. LIFT VS ANGLE OF ATTACK AT M 0.9 δ_n=16°

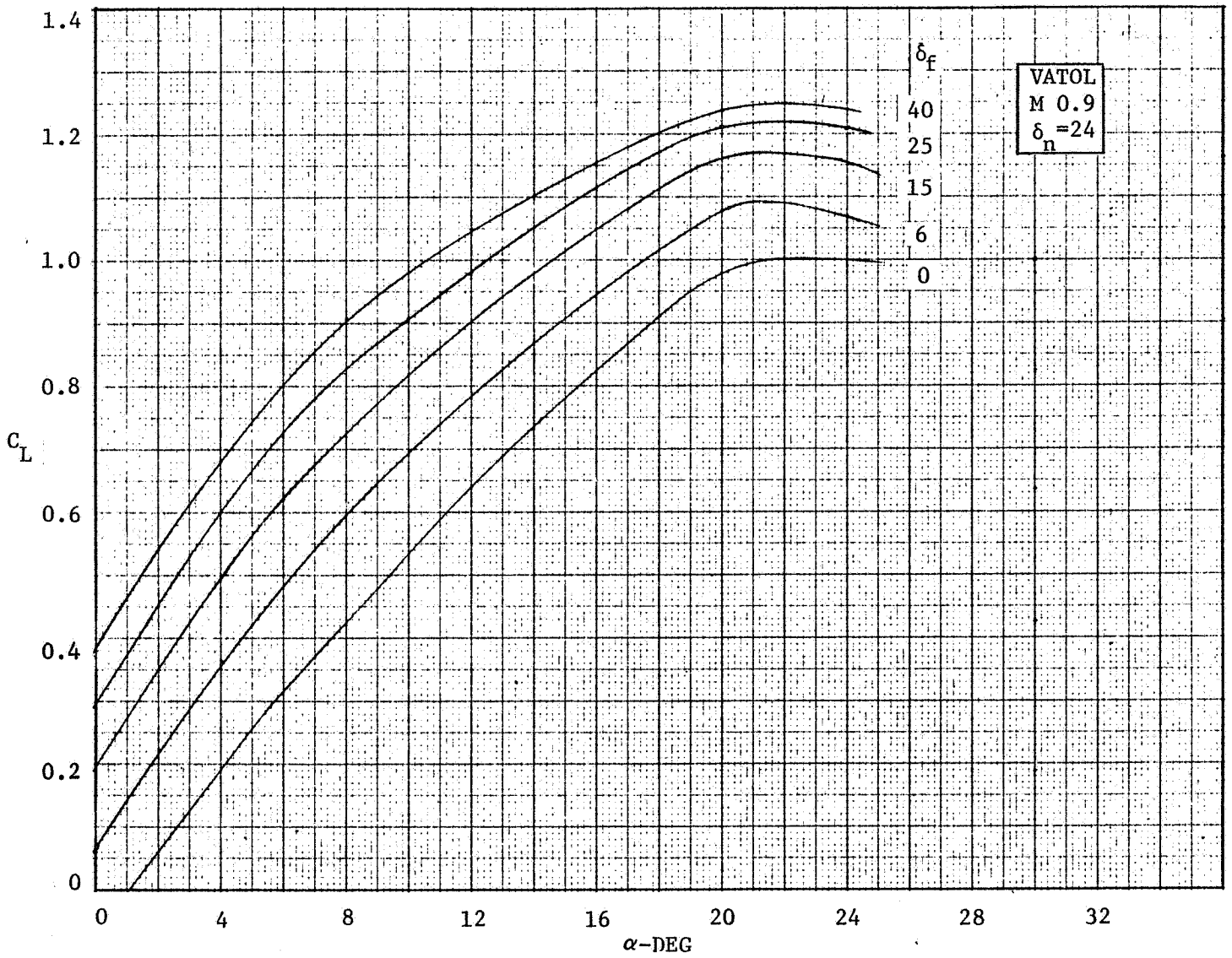

FIGURE 3-26. LIFT VS ANGLE OF ATTACK AT M 0.9, δ_n=24°

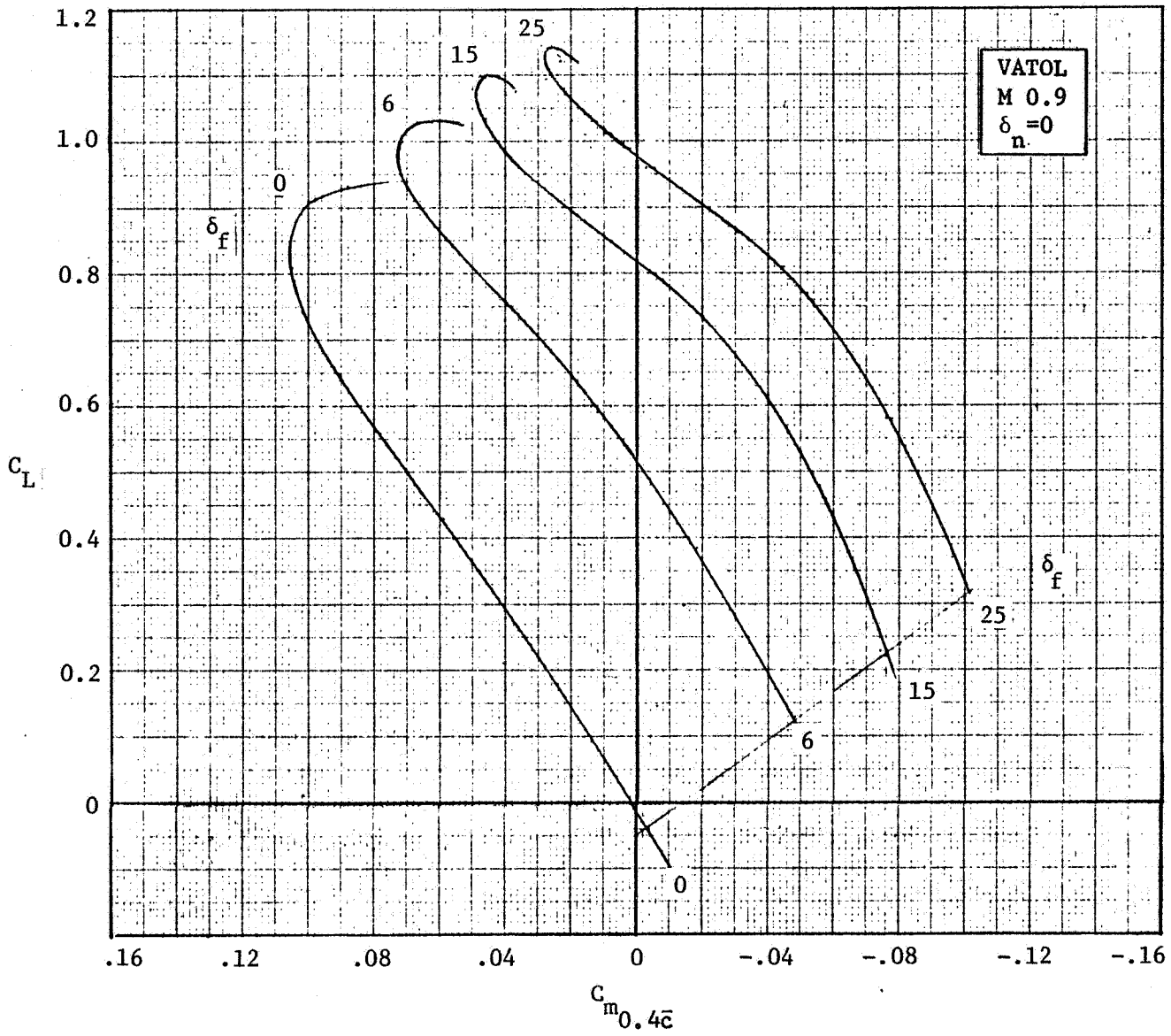

FIGURE 3-27. TRAILING-EDGE FLAP EFFECTIVENESS AT M 0.9, δ_n=0

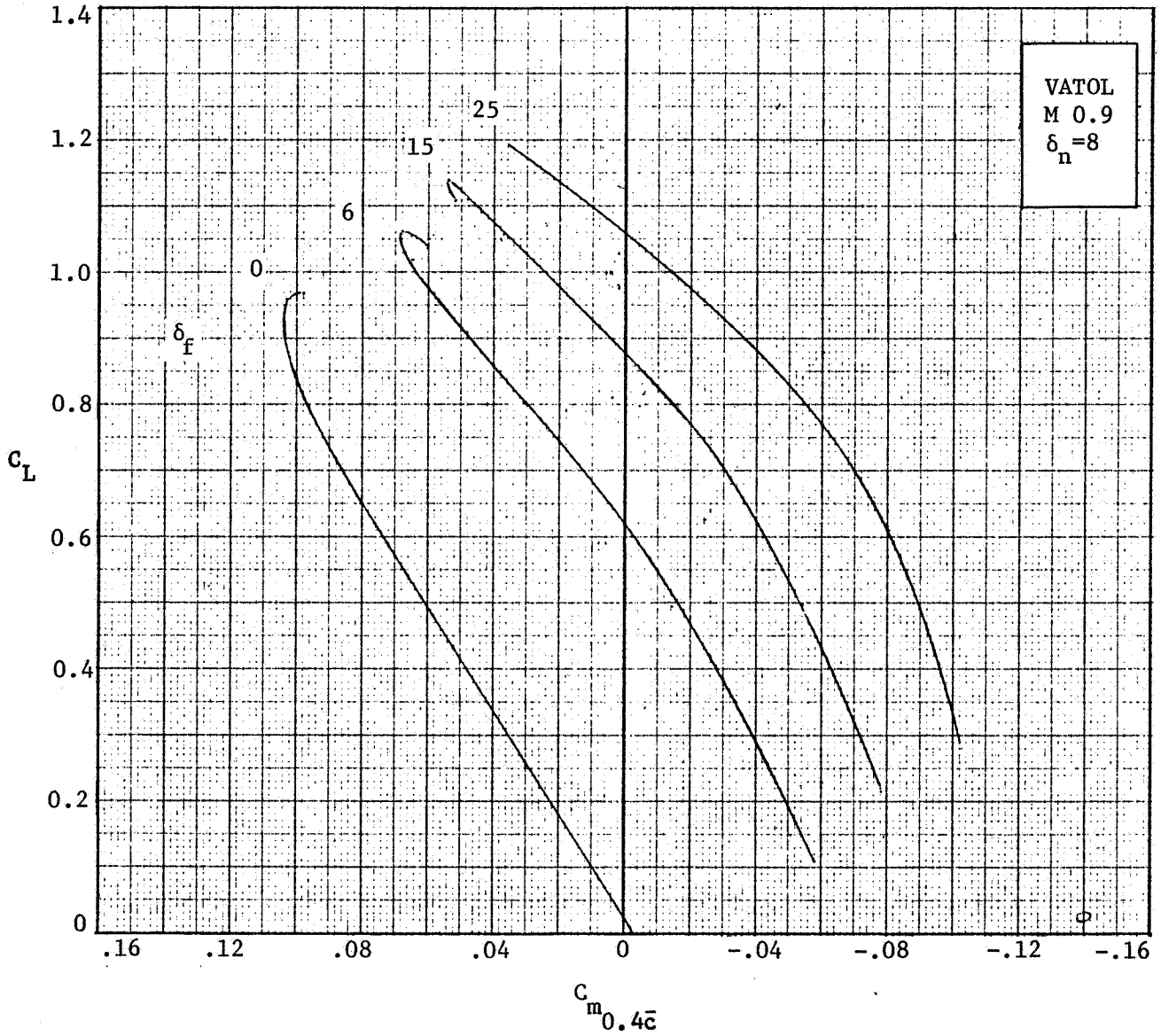

FIGURE 3-28. TRAILING EDGE FLAP EFFECTIVENESS AT M 0.9, δ_n=8°

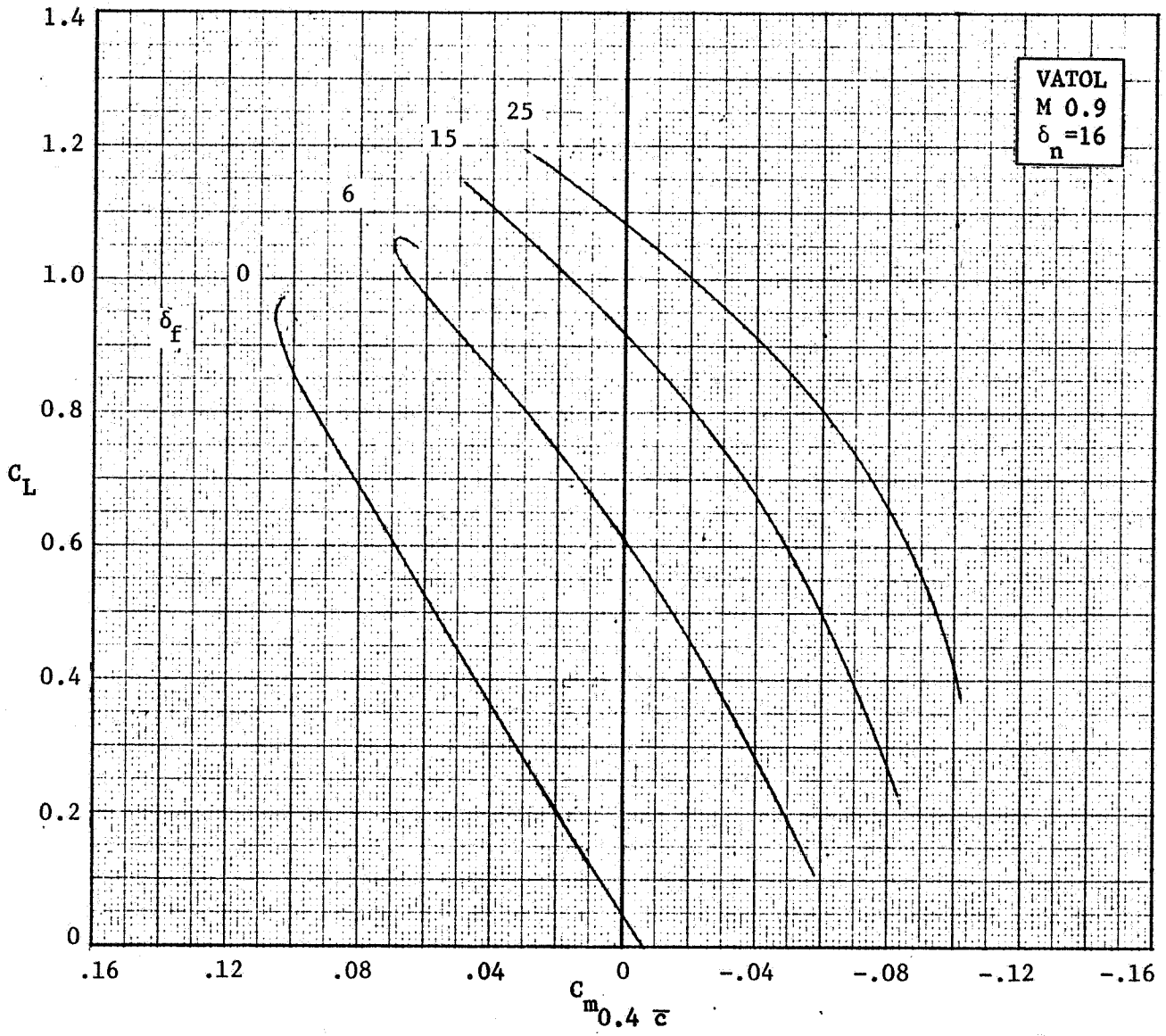

FIGURE 3-29. TRAILING-EDGE FLAP EFFECTIVENESS AT M 0.9, δ_n=16°

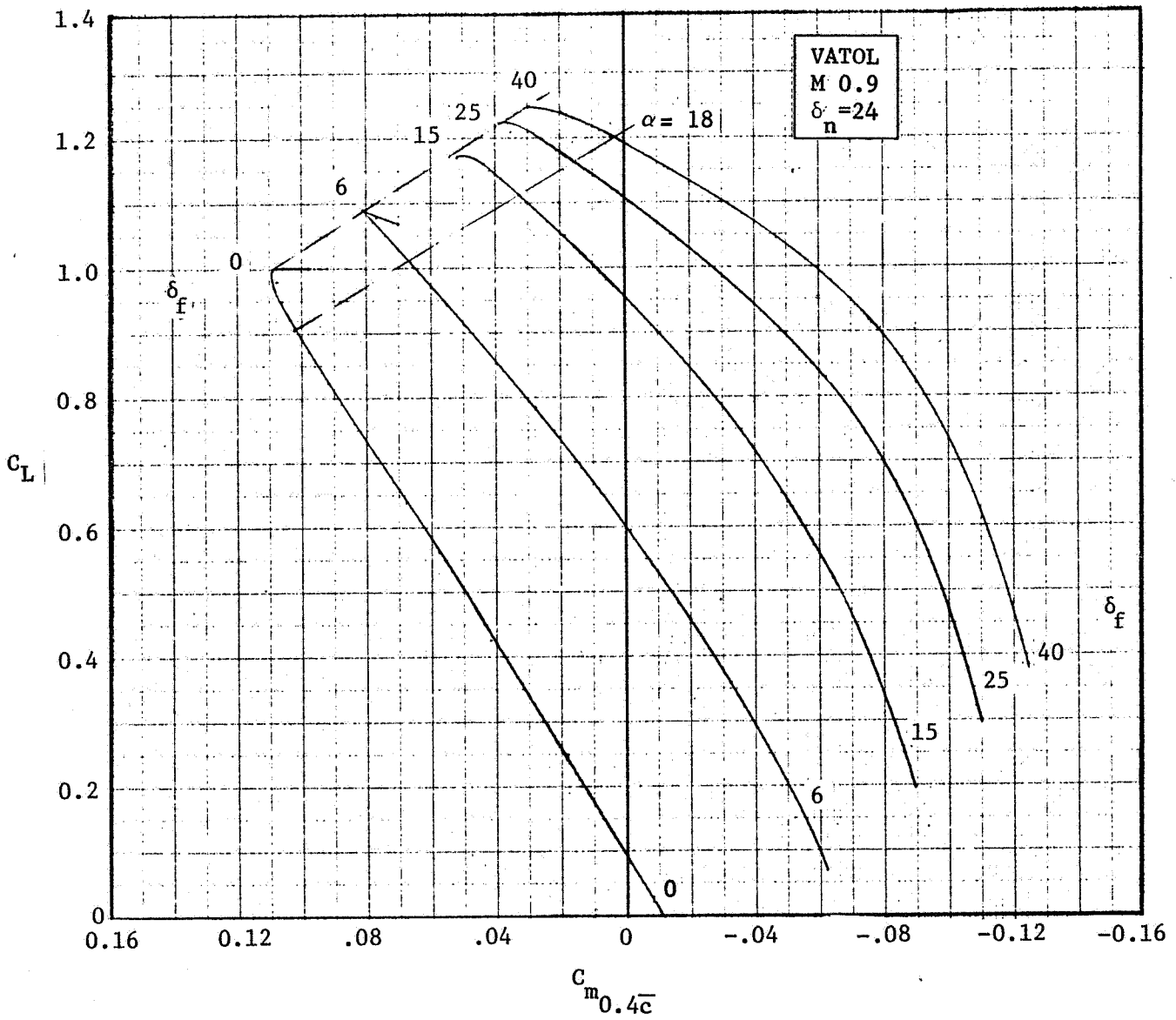

FIGURE 3-30. TRAILING-EDGE FLAP EFFECTIVENESS AT M 0.9, δ_n=24°

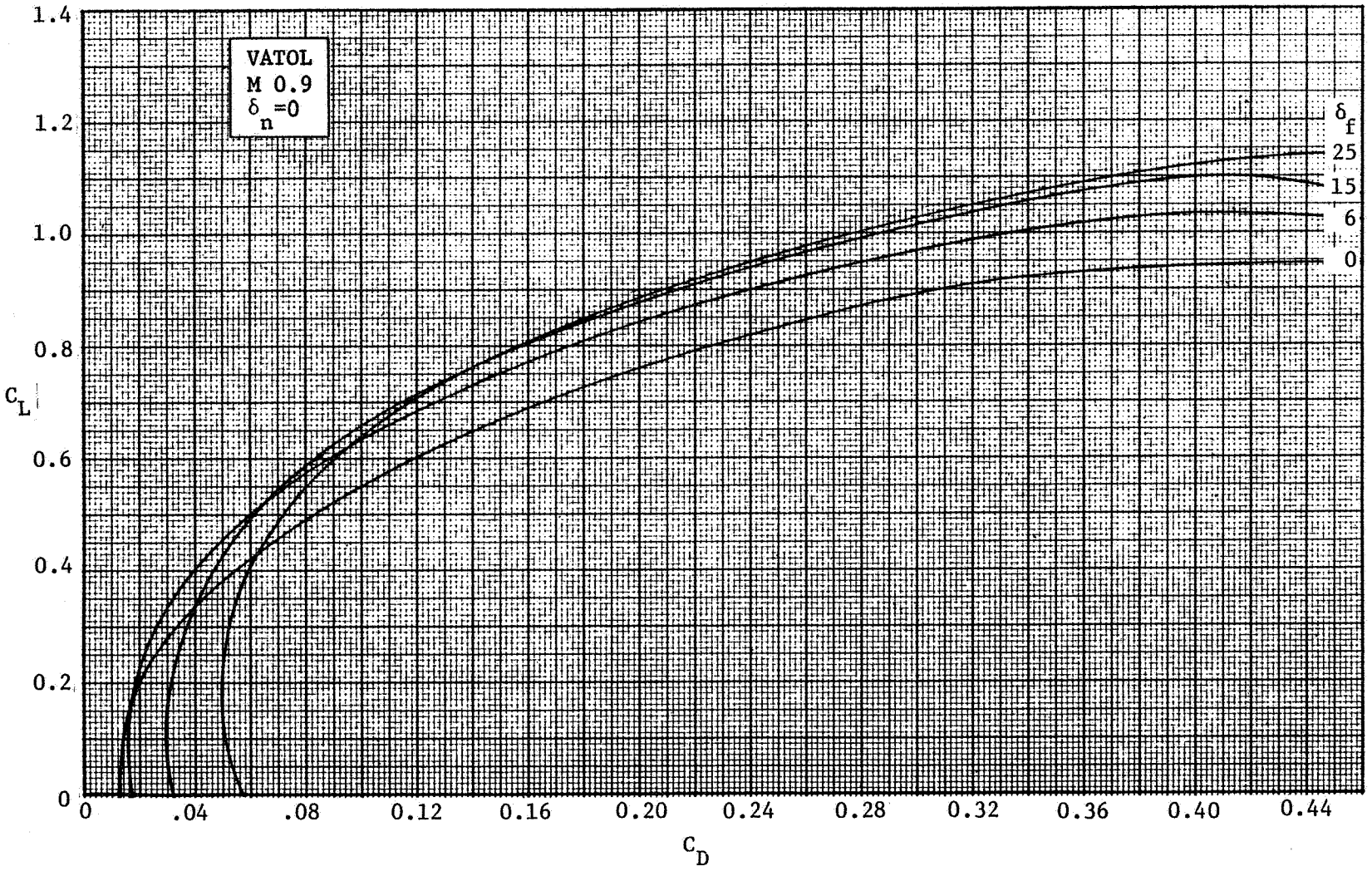

FIGURE 3-31. LIFT-DRAG POLAR AT M 0.9, δ_n=0

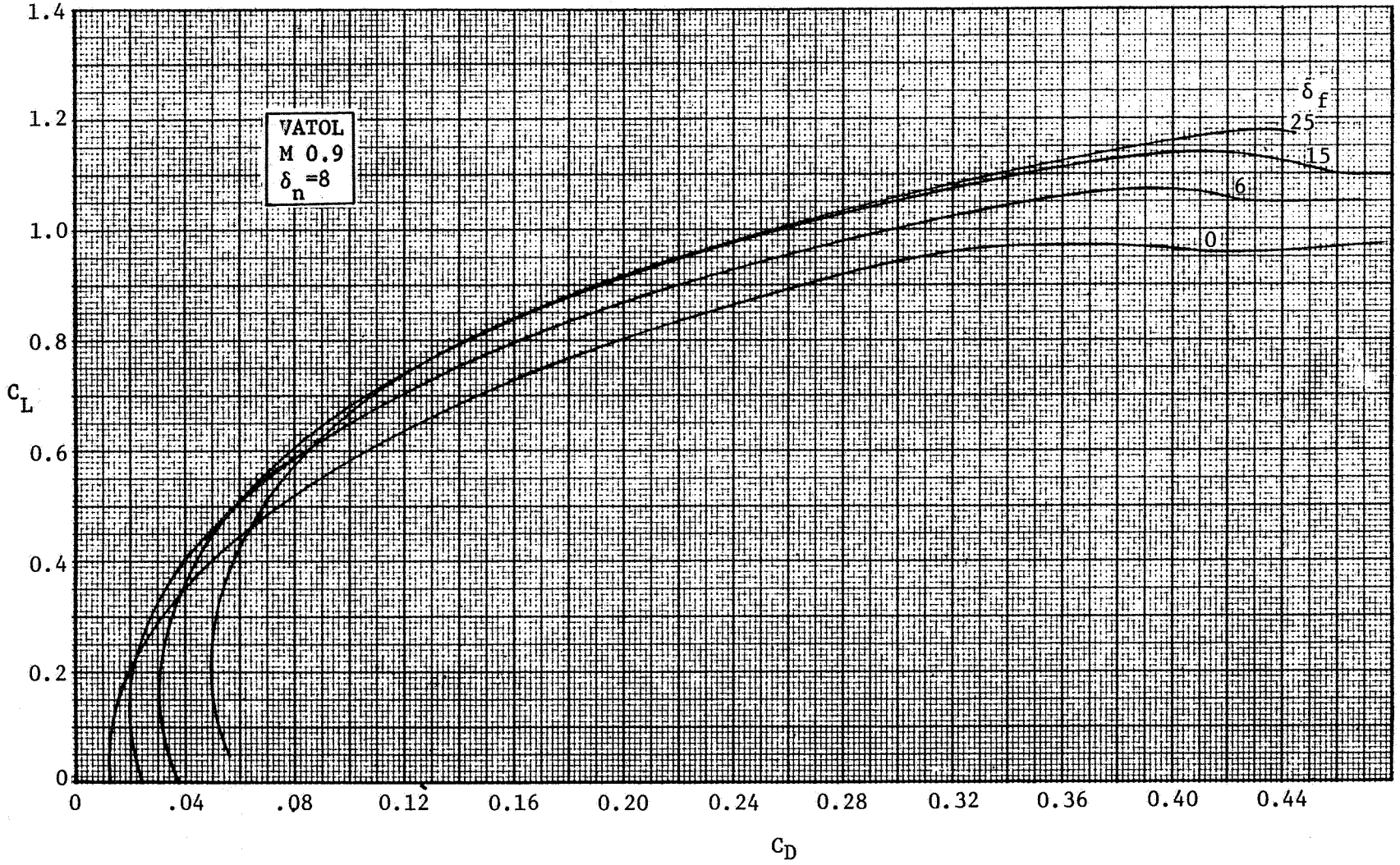

FIGURE 3-32. LIFT-DRAG POLAR AT M0.9, δ_n = 8°

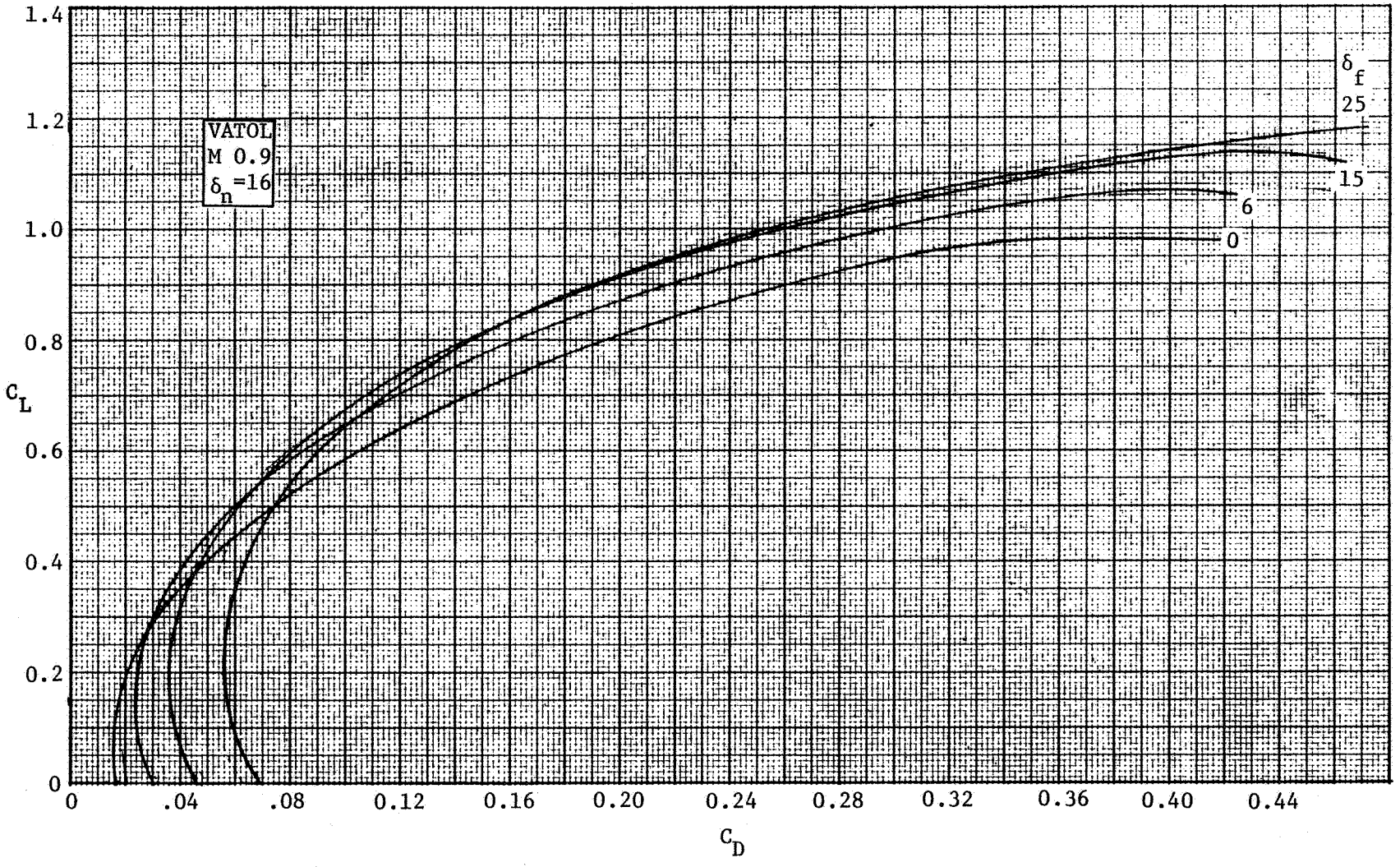

FIGURE 3-33. LIFT-DRAG POLAR AT M 0.9, δ_n=16°

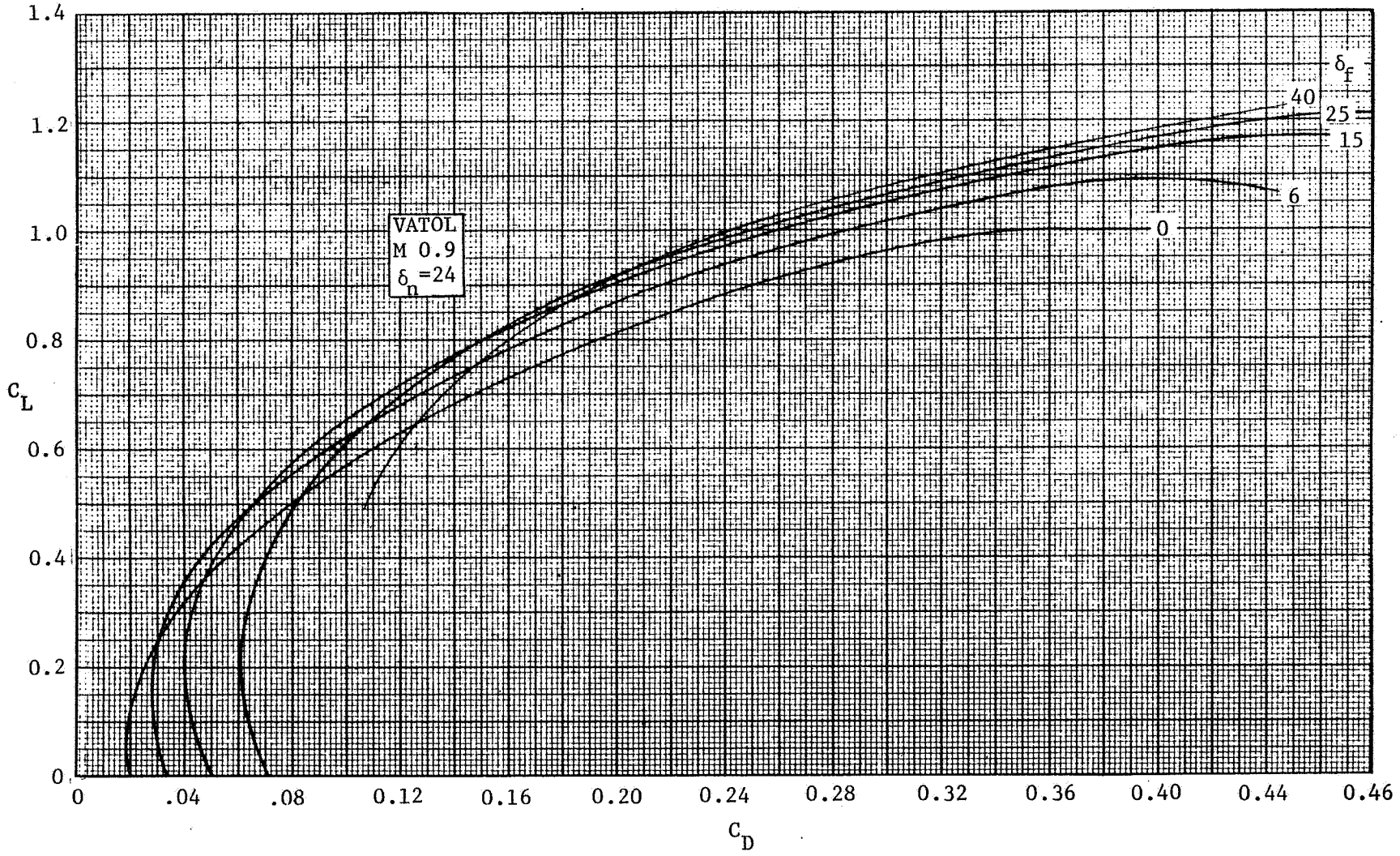

FIGURE 3-34. LIFT-DRAG POLAR AT M 0.9, δ_n=24°

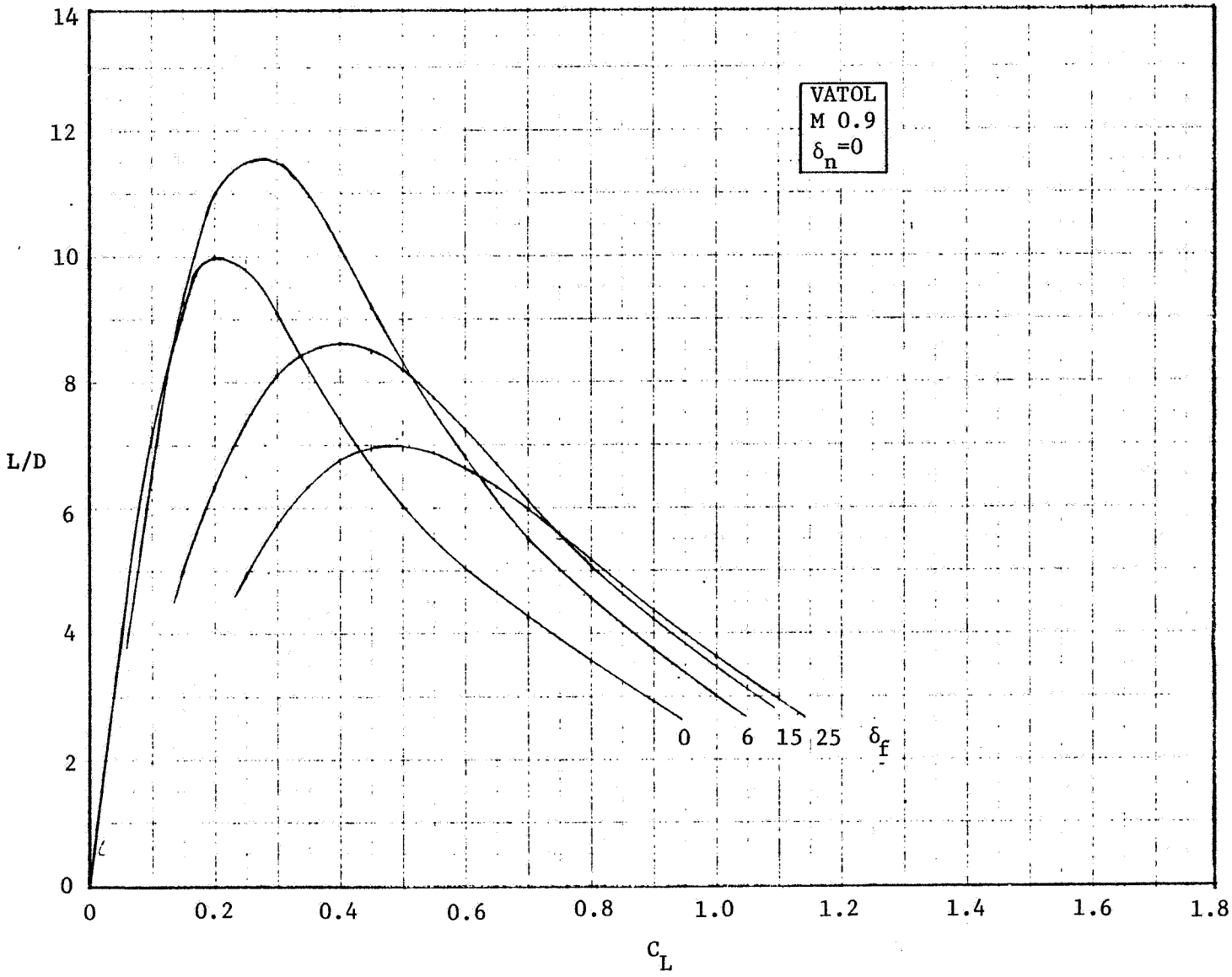

FIGURE 3-35. LIFT-DRAG RATIO AT M 0.9, δ_n=0

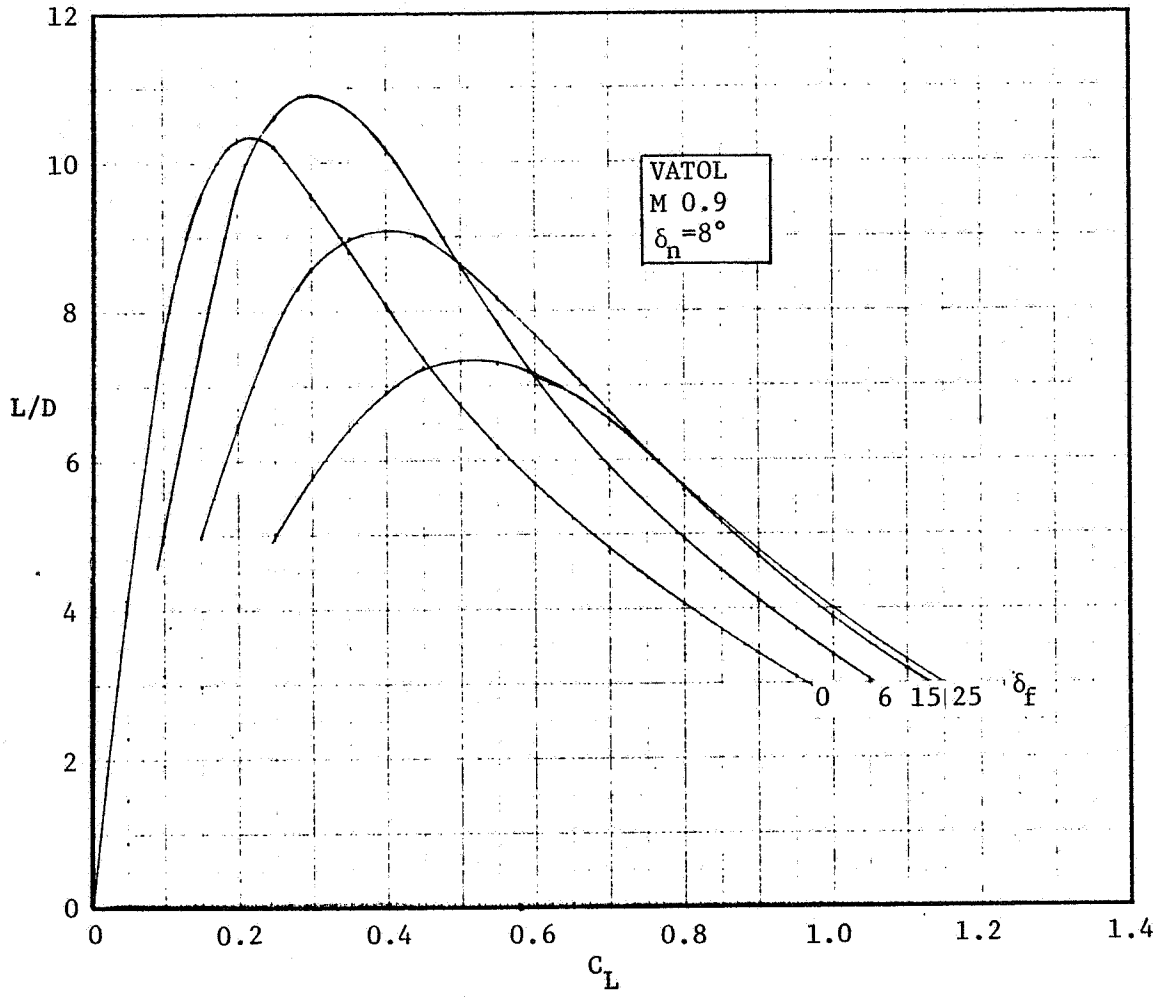

FIGURE 3-36. LIFT-DRAG RATIO AT M 0.9, δ_n=8°

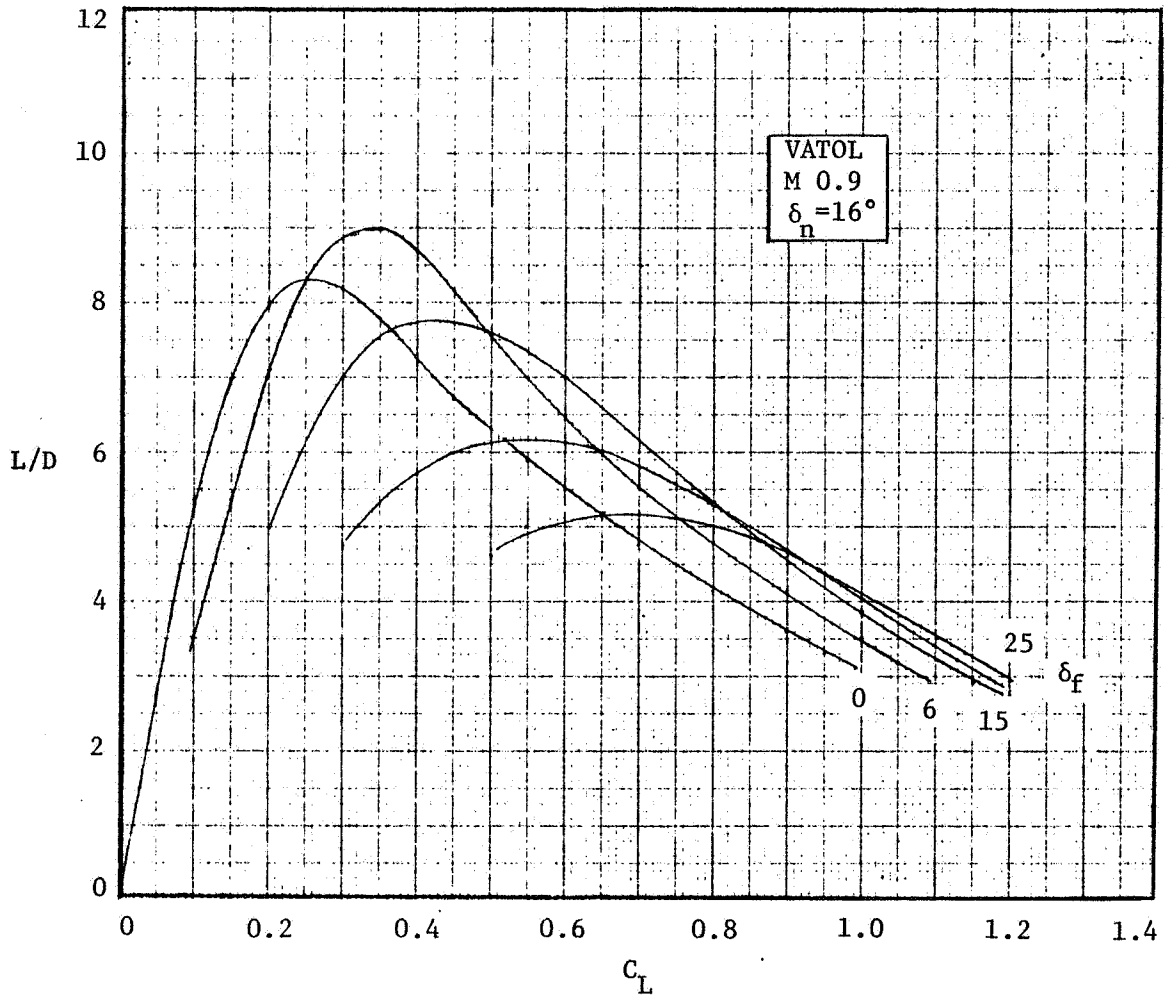

FIGURE 3-37. LIFT-DRAG RATIO AT M 0.9, δ_n=16°

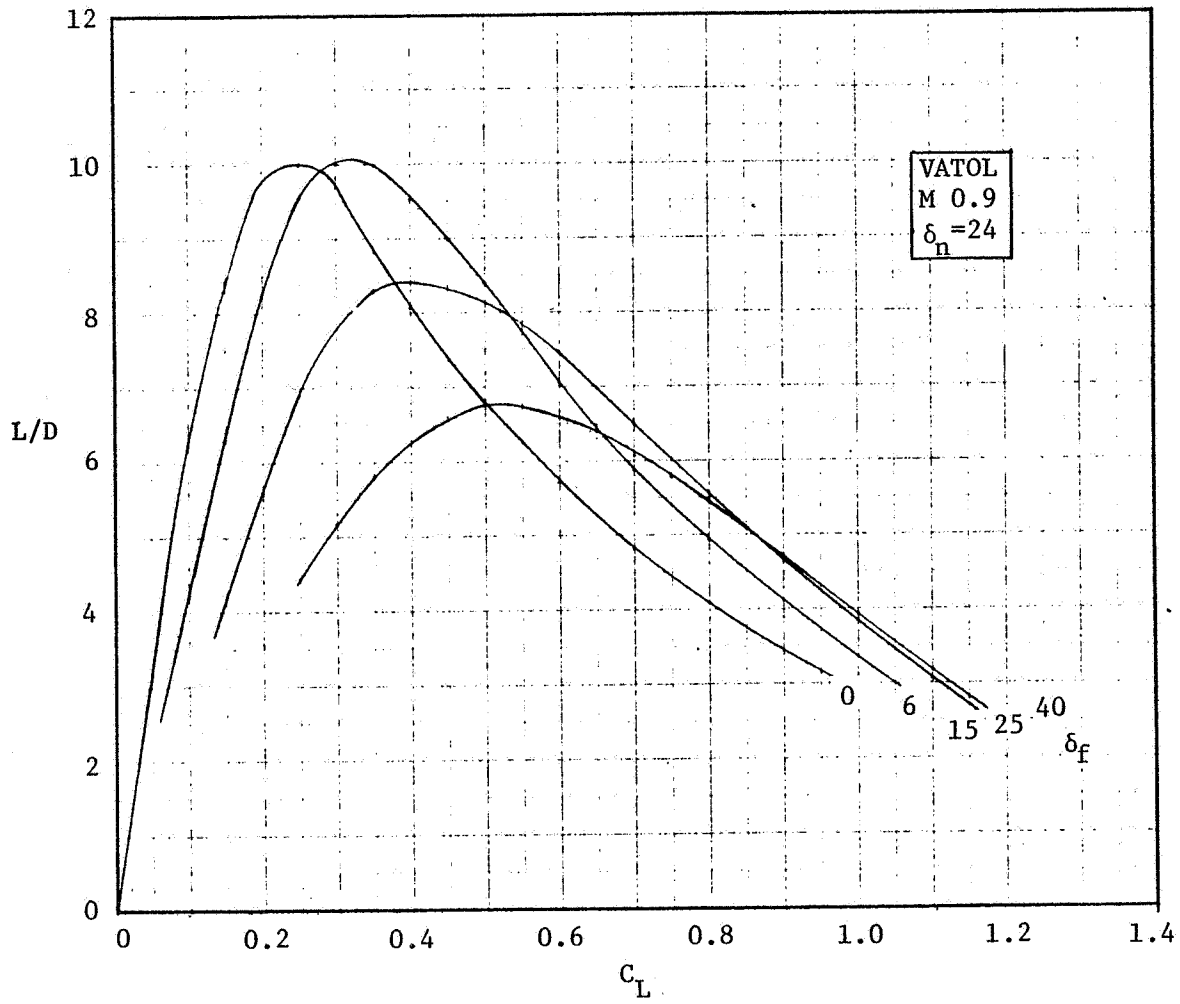

FIGURE 3-38. LIFT-DRAG RATIO AT M 0.9, δ_n=24°

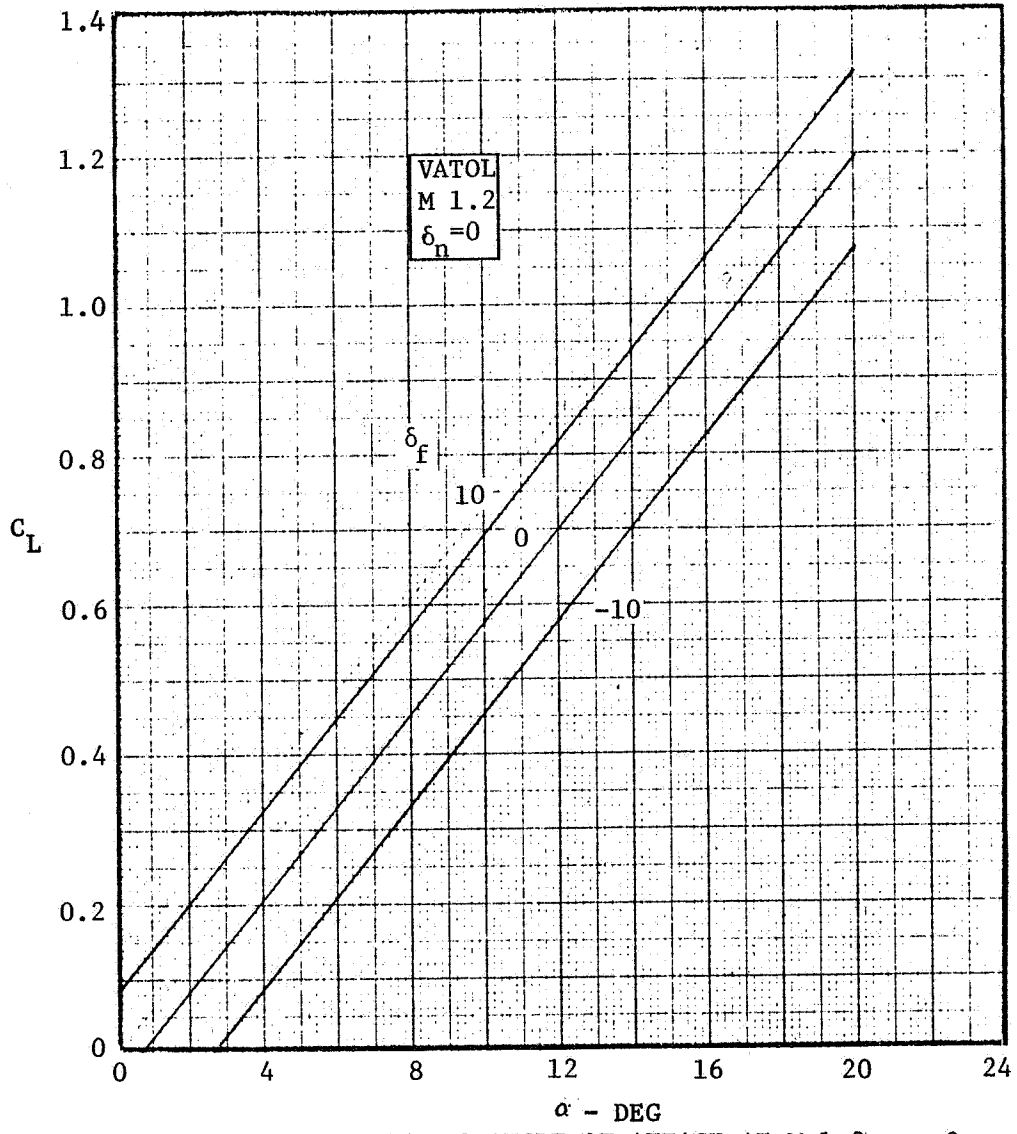

FIGURE 3-39. LIFT VS ANGLE OF ATTACK AT M 1.2, δ_n=0

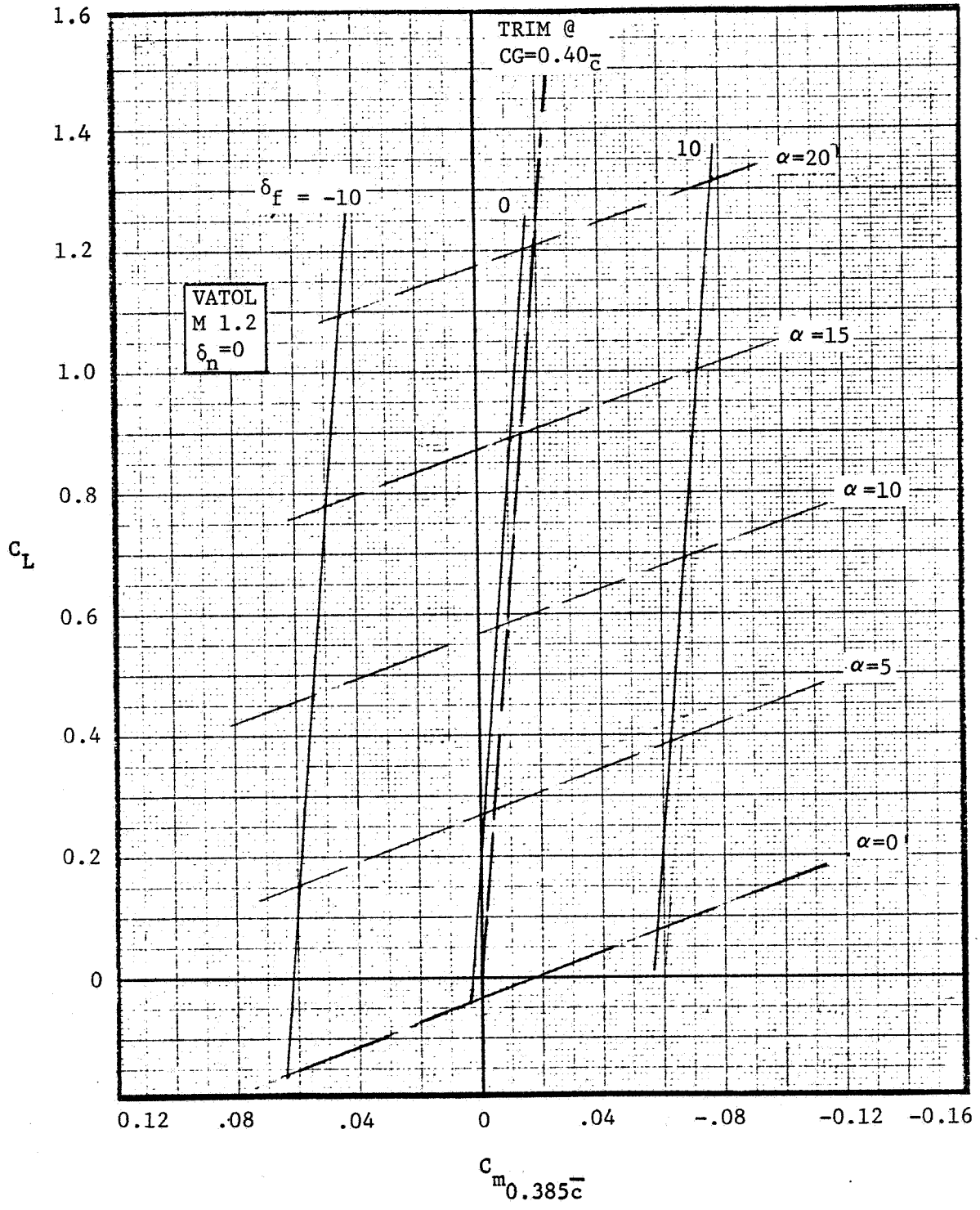

FIGURE 3-40. TRAILING-EDGE FLAP EFFECTIVENESS AT M 1.2, δ_n=0

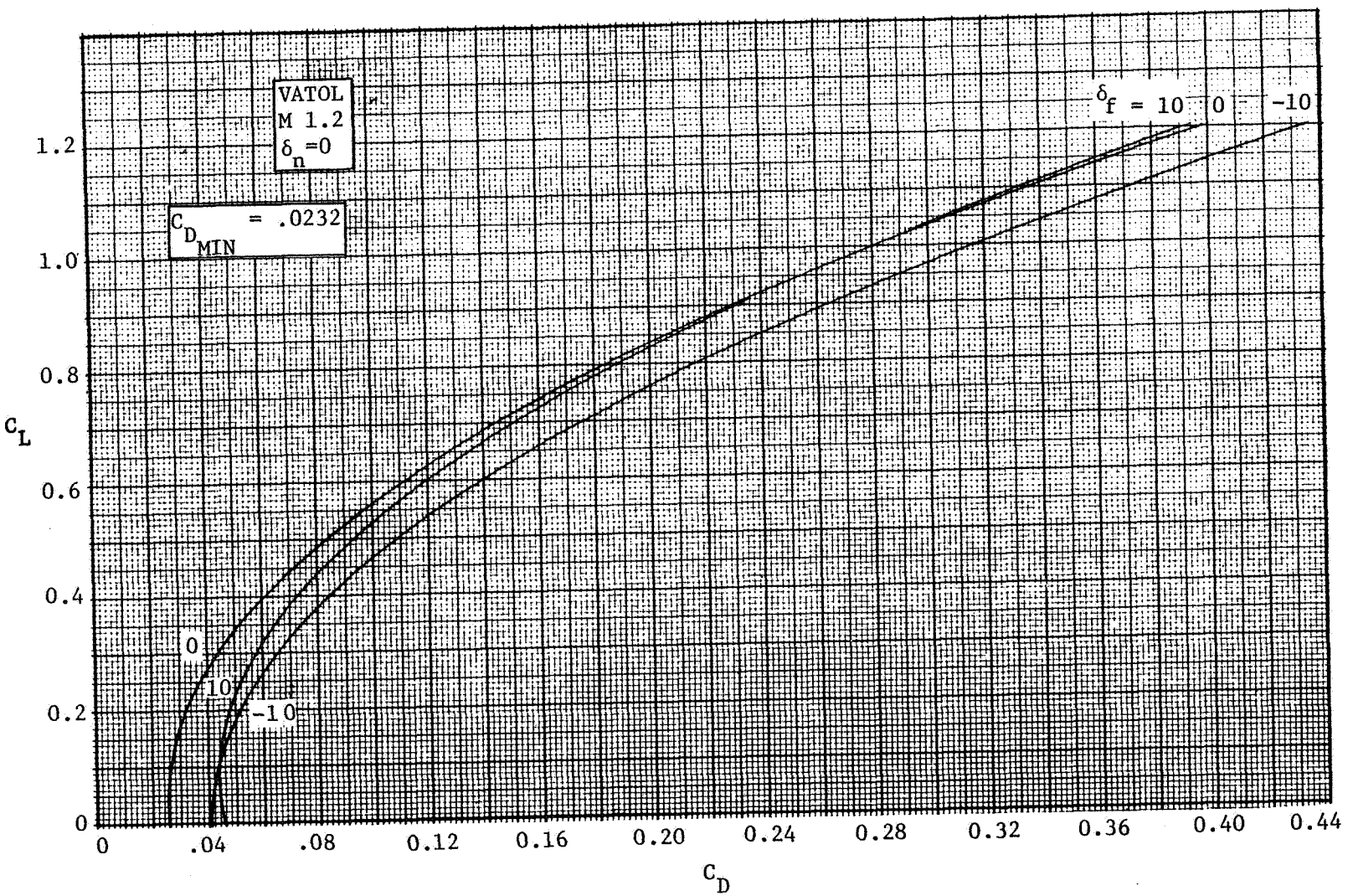

FIGURE 3-41. LIFT-DRAG POLAR AT M 1.2, δ_n=0

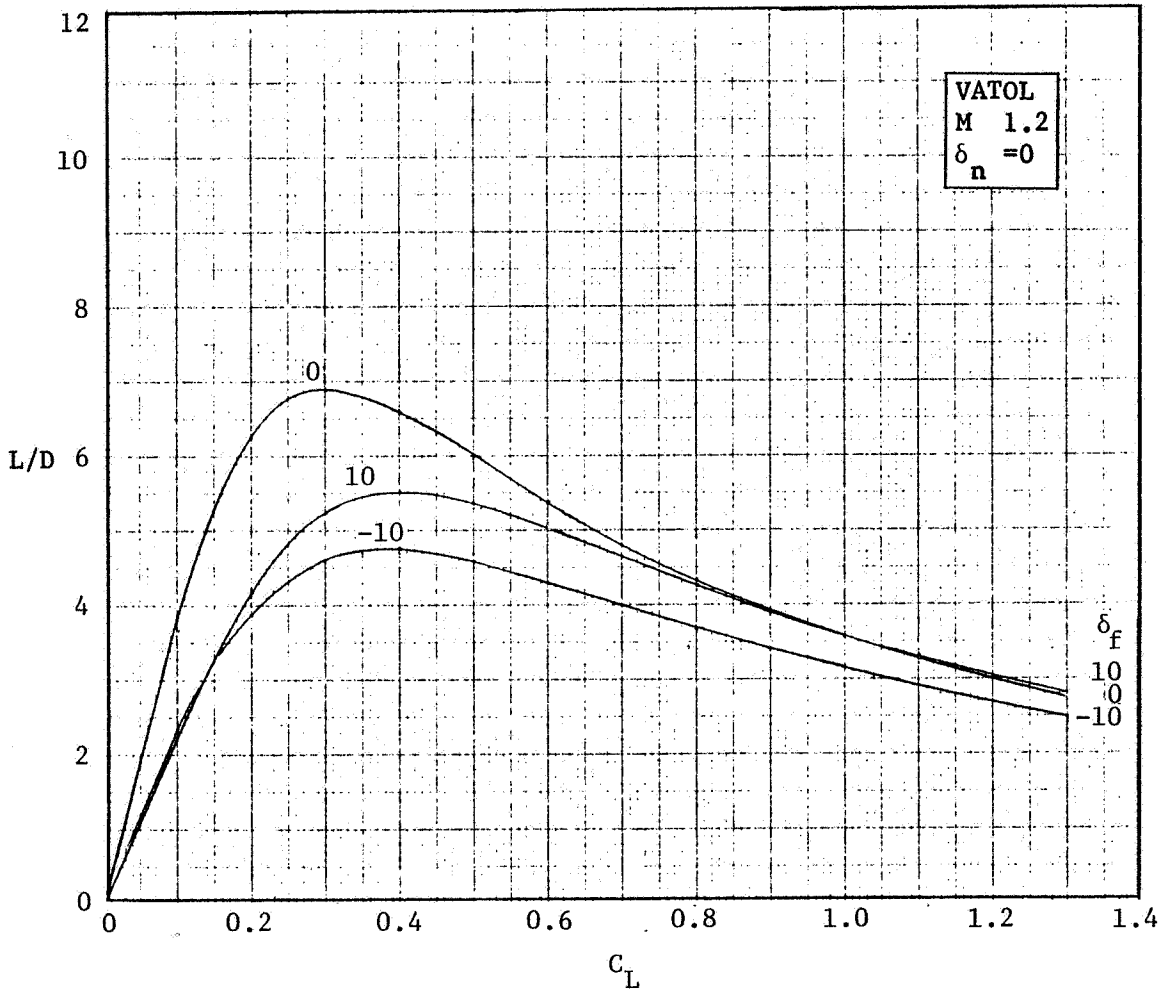

FIGURE 3-42. LIFT-DRAG RATIO AT M 1.2, δ_n=0

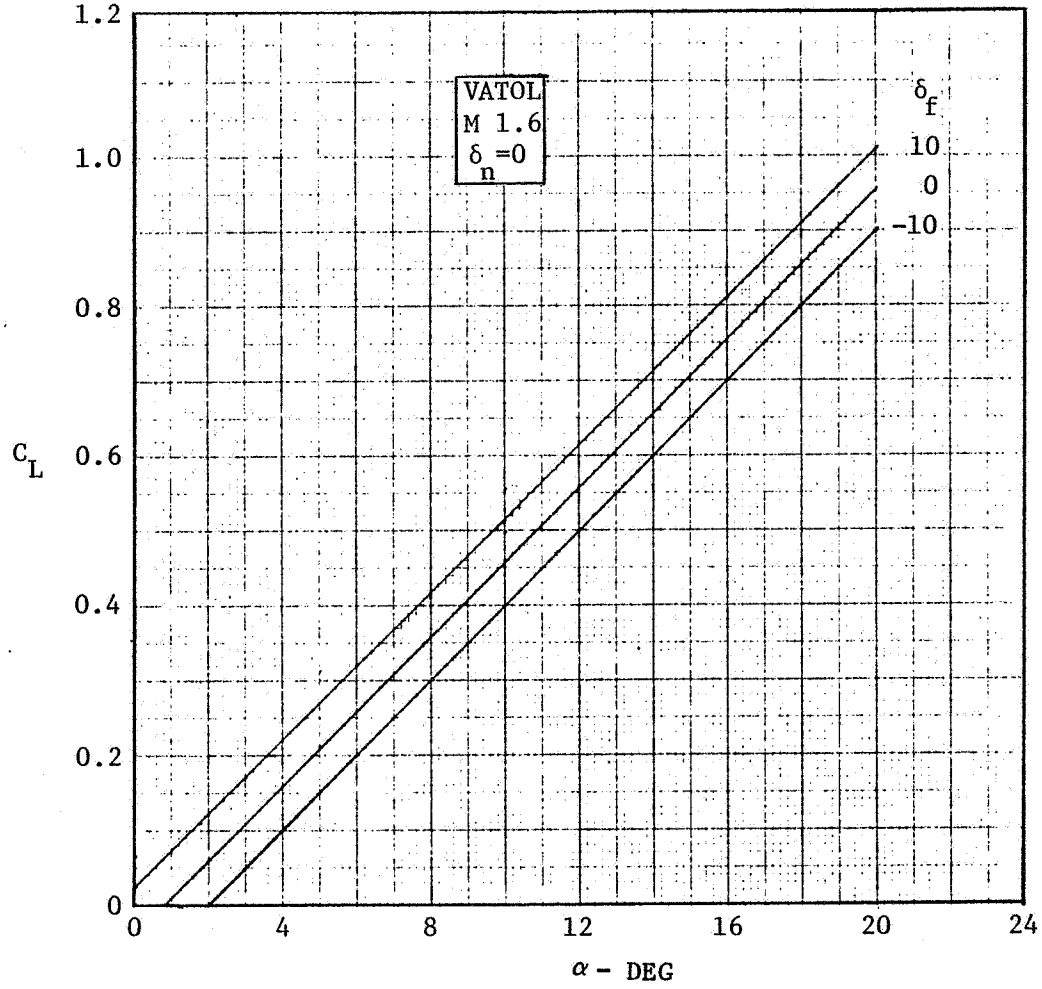

FIGURE 3-43. LIFT VS ANGLE OF ATTACK AT M 1.6, δ_n=0

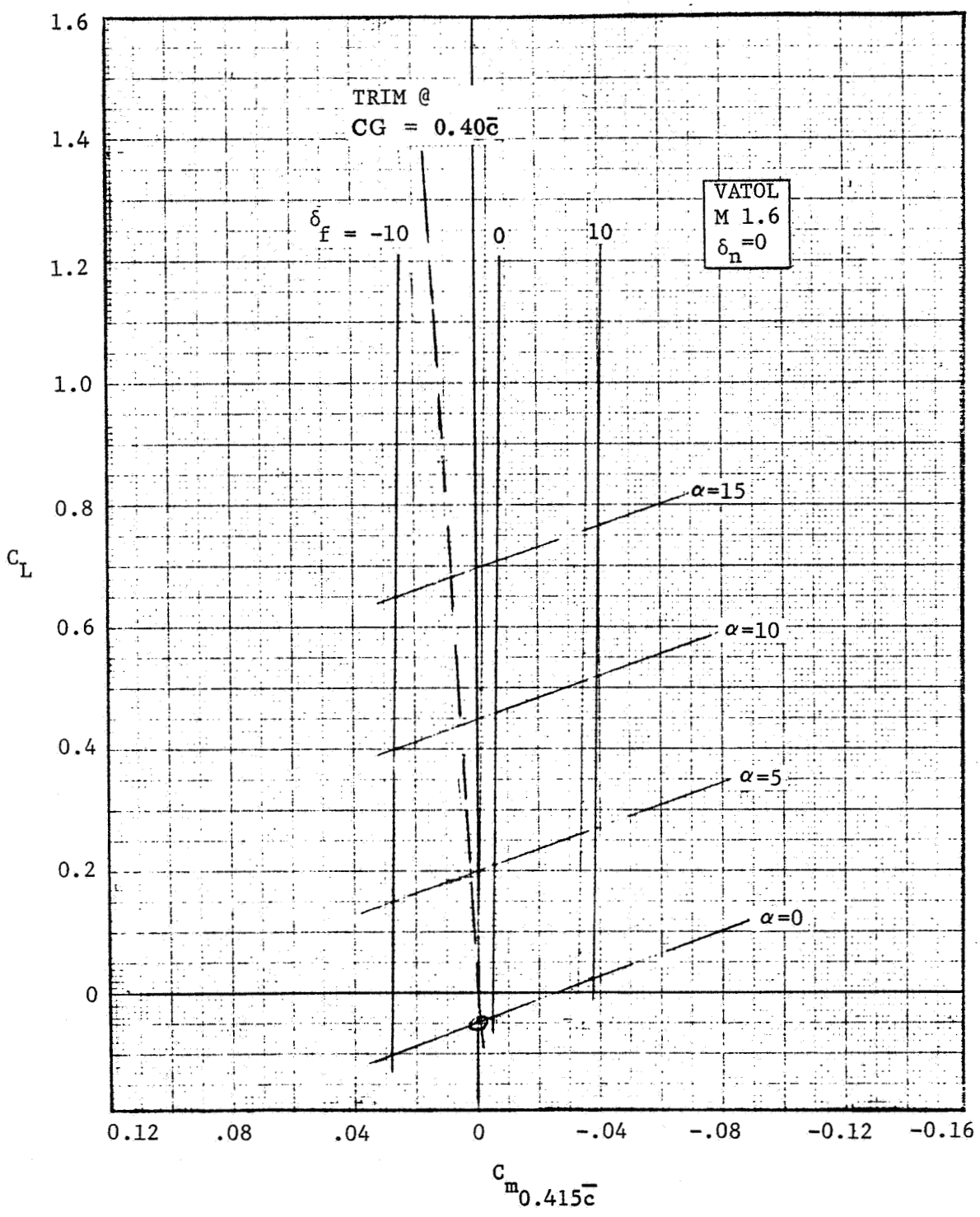

FIGURE 3-44. TRAILING-EDGE FLAP EFFECTIVENESS AT M 1.6, δ_n=0

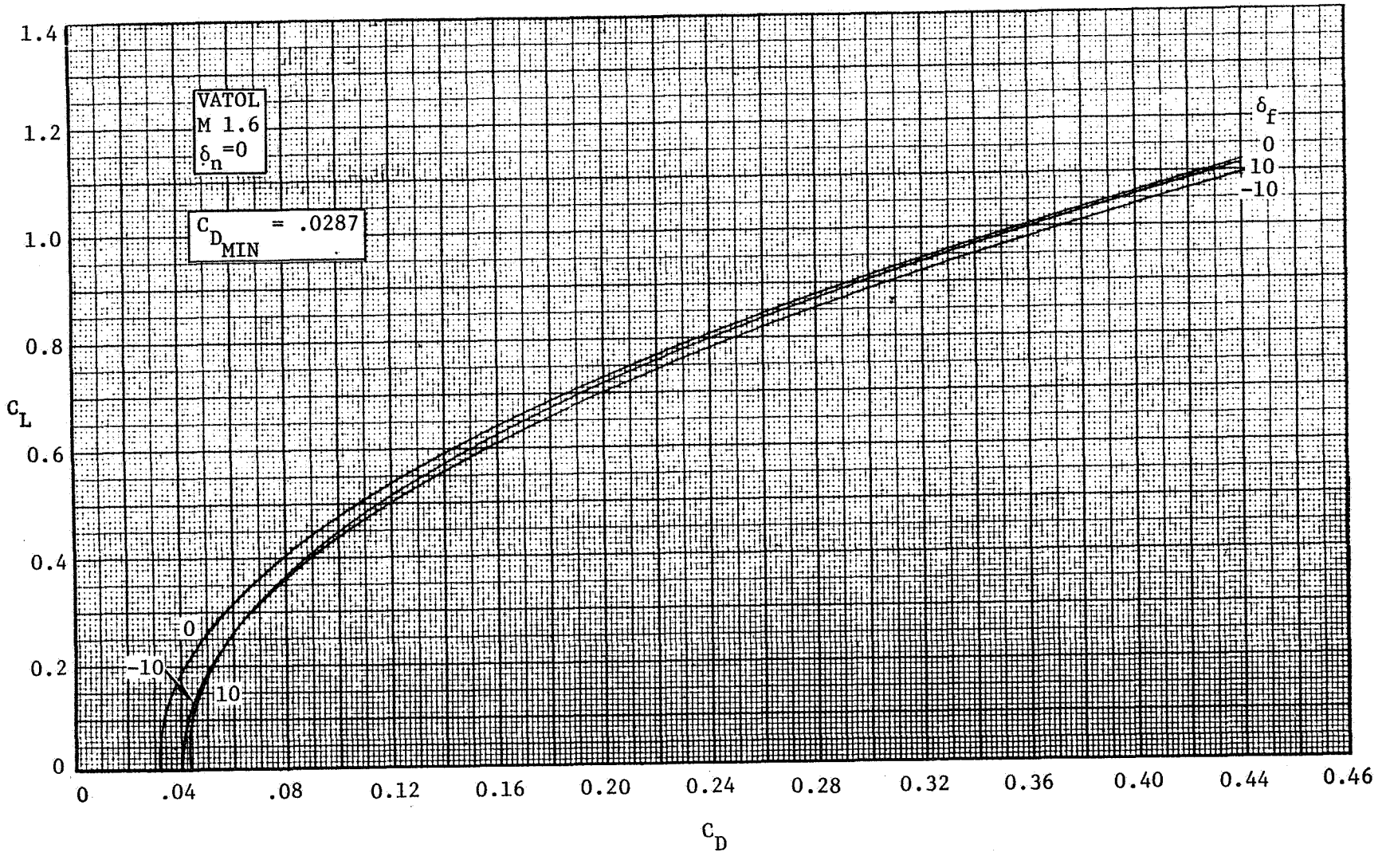

FIGURE 3-45. LIFT-DRAG POLAR AT M 1.6, δ_n=0

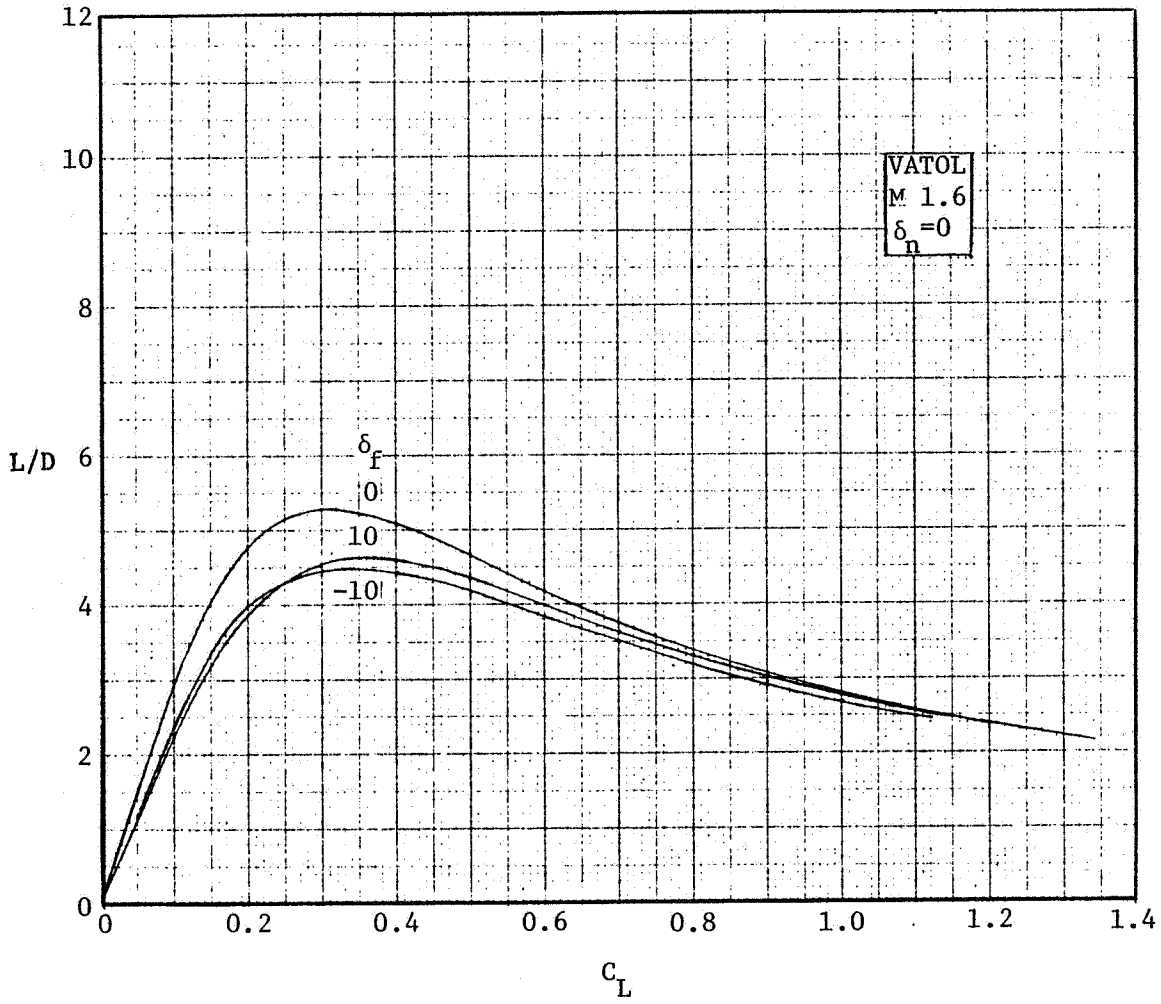

FIGURE 3-46. LIFT-DRAG RATIO AT M 1.6, δ_n=0

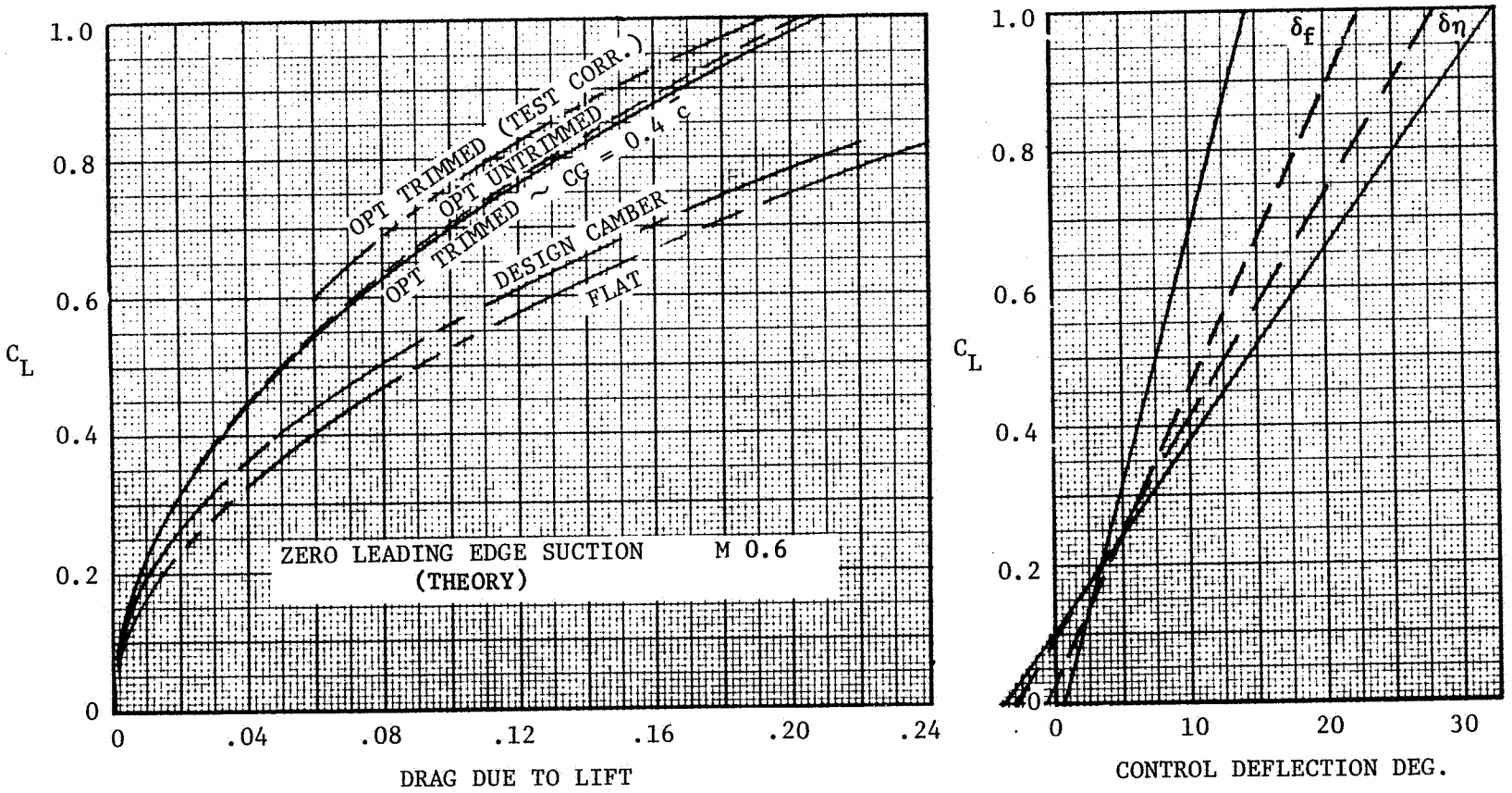

FIGURE 3-47. DRAG DUE TO LIFT

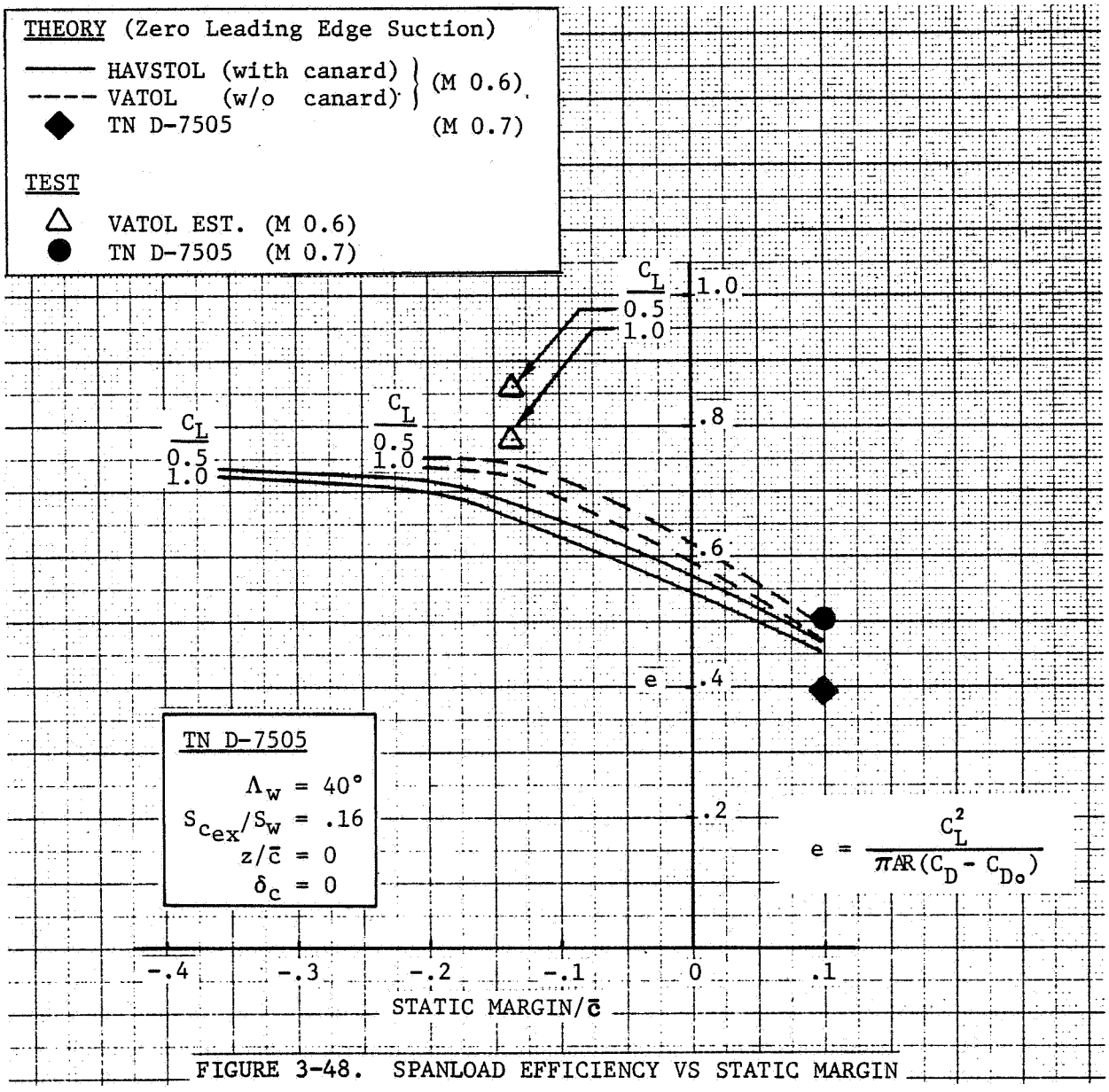

FIGURE 3-48. SPANLOAD EFFICIENCY VS STATIC MARGIN

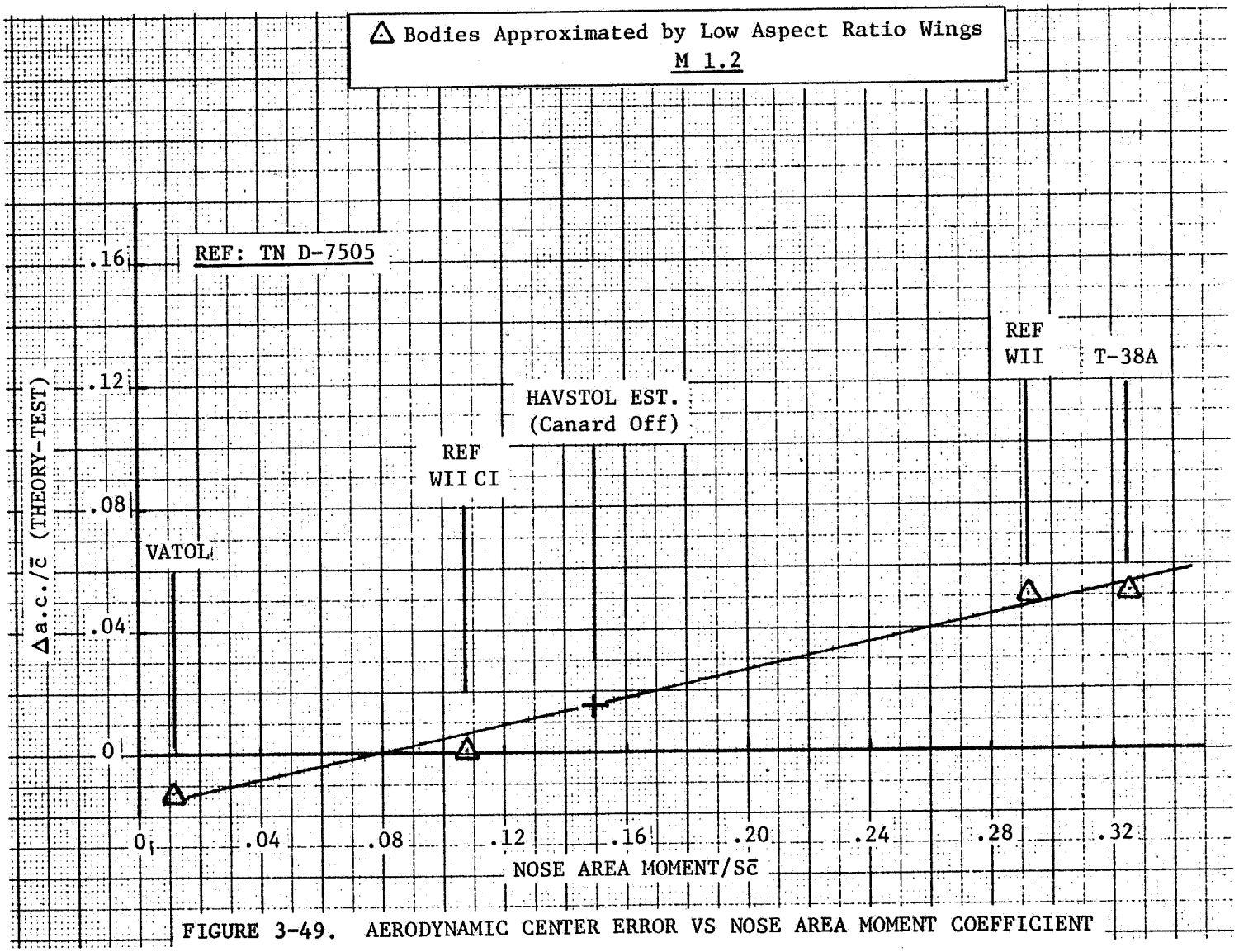

FIGURE 3-49. AERODYNAMIC CENTER ERROR VS NOSE AREA MOMENT COEFFICIENT

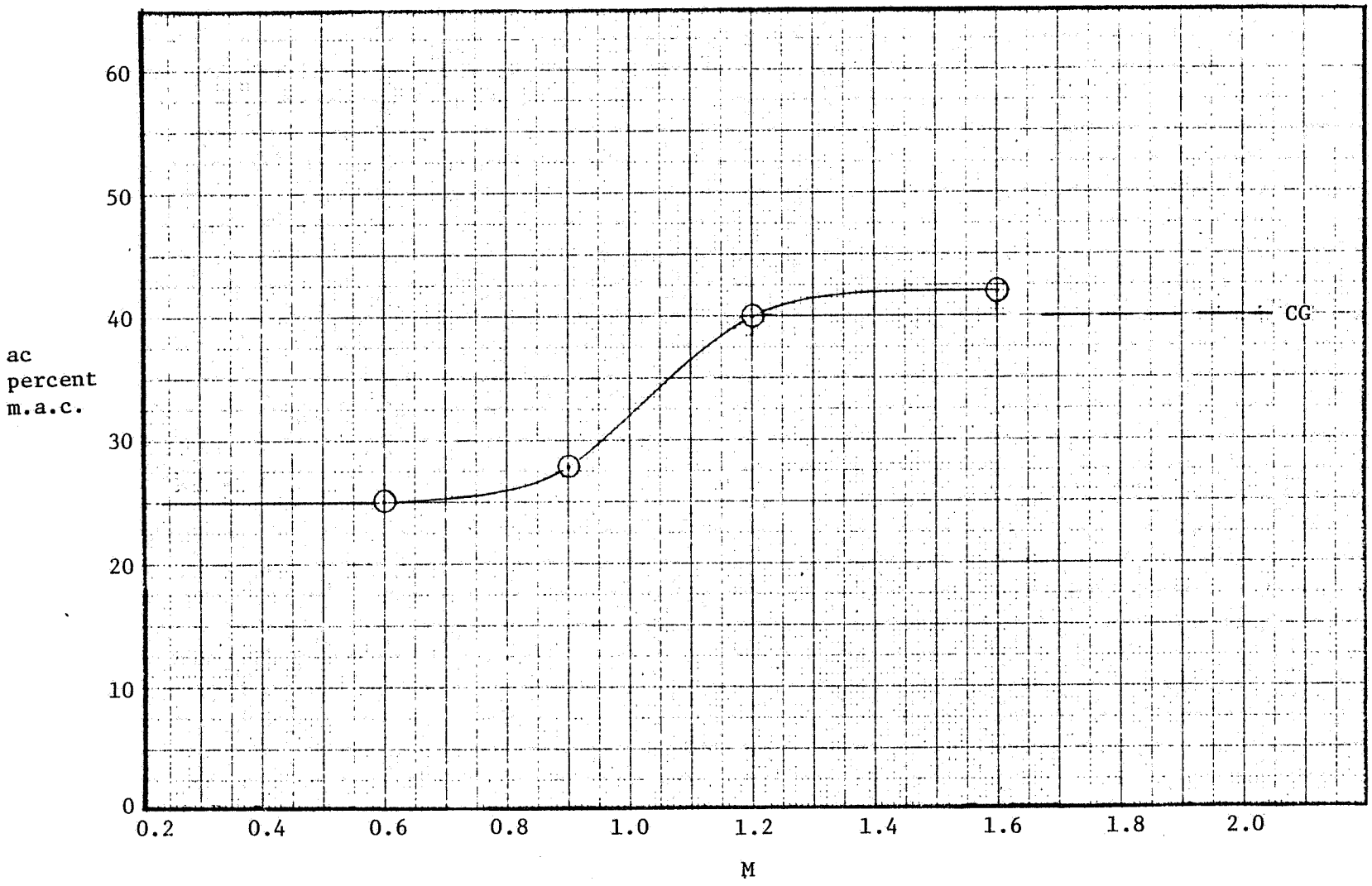

FIGURE 3-50. AERODYNAMIC CENTER LOCATION

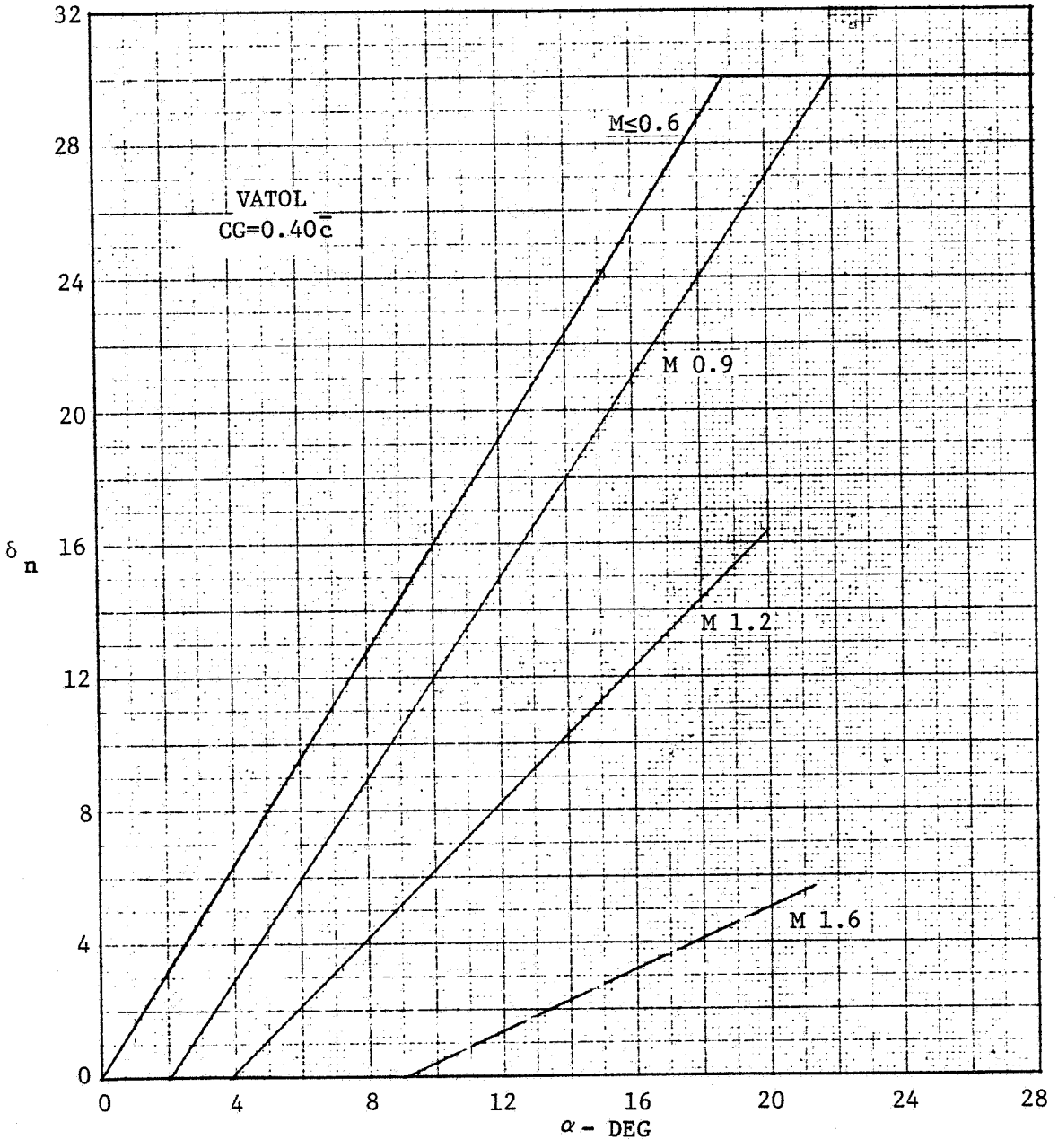

FIGURE 3-51. LEADING-EDGE FLAP SCHEDULE

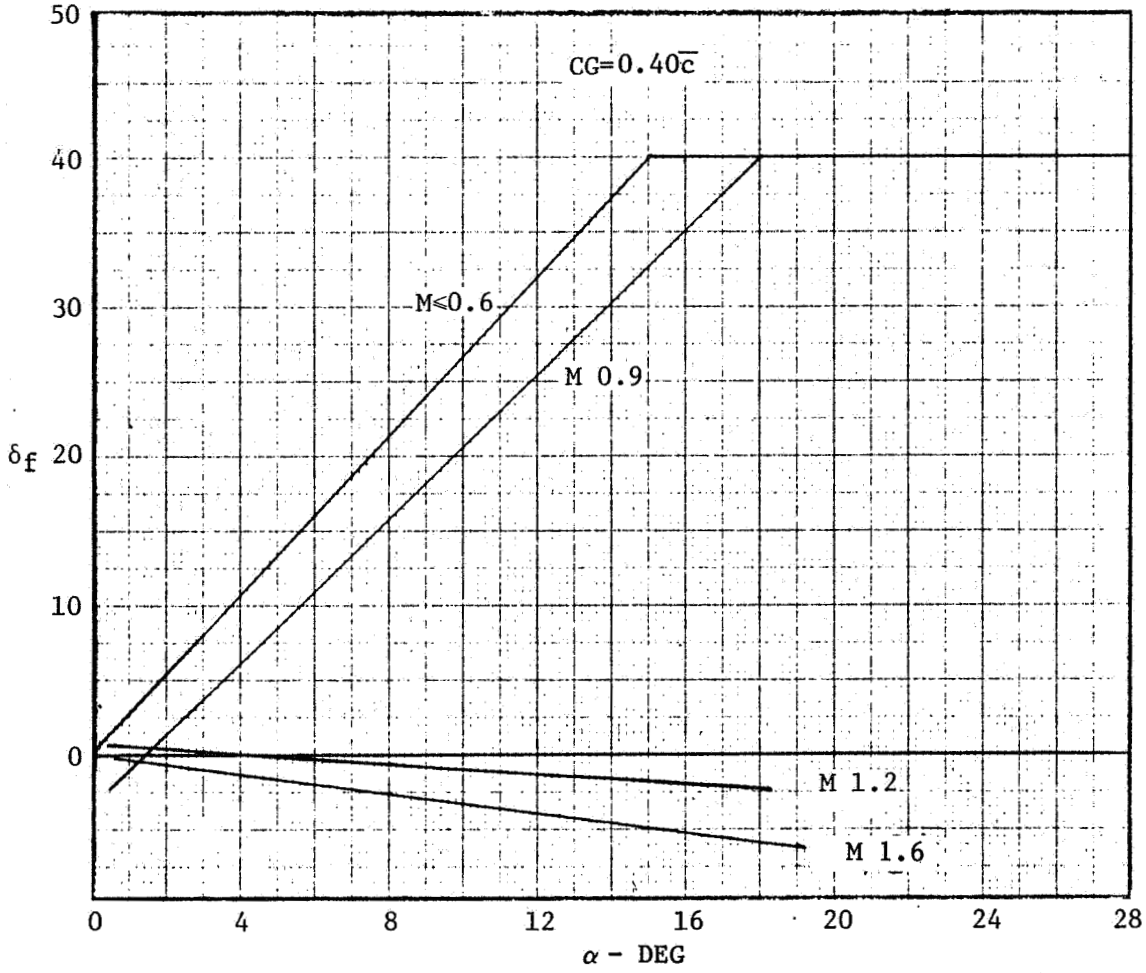

FIGURE 3-52. OPTIMUM TRAILING-EDGE FLAP DEFLECTION FOR TRIM

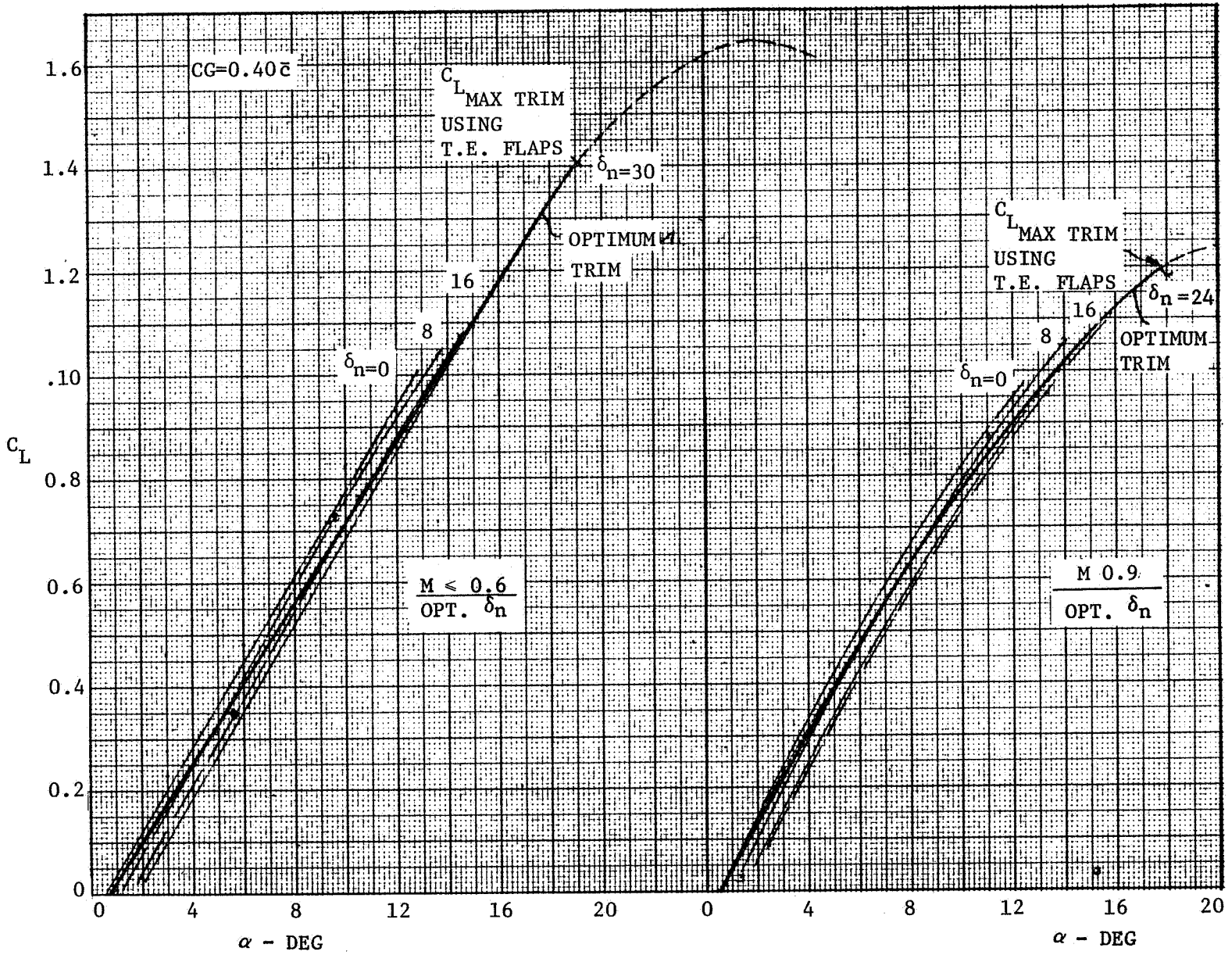

FIGURE 3-53. SUBSONIC TRIM LIFT CURVES

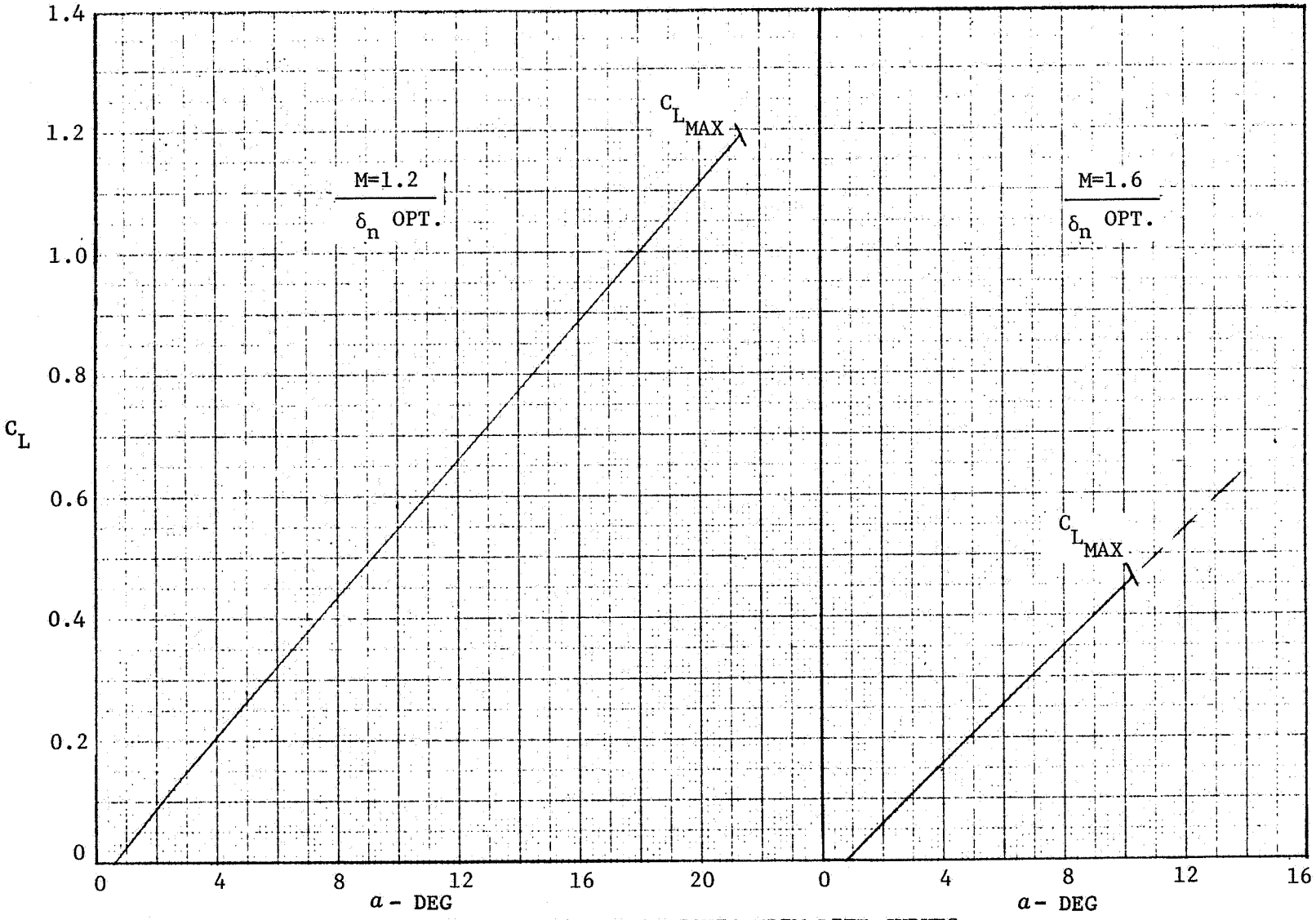

FIGURE 3-54. SUPERSONIC TRIM LIFT CURVES

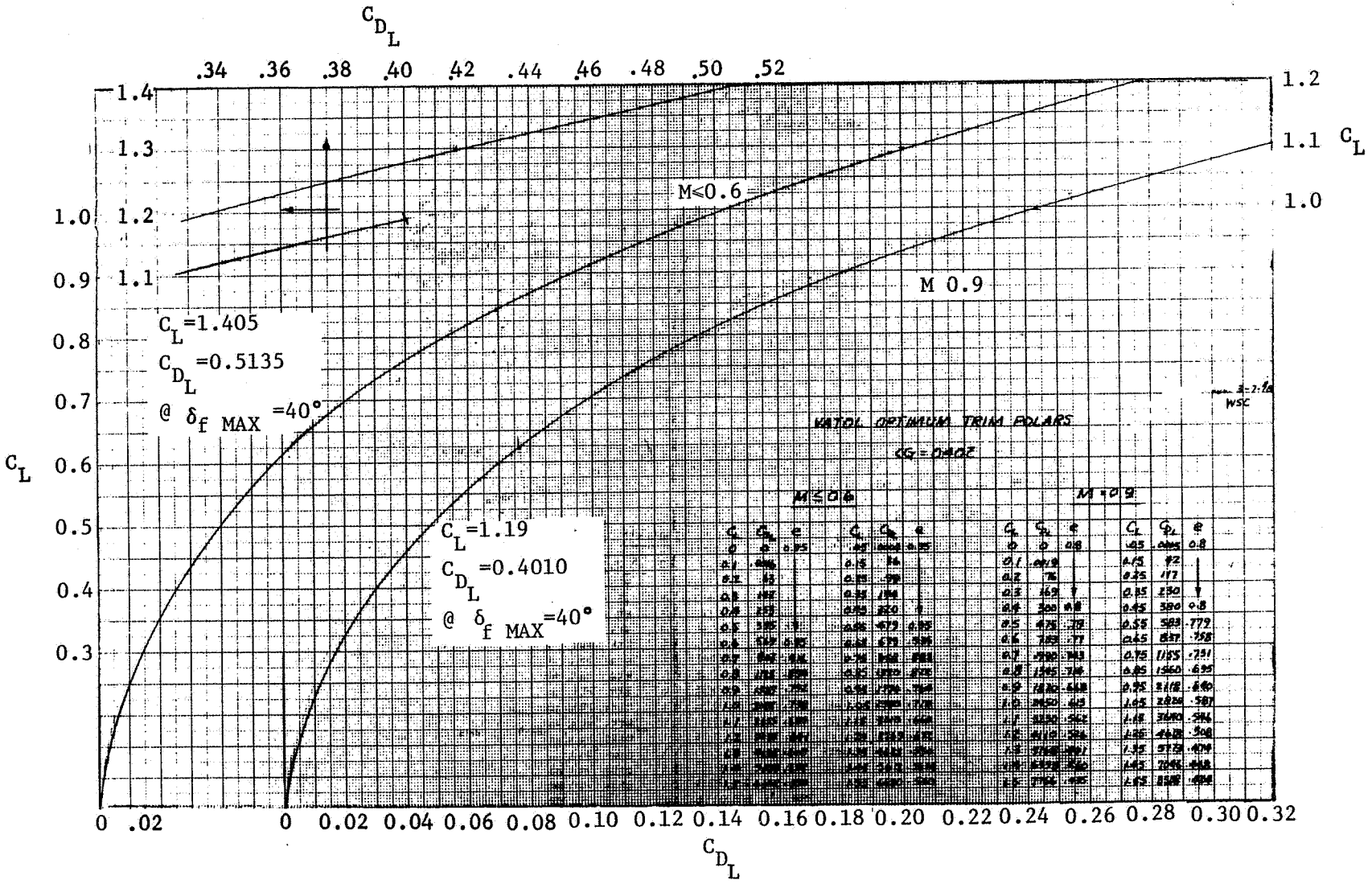

FIGURE 3-55. SUBSONIC TRIM POLARS

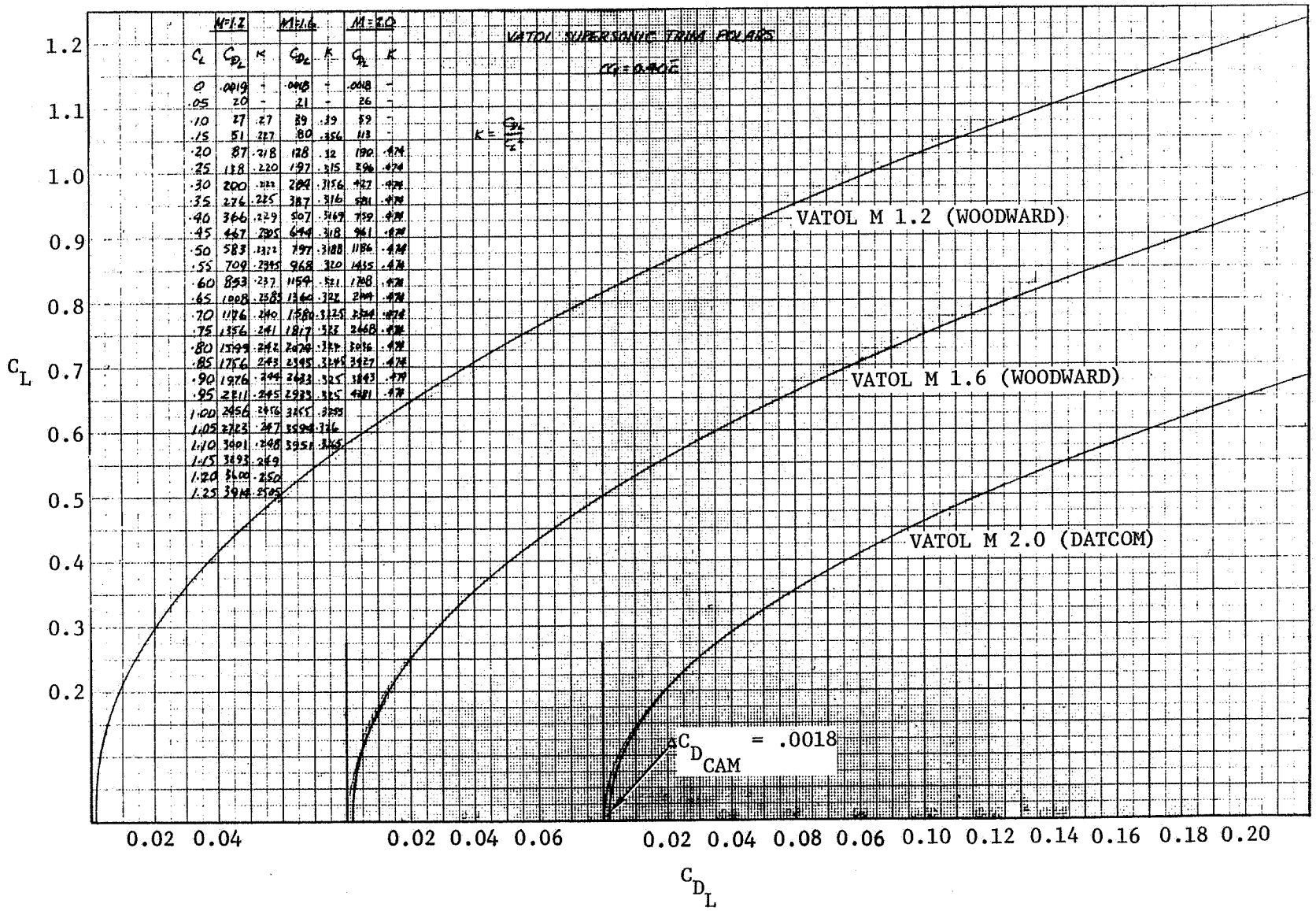

FIGURE 3-56. SUPERSONIC TRIM POLARS

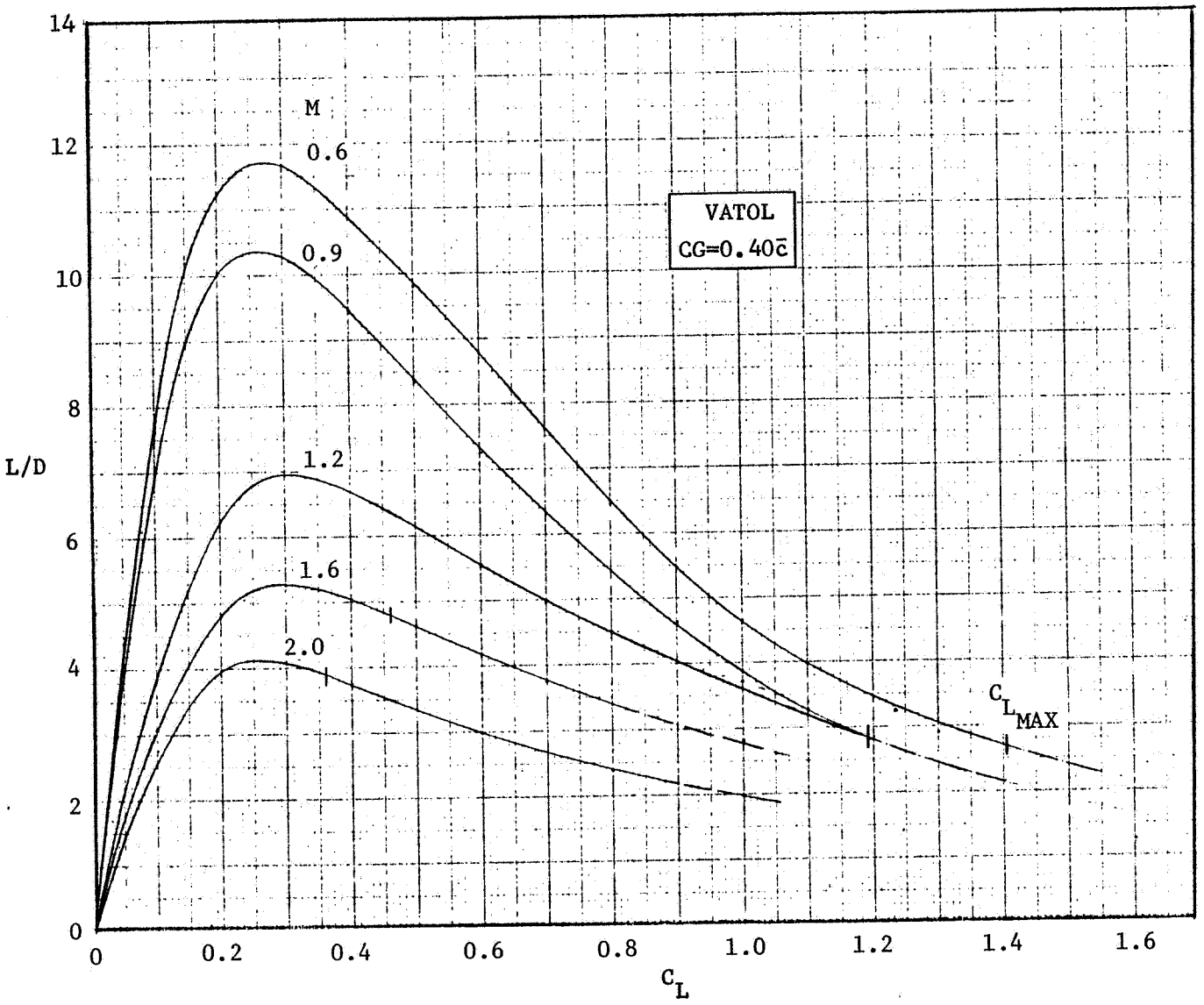

FIGURE 3-57. OPTIMUM TRIM LIFT-DRAG RATIO

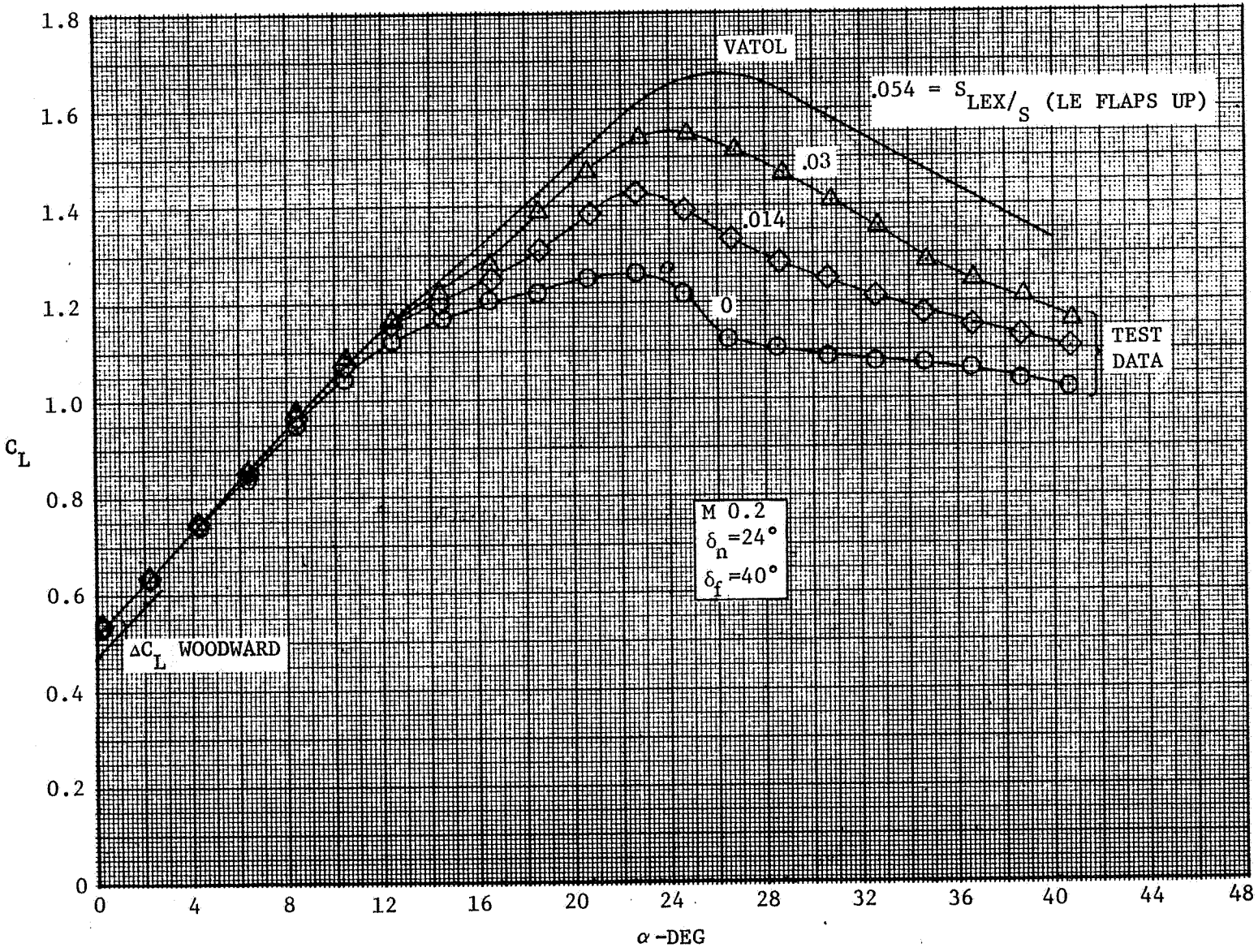

FIGURE 3-58. EFFECT OF LEX SIZE ON LIFT AT ANGLE OF ATTACK

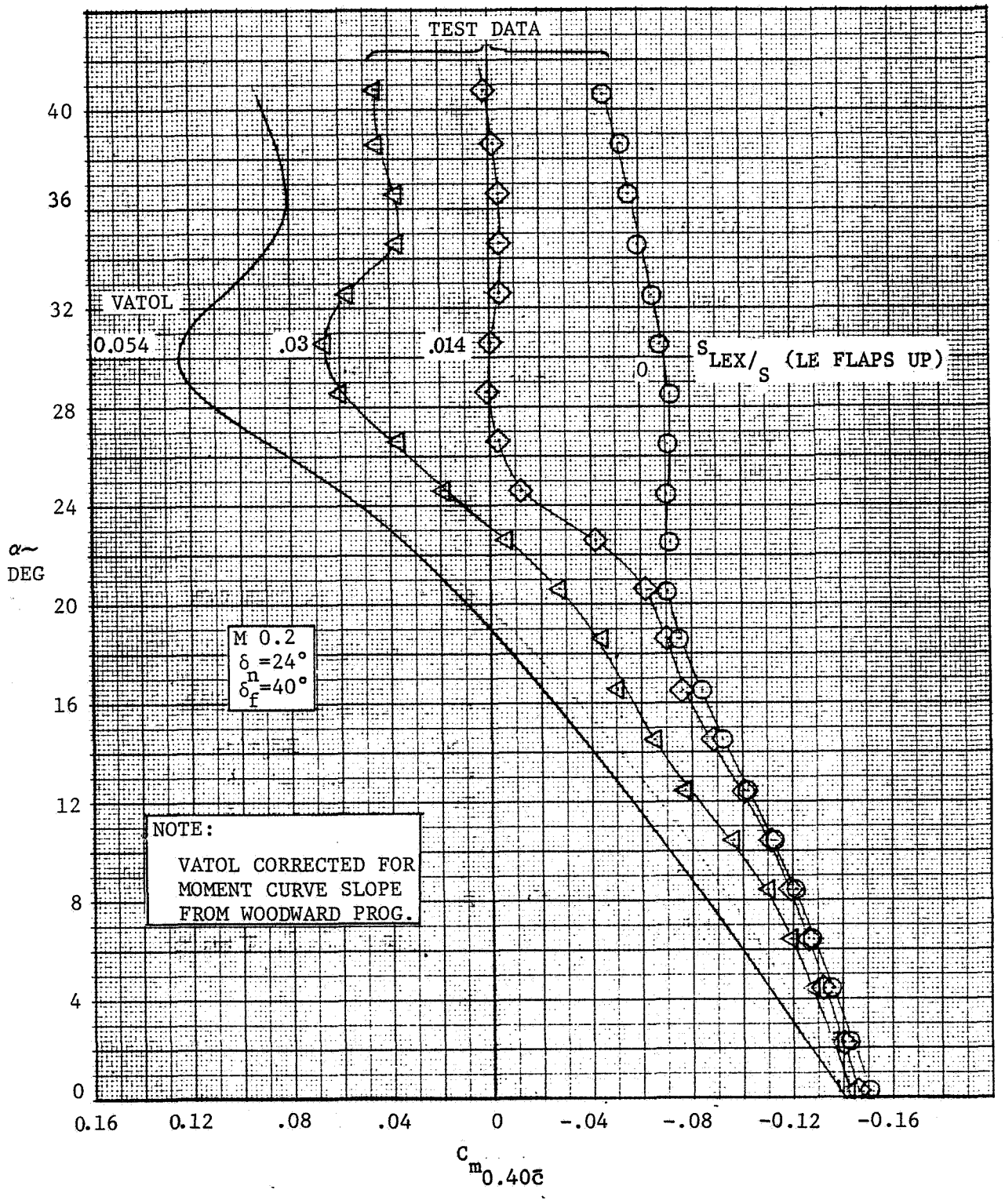

FIGURE 3-59. EFFECT OF LEX SIZE ON PITCHING MOMENT AT ANGLE OF ATTACK

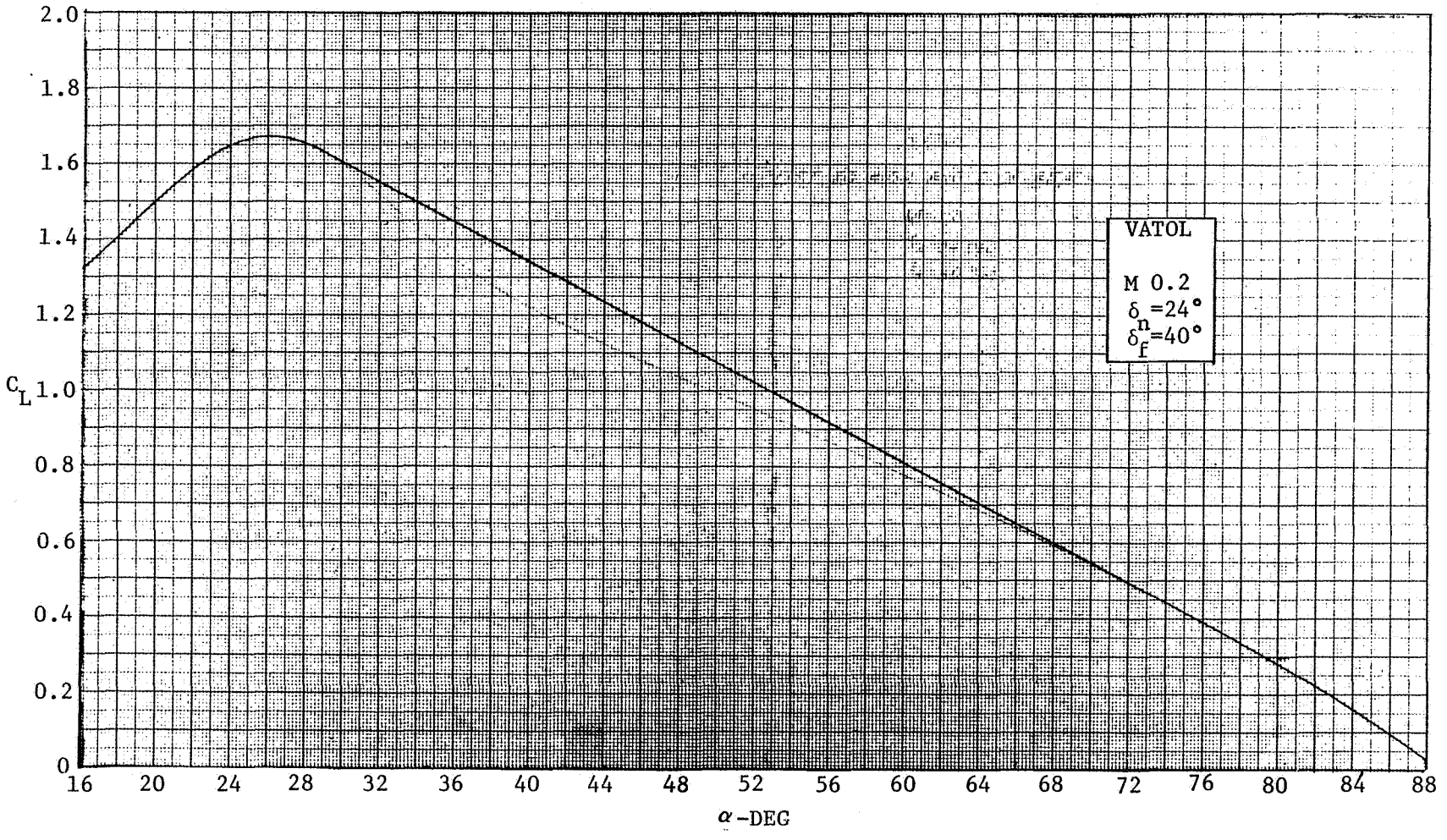

FIGURE 3-60. LIFT TO HIGH ANGLE OF ATTACK

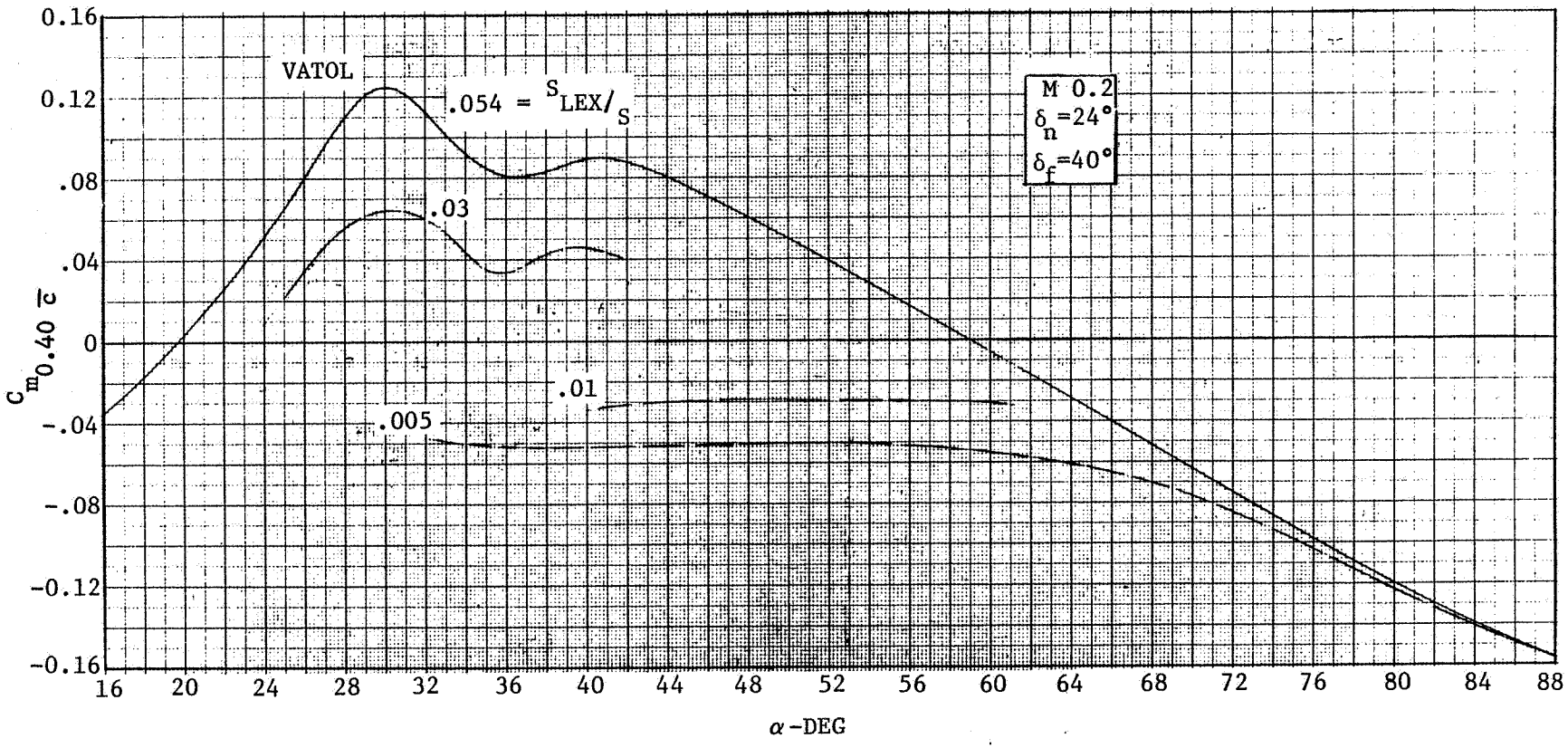

FIGURE 3-61. PITCHING MOMENT TO HIGH ANGLE-OF-ATTACK

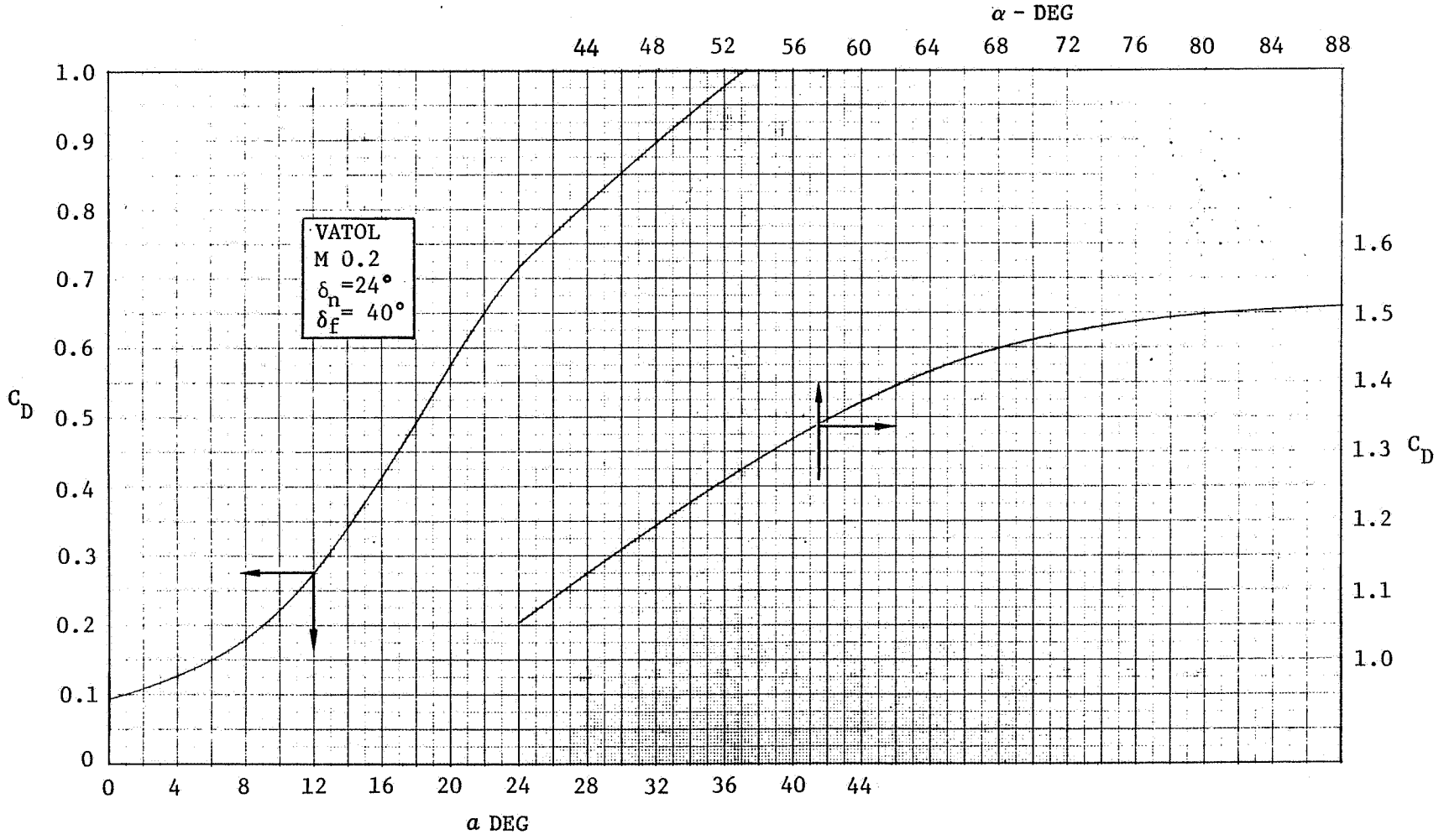

FIGURE 3-62. DRAG TO HIGH ANGLE-OF-ATTACK

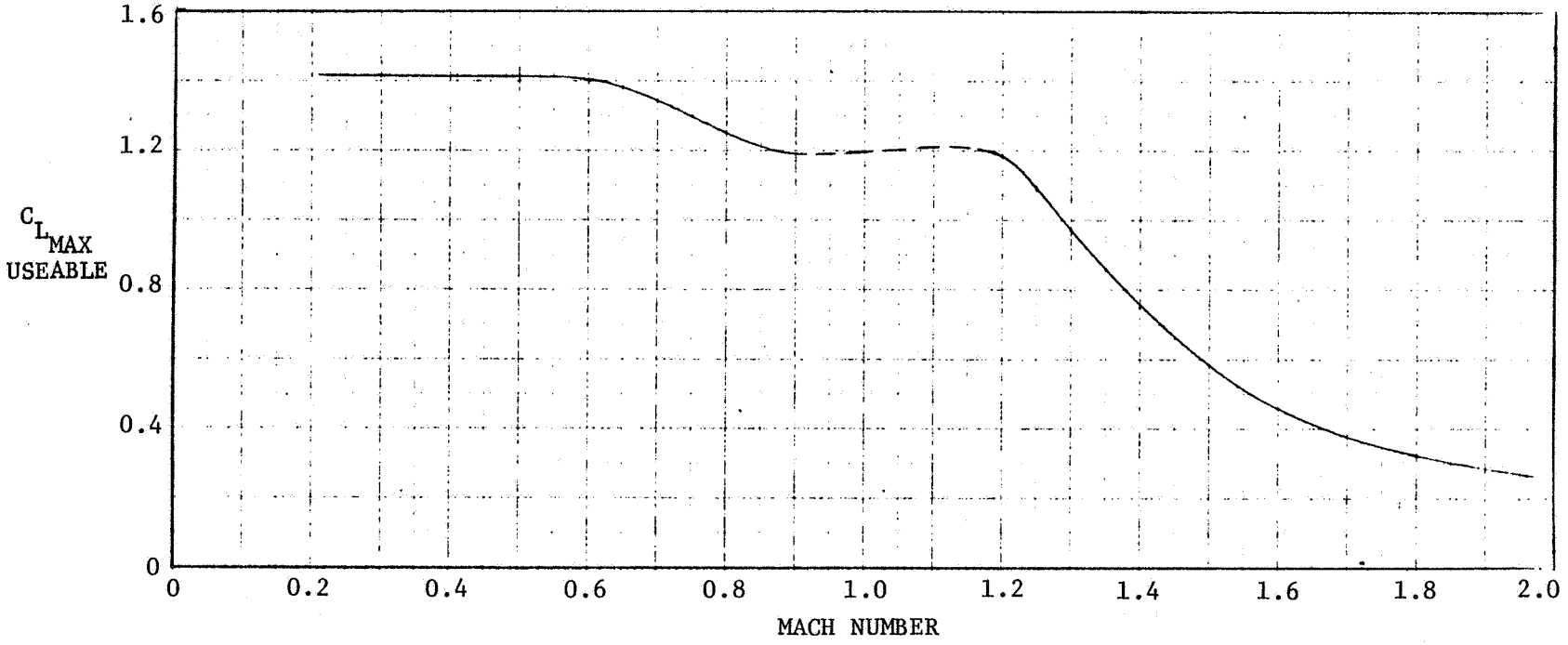

FIGURE 3-63. MAXIMUM USEABLE LIFT

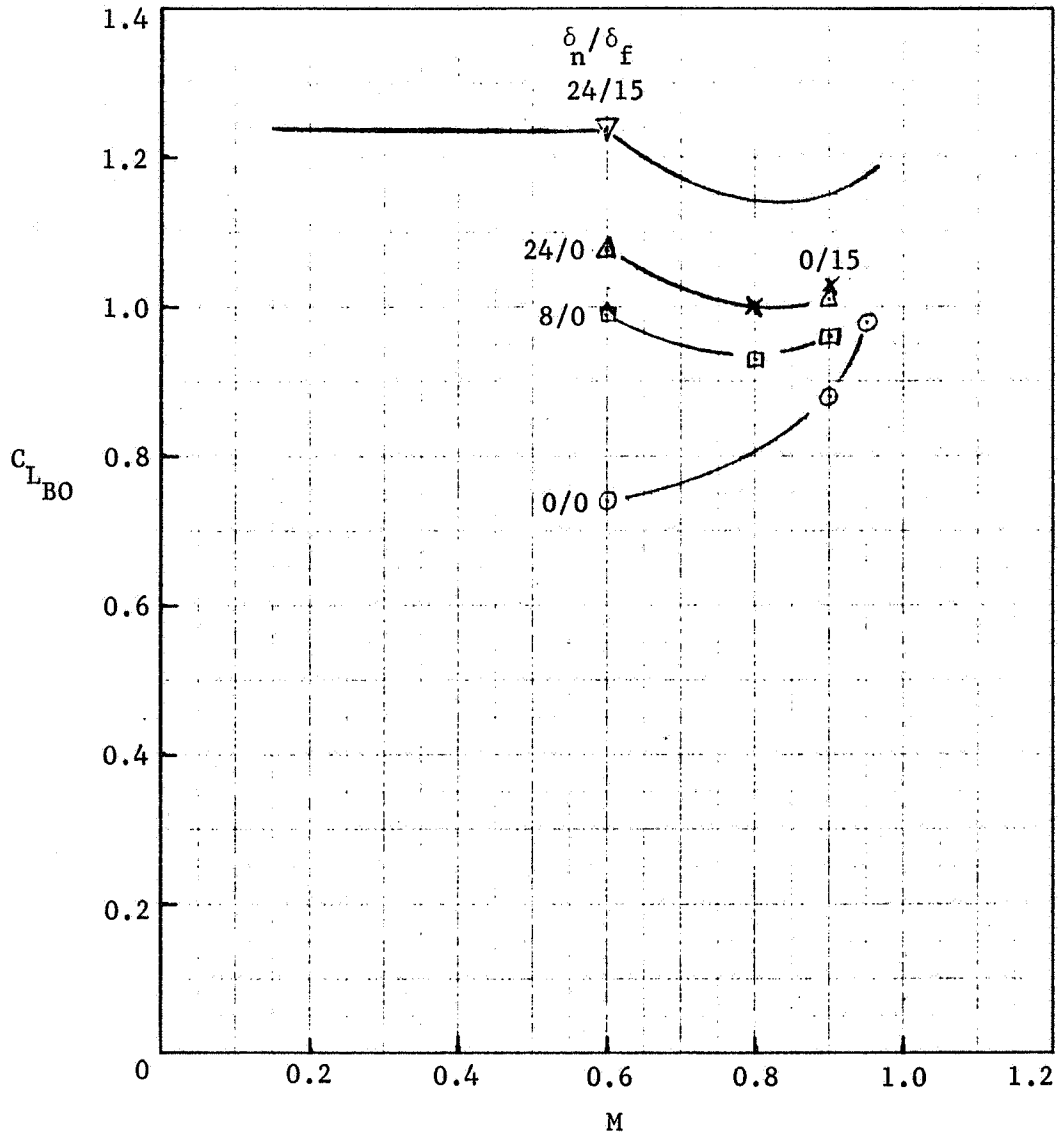

FIGURE 3-64. LIFT COEFFICIENT FOR BUFFET ONSET

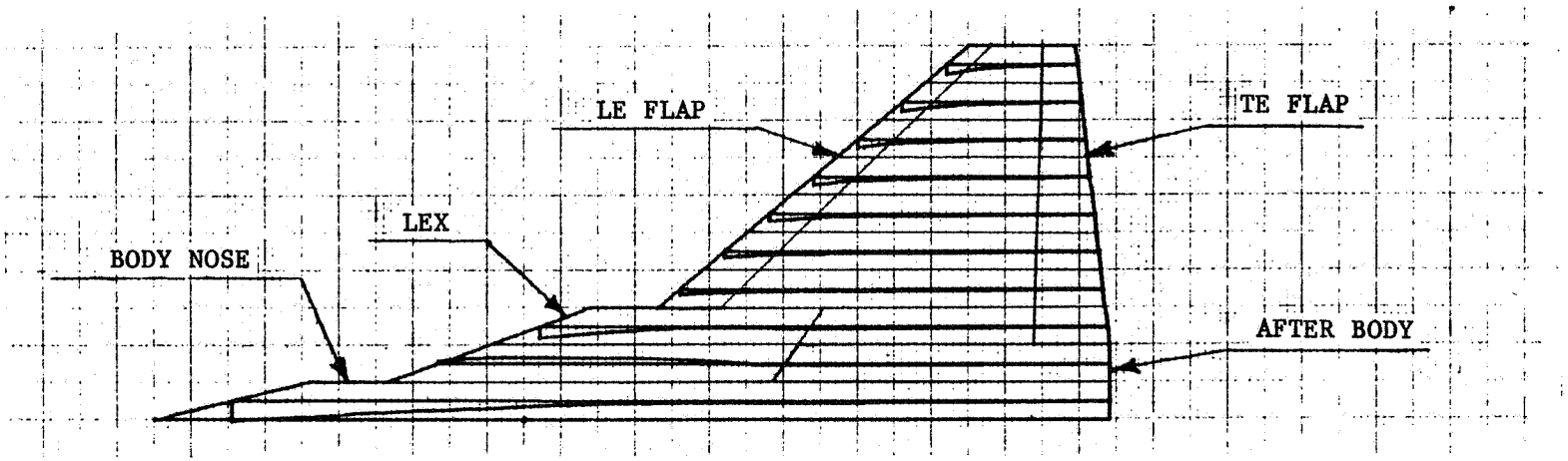

FIGURE 3-65. GEOMETRY MODEL FOR AERODYNAMIC ANALYSIS

3.3 LATERAL/DIRECTIONAL ANALYSIS

Lateral/Directional data are presented in the body axes system for a rigid aircraft with a reference moment center of $0.40\bar{c}$. The data are derived essentially from wind tunnel test results.

3.3.1 Lateral/Directional Stability

A Northrop transonic wind tunnel test (NAL-171) of a tailless design having the same wing planform (but a smaller LEX) and a very similar vertical tail planform compared to the VATOL configuration, was used as a data base which was suitably modified by theory to obtain the estimated lateral/directional data. The test body characteristics, ΔCy and ΔC_n, as a function of α and β, were estimated and subtracted from the wing body test data. The body alone ΔC_l was assumed negligible (body axes). The VATOL body characteristics were similarly estimated and added back in. The body estimation procedure used modified incremental slender body theory, a technique which has been found to give reasonable approximations in most cases. A self-correcting tendency is inherent in the process just described, provided consistency in the body estimation details is maintained. The wind tunnel test model was nominally a midwing configuration with zero dihedral. The VATOL is essentially a midwing configuration also, but with three degrees of cathedral. Corrections were made to VATOL for three degrees of cathedral, using standard DATCOM procedures.

The vertical tail effects were then estimated, using the test data modified by moment area relationships, and added in to the wing body estimates. The effects of the increased LEX size, relative to the model tested, are difficult to estimate in the absence of specifically applicable test data because of the strong aerodynamic interrelationship of the LEX, wing and vertical tail surfaces. For the VATOL configuration, it was assumed on the basis of Northrop test experience, that the lateral/directional stability would fall off less rapidly because of the increased LEX size at angles of attack above twenty degrees. This beneficial effect may require wind tunnel investigation, particularly with regard to vertical tail location.

Wind tunnel test data were available as a base for M0.6, 0.9, and 1.2, but not at 1.6. As a result, the data had to be extrapolated to 1.6, using trends characteristic of delta wing airplanes, and are therefore not as well substantialized at 1.6 as at the other Mach numbers.

The static lateral/directional parameters C_y, C_n and C_l are plotted at constant angles of attack versus sideslip angle for M0.6, 0.9,. 1.2 and 1.6 in

Figures 3-66 through 3-77. Each figure shows the configuration with the vertical tail off and on. The controls are fixed at zero deflection angle in these figures, but will in fact move as required to supplement the aerodynamic stability characteristics via the active control system.

Side force due to sideslip is shown in Figures 3-66 through 3-69. Conventional trends are apparent for the wing-body and wing-body vertical tail configurations. The fixed-vertical-tail directional stability of the complete configuration, as seen in Figures 3-70 through 3-73, is positive for the low and moderate range of angles of attack. Adequate aerodynamic directional control is available via the vertical tail at the higher angles of attack to provide apparent stability even at statically unstable conditions. The corresponding dihedral effect, Figures 3-74 through 3-77, is favorable for much of the angle of attack and sideslip range shown without the active control system, although the goal of good flying qualities and control harmony will dictate the active control system stability inputs.

As a result of the use of electronic adaptive flight control systems, the stability and control characteristics of the aircraft are not as clearly related to the static aerodynamic parameters as they have been for the more conventional control systems. The apparent aircraft stability is, instead, a combined function of the aerodynamic stability, the aerodynamic control power, and the control system mechanization. Angle of attack or sideslip limitations can be designed into the control system to avoid any situation where the aircraft aerodynamics might lead to an uncontrollable condition. This section of the report does not treat the control system, and the reader is referred to Section 5.2.

3.3.2 Lateral/Directional Control Effectiveness

Control effectiveness of the all movable vertical tail and of the elevons in roll was estimated by correcting the wind tunnel test data described in 3.3.1 using moment area relationships. The vertical tail was sized to satisfy the cross wind landing requirement of MIL-F-8785B (ASG) for conventional aircraft. The vertical tail is not required for trim, in a failed engine case, as the thrust line of the remaining engine can be vectored to pass through the center of gravity to eliminate assymmetric thrust moments.

Vertical tail and elevon roll control effectiveness are presented in derivative form versus angle of attack for M0.6, 0.9, 1.2 and 1.6.

Figures 3-78 through 3-81 present the control power derivatives of the all movable vertical tail. The vertical tail provides good directional control power to high angles of attack at all Mach numbers. The rolling moment due to vertical tail deflection is small. The comparatively small size of the vertical tail warrants more careful scrutiny throughout the flight envelope than was possible in this conceptual study.

Elevon roll control power appears in Figures 3-82 through 3-85. The roll control power holds up well to high angles of attack except at M 0.9 where it falls to about 15 percent of its $\alpha = 0$ value at $\alpha = 26$ degrees. The yawing moment due to roll control is very small.

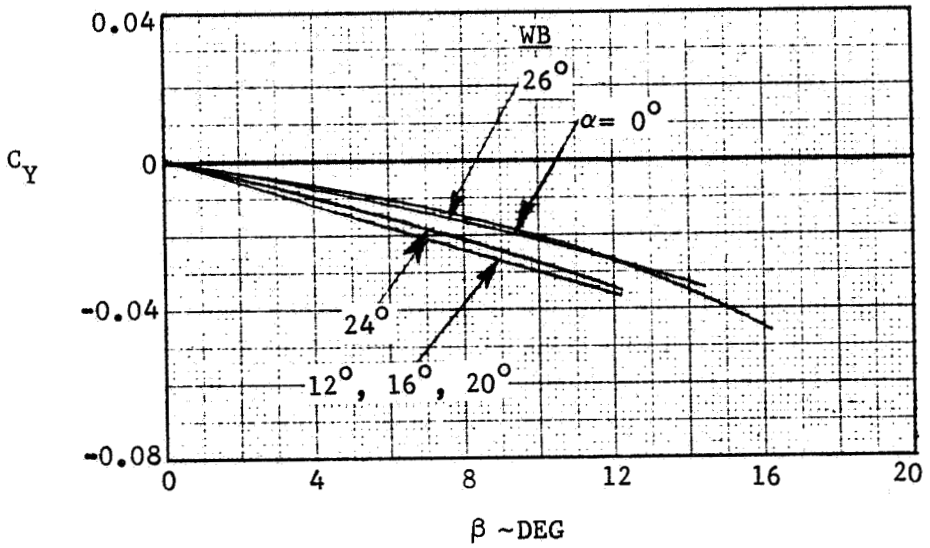

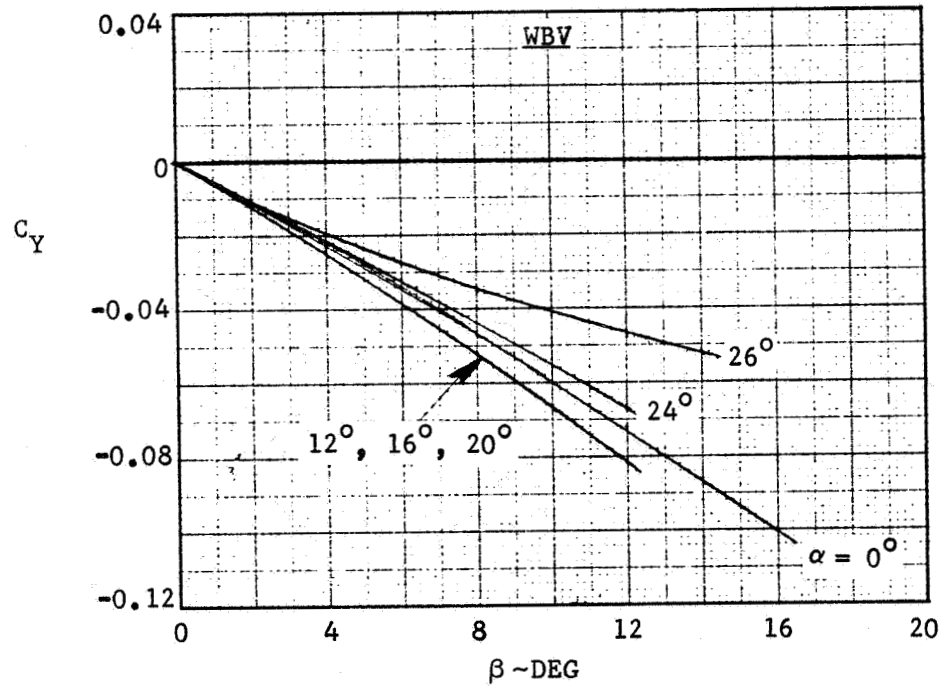

FIGURE 3-66. SIDE FORCE AT M 0.6

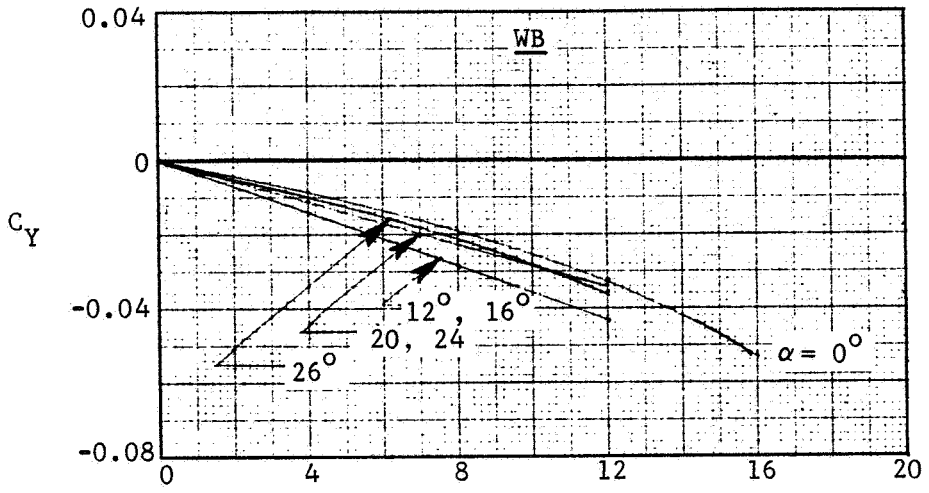

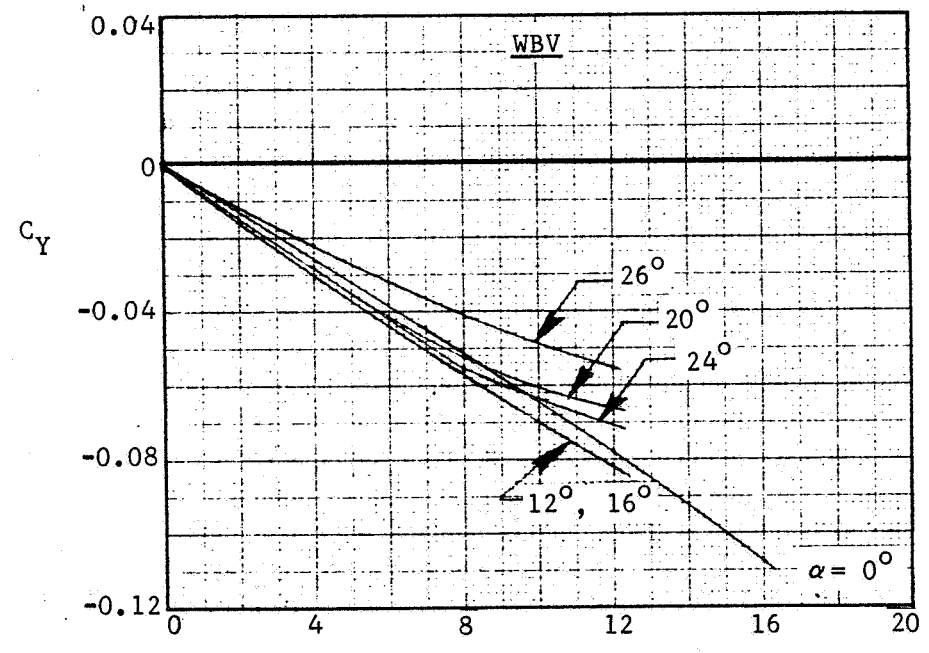

FIGURE 3-67. SIDE FORCE AT M 0.9

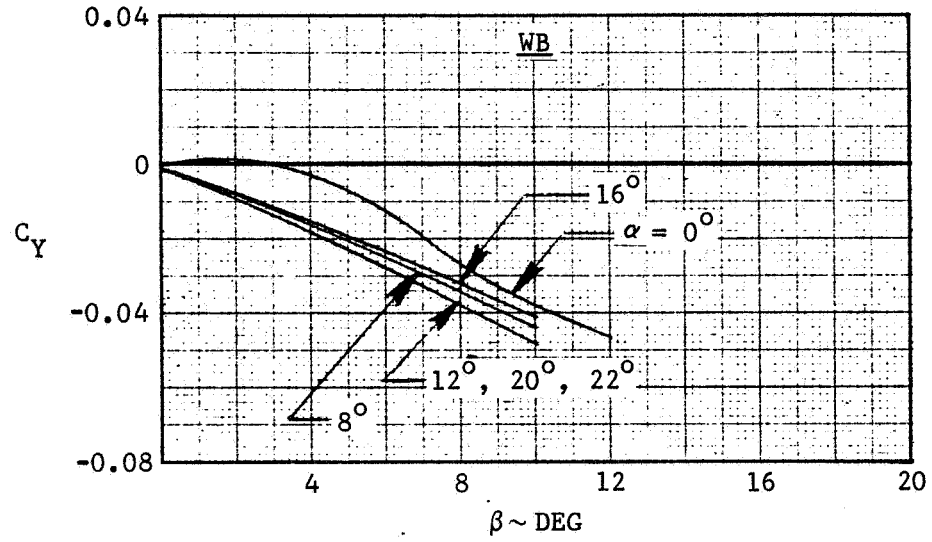

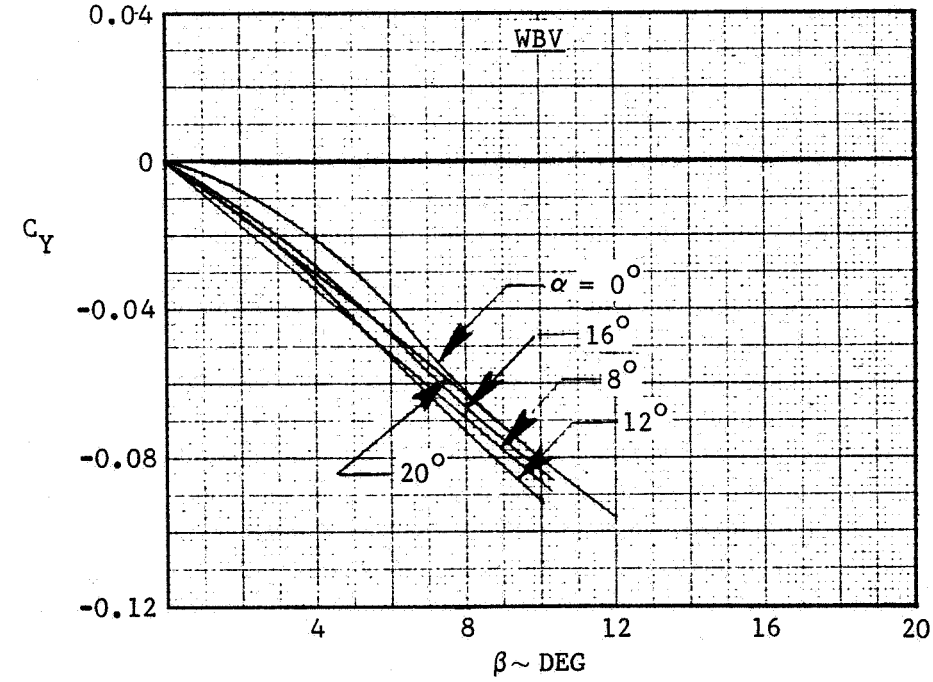

FIGURE 3-68. SIDE FORCE AT M 1.2

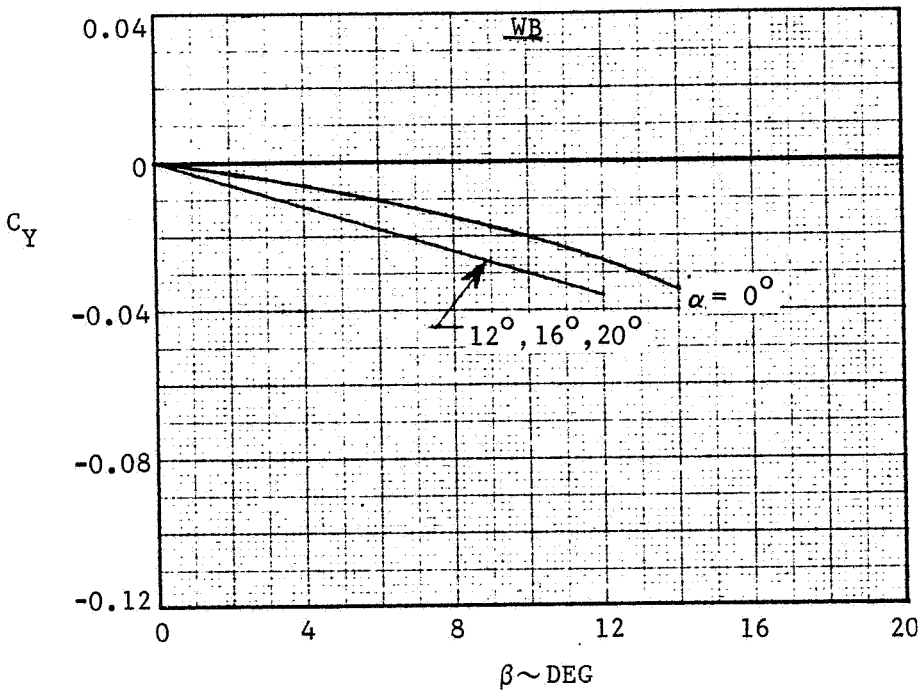

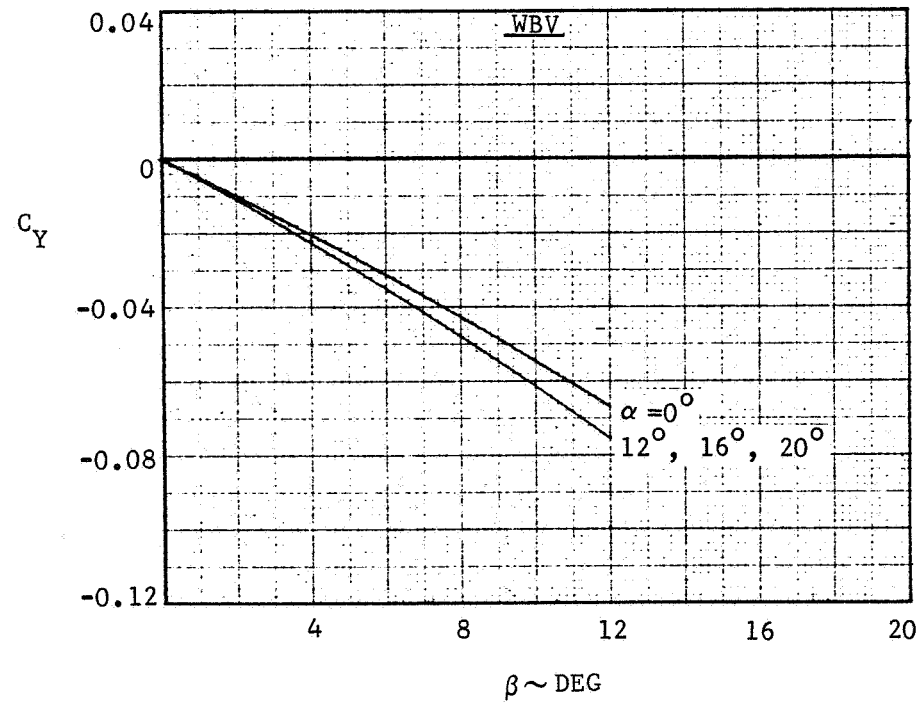

FIGURE 3-69. SIDE FORCE AT M 1.6

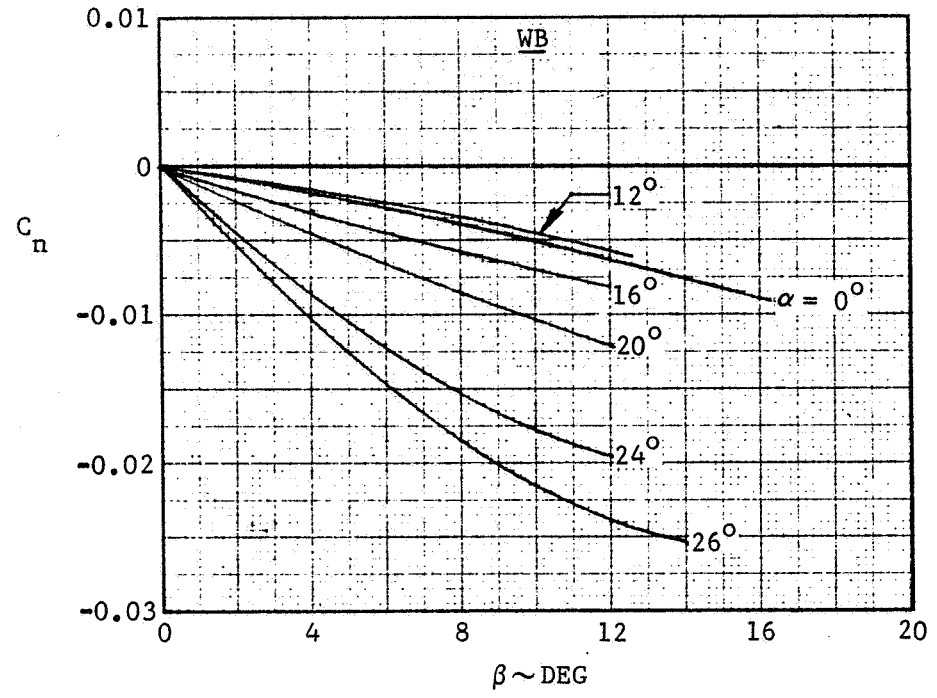

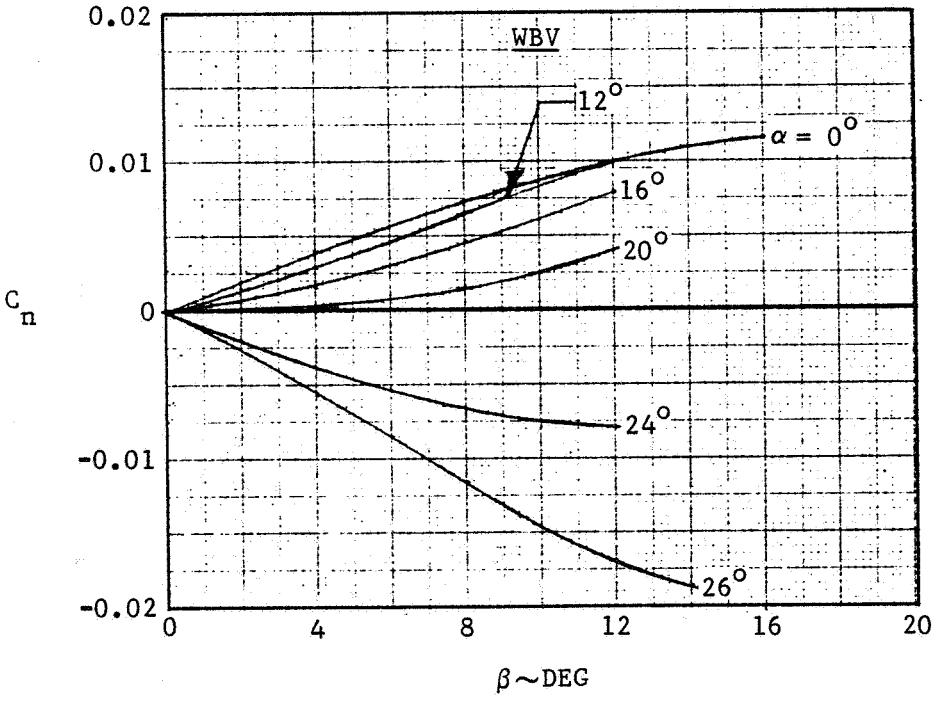

FIGURE 3-70. YAWING MOMENT AT M 0.6

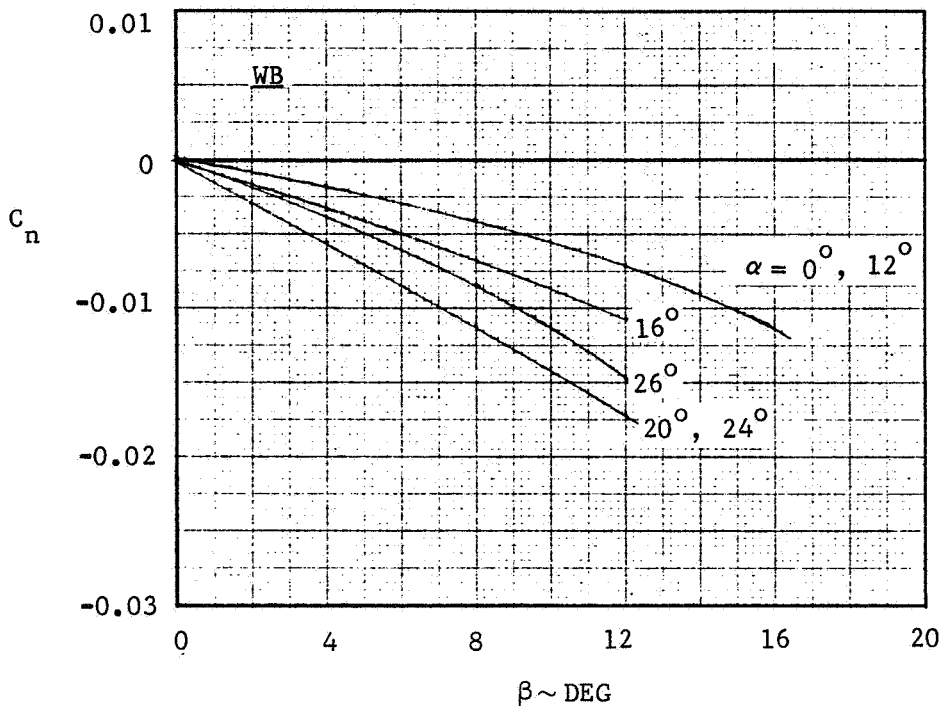

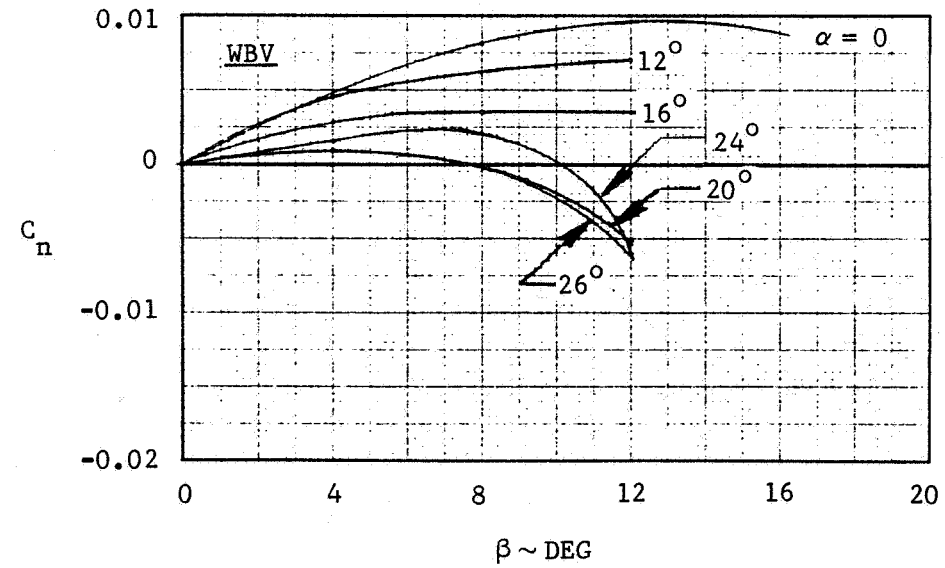

FIGURE 3-71. YAWING MOMENT AT M 0.9

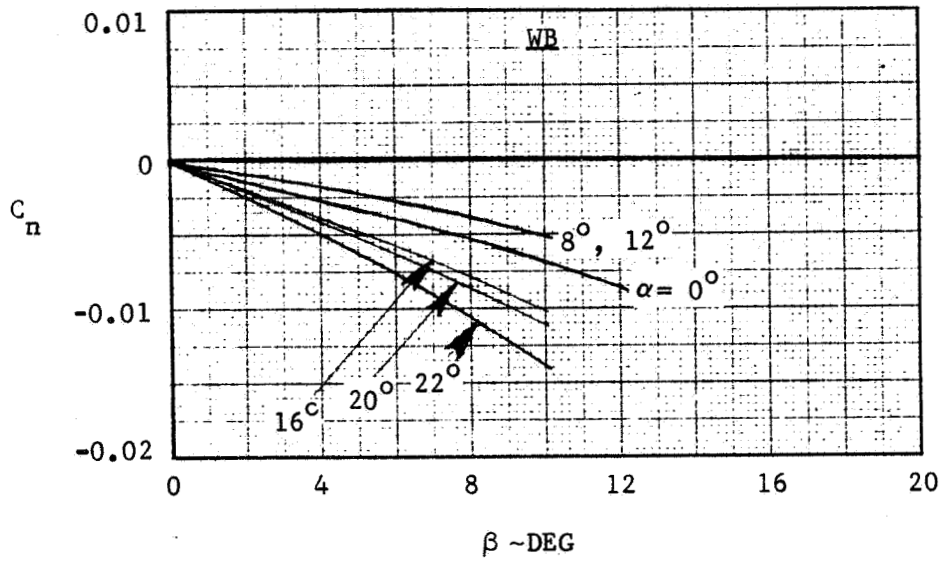

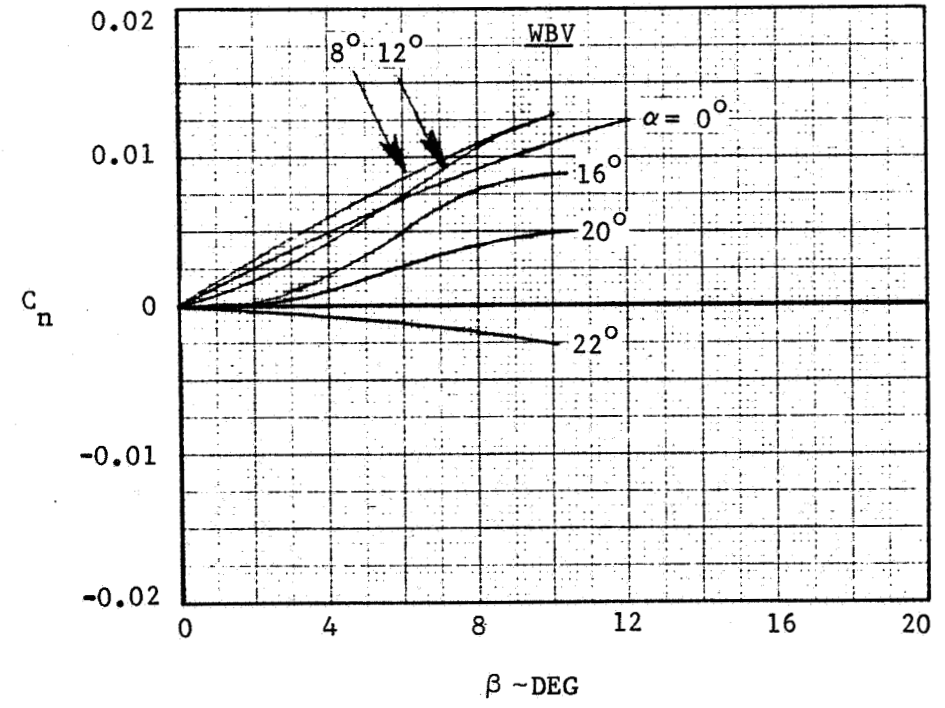

FIGURE 3-72. YAWING MOMENT AT M 1.2

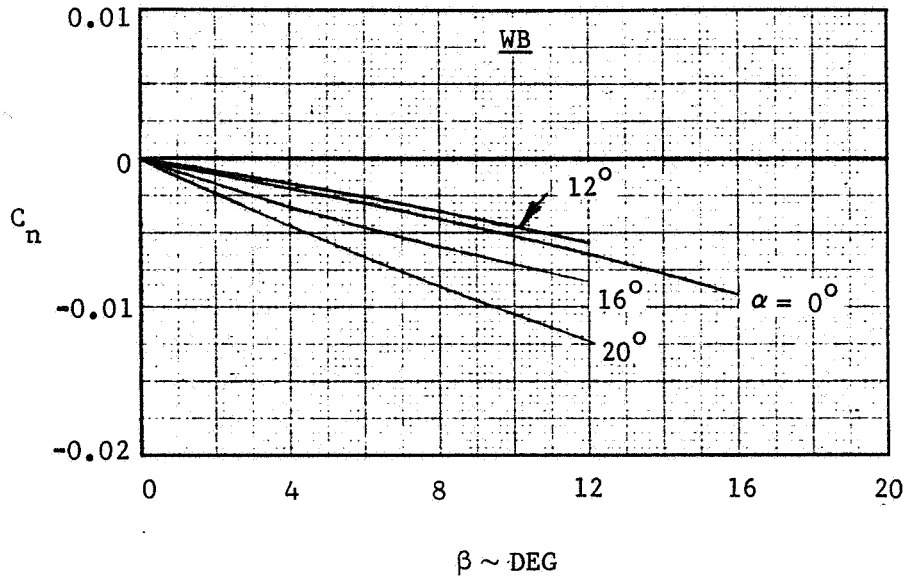

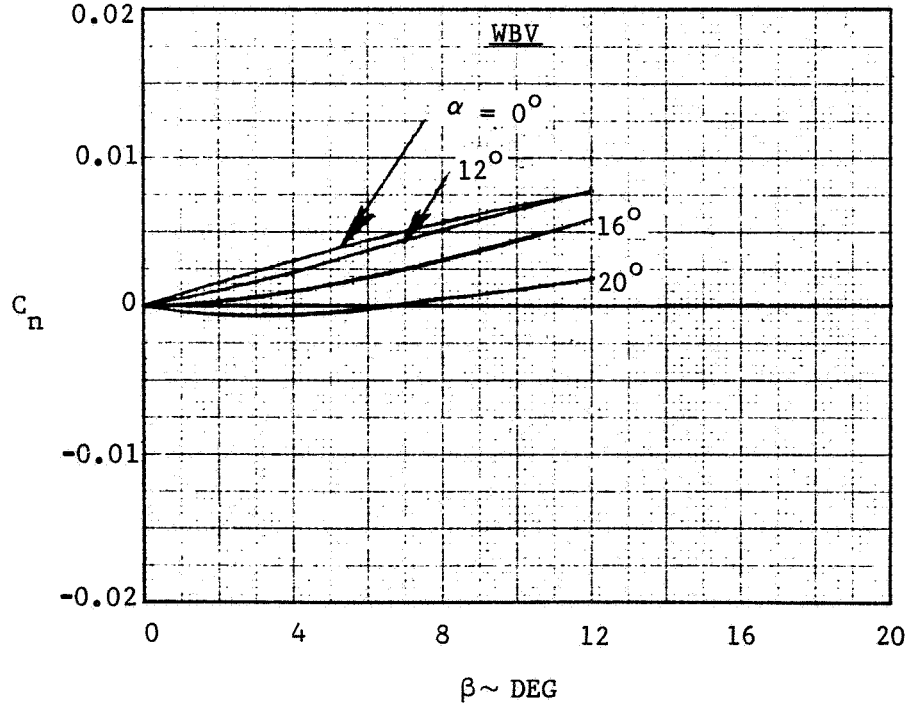

FIGURE 3-73. YAWING MOMENT AT M 1.6

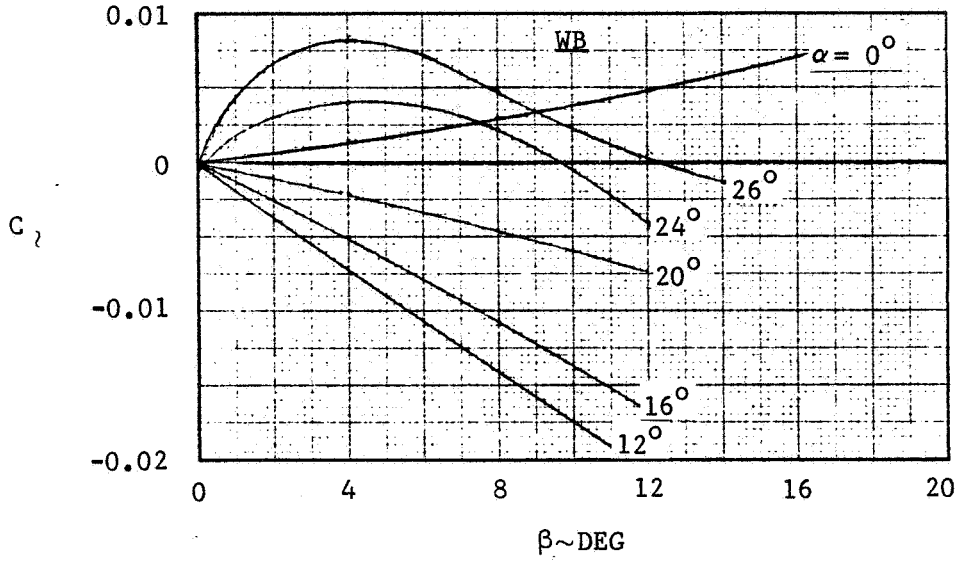

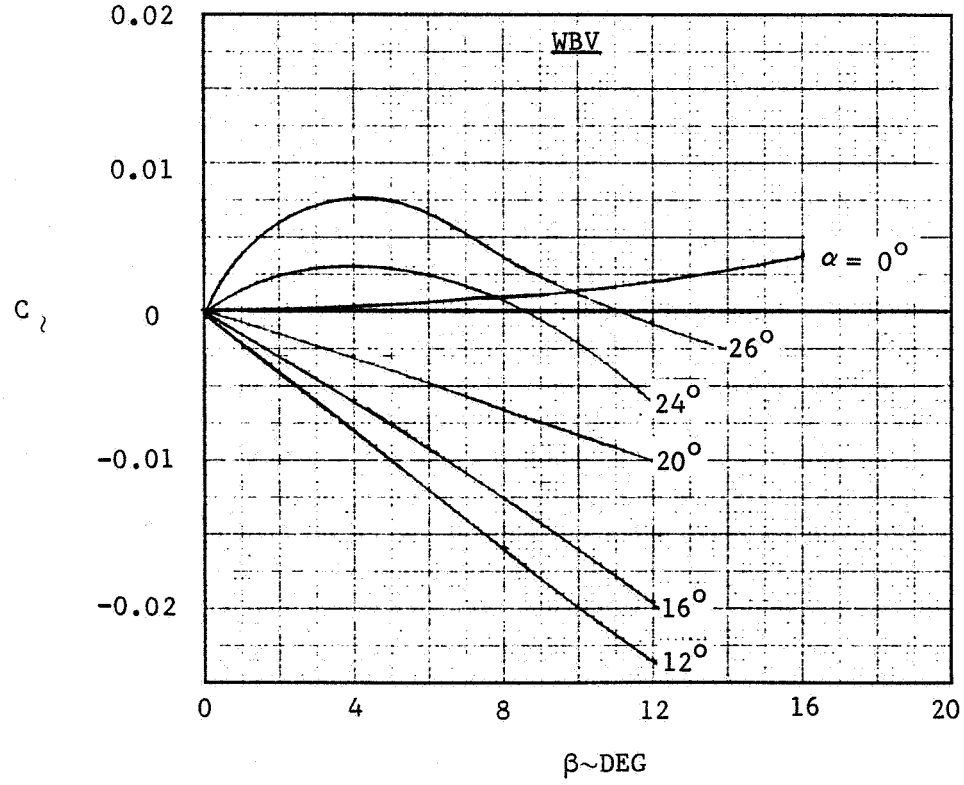

FIGURE 3-74. ROLLING MOMENT AT M 0.6

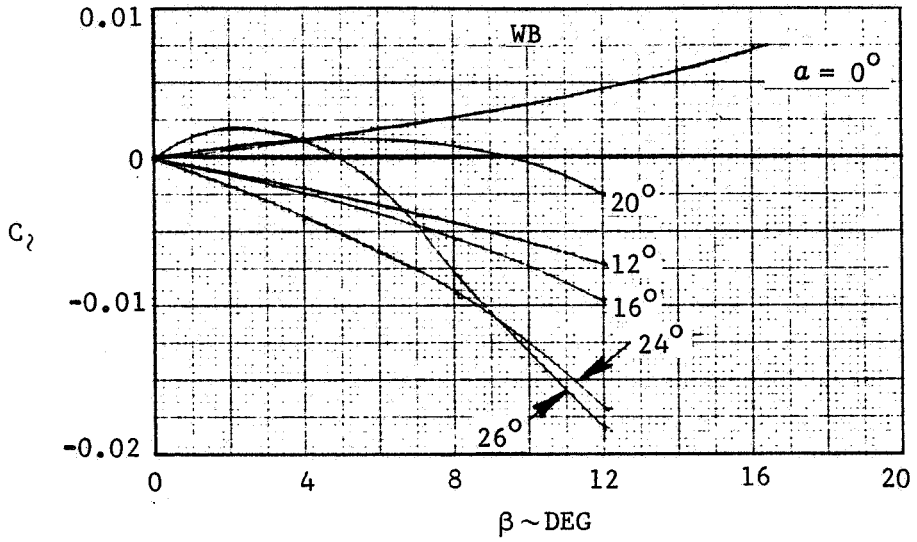

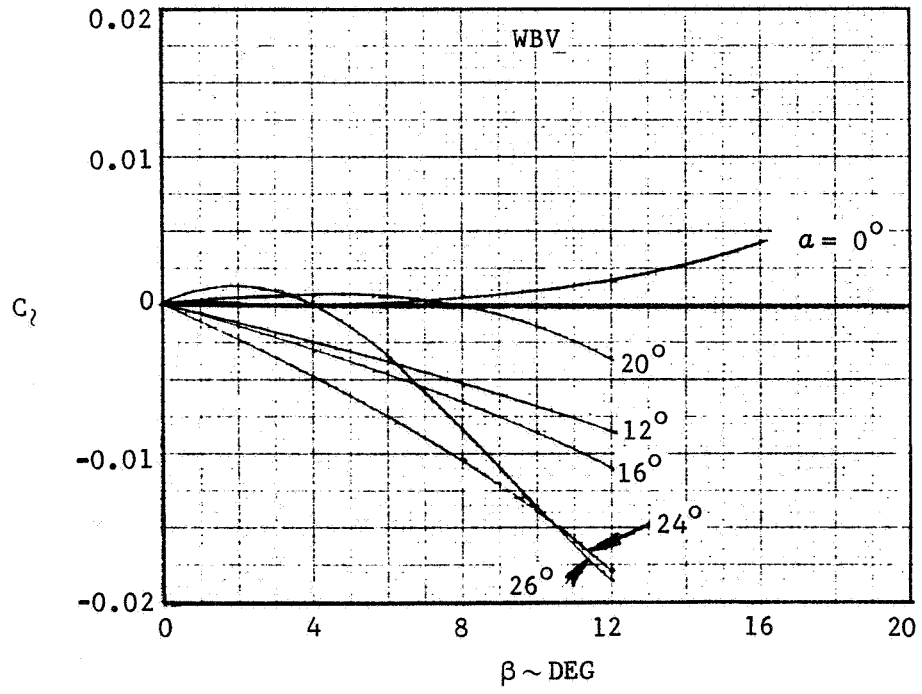

FIGURE 3-75. ROLLING MOMENT AT M 0.9

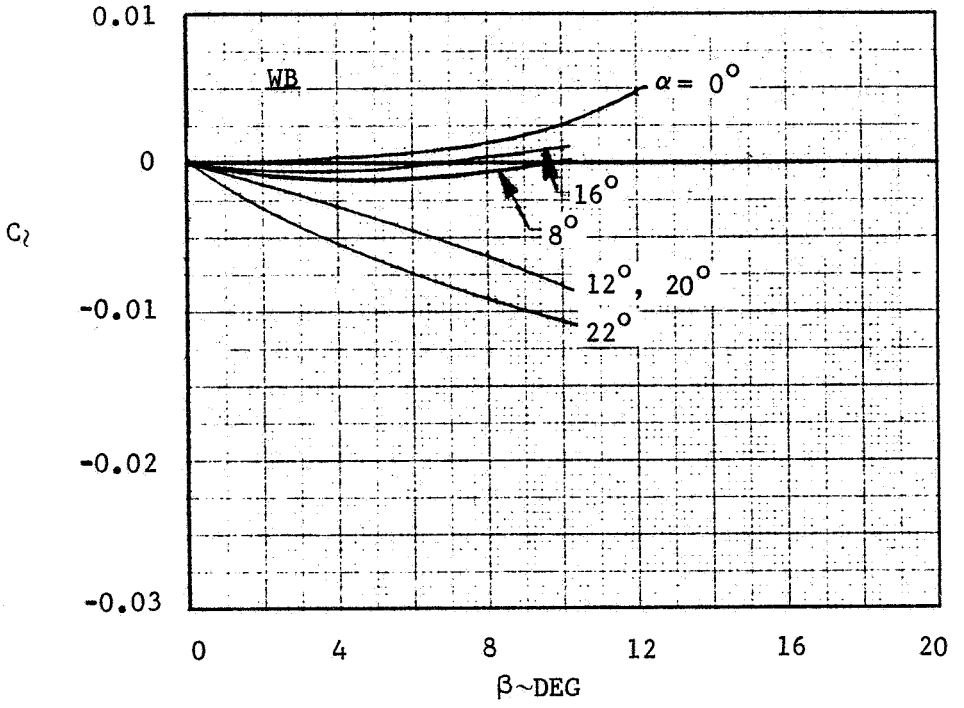

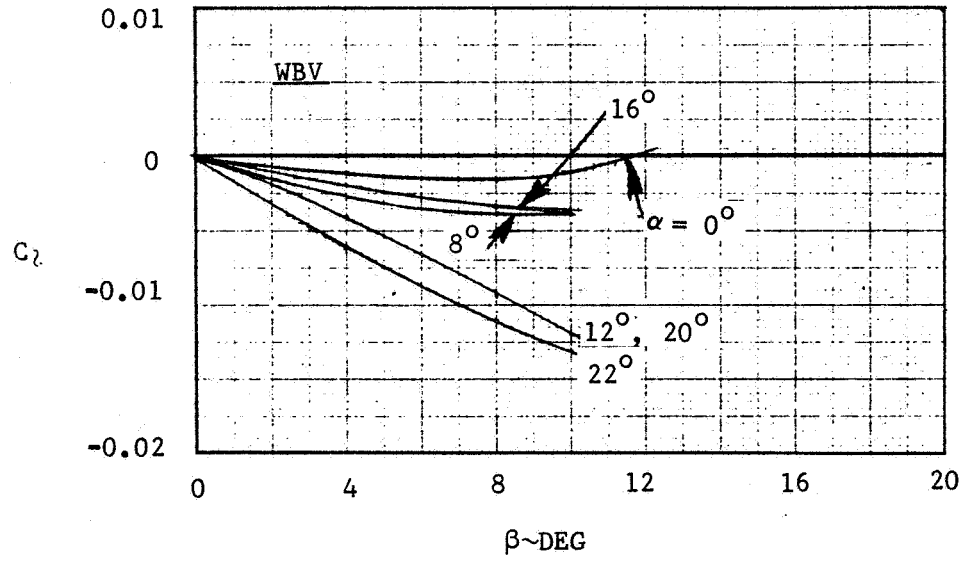

FIGURE 3-76. ROLLING MOMENT AT M 1.2

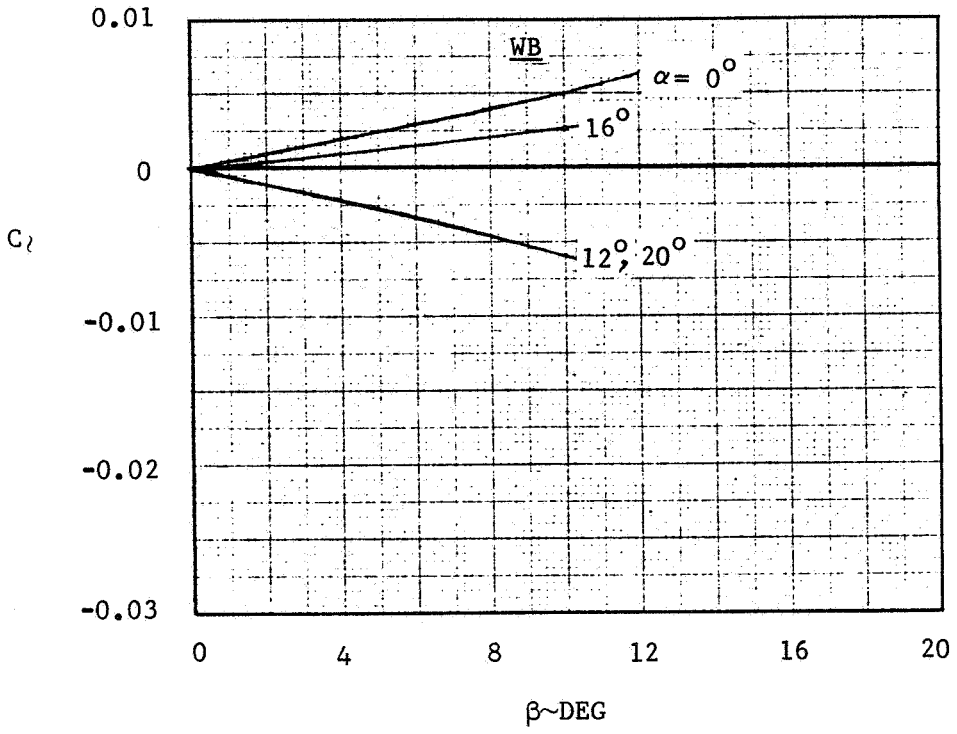

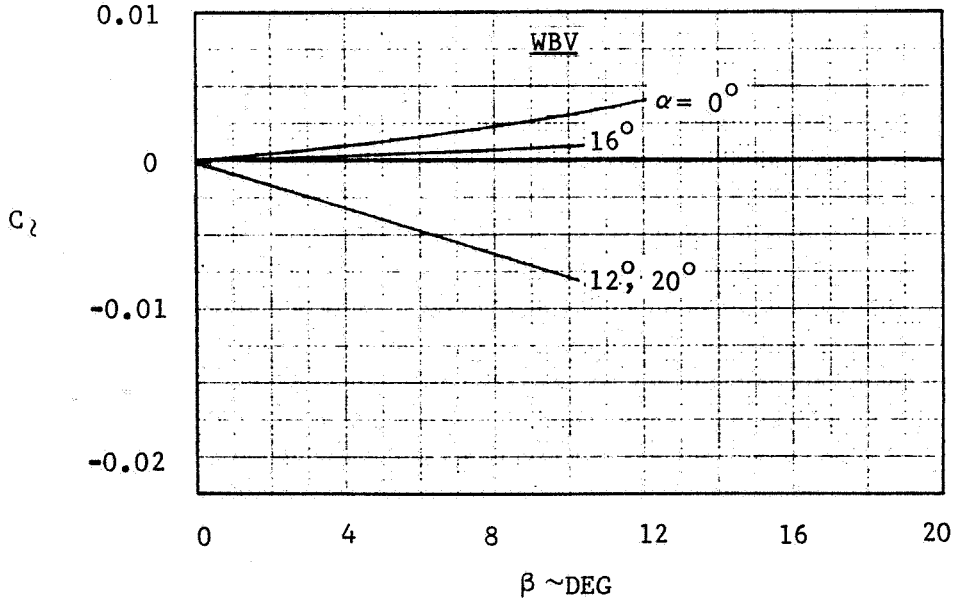

FIGURE 3-77. ROLLING MOMENT AT M 1.6

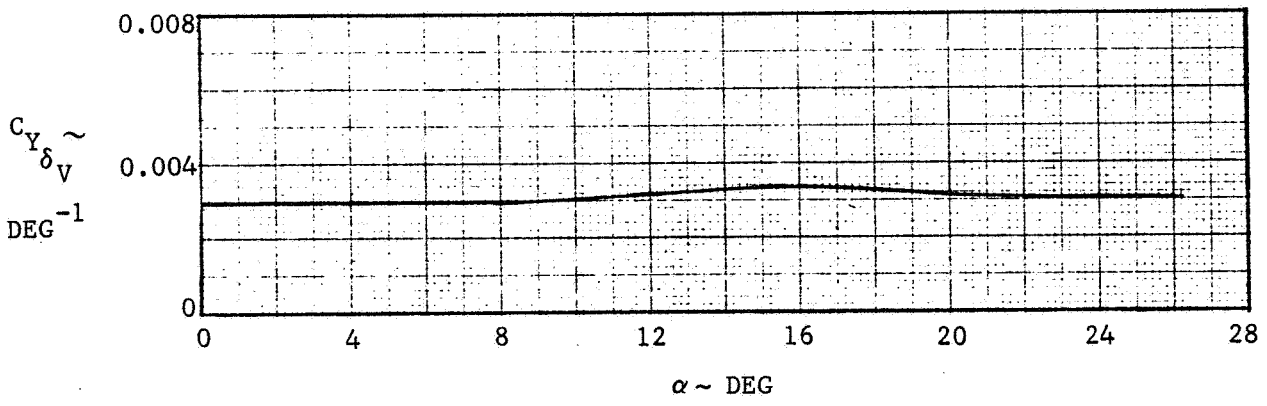

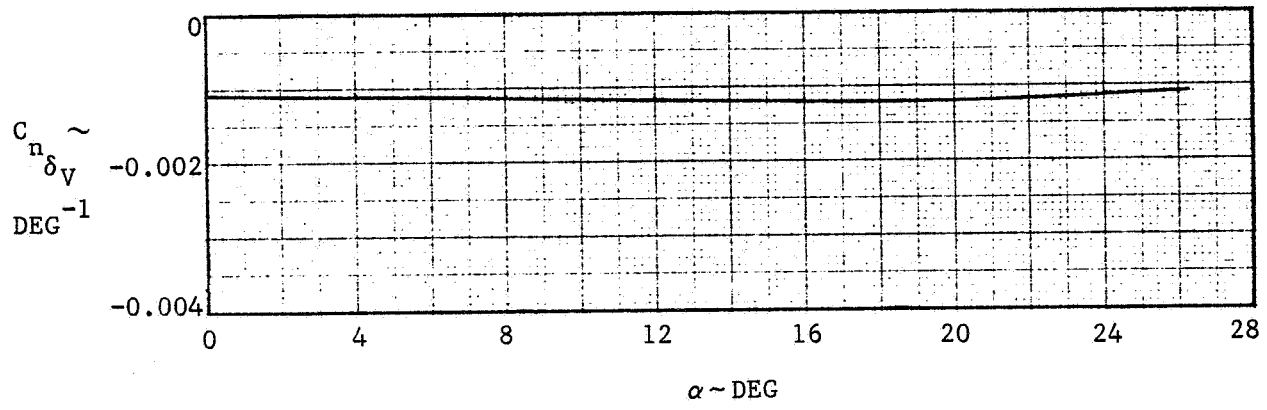

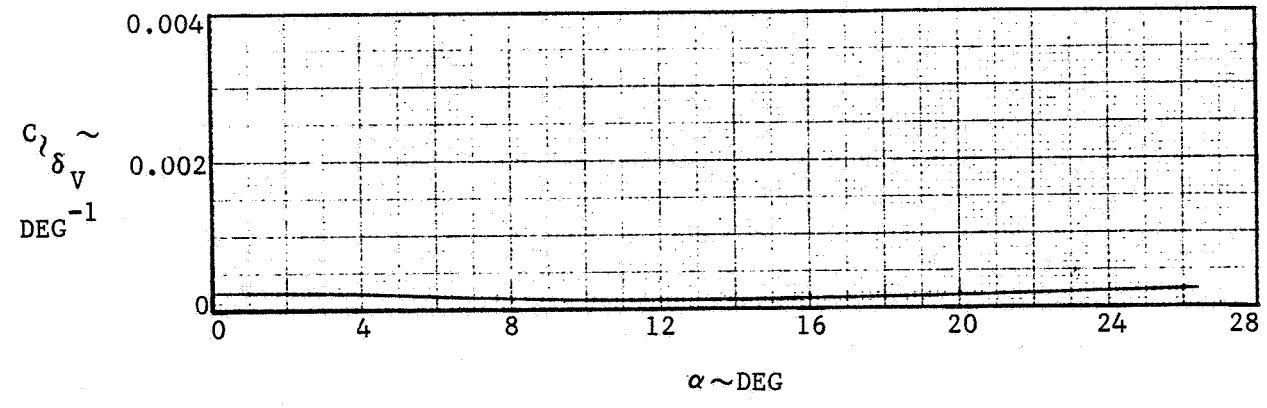

FIGURE 3-78. VERTICAL TAIL CONTROL EFFECTIVENESS AT M 0.6

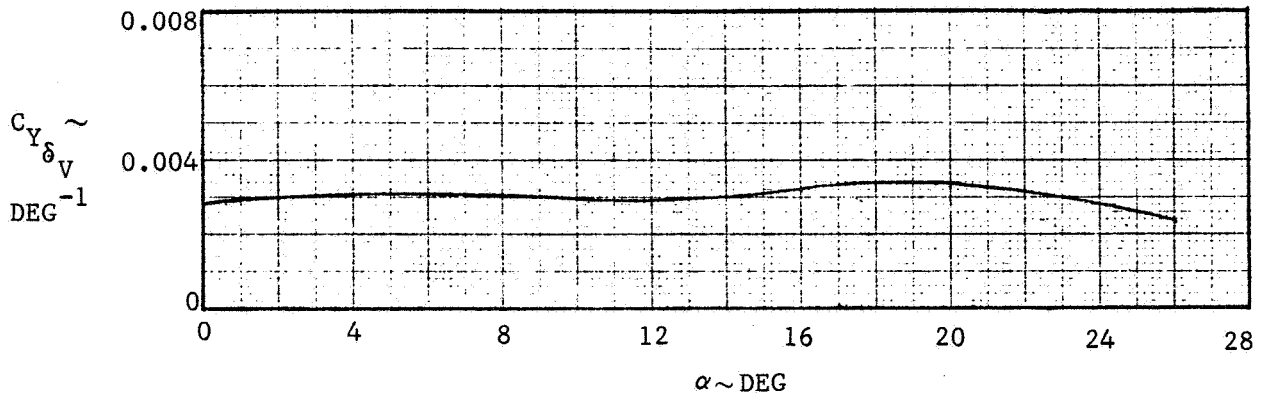

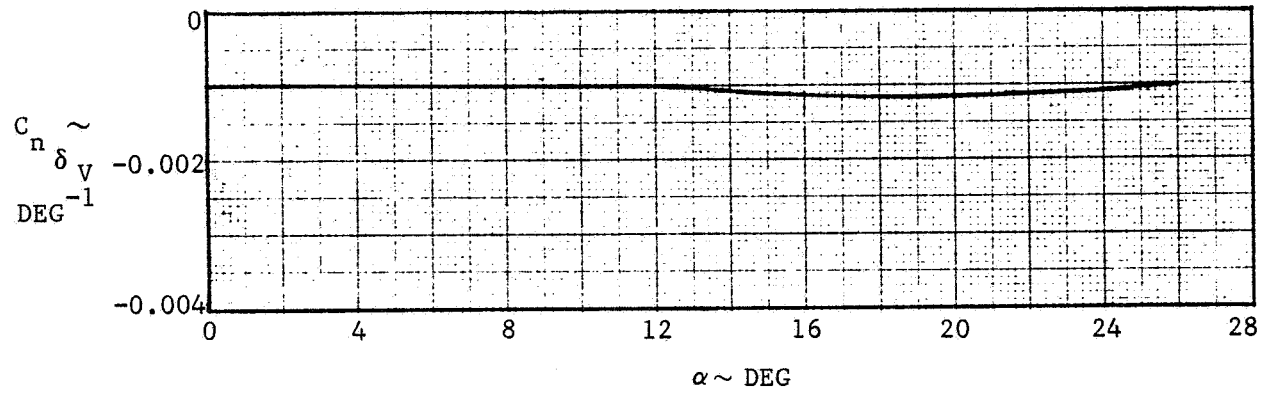

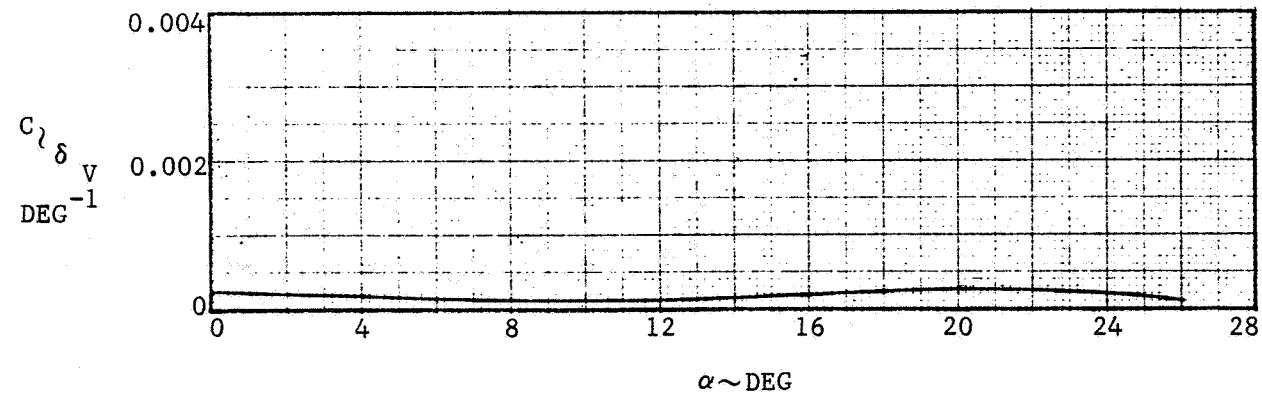

FIGURE 3-79. VERTICAL TAIL CONTROL EFFECTIVENESS AT M 0.9

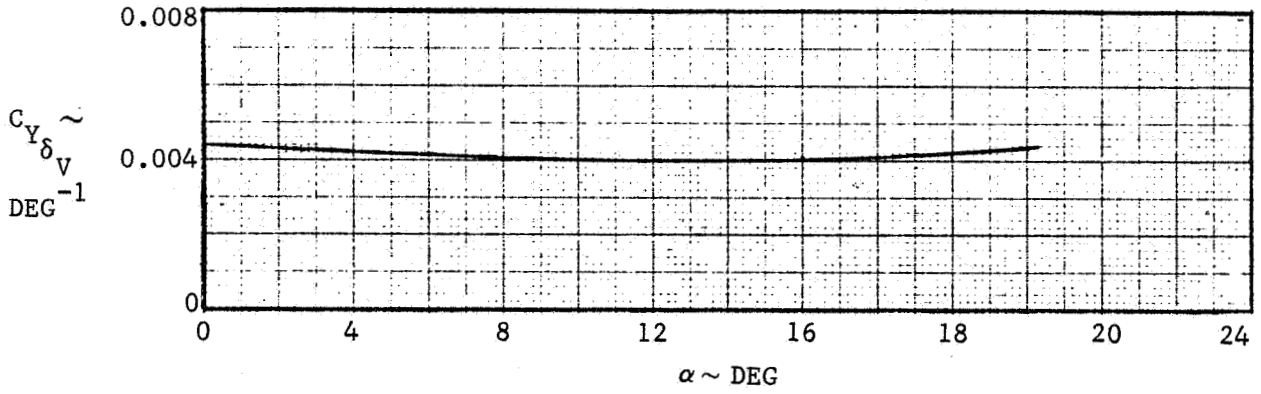

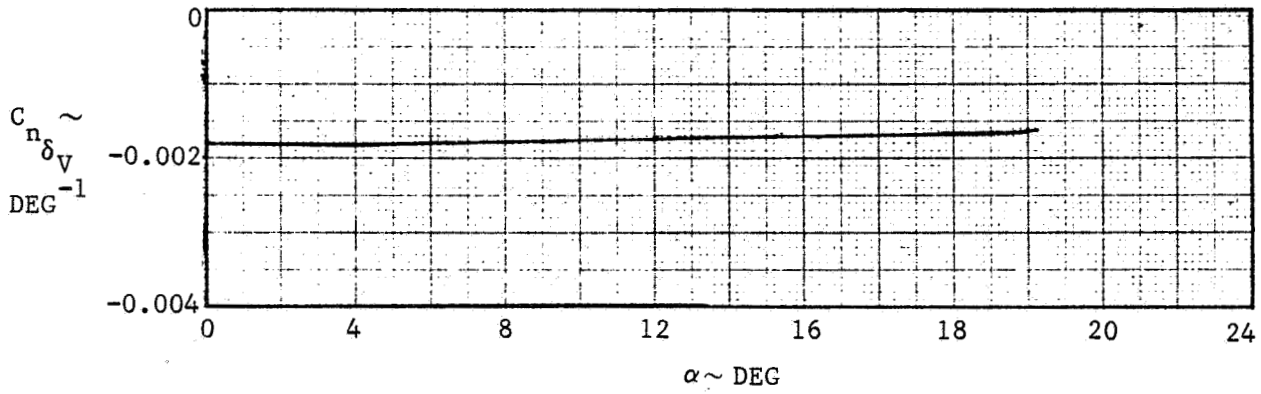

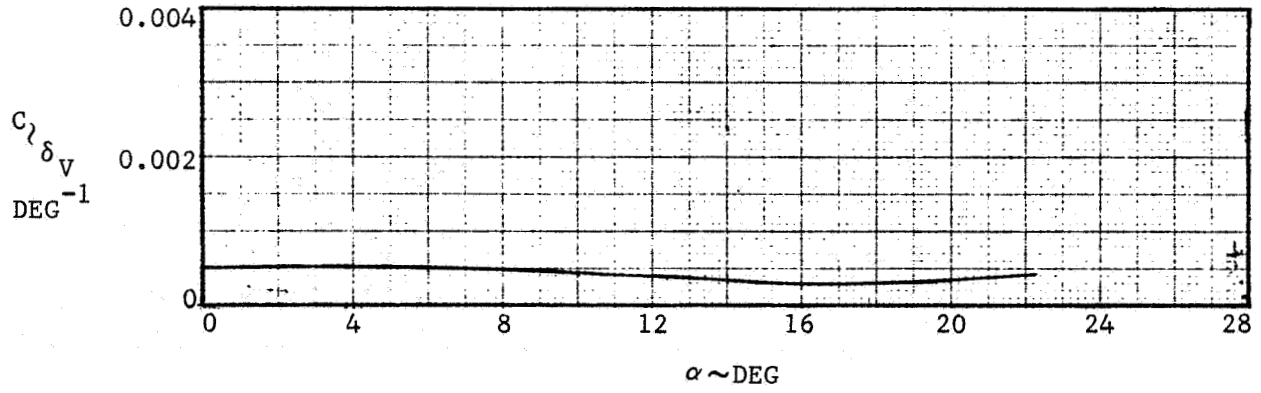

FIGURE 3-80. VERTICAL TAIL CONTROL EFFECTIVENESS AT M 1.2

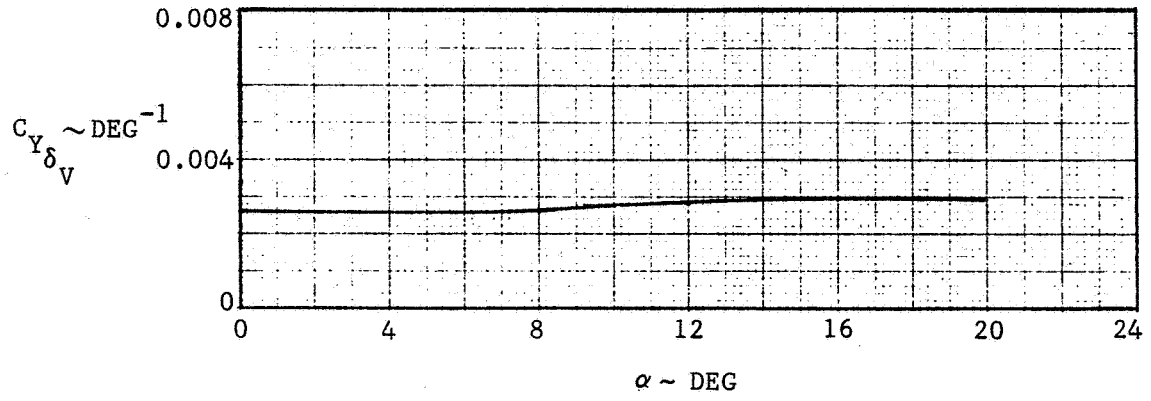

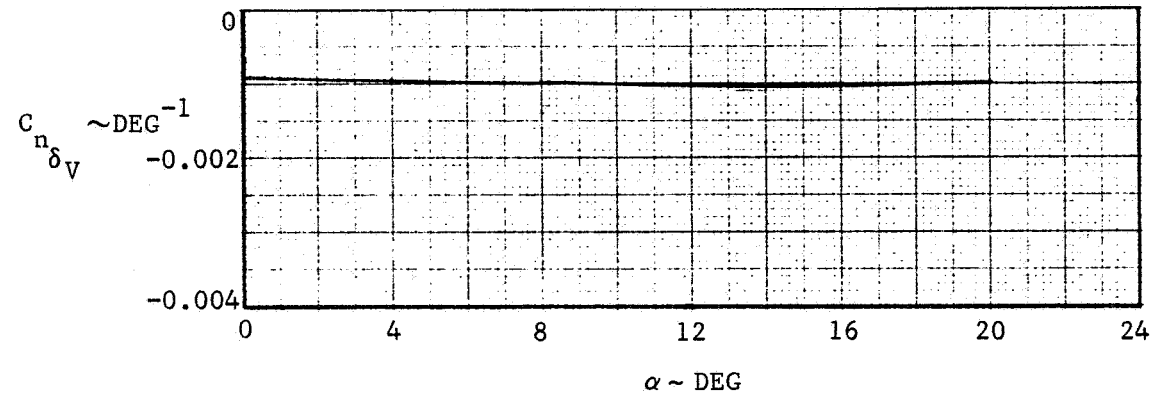

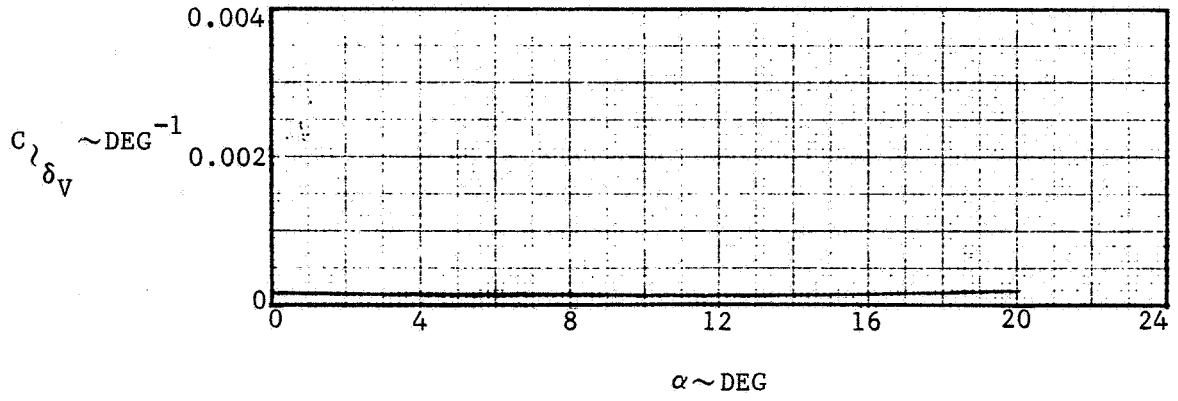

FIGURE 3-81. VERTICAL TAIL CONTROL EFFECTIVENESS AT M 1.6

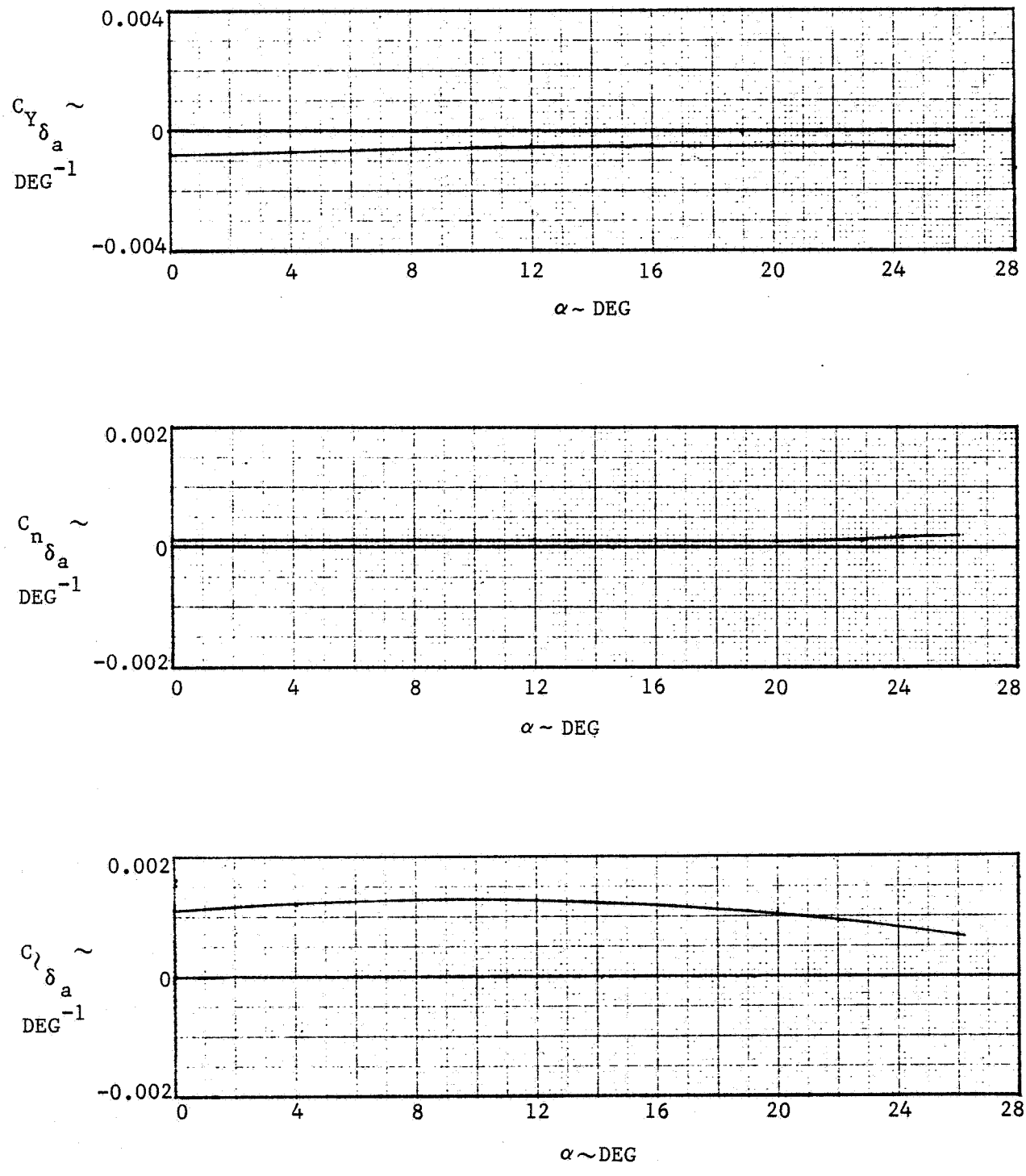

FIGURE 3-82. ELEVON ROLL CONTROL EFFECTIVENESS AT M 0.6

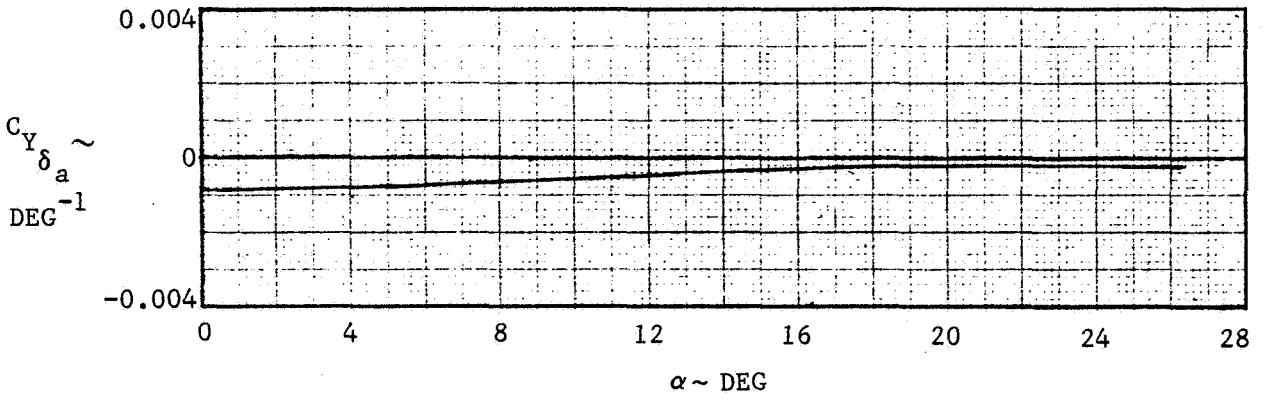

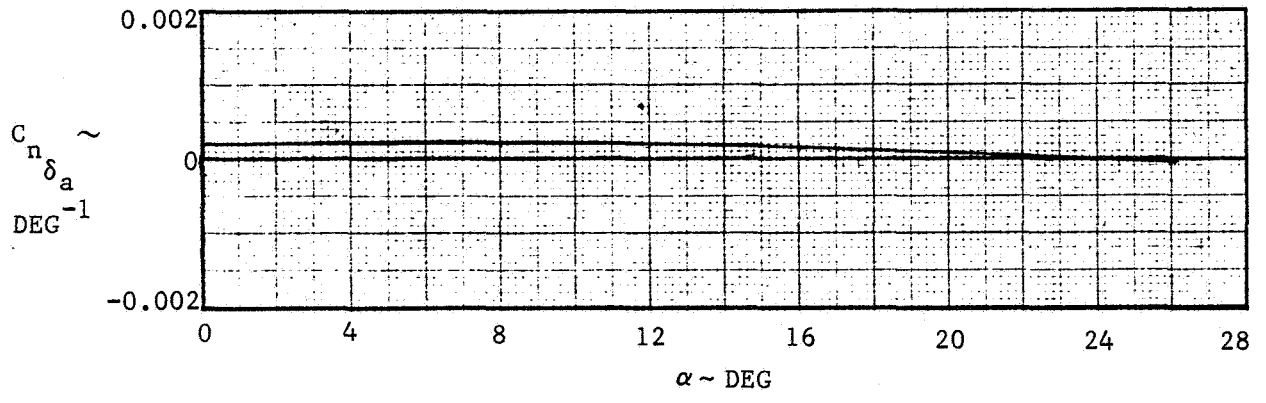

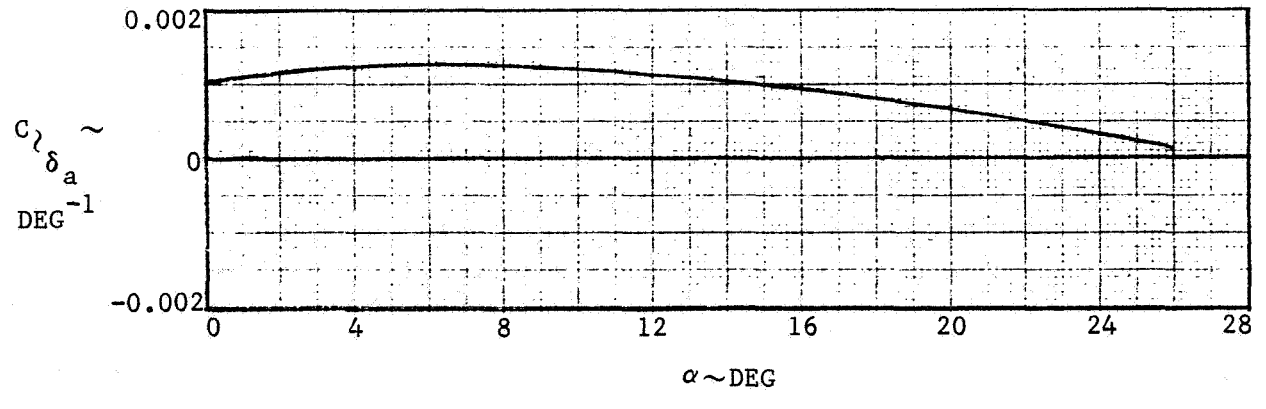

FIGURE 3-83. ELEVON ROLL CONTROL EFFECTIVENESS AT M 0.9

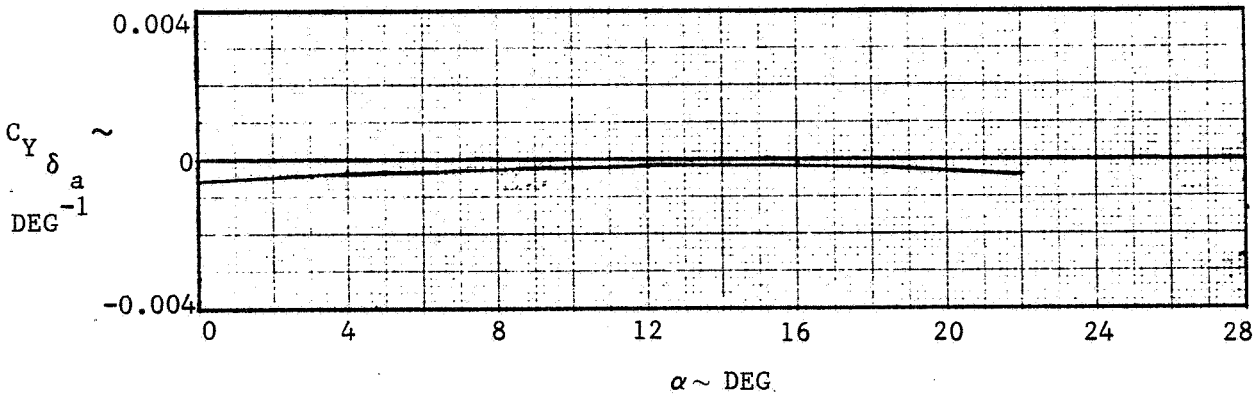

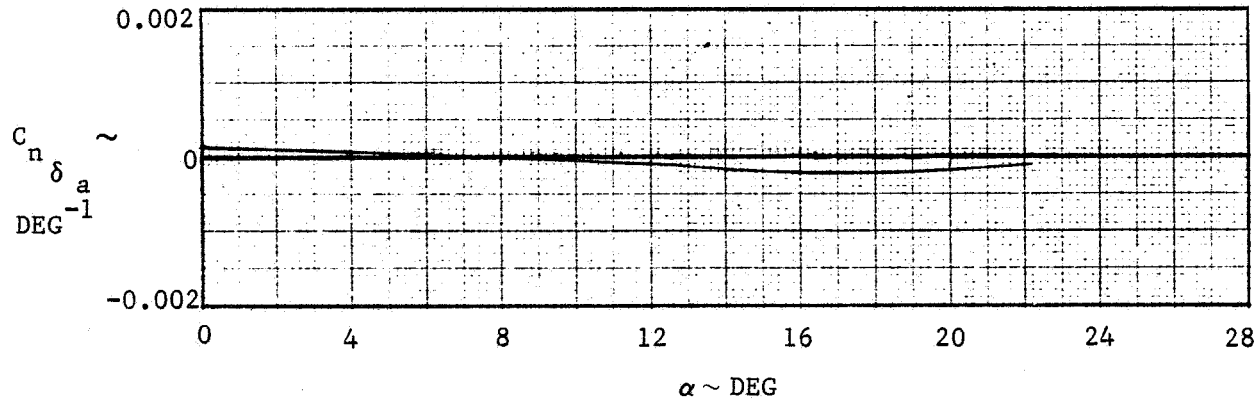

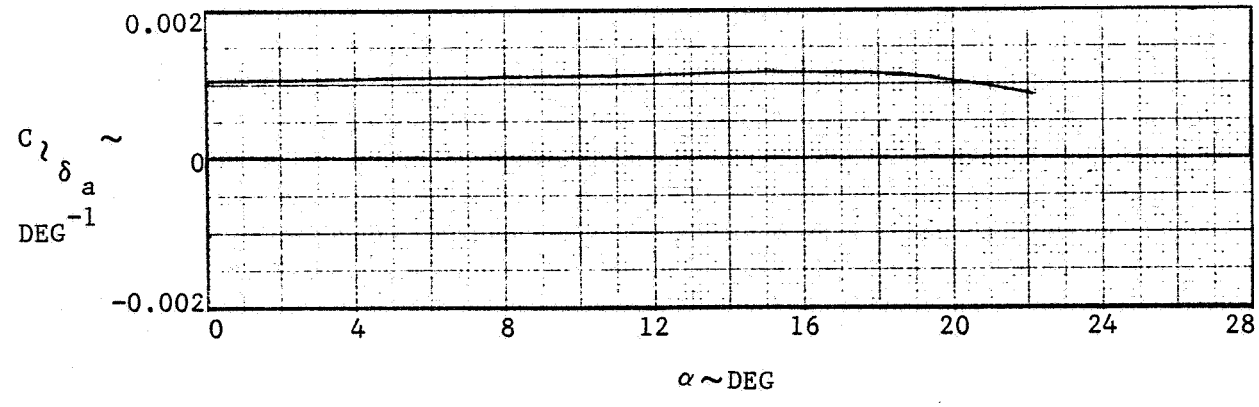

FIGURE 3-84. ELEVON ROLL CONTROL EFFECTIVENESS AT M 1.2

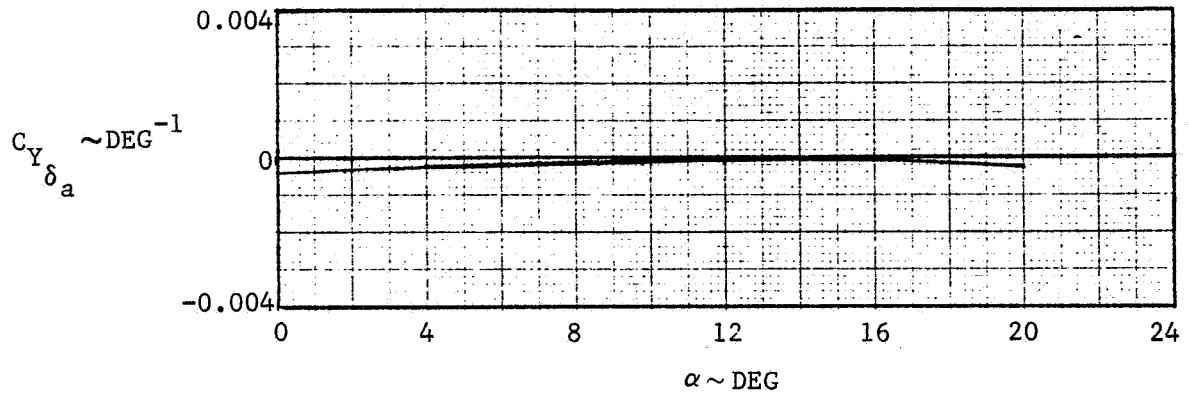

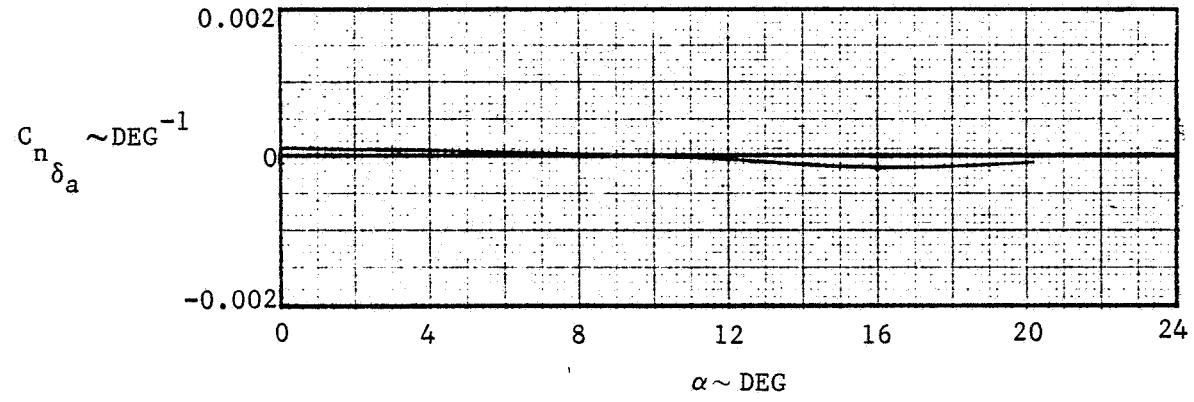

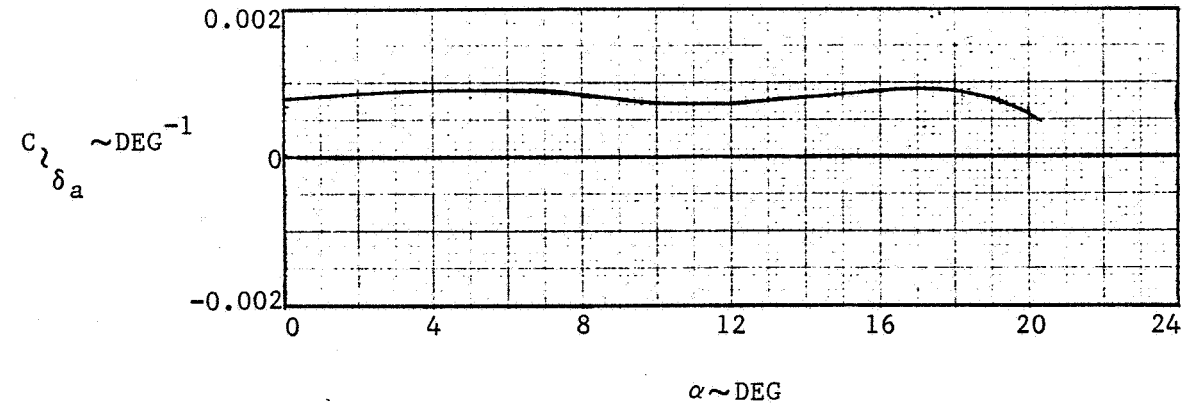

FIGURE 3-85. ELEVON ROLL CONTROL EFFECTIVENESS AT M 1.6

3.4 PROPULSION INDUCED EFFECTS

A vertical attitude vehicle inherently minimizes propulsive lift interference problems and ingestion of exhaust gases. In contrast to the horizontal attitude configuration, neither large nozzle deflections nor multiple exhaust locations are required. However, there is the potential for generation of sea spray which could intefere with pilot visibility, be ingested into the engine and impinge on aircraft structure. A limited study of available data has been made, a simple correlation formula generated and spray height estimates made.

Experiments done with small-scale jet nozzles at NASA Langley and observations of the X-13 suggest that operation of a VATOL vehicle may produce considerable salt water spray. The effects of this spray on visibility, corrosion, and thrust loss (due to water ingestion) could be considerable. Although a few experiments have been conducted with scale model jets to determine spray height as a function of various flow parameters (references 13 and 14), none resulted in a parametric formula for spray height that satisfactorily predicts full-scale results. This section presents the results of an analysis to find a parameter which correlates the available jet nozzle data, so that the spray height for the configuration may be estimated.

Considering the physics of this problem, spray height (H_S) is assumed to be a function of the nozzle exit dynamic pressure (Q_N), the height of the nozzle above the water's surface (H_N), the nozzle diameter (D), the density of the water (ρ_W), and the acceleration due to gravity (g).

Thus,

$$H_S = F(Q_N, H_N, D, \rho_W, g)$$

Writing H_S as a power series,

$$\sum_{\alpha=-\infty}^{\infty} \sum_{\beta=-\infty}^{\infty} \sum_{\gamma=-\infty}^{\infty} \sum_{\epsilon=-\infty}^{\infty} \sum_{\lambda=-\infty}^{\infty} C_{\alpha\beta\gamma\epsilon\lambda}\, Q_N^{\alpha}\, H_N^{\beta}\, D^{\gamma} \rho_w^{\epsilon} g^{\lambda}$$ in which $C_{\alpha\beta\gamma\epsilon\lambda}$ are constants,

Dimensional analysis shows that

$$\lambda = -\alpha$$

$$\epsilon = -\alpha$$

and

$$\gamma = 1 \quad -\alpha - \beta$$

so that

$$H_S/H_N = \sum_{\alpha=-\infty}^{\infty} \sum_{\beta=-\infty}^{\infty} C_{\alpha\beta} \left(\frac{Q_N}{\rho_w g H_N}\right) \left(\frac{H_N}{D}\right)^{\alpha+\beta-1}$$

Data on the spray height produced by jet nozzles, expressed in the form of the parameters used in this analysis (Q_N, H_N, D) were obtained from Richard Kuhn of NASA Langley, and are summarized in Table 3-6. Data on the X-13 airplane was obtained from photographs of the aircraft in operation. These data are used to determine α, β and C. To determine α; H_N and D are held constant. This gives the relation

$$H_S = \sum \quad K_\alpha Q_N^\alpha \text{ where "}K_\alpha\text{" is a constant.}$$

This is seen plotted on log-log scale in Figure 3-86 for a number of values of H_N and D. It is observed that the data for each H_N/D lie reasonably well on a straight line. The slopes of these lines were determined using a linear regression curve fitting procedure. The value of α is determined from the average of the slopes of these lines.

$$\alpha = \frac{0.92 + 0.95 + 0.78 + 1.36}{4} = 1.00$$

This gives

$$\frac{H_S}{H_N} = \sum_{\beta=-\infty}^{\infty} C_\beta \left(\frac{Q_N}{\rho_w g H_N}\right) \left(\frac{H_N}{D}\right)$$

Note that this dimensionless equation contains the group $(Q_N/\rho_w g H_N)$ which is a Froud number for this problem. The Froud number is an important scaling parameter for systems involving the free surface behavior of water (reference 15).

The value of β is determined in a similar manner. The data have been plotted on log-log scale in Figure 3-87. A linear regression curve fitting procedure was used to determine a line through these points. The resulting equation is:

$$\log \left(\frac{H_S}{Q_N}\right) = 0.539 \log \left(\frac{H_N}{D}\right) + \log (0.1407)$$

This becomes, upon rearranging,

$$\frac{H_S}{H_N} = 0.1407 \left(\frac{Q_N}{H_N}\right) \left(\frac{H_N}{D}\right)^{-0.539}$$

indicating that

$$\beta = 0.539$$

and

$$C_\beta = 0.1407\ \rho_w g = 282.$$

The final equation for estimating spray height in terms of nondimensional quantities is

$$\frac{H_S}{H_N} = 282 \left(\frac{Q_N}{H_N \rho_w g}\right) \left(\frac{H_N}{D}\right)^{-0.539}$$

The data are plotted in Figure 3-88, as a function of the calculated value of H_S/H_N. Although there is a great deal of scatter, the results appear to be randomly spread about the predicted values. Note that the full scale X-13 points lie very close to the predicted values. Also note that essentially all of the data lies within 20 percent of the predicted values. For an analysis of this sort, 20 percent error is most reasonable.

The following approximations of the VATOL spray height are based on the information and assumptions in Table 3-7. Nozzle conditions at maximum power are used for both takeoff and landing. The equivalent jet diameter is

$$D = 2\sqrt{\frac{2A_e}{\pi}} = 0.719 \text{ m } (2.36 \text{ ft})$$

where D = diameter of a single jet with the same area as the two VATOL jets.

Spray heights calculated for operation from two types of carriers are:

	LPH	CVN
	H_S, m (ft)	H_S, m (ft)
Takeoff	29.3 (96)	22.9 (75)
Landing	21.3 (70)	16.8 (55)

Figure 3-89 is a carpet plot showing how each of the physical parameters affects the spray height. Two X-13 operating points, as well as the operating points for the VATOL configuration during both takeoff and landing for the two different carriers, are indicated on this plot.

Clearly, more test data on this problem, particularly for large nozzle diameters (1-2 feet) and high nozzle dynamic pressures (1000-3000 lbs/ft^2), are needed before an accurate prediction of spray height can be made. The effects of temperature, insofar as steam may be produced, have been ignored and should be investigated in future tests. In spite of this, an estimate of spray height can be made using the empirical equation derived here. For the VATOL concept operating from an LPH carrier, spray heights between 70 and 96 feet are predicted, and between 55 and 75 feet for the VATOL operating from a CVH carrier. This spray will clearly affect the operating environment of the aircraft in takeoff and landing and is a potentially serious problem.

TABLE 3-6 SPRAY HEIGHT DATA

	D		Q_N		H_N		H_S	
	m	ft	N/m^2	lb/ft^2	m	ft	m	ft
	0.102	0.33	1355	28.3	0.203	0.67	0.813	2.67
	0.102	0.33	876	18.3	0.203	0.67	0.508	1.67
	0.102	0.33	397	8.3	0.203	0.67	0.356	1.17
	0.102	0.33	158	3,3	0.203	0.67	0.102	0.33
	0.102	0.33	1355	28.3	0.406	1.33	0.569	1.87
	0.102	0.33	876	18.3	0.406	1.33	0.406	1.33
	0.102	0.33	397	8.3	0.406	1.33	0.179	0.59
	0.102	0.33	3433	71.7	0.610	2.00	1.219	4.00
	0.102	0.33	1518	31.7	0.610	2.00	0.610	2.00
	0.102	0.33	239	5.0	0.610	2.00	0.152	0.50
	0.102	0.33	4788	100.0	0.813	2.67	1.138	3.73
	0.102	0.33	3433	71.7	0.813	2.67	0.950	3.12
	0.102	0.33	1273	26.7	0.813	2.67	0.203	0.67
*	0.509	1.67	61960	1294.0	17.307	56.75	9.866	32.36
*	0.509	1.67	61960	1294.0	22.256	73.00	6.098	20.00

* RYAN X-13 DATA

TABLE 3-7. Nozzle Conditions for Calculating VATOL Spray Height

T_t	Nozzle exit total temperature	2572 (^oR)	1429 (^oK)
P_t	Nozzle exit total pressure	76.2 (lb/in^2)	5.25×10^5 (N/m^2)
A_e	Nozzle exit area	2.63 (ft^2)	0.245 (m^2)
γ	Ratio of specific heats	1.4	1.4
R	Gas constant for air	53.35 ($ft/^oR$)	29.27 ($m/^oK$)
g	Acceleration due to gravity	32.17 (ft/sec^2)	9.81 (m/sec^2)
P_o	Ambient pressure	14.7 (lb/in^2)	1.01×10^5 (N/m^2)
H_N	Height of nozzle above water	*	*
ρ_w	Density of water	62.3 (lb/ft^3)	998 (kg/m^3)

*H_N = 9.14 m (30 ft) for LPH

H_N = 14.63 m (48 ft) for CVN

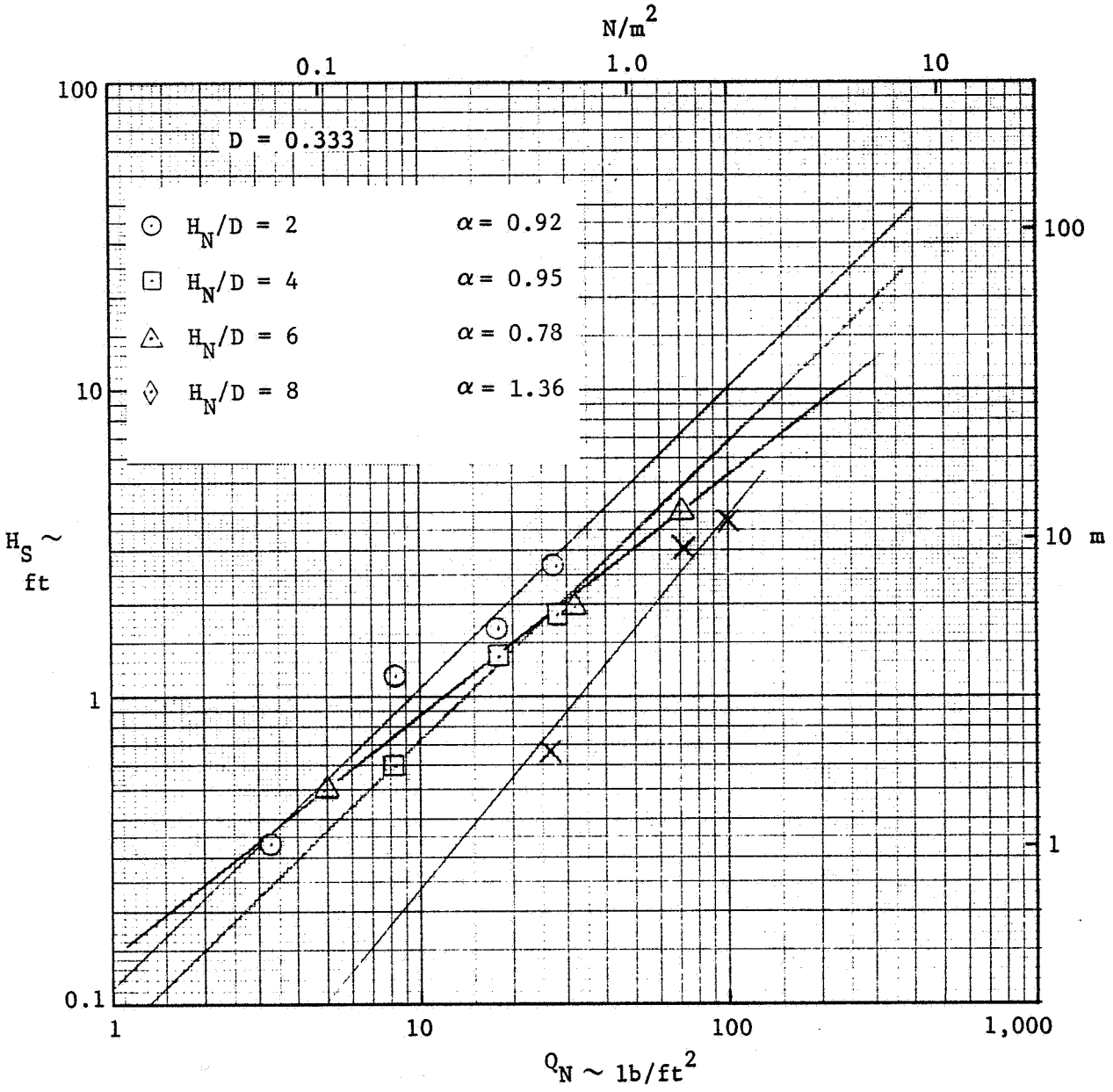

FIGURE 3-86. CORRELATION OF SPRAY HEIGHT FOR VARYING NOZZLE HEIGHT AND DYNAMIC PRESSURE

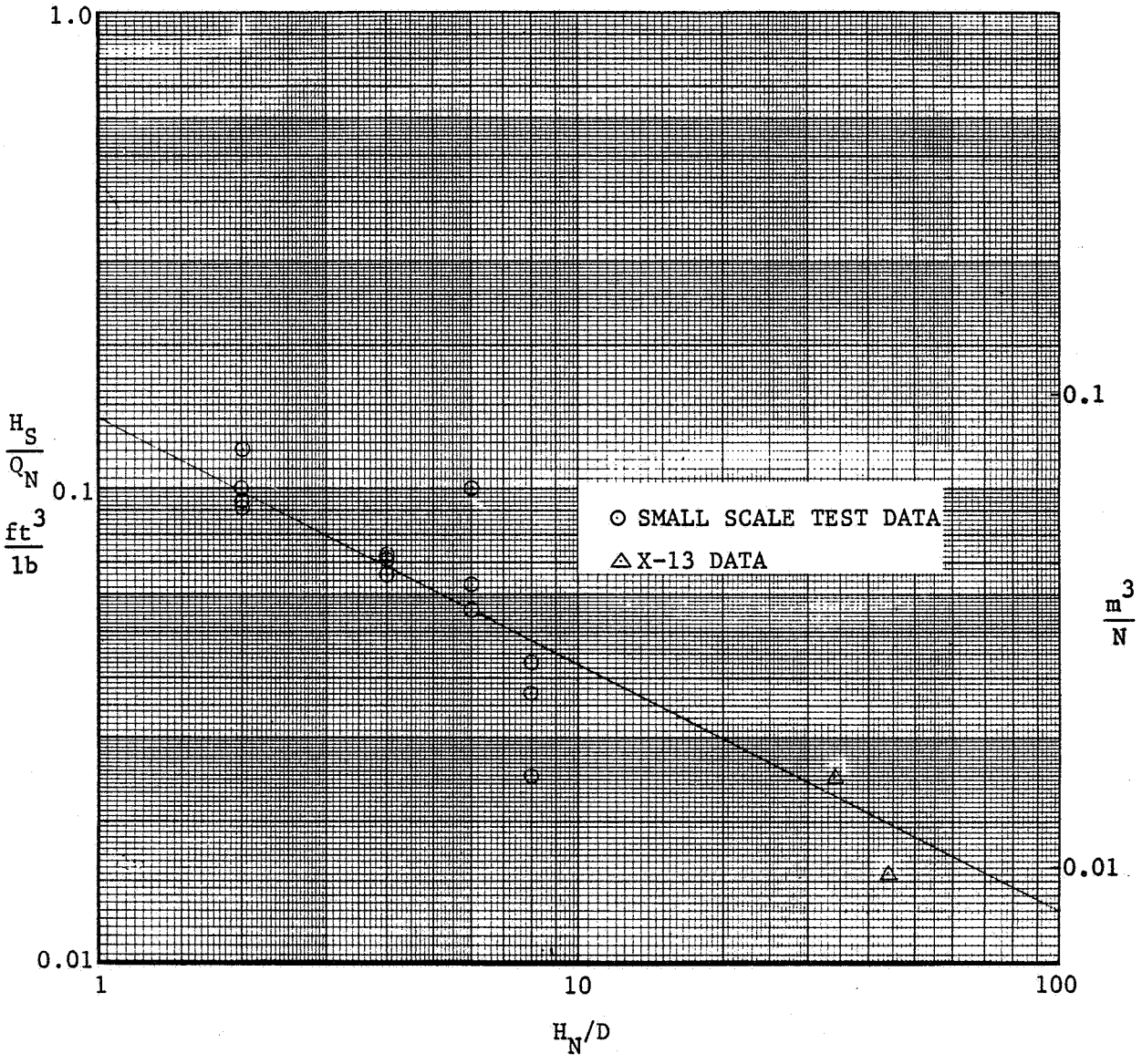

FIGURE 3-87. CORRELATION OF SPRAY HEIGHT DATA

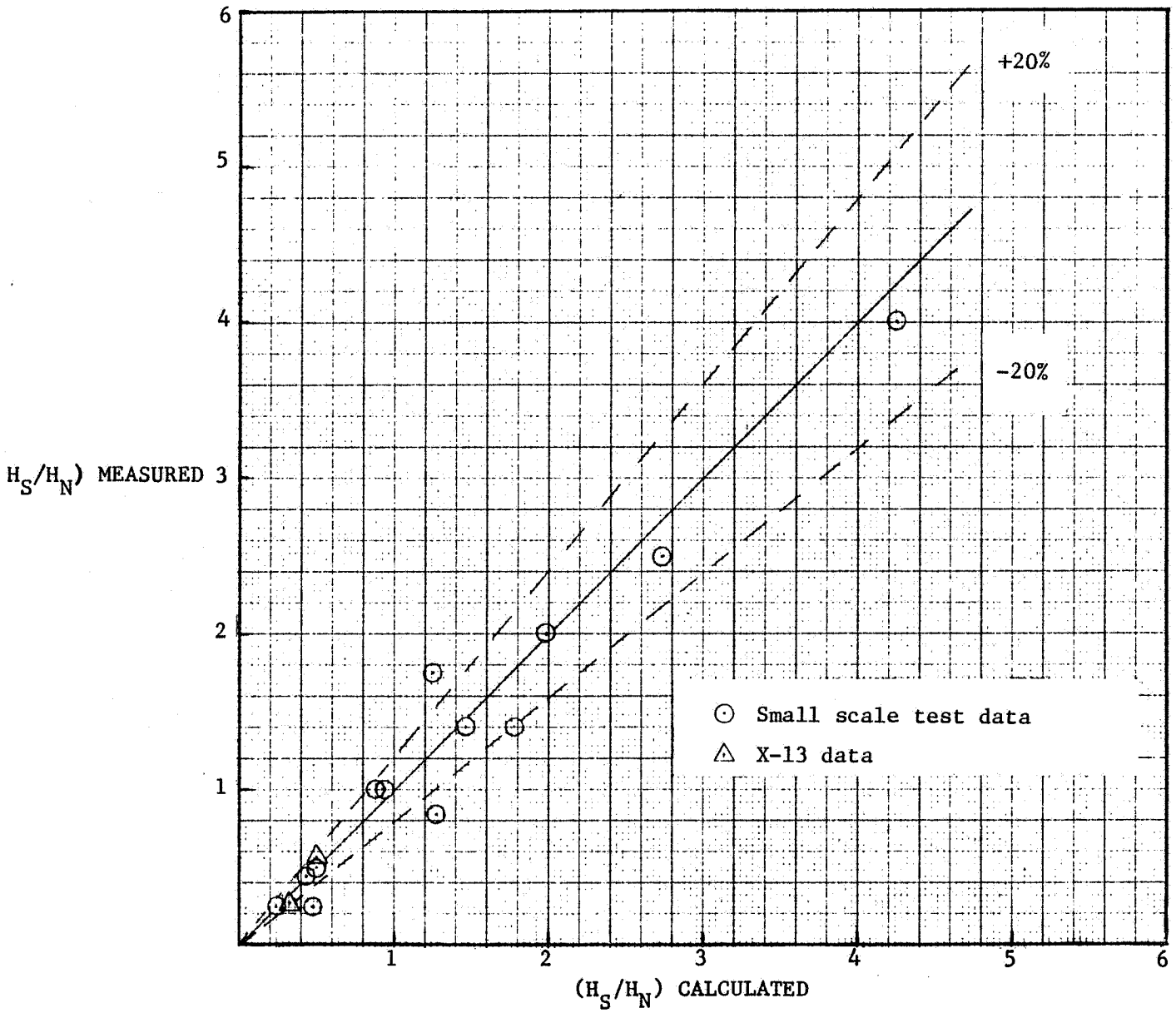

FIGURE 3-88. COMPARISON OF CALCULATED AND TEST SPRAY HEIGHT

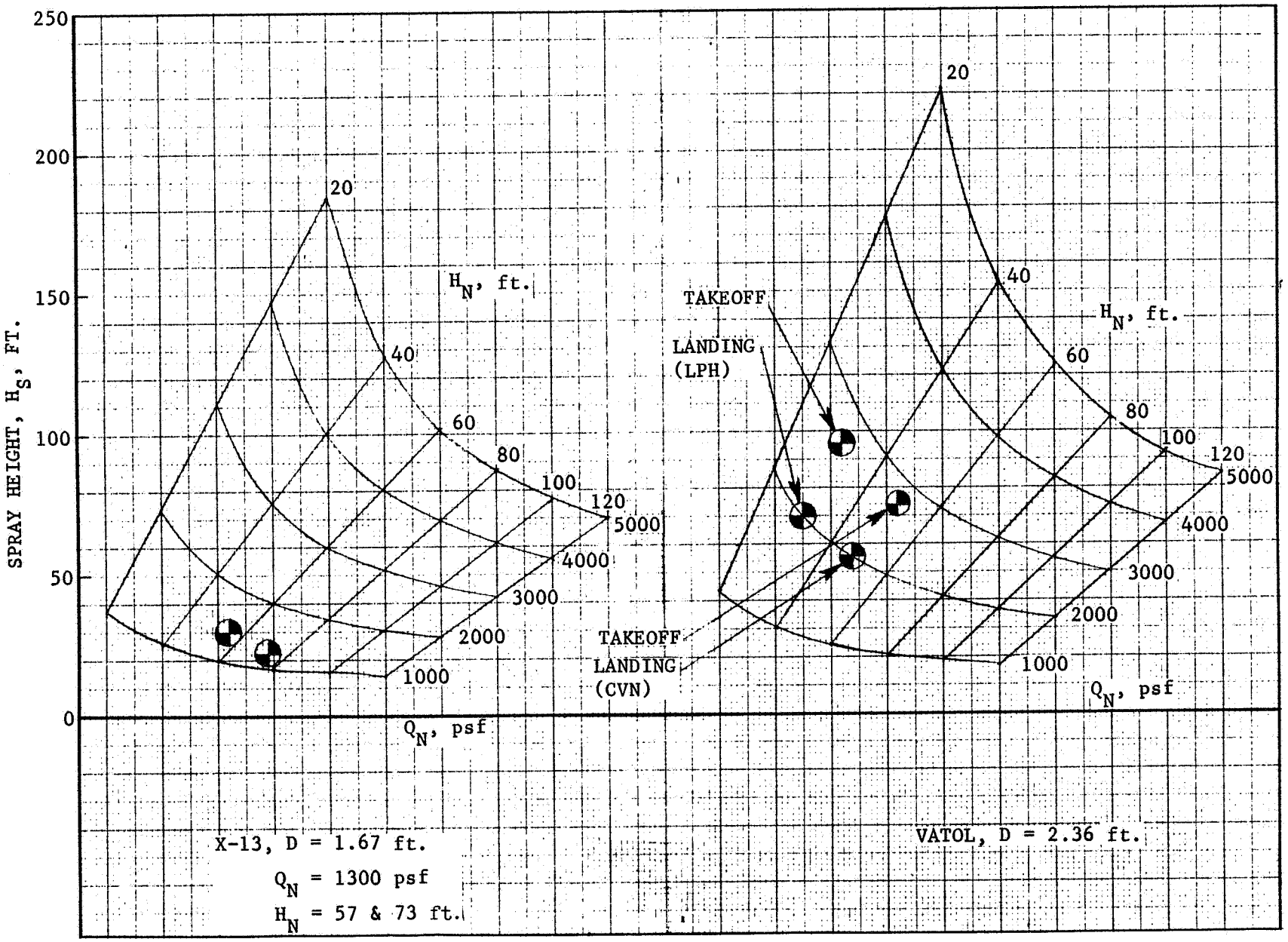

FIGURE 3-89. EFFECTS OF PHYSICAL PARAMETERS ON SPRAY HEIGHT

3.5 CONTROLS BLENDING

Stability and control estimates show positive aerodynamic effects throughout most of the angle of attack range of interest. Propulsion-induced airflows are expected to add to the innate aerodynamic characteristics. Only at high angle of attack combined with sideslip, large unstable yawing moments are developed. The yawing moment available from vertical tail and nozzle deflections, however, are assumed adequate to trim these moments.

Providing adequate roll control is the most critical requirement for a VATOL vehicle. During a landing transition, especially when deceleration takes place along a sloping flight path, the engines are temporarily at a rather low thrust setting while the airplane pitches through the C_{Lmax} regime. As aileron roll control is lost within that range, all roll control must come from differential main nozzle deflection and wing tip reaction control, both of which are affected by low engine power. Roll control available from anti-symmetric main nozzle deflection for the landing transition case is given in Figure 3-90. Using 1.4 rad/sec^2 as the roll control requirement[1], it is shown that this can be achieved down to a thrust setting of 64.6 kN (14,500 lb), (i.e., 42 percent of maximum thrust) given a maximum differential deflection of ±30 degrees. If wing tip reaction control is added, assuming that 5 percent airflow can be bled from the compressor, the minimum engine thrust at which the specified roll control can be achieved drops to about 22.24 kN (5000 lb) as shown in Figure 3-91.

[1] Mean value of roll control requirement range specified in AGARD 577.

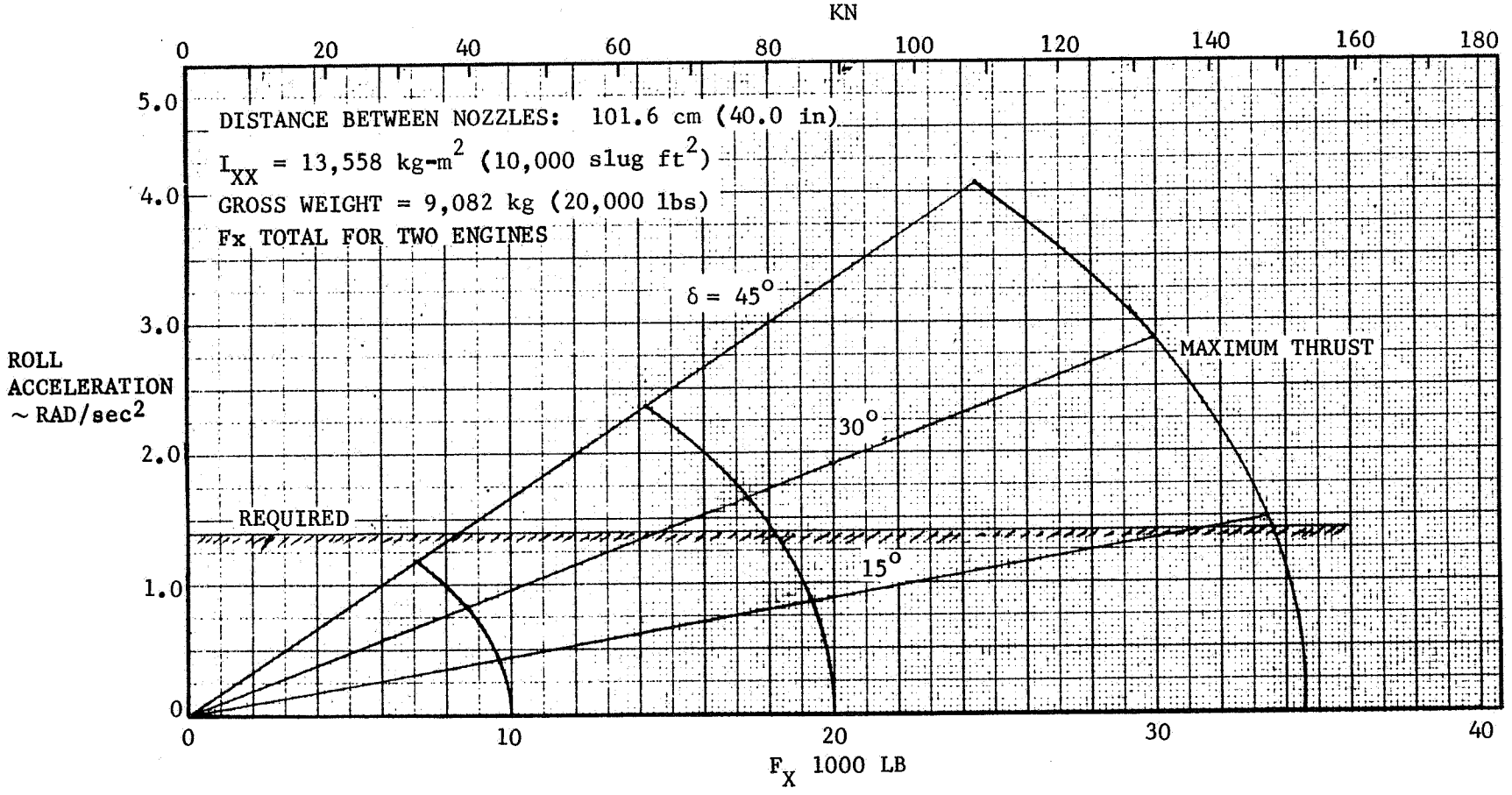

FIGURE 3-90. ROLL CONTROL POWER WITHOUT TIP JETS

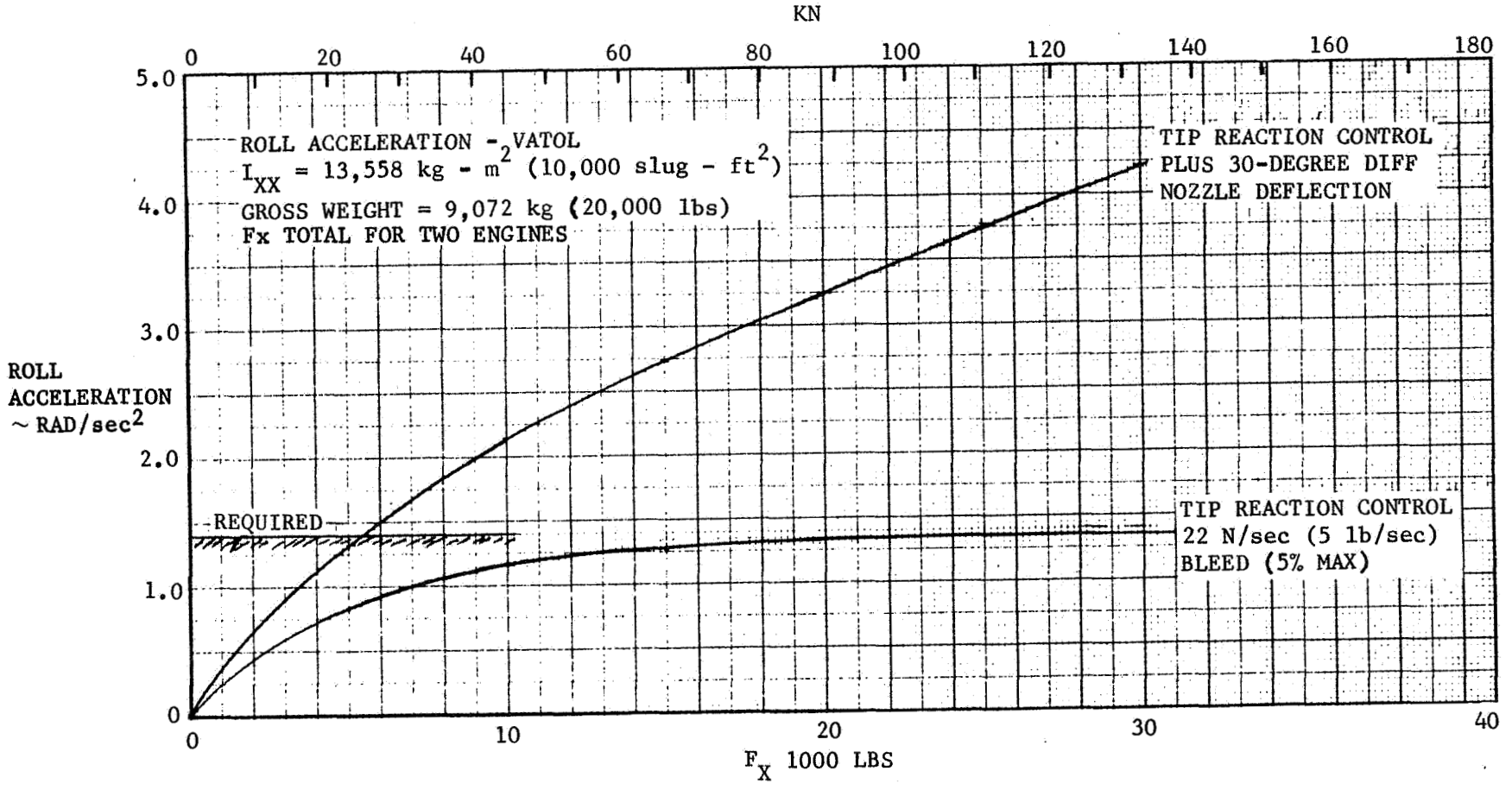

FIGURE 3-91. TOTAL ROLL CONTROL POWER

SECTION 4

PROPULSION CHARACTERISTICS

An advanced turbojet engine as described by Pratt and Whitney in PWA Report INST. 801 was selected for this study. The concept is an unaugmented single spool engine with variable turbine area. The high turbine inlet temperature capability of the engine provides a large engine thrust-to-weight ratio.

4.1 ENGINE SELECTION AND DESCRIPTION

The Pratt and Whitney Parametric Variable Turbine Geometry Turbojet Engine computer program (CCD 0260) was used to obtain engine characteristics. This deck allows the simulation of dry or afterburning engines incorporating a variable turbine inlet temperature and engine scheduling. The program estimates engine performance and weights based on mid-1980's technology and will be slightly conservative for the time period in question.

The selected engine and its static performance are illustrated in Figure 4-1. The turbojet was selected for the high level of thrust available at high speed without afterburner. In this manner, the engine can be sized for takeoff conditions, and the engine weight is minimized. The high turbine inlet temperature also minimizes the engine weight. The non-afterburning concept was chosen for its lower SFC at maximum power enhancing persistence in hover and combat tasks. Further, the exhaust gas and hot metal temperatures, although comparatively high, are still lower than those which would result from an afterburning engine and, as such, will result in a reduced infrared signature of the vehicle. One disadvantage of the dry engine concept is the SFC rise associated with cruise and loiter operation where the engine will operate at a lower percentage of intermediate power. This is minimized by the use of a variable turbine for which the rise in SFC at low power is delayed considerably. The variable turbine will also reduce inlet spillage drag at reduced throttle settings since the engine will operate at a high airflow over a wide range of operational conditions.

4.2 PROPULSION TRADES

The vehicle makes use of an advanced technology dry turbojet engine. In the selection of the cycle using this concept, the tradeoff between engine weight and fuel weight caused by varying cycle pressure ratio must be considered. An analysis was made to determine the optimum cycle pressure ratio for the VATOL turbojet engine. In this analysis, the maximum turbine inlet temperature was held constant (T_{4max} = 3200°F).

The study of the effects of cycle pressure ratio on engine cycle selection was performed with the Pratt and Whitney Variable Geometry Turbine Turbojet computer program (CCD 0260). An engine performance installation deck, representative of the engine installation, was used in conjunction with the PWA cycle deck to obtain installed engine data.

Four engine cycles varying in cycle pressure ratio were studied. The pressure ratios ranged from 12 to 25.

In order to evaluate the overall effects of cycle pressure ratio on aircraft performance, a mission performance study was made. A fighter escort mission, as shown in Table 4-1, was selected. In this table, fuel consumption is shown for the various mission segments for aircraft using an engine pressure ratio (12) and an engine pressure ratio of 20.

In making this comparison, aircraft gross takeoff weight was held constant, while the fuel weight was reduced by the engine weight increment. The results showed a substantial improvement in mission radius as the engine pressure ratio was increased (the airplane configuration was virtually unaffected). A 13 percent increase in radius capability resulted from an increase in the engine pressure ratio from 12 to 20. The engine size necessary for the design sustained load factor capability (n_z = 6.2g, M 0.6, 3.05 km altitude) showed a small increase of about 0.6 kN (130 lb) per engine in terms of rated thrust.

For the change in pressure ratio from 12 to 20, the engine weight increased by less than 20 kg (50 lb), the length increased by less than 30 cm (12 in), and the diameter decreased by less than 8 cm (3 in). The resulting maximum wetted area variation for the design was less than 0.2m^2 (3 ft^2). The change in drag would be less than inherent errors in the drag estimation procedure.

Increases in the pressure ratio above 20 produced performance improvements at a reduced rate, and the benefits became more difficult to substantiate. Such higher pressure ratios would most likely require twin-spool arrangements. In addition, more detailed analyses considering engine design, complexities and costs would be required to determine an optimum design pressure ratio. In anticipation of only minor performance improvements, these more exhaustive studies were not justified at this stage of development. Thus, a pressure ratio of 20 was selected as the engine pressure ratio.

4.3 AIR INDUCTION SYSTEM

The air induction system is designed to operate efficiently at the critical takeoff, maneuvering, and maximum speed conditions. The baseline design concept features a 2-D topside inlet arrangement which has certain advantages such as RCS reduction, FOD problem reduction, and relaxation of lower fuselage constraints associated with landing gear placement, location of stores, store/inlet interference, access doors, etc.

The inlet has a fixed-seven degree ramp with shock-on-lip operation at a local inlet M 2.0 (M_∞ 1.8). The configuration utilizes a horizontal ramp.
The leading edge extension (LEX) on the wing provides a favorable flow field for surface of the aircraft. The 7-degree ramp provides a good compromise between recovery and spillage over the required Mach range. Pressure recovery at takeoff and transition is improved by the use of auxiliary inlet doors located in the duct immediately upstream of the compressor face. These doors are sized to minimize the amount of air passing through the main inlet, thus minimizing lip-induced pressure losses. Spillage drag for the main inlet is held to a minimum by proper scheduling of the variable turbine features of the engine.

The sized, main air inlet has the following characteristics (per engine):

- 4613cm^2 (715 in^2) capture area
- 3620cm^2 (56lin^2) throat area
- Inlet lip thickness of 1.3cm (1/2 in)

The auxiliary inlet doors are sized to provide 4335cm^2 (672 in^2) of flow area. The inlet duct area distribution is shown in Figure 2-3. The main inlet system incorporates a ramp bleed system which removes most of the ramp boundary layer, improves pressure recovery, and lessens shock/boundary layer interaction problems. This

type of ramp bleed system is used on the F-17 air induction system. Tests have shown it capable of providing stable inlet operation to flight speeds of M 2.2.

4.4 TOPSIDE FLOW FIELD EFFECTS

The leading edge extension (LEX) on the wing provides a favorable flow field for the air inlets located above the rear part of the wing. The strong vortices generated by the LEX improve the upper fuselage flow field at angle of attack by removing the low energy boundary layer flow outboard and replenishing it with high energy external flow. Furthermore, the downwash induced on the center plane serves to align the flow with the upper fuselage, even at considerable heights above the fuselage. Previous aerodynamic investigations have shown the vortex system is stable to relatively high angles of attack, thus providing the desired inlet flow field characteristics at all maneuvering conditions. The vortex system eventually breaks down at very high angles of attack/sideslip as a result of the increasing adverse pressure gradients on the upper wing fuselage. Vortex stability is achieved by proper shaping of the LEX planform. Test data generated at Northrop provided design guidance.

A low speed wind tunnel test has been conducted on an advanced fighter model having the same wing, LEX planform, and inlet location as the VATOL concept. Figure 4-2 shows experimental low speed (M 0.3) α/β envelopes for an inlet pressure recovery of 0.99. The effects of LEX-off, wing height, and leading edge flap deflection on the α/β envelopes are also shown. Figure 4-2 shows that an inlet recovery of 0.99 can be obtained for angles of attack up to 40° within a sideslip range of $\pm 6^{\circ}$. The data indicate that the inlets should operate satisfactorily up to a high angle of attack with moderate sideslip. During the very low speed portion ($M < 0.2$) of the VATOL landing transition maneuver, however, the aircraft angle of attack may exceed 90°. High inlet recovery should still be obtainable by use of the auxiliary inlet doors at this very low speed condition.

4.5 EXHAUST NOZZLE/AFT END DESIGN APPROACH

The exhaust nozzles are of the variable geometry, balanced beam, axisymmetric type used with the PWA F100 turbofan engine. This type of nozzle can schedule throat area and exit area independently so as to provide nearly optimum thrust for a wide

range of flight conditions. The nozzle has a gimbal capability of 30 degrees in the pitch plane and 15 degrees in the yaw plane. This provides the pitch, yaw, and roll control capability (differential gimballing) required of the propulsion system during VTOL flight. The engines have been placed close together to provide smooth aft end slopes similar to the approach taken in the F-17/F-18 aircraft.

4.6 ENGINE INSTALLATION LOSS ASSESSMENT

Propulsion installation losses can be divided into two categories: (1) engine cycle losses, and (2) propulsion-related subsystem losses. Installation factors causing engine cycle performance losses are:

a. Extraction horsepower for aircraft power systems (hydraulic and electrical).

b. Engine air bleed for the environmental control system.

c. Inlet total pressure recovery.

Drag components assigned to the propulsion system are as follows:

a. Environmental Control System (ECS) and avionics system cooling airflow momentum losses.

b. Engine bay ventilation airflow momentum loss.

c. Inlet ramp and/or throat bleed airflow momentum losses.

d. Inlet spillage drag.

e. Throttle-affected nozzle/afterbody drag.

The engine installation computer program is written such that the engine cycle losses are computed by the engine manufacturer's cycle deck (CCD0260). The compressor bleed flow rates are shown in Figure 4.3. They vary from 0.5 kg/sec c1.1 lb/sec) at sea level to about 0.14 kg/sec (0.3 lb/sec) at 15.2 km (50,000 ft) altitude. The external losses are calculated by a program developed specifically by Northrop for the aircraft installation. The assessments of these propulsion loss items are summarized in Table 4-2. The thrust-drag bookkeeping procedure relative to the inlet spillage and afterbody drags is the same as the "Navy" procedure used for the F-18. In this procedure, at Mach numbers of and above one, the critical inlet spillage drag is assigned to the aircraft minimum drag. Only the subcritical portion of the

spillage drag is assigned to the propulsion system. Throttle-dependent nozzle/afterbody drag is handled in the same manner. The reference condition is a wide-open, fully-expanded flow, cylindrical nozzle. Since this is the same reference condition assumed by the aerodynamic group, there is no need to add another drag increment to the aircraft minimum drag.

Typical build-ups of installed thrust losses at maximum power for M0.6 and M0.9 at 3 km (10,000 ft) altitude are shown in Figure 4-4. The build-ups for M1.2 and M1.8 at 11 km (36089 ft) are shown in Figure 4-5. These figures show that for subsonic and transonic Mach numbers, installed thrust losses at maximum power are only 4 percent or less. At higher supersonic speeds, however, these losses increase rapidly to 35 percent at M1.8. The reasons are increasing inlet recovery loss and increasing spillage drag.

The effect of the tropical day atmosphere (T - 305^{o}K, sea level) on installed engine takeoff performance was calculated with the installation program.

4.7 INSTALLED ENGINE PERFORMANCE

Installed engine performance was obtained for intermediate (maximum dry) and cruise power settings over the range of Mach numbers from 0 to 2.4 and altitudes from sea level to 18.3 km (60 kft). However, the data are proprietary to Pratt and Whitney and are therefore not included in this report.

4.8 REACTION CONTROLS

In the hover and transition flight regimes, roll control is provided primarily by wingtip mounted reaction nozzle jets. Additional roll control capability is obtained by differential deflections of the gimballed main engine nozzles. This helps to reduce the size of the reaction control system, compressor bleed air requirements, and installed engine performance losses. The reaction control system is composed of a left hand and right hand subsystem. Each subsystem consists of a (1) feeder pipe which transfers bleed air from the engine compressor through the wing to (2) a wingtip plenum chamber, and then exhausted through (3) a reaction nozzle to create thrust and rolling moment. The reaction control subsystem for each wing has been designed for a maximum flow rate of 2.5 kg/sec (5.5 lb/sec). The compressor bleed air is supplied at a

stagnation temperature of 730°K (850°F) and pressure of 1630 kN/m^2 (236 psia). To ensure low feed pipe pressure losses, the pipe is sized so that the pipe flow Mach number is only 0.2 at the maximum flow rate. This means a pipe inner diameter of 6.4 cm (2.5 in). The wingtip reaction nozzle is of the convergent type and has an exit diameter of 3.7 cm (1.6 in). The maximum reaction thrust from each wingtip nozzle is 2 kN (450 lb).

TABLE 4-1. FIGHTER ESCORT SIZING MISSION

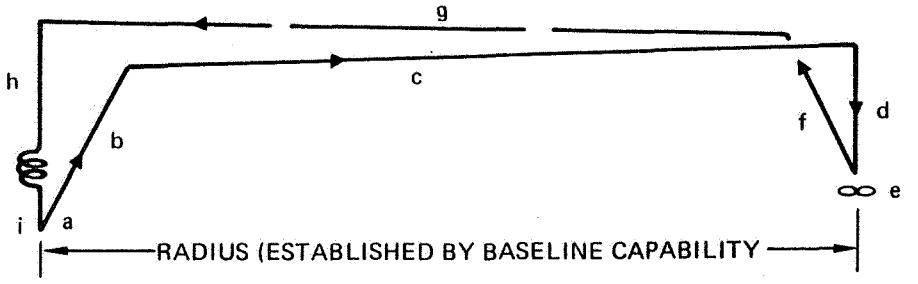

SEGMENT	MISSION EVENT	FUEL REQUIREMENT BASIS	FUEL USED RADIUS 926 KM (500 NM) PR = 12	FUEL USED RADIUS 1046 KM (565 NM) PR = 20
A	START, T.O. TRANSITION AND ACCELERATE TO BEST CLIMB SPEED	45 SEC EACH, INTERMEDIATE AND MAX THRUST (VSTOL MODE). 1 MIN INTERMEDIATE THRUST (UP-AND-AWAY MODE) (S.L. TROPICAL DAY)	692 KG (1525 LB)	621 KG (1370 LB)
B	CLIMB TO BEST CRUISE ALTITUDE	MAX R/C AT INTERMEDIATE THRUST	283 KG (625 LB)	259 KG (570 LB)
C	CRUISE OUT	BEST ALTITUDE AND MACH NO	1361 KG (3000 LB)	1490 KG (3285 LB)
D	DESCENT TO 9144 m (30,000 ft)	NO DISTANCE OR FUEL CREDIT		
E	TASK ORIENTED COMBAT	(1) ACCELERATION FROM M0.8 TO M1.2. 9144 m (30,000 FT) (2) 360° SUSTAINED TURNS AT MI. 2. 30,000 FT (4) 360° SUSTAINED TURNS AT MO. 6. 10,000 FT	739 KG (1630 LB)	671 KG (1480 LB)
F	CLIMB TO BEST CRUISE ALTITUDE	MAX R/C AT INTERMEDIATE THRUST FROM 10,000 FT	206 KG (455 LB)	190 KG (420 LB)
G	CRUISE BACK	BEST ALTITUDE AND MACH NO	1107 KG (2440 LB)	1225 KG (2700 LB)
H	DESCENT TO S.L.	NO DISTANCE OR FUEL CREDIT		
I	RESERVES AND LANDING	VSTOL MODE 1 MIN EACH INTERMEDIATE AND MAX THRUST ALLOWANCE UP AND-AWAY MODE 10 MIN AT BEST LOITER SPEED PLUS 5% INTERNAL FUEL RESERVE	1191 KG (2625 LB)	1123 KG (2475 LB)
TOTAL FUEL			5579 KG (12300 LB)	5579 KG (12300 LB)

TABLE 4-2. PROPULSION LOSS ASSESSMENT

ITEM	ASSESSMENT
POWER EXTRACTION	37 kw (50 HP) per engine except for certain takeoff, landing, and combat conditions where 63 kw (85 HP) is assumed.
ENGINE BLEED AIR	As shown in Figure 4-3.
INLET RECOVERY	Use modified F-17 7° ramp inlet data. Corrections made for shorter VATOL inlet diffuser length, local Mach number, and use of auxiliary inlet doors.
ECS, AVIONICS SYSTEM DRAG	ECS and Avionics ram airflows equal to three times engine air bleed. Drag equal to 1/2 freestream momentum.
ENGINE BAY VENTILATION DRAG	F-17/F-18 procedure with ventilation airflow scaled to engine size. Cooling air velocity change determined with semi-empirical technique. Drag proportional to product of airflow and velocity change.
RAMP BLEED DRAG	Scaled F-17 7° ramp bleed data used for airflow and bleed airflow velocity change. Drag proportional to product of airflow and velocity change.
INLET SPILLAGE DRAG	Calculated with Sibulkin method. For Mach numbers ≤ 1 only the subcritical inlet spillage drag is assigned to the propulsion system. The critical spillage drag is assigned to the aircraft minimum drag.
THROTTLE - DEPENDENT NOZZLE/ AFTERBODY DRAG	Based on F-17 nozzle/afterbody drag data. Reference nozzle is a fully-open cylindrical PWA-type balanced beam nozzle with fully expanded exhaust ($P_{s9}/P_{am} = 1$).

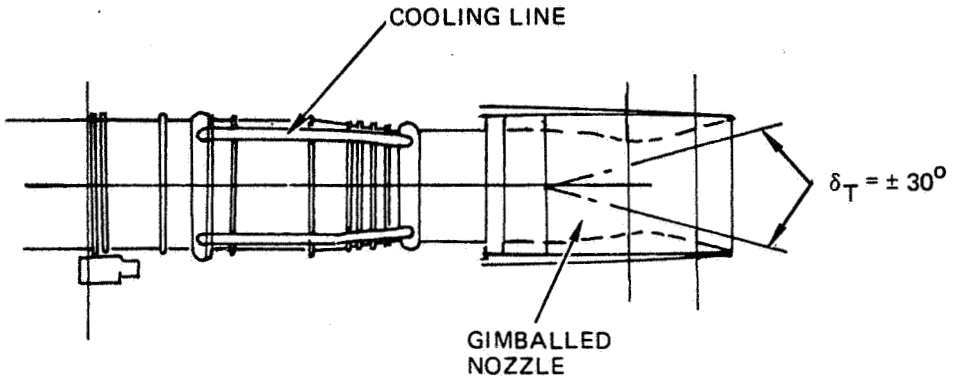

- PR = 20
- T_4 = 2030°K (3200°F)
- VTOL THRUST* = 77.8 KN (17500 LB)
- T/W = 35000/30000 = 1.17*
- TURBOJET
- VARIABLE TURBINE
- NON-AUGMENTED
- SELF-COOLED

* INSTALLED, TROPICAL DAY (T = 305°K, 90°F)

FIGURE 4-1. TURBOJET ENGINE DESCRIPTION

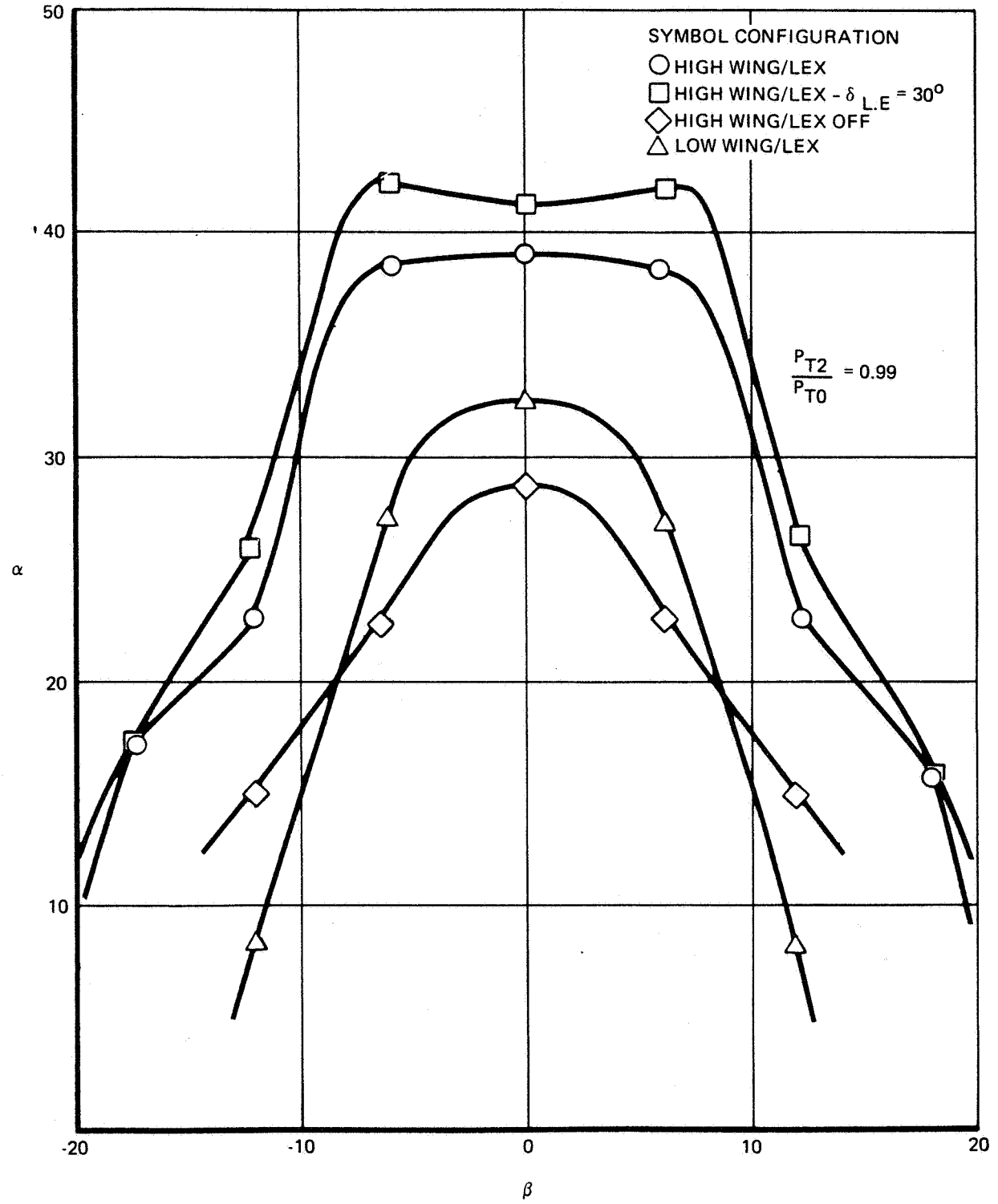

FIGURE 4-2. EFFECT OF WING CONFIGURATION AND LOCATION ON PERFORMANCE ENVELOPE

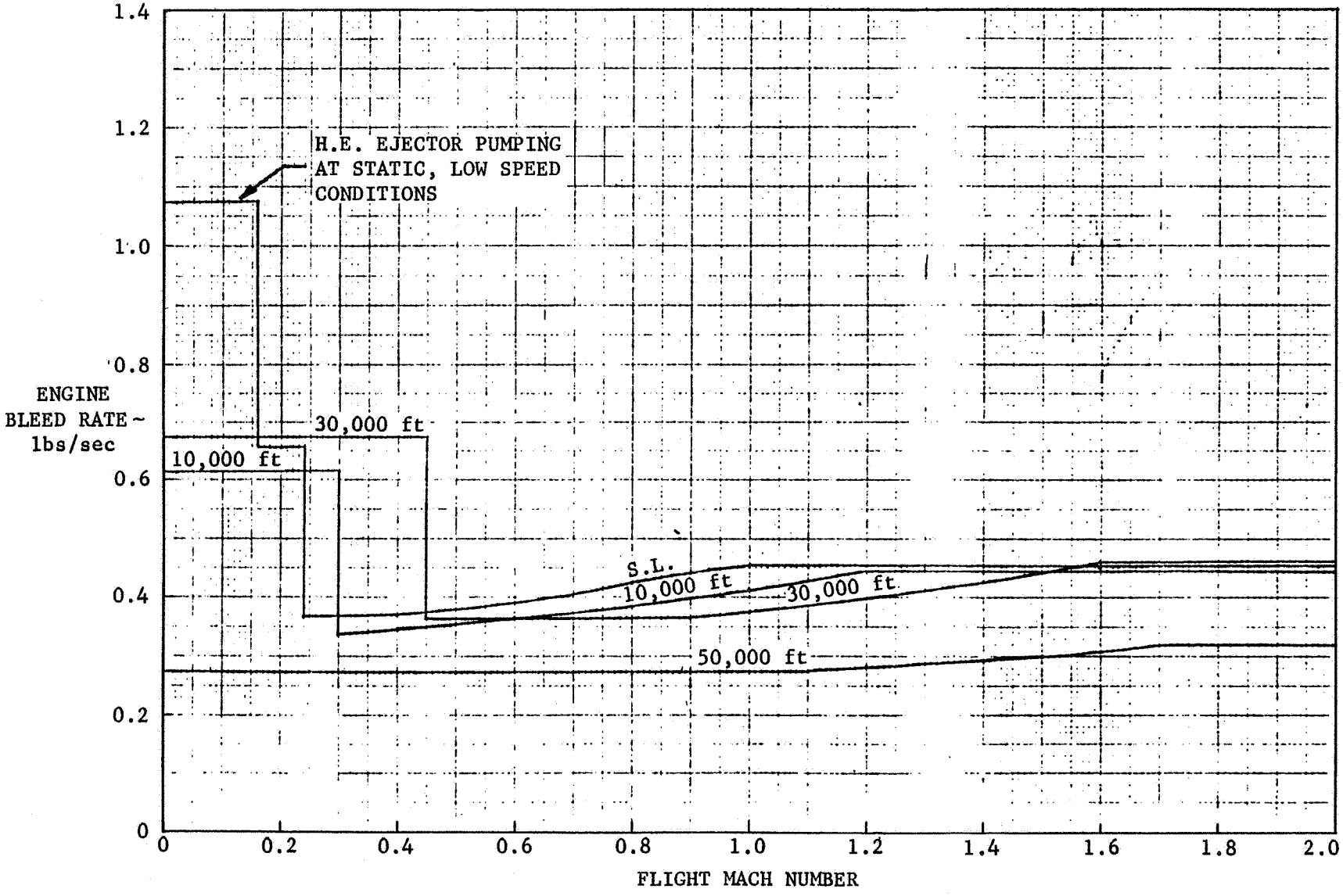

FIGURE 4-3. ENGINE COMPRESSOR BLEED RATES

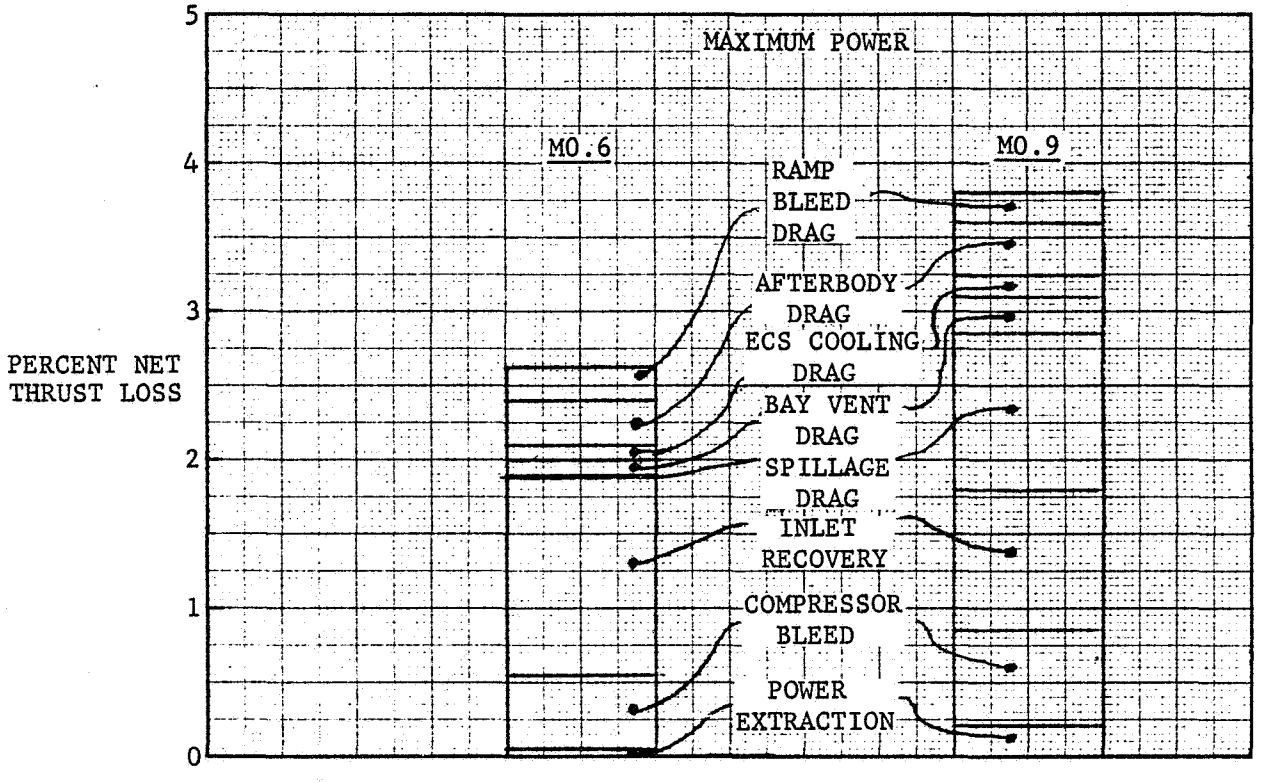

FIGURE 4-4. BUILD-UP OF INSTALLED NET THRUST LOSSES AT 3 KM (10,000 ft) ALTITUDE

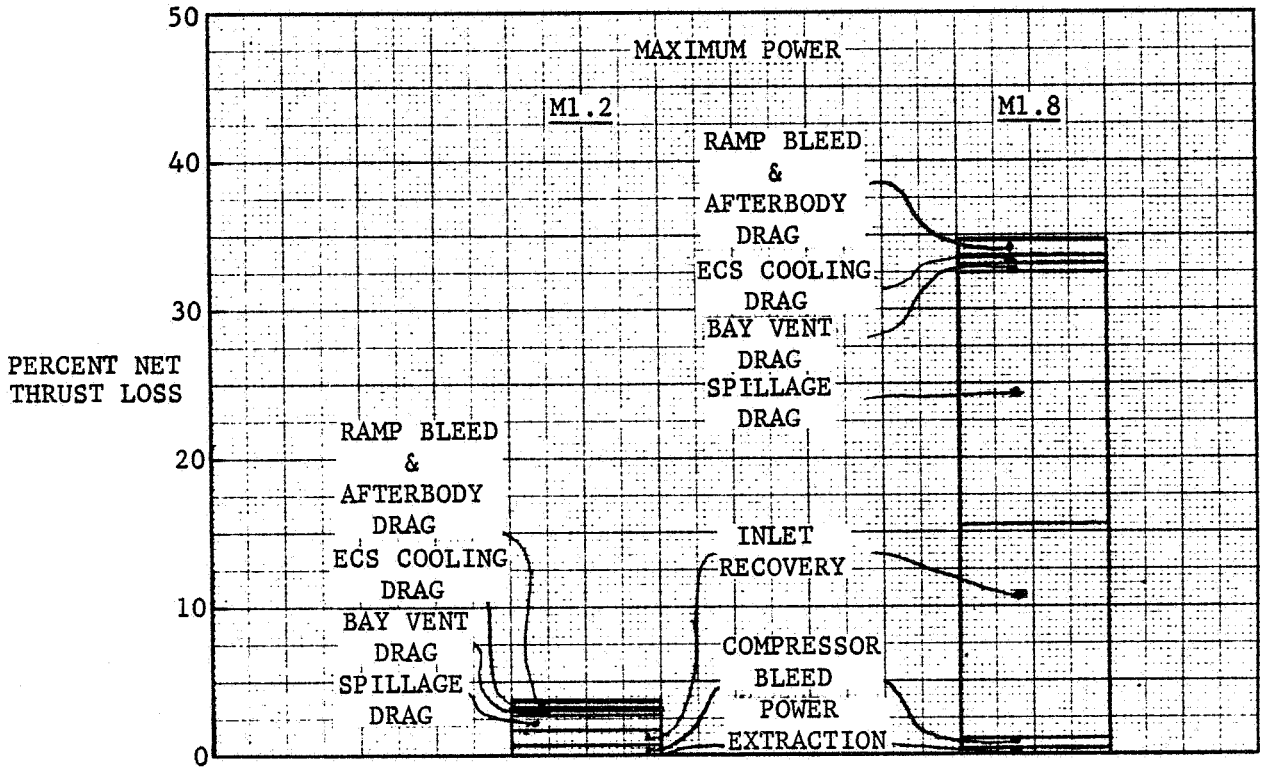

FIGURE 4-5. BUILD-UP OF INSTALLED NET THRUST LOSSES AT 11 KM (36,089 ft) ALTITUDE

SECTION 5

AIRCRAFT DESIGN

The aircraft structural design and system study was conducted to a limited depth. The intent was to ensure that the configuration was sufficiently credible to justify a detailed aerodynamic and propulsion integration analysis.

5.1 STRUCTURAL DESIGN AND ANALYSIS

5.1.1 Design Criteria

Current military specifications were reviewed to establish the applicability of available requirements for structural design of VSTOL aircraft. Results indicated that although current MIL-SPEC requirements provide adequate criteria for operation as a conventional airplane; appropriate criteria must be developed to provide a basis for structural design during both hover and transition modes of flight. Criteria for hover require specification of thrust forces, inertia effects, engine gyroscopic effects, and crosswind forces. Control requirements for maximum load factor maneuvers and for maneuvers induced with maximum control deflection must be defined to provide for evaluation of the effects of rapid changes in trim, moment shifts, and interactions between aerodynamics and propulsion forces during transition.

The thermal environment of structure in areas exposed to propulsion system effects has been reviewed utilizing F-18A design experience and available data. Temperature limitations were established as follows:

1. Engine Compartments were designed with appropriate cooling flows such that the temperature distribution did not exceed the design limits of adjacent structure. Engine cooling airflows were sized such that aluminum or composite airframe components were not exposed to temperatures in excess of $120^{\circ}C$ ($250^{\circ}F$) with titanium used in areas where higher temperatures may be experienced. Steel structural components were not exposed to temperatures greater than the design thermal level.

2. Reaction control duct walls were considered exposed to the same temperature as bleed air from the compressor; approximately 455°C (850°F).

5.1.2 Structural Materials

Advanced composite materials were selected as the primary materials of construction for both strength and stiffness-critical applications. Not only are lightweight structural components possible through efficiently tailored properties and lower specific strength/stiffness, but lower fabrication costs result through integral or one piece design concepts.

Advanced metallic materials were selected for areas of extremely localized loading as well as severe thermal, acoustic, moisture, and corrosive environmental/operational conditions. A proper blend of the application of aluminum powder metallurgy, titanium superplastic forming plus diffusion bonding will result in lightweight, low cost, and durable advanced metallic material airframe components in the 1990's.

5.1.3 Structural Description

The aircraft structure is shown in Figure 5-1. Major structural components include a fuselage with integrated nacelles, a carry-through wing, and single pivoted vertical stabilizer.

Fuselage Structure. The fuselage is a semi-monocoque structure of stressed skin panels stabilized by edge members, bulkheads, and frames. Frame spacing is based on trade studies made for both honeycomb sandwich and integrally stiffened skin panel designs. Typical of most airframe designs, a common frame spacing is not achievable due to support frame or compartment bulkhead location constraints. However, studies have shown that by optimizing honeycomb panel thickness or integral stiffener heights within any specific bay based on local loading conditions, near optimum panel weight is obtainable for frame spacing varying from 38 cm (15 in) to 102 cm (40 in). An average frame spacing of approximately 51 cm (20 in) has been selected for this design based on system routing support and battle damage considerations.

For ease of producibility the fuselage was divided into three major sections: a forward section from FS 25 (10) to FS 564 (222), a center section from FS 564 (222) to FS 1067 (420, and an aft section from FS 1067 (420) to FS 1488 (586).

The Forward Fuselage contains radome, radar bay, nose landing gear, cockpit, avionics bay and ECS system. The cockpit module extends from FS 262 (103) to canted bulkhead FS 394 (155) and contains all crew accommodations, aircraft and system controls, pilot's enclosure, and associated mechanisms. The cockpit module pivot point is at FS 249 (98), and the actuators are housed between FS 262 (103) and FS 394 (155) below the module.

The Center Fuselage extends from the fuel bulkhead at FS 564 (222) aft to FS 1067 (420). Fuel is contained within the entire basic fuselage shell from FS 571.5 (225) to FS 998 (393). Panels in the lower skin and doors in the fuel floor provide for access to the tanks. The ECS system is housed forward of the fuel boundary between FS 526 (207) and FS 564 (222). A removable section of the engine air intake above the wing permits installation of the carry-through wing.

The Aft Fuselage extends from FS 1067 (420) to FS 1488 (586). This section contains engines and engine mounts. The primary structure consists of two side panels, a center keel fire wall and an upper panel. Engine mounts are located between FS 1261 (496.5) and FS 1287 (506.5) and are metal components. Intercostals forward and aft of these frames support engine thrust loads. A machined steel spindle fitting centered between FS 1321 (520) and FS 1346 (530) mounts the all movable vertical stabilizer. The vertical stabilizer acutator is installed between FS 1321 (520) and FS 1407 (554), and an access panel on the left side of upper fuselage is provided.

Wing Structure. The wing has a carry-through main box structure which is trunnion mounted to the fuselage between FS 856 (337) and FS 1067 (420) bulkheads.

The wing consists of a fuel containing main structural box, leading edge flaps, flaperon, LEX, and wingtip jet reactor fairings.

The main structural box is of thick skin, multispar construction fabricated of advanced composite materials. Flaperon actuators at WS 203 (80) are located below the wing. The front spar supports leading edge flap rotary actuators. All wing access panels are structural and located on the upper surface. A wing shear attach fitting is located at the inboard end of the aft spar.

Leading edge flaps and trailing edge flaperon panels will be of full depth honeycomb sandwich construction fabricated of advanced composite materials. Metallic inserts, cocured with the panel, will be used at hinge or actuator attach locations.

Vertical Stabilizer Structure. The vertical stabilizer main structural box is a bonded assembly of graphite/epoxy skins, spars, ribs and full depth fiberglass honeycomb core. A machined titanium root rib is attached with mechanical fasteners. The tip and leading edge antenna covers are of fiberglass/epoxy.

5.1.4 Structural Analysis

The basic structural concepts used are standard military aircraft approaches and can be adequately substantiated using current military specifications estblished for structural integrity. Construction of the aircraft is such that compliance with the appropriate manufacturing and process requirements together with adequate stress/damage tolerance analysis and static/fatigue testing will result in unrestricted service operation within the strength envelope.

The wing structural configuration is similar to that of an existing finite element wing model upon which comprehensive flutter analysis was performed considering various flaperon actuator arrangements. Results of the analysis revealed that the wing equipped with a full span flaperon actuated by a mid-span actuator met flutter speed requirements. It was also shown to be the optimum design in terms of incremental structural weight and cost over the baseline design of two actuators installed per side. It should be noted that the analysis conducted was on a low elastic-to-rigid ratio delta wing structure and the VATOL wing will be expected to be much stiffer.

The flutter analysis could necessitate a change in the flaperon actuator location. However, the basic concept of the wing design provides assurance that no significant problems involving aeroelastic stability exist within the flight envelope of the aircraft. In summary, the studied concept was considered to be a straightforward airplane unlikely to be subjected to flutter problems.

5.2 FLIGHT CONTROL SYSTEM

5.2.1 Hover and Transition Regimes – Normal Operation

One of the most frequent complaints about previous VSTOL aircraft is the excess pilot workload during the transition between aerodynamic and powered-lift configurations and during the hover period. The study aircraft has 10 parameters available at

the beginning of the landing transition (and end of the takeoff transition) to control its forces and moments, and seven controllable parameters when solely in the powered-lift configuration. Such a large number of controls, along with their mutual interactions, would make extraordinary demands on the abilities of even a highly-skilled pilot. Consequently, the control system shown conceptually in Figure 5-2 was conceived to reduce pilot workload. Its main features are:

1. The number of cockpit controls remains at the familiar five (pitch and roll stick, rudder pedals, and left and right throttle controls).
2. The cross-axis coupling between controls is greatly reduced.
3. The aircraft response to cockpit controls is "natural"; i.e., similar to its response when in the conventional aerodynamic-lift mode.
4. The transition phase, including cockpit rotation, is fully automatic; however, however, manual override can be used to modify all automatic functions.
5. The system readily lends itself to expansion to fully automatic landings and takeoffs, depending upon the quantity of earth-referenced data available.

The sketches at the bottom of Figure 5-2 define the symbols used.

The heart of the control system is the Crossfeed Matrix and the two Augmentation blocks. As a result of these blocks, in the Manual mode the cockpit controls produce the following results. At the beginning of transition, to hover regime fore-aft stick movements produce pitch attitude changes proportional to stick displacement. Altitude rate is proportional to throttle lever at airspeeds below 1.1 V_s. When airspeed is below about 55.6 km/hr (30 knots) and attitude is greater than about 70^o, fore-aft stick movements cause speed change commands in a fore and aft direction. When pitch attitude is less than 45 degrees, lateral stick and pedal movements cause roll and yaw rates, respectively, proportional to displacement. When the controls are at neutral, roll attitude hold and heading hold are maintained. When pitch attitude exceeds 45 degrees, lateral stick movements command the yaw axis (yaw-rate/heading hold) and pedal movements command the roll axis (roll rate/attitude hold). This swapping of the lateral controls was found to be highly desirable during Ryan X-13 VATOL tests. Note that in the current design, the pilot will rotate during transition by 45^o as was done in the X-13.

The sequence of events during a landing transition is shown in Figure 5-3. Figure 5-4 gives the details of the Pitch Augmentation block. At the transition initiation point, a 90^{o} step is applied to the Rate Limit. Its output commands a nominal pitch rate of 5 degrees/sec. When airspeed drops below 1.1 V_S, SW1 transfers to the -0.1g position and is summed with a horizontal acceleration signal. The resulting acceleration error signal modulates the nominal pitch rate to null itself. Pilot fore-aft stick movements, ΔSp, can also be used to modulate the pitch rate to modify the automatic transition if required. As horizontal speed (obtained by integrating horizontal acceleration) drops below about 55.6 km/hr (30 knots), a speed hold loop is engaged. The pilot now uses his stick to command speed in a fore-aft direction.

Prior to transition, the sink rate and horizontal acceleration were being synchronized to zero by K5/S. At transition, SW2 moves to the center position and the output of K5/S is held at a constant value, the initial sink rate. Subsequent changes in sink rate produce errors signals which vary thrust to maintain initial sink rate. When pitch exceeds 80^{o} or altitude drops below 15.2 m (50 ft.), SW2 transfers to position A and the commanded sink rate expotentially decays to zero. The pilot takes control and manually uses throttle levers to control sink rate.

Since the thrust level required prior to transition is small (especially if a steep descent angle is being flown), and a large thrust level is required during hover, a means must be provided to maintain the thrust difference. The output of integrator K_{IH}/S can provide the required difference, but since its input is the altitude rate error, relying solely upon the integrator, forces the aircraft's sink rate to be greater than the commanded value. To reduce the demands upon the integrator, a bias, whose magnitude increases as pitch increases, provides about 2/3 of the increased thrust level required. The integrator provides the remainder.

Nozzle motions away from the vertical are passed through absolute value circuits and increase the thrust level, thus providing additional decoupling (over what the vertical acceleration signal provides) between changes in horizontal or lateral speed and altitude rate.

Details of the Lateral Augmentation block are given in Figure 5-5. (Roll means rotation about the X – body axis; yaw about the Z – body axis.) Roll rates are

proportional to lateral stick movements for small pitch angles or to pedal movements for large pitch angles. Centered controls provide attitude hold. During transition, the bank signal is generated by approximately integrating roll rate with a long-time-constant lag. During hover, the "bank" signal would come from a heading error source.

In aerodynamic flight, the rudder is driven to maintain turn coordination. In powered-lift flight, yaw rate is proportional to pedal displacement for small pitch attitudes and lateral-stick displacements for large pitch attitudes. During transition, heading changes are held to zero. Heading changes are generated by approximately integrating yaw rate with a long-time-constant lag. During hover, the "heading" error signal would come from a bank angle source.

Figure 5-6 shows the details of the Crossfeed Matrix. Its 5 inputs, which are the various error signals from the two Augmentation blocks, are distributed to its 10 force and angle outputs as shown. To illustrate its use, consider δ_{ac}, which is commanded aileron position. Reading down the fourth column to the first non-zero elements, a_{14} and a_{24} and then reading to the left end of the row, we see that the primary effect of δ_{ac} in the powered-lift regime is on thrust from the wingtip reaction jets, R_R and R_L. Continuing down, elements a^s_{34} and a^s_{44} show that δ_{ac} also produces thrust from the rear nozzles ($a^s_{34} = -a^s_{44}$). Finally, a_{94} indicates that δ_{ac} also drives the aileron, whose effectiveness goes to zero as airspeed goes to zero. In the cruise-combat regime, δ_{ac} affects the aileron only. Although the matrix elements are shown as constants, most of these elements have first or second order denominators representing the transfer functions of the surface and nozzle actuators, and the engine dynamics. Also, gain scheduling might be required for some of these gains.

The Outer Loop Control Laws block and the Auto-Man switch in Figure 5-2 provide the means of readily adding modes such as Altitude Hold, VOR, glide slope and localizer and even a fully automated landing mode. The main restriction on these modes is the availability of the appropriate earth-referenced and air-data signals.

The Auto-Man switch is shown as having all signal paths either from the pilot or from the Outer Loop Control Laws block. The actual hardware could easily be implemented to permit split-axis operation.

Note that in the above discussion, parameter values such as -0.1g, 15.2 m (50 feet), 1.1 V_A, etc., were chosen arbitrarily to illustrate the control system

concept and to provide approximate estimates. More exact values will be obtained from simulator studies. Note also that switching details to lock the system out during combat conditions when, for example, V_A might drop below 1.1 V_S, are not shown. Finally, it was assumed that all of the pilot's cockpit controls only move as a result of his inputs, and that electrical signals generated by the control system do not move the pilot's controls.

During the takeoff transition, the reverse sequence occurs with some of the switching occurring at slightly different points than shown in Figures 5-4 and 5-5, which are drawn to mainly show a landing sequence.

Since takeoff is generally less demanding than landing, fully automated takeoffs can readily be provided without having to add additional earth-referenced signals. One easily implemented profile might be to command a 0.1g upward acceleration for about 4 or 5 seconds, and then maintain the existing climb rate while commanding a maximum forward acceleration.

5.2.2 Engine Failure in Hover or Transition

Since the maximum thrust level from each engine is less than the landing weight of the aircraft, an engine loss in a certain range of altitudes with airspeed below some critical value will result in loss of the aircraft. The problem now becomes one of pilot-escape before the aircraft reaches an attitude where safe ejection is impossible. Assuming the airplane was in steady hover with the nose vertical when engine loss occurs, the effects of an engine loss are unbalanced vertical forces, which increase the sink rate, and a yawing moment because the thrust from the remaining engine is laterally offset from the center-of-gravity. Since the moment arm is so short, the yawing moment is readily eliminated by the control system by vectoring the remaining engine such that the thrust goes through the c.g. and by leaning the aircraft such that the thrust is aligned with the gravity vector.

One possible approach to an engine monitor is as follows. The most basic engine input, commanded fuel flow rate, is fed to the input of a model whose dynamic response simulates the engines' dynamic response. The output of the model is compared to some thrust-indicating parameter such as pressure ratio or exhaust gas temperature. Differences between the compared signals exceeding some threshold for some time period would indicate a lost engine and provide appropriate warnings.

5.2.3 Conventional Flight Regime

The aircraft is designed to operate with 15 percent negative static margin at subsonic speeds in pitch. With this level of static instability, the aircraft cannot be flown unaugmented with mechanical controls. Hence, a full authority fly-by-wire stability and command augmentation system (SCAS) with proper redundancy is used to provide good flying qualities and to ensure flight safety.

With static instability, the amount of control power available at high angles of attack is insufficient to counteract moments due to inertial and aerodynamic cross-coupling, engine gyroscopic effects, and thrust offset. Hence, high angle of attack maneuvering capability has to be restricted to prevent uncontrolled departures from which the aircraft cannot be recovered. An automatic departure prevention system has been designed for an aircraft having a 15 percent negative static margin and a wing planform similar to that used for this concept. The automatic departure prevention system is integral with the SCAS so that the pilot can use any combination of control inputs without the danger of the aircraft becoming uncontrollable, and he can fly with "head out of the cockpit." Nonlinear control laws are used to maximize the lift and turn rate capability. For structural protection, the SCAS limits the maximum load factor that the pilot can command.

The performance at low dynamic pressures is enhanced by using the thrust vectoring capability. The Thrust Vector Control System (TVC) is designed integral with SCAS and is phased in automatically at low dynamic pressures. With additional control power available, the angle of attack flight envelope and roll rate capability are substantially expanded. The inputs to the TVC are provided, along with inputs to aerodynamic control surfaces, by pitch and roll stick displacement. The pilot task is thus made easier by not requiring extraordinary control input.

An extensive air combat simulation was recently concluded, using an aircraft in which this flight control system was modeled, in which the pilot on a moving base simulator was engaged with an interactive target. This target, computer controlled, took defensive as well as offensive action. The resulting maneuvering was very realistic, with the aircraft driven to its performance limits. In a total of 500 combat engagements, not a single departure from controlled flight occurred.

5.3 MASS PROPERTIES

A parametric weight estimation procedure in conjunction with the Northrop D-SYN sizing program was used for the sizing and sensitivity studies of the aircraft under study. The weight prediction equations are of the rational-empirical type applicable to conventional aircraft configurations, and supplemented to include the appropriate increments and penalties peculiar to the VSTOL aircraft (e.g., reaction controls, thrust vectoring devices). Factors are applied to the structural weight estimates to account for different materials, fatigue life and thermal environment.

The resulting individual group weight estimates are then accumulated for several assumed design gross weights, including the effect of fuselage sizing for the required fuel volume. The corresponding fuel available is then found from mission performance computations and is subsequently used to iterate for a takeoff gross weight (fuel required = fuel available).

Identical weight computations may also be performed by a stand-alone computer program utilizing the formulas to estimate the weights of individual design groups (wing, tail, body, flight controls, etc.) for a specific aircraft and design mission. Each formula employs significant design parameters affecting weight; such as, design weight, load factor, basic dimensions, and yields a predicted weight for a particular design group.

Appropriate to the 1990+ time period, service introduction of advanced composite materials was reflected in the use of the following structural weight savings: wing and tail surfaces 26 percent, fuselage 25 percent, and landing gear 18 percent.

5.3.1 Weight Estimates

The weights are presented in the group weight statement in Table 5-1.

5.3.2 Balance

The baseline configuration is balanced for the center of gravity position (corresponding to 13,608 kgf (30,000 lb) T.O.W.) at 36 percent mac. At zero fuel weight of 7885 kgf (17,442 lb) the c.g. location is at 40.2 percent mac. By nature, the VATOL concept in the VTOL mode is less sensitive to longitudinal c.g. travel and loading conditions than the HAVSTOL concept.

5.3.3 Moments of Inertia

Moments of inertia of the baseline configuration were calculated for two loading conditions and are given below:

Loading Condition	Iyy (Pitch)	Ixx (Roll)	Izz (Yaw)	Units
Take-Off Weight, 13,608 kgf	134,401	19,935	171,434	kg. m^2
(30,000 lb)	99,129	14,703	126,443	sl. ft^2
Zero-Fuel Weight, 7,885 kgf	77,760	11,634	98,618	kg. m^2
(17,442 lb)	57,353	8,581	72,737	sl. ft^2

5.4 CREW STATION

5.4.1 Design Philosophy

In a vertical takeoff and landing aircraft, the critical function of pilot operation over the range of flight attitudes is of primary concern. The pilot must be afforded excellent visibility and comfort so that he can operate his aircraft precisely in the liftoff and touchdown maneuvers. The unique problem facing VSTOL operations is the necessity to maximize pilot vision while still maintaining a good supersonic area distribution. An overnose vision angle of 15 degrees in conjunction with overside vision of 40 degrees was deemed necessary for operation during liftoff and touchdown as well as transition.

In the case of a vertical attitude VTOL aircraft, there is an extreme attitude change from horizontal to vertical; i.e., 90 degrees. This special case requires a more dramatic solution so that reasonable pilot vision can be maintained as well as a position that will allow him to retain his orientation during the transition maneuver.

As this VSTOL aircraft is also a high performance fighter, it is essential that the pilot has good aft visibility and that he maintains a high level of proficiency during air combat high "G" maneuvers. There is a contradiction in the requirement for high "G" tolerance and VSTOL visibility. Greater proficiency results from a reclined seat position in the former case, and an upright position for the latter.

Pilot safety is of primary concern during VSTOL operations with a necessity that the aircraft provide an escape system for all modes of flight. This escape criterion is referred to as the "pilot ejection envelope" and, in the case of VSTOL aircraft, must cover the flight regime from low altitude no speed to high altitude high speed. In some cases, the extreme attitude of the aircraft will require some kind of "vertical seeking seat" so that altitude may be gained before chute deployment.

During VTOL operations, pilot workload is high, a condition exacerbated by the need to monitor critical controls and displays to assure safe operations while permitting major emphasis on the exterior situation. Engine health must also be monitored to assure sufficient thrust for safe vertical flight. Any instrument operation that must be completed during the vertical flight mode must be operable from either the control stick or the throttle.

5.4.2 Crew Seat Positioning

The problem of pilot orientation and visibility through the transition maneuver arises as a result of the extreme attitude change from horizontal flight to vertical flight. How the aircraft interfaces with the ship in the vertical attitude presents a formidable problem combined with the added difficulties of reducing risks and making this mode of operation acceptable to pilots. The solutions to these problems may result in a complex articulation system with associated weight and drag penalties. Three crew station articulation concepts have been developed for possible application on the VATOL aircraft: forward articulating seat, forward articulating crew station, and articulating forward fuselage. The fundamental considerations of each are discussed below.

Forward Articulating Seat. The concept of articulating the seat represents the simplest system and is similar to that used on the X-13 research aircraft developed by Ryan to investigate VTOL technology. (See Figure 5-7). The seat is rotated through an angle of 45 degrees while the aircraft changes attitude by 90 degrees, resulting in the effective pilot attitude change of only 45 degrees. This attitude reduction helps to maintain the pilot's orientation through the transition maneuver. The seat is pivoted about a point that will permit the pilot's feet and hands to remain in a stationary

position, allowing him to use a single set of controls during transition. Control for the seat position is provided by a switch on the control stick that initiates and terminates seat articulation. Careful attention must be paid to cockpit instrumentation to compensate for the pilot's eye movement relative to the instrument panel. An effect this system has on the basic aircraft is the requirement for additional volume to accommodate the seat articulation. This results in an increase in cross-sectional area at the critical cockpit location.

Pilot ejection from the vertical attitude is accomplished by returning the seat to the back position and then firing the seat in a normal sequence. The seat back angle from this position combined with the vertical attitude results in a downward trajectory which must be compensated for by the use of a vertical seeking seat.

This crew station concept has the minimum of shipboard interface difficulties because the entire articulating seat remains within the basic mold lines of the aircraft. One area that may develop as an interface problem is a requirement for shipboard visual aids during gantry engagement because of the restricted visibility from the forward seat position.

Articulating Crew Station. The second crew station concept considered for the vertical attitude aircraft incorporates the idea of rotating the entire crew station out of the basic aircraft fuselage as shown in Figure 5-8. This concept permits the pilot to remain in the same relative position with the instrument panel, flight controls, and horizon through the transition thus retaining his orientation. Operation is automatic during the transition maneuver, with an additional override switch provided on the stick. The crew station is a capsule which during transition is unlatched about the canopy and rotated out unpressurized through an angle of 45 degrees. The effect of this rotation is to reduce the angle that the pilot is rotated from 90 degrees to 45 degrees. As a result of the crew station rotating away from the body, visibility is improved during vertical attitude operation. Critical areas for design emphasis are the hermetic sealing of the unpressurized capsule in the out position, and the method of articulation and support for the capsule. These detail design considerations may result in an increase in volume and weight for the cockpit area.

Pilot ejection is possible from any attitude during transition because the seat back angle is maintained in an upright direction. Wheter this angle is sufficient to make a safe escape without the necessity of a vertical seeking seat has not been determined.

Shipboard interface of this crew station is essentially the same as the previous concept, with the exception of vertical attitude visibility. While the seat back angle in the vertical attitude is the same as on the articulating seat, visibility is improved by the capsule rotating out away from the fuselage, thus providing a less obstructed view.

Articulating Forward Fuselage. The third crew station concept for use on the vertical attitude VSTOL utilizes a completely articulating forward fuselage which is hinged just aft of the cockpit (see Figure 5-9). This system rotates the pilot through an angle of 75 degrees during transition so the net effect is that the pilot maintains almost the same attitude while aircraft translates into the vertical position. With this concept, the pilot not only retains his orientation but also most of the forward visibility. While this concept articulates the most mass, resulting in the largest weight increase, it also results in the minimum volume buildup at the cockpit, and thus the least amount of wave drag.

Escape from this concept is similar to the horizontal attitude aircraft as the forward fuselage always remains in a horizontal attitude. With this simplified system, pilot ejection can be accomplished with a "0-0" ejection seat.

Significant development would have to be undertaken to determine the possibilities of adapting this concept to shipboard operations. While this system offers superior visibility and pilot attitude, it also introduces an interference between the gantry and the projecting nose.

A subject reevaluation of the candidate crew station design approaches has been made, Figure 5-10, with the articulating crew station selected to be in the configuration.

5.5 SUBSYSTEMS

Primary study effort for aircraft subsystems was to define preliminary concepts to support the configuration development. Specific systems such as landing gears and propulsion installation were evaluated in more depth than other systems since they had a major impact on the configuration development. Other systems discussed below include hydraulics, environmental control, fuel, and electrical. General location of system components are shown on the inboard profile drawing, Figure 2-4.

The propulsion installation utilizes two engines mounted in the aft fuselage. A three point mount system is used to attach each engine to the airframe. The air induction system consists of closely-spaced rectangular fixed geometry inlets positioned above the wing and fuselage, internal ducting terminating at each engine compressor face and a plenum with auxiliary air inlet doors located forward of the engine compressor face. A single splitter plate separates the two inlets and a boundary layer diverter is positioned below the inlets. A variable C-D, axisymmetric, gimbled nozzle, capable of 30^{o} pitch, 15^{o} yaw of swiveling, is provided on each engine. Aircraft accessories consisting of generator and hydraulic pump are mounted on and driven by the engine. Firewalls, fire detection, and extinguishing systems are provided. Access doors are located on the lower surface of the aft fuselage to facilitate engine servicing, maintenance and engine installation/removal.

Fuel is carried in three bladder cells in the fuselage and in two integral wing tanks. Two of the bladder cells are engine feed tanks, one supplying each engine. All other tanks supply fuel to the feed tanks by automatic sequence transfer of fuel. Booster pumps installed in inverted flight compartments, within the engine feed tanks supply fuel to the engines. Cross feed fuel capability is provided. Other fuel system components include a vent system, fuel quantity and flow measurement, pressuring fueling, fuel dumping and external fuel provisions.

The environmental control system is located in the center fuselage aft of the nose gear compartment. The system provides air to the cockpit for pressurization and defog, anti-G suit, canopy seal, and avionics equipment cooling. Hot air anti-icing and rain repellant/removal systems are provided for the windshield. Closed loop air cycle environmental control concepts are proposed and require further study to define specific system arrangements and performance capabilities.

Aircraft electrical power is provided by two alternating current generators, transformer rectifiers, a battery, and the power distribution system. The generating system is of the constant hertz type with the generators mounted on and driven by the engine gearbox. Use of electrical technology concepts such as solid state switching, multiplexing, power monitoring, fibre optics for signal transmission and use of advanced permanent magnet materials in generator and electric motor construction, provide for an efficient lightweight electrical system.

Dual independent high pressure (8,000 psi) hydraulic systems are used. Primary flight control actuators are dual and receive one-half of their power from each system. Each system consists of multiple circuits which can be isolated from the main system in the event of a leakage failure. An engine-driven pump, sealed pressurized reservoir, return pressure sensing switching valves, filters, and ground power connections are provided for each system. High strength steel and titanium lines and low flammability fluid are used. Adequate power is provided in each system to control the airplane in the event of a complete failure of a single system.

The landing gear is compatible with the vertical platform takeoff and landing system as well as an emergency landing on a conventional carrier deck. Adequate tip-back and turn-over angles are provided for deck and ground handling. The gear system is not designed for conventional carrier catapult launch. Adequate wheel brakes and a nose gear steering system are installed for deck/ground handling and taxi on/off the platform.

The nose gear is specifically designed to engage one of the vertical platform cables as well as absorb the shock of an emergency conventional carrier landing. The basic shape and angles of the shock strut housing and trailing arm are configured to guide the platform cable into the locking slot when the aircraft is allowed to settle downward. The cable will be guided into the slot when the nose tire is within several inches of the platform or fully loaded against the platform. The latch will retain the nose gear in the slot while the cable stanchions are rotated and the platform lowered to the horizontal position. Replaceable wear plates are attached to the housing and trailing arm where cable contact is made. The shock absorber unit is fully protected within the outer housing.

A baseline avionics suite is shown in Table 5-2 which also lists certain options and alternatives. Options are additions to the baseline which provide significant supplemented capability and may be adopted either through missionizing a single version of the aircraft, or in alternate versions of the fighter/attack aircraft.

The avionics have been configured to support the anticipated missions of the aircraft. The multi-mode radar has a full air-to-air search and track capability along with an air-to-ground synthetic-aperture high-resolution ground-mapping and target-designating capability. It would be capable of detecting a 5-square meter target at a range of 35 to 45 NMI in a look-down situation over ±60° azimuth coverage and track up to 10 targets simultaneously. The radar will include reduced probability-of-intercept features and have its emissions controlled by the Observables Control and Management system. The avionics will be covert, i.e., designed to minimize observables throughout the rf, IR and visible spectrum. The air-to-air features and characteristics of the avionics suite are only gross estimates at this time and would be refined as the capabilities and characteristics of the supporting functions (GCI, AEW, Defense Suppression, etc.) and the advanced weapons are better defined.

TABLE 5-1. GROUP WEIGHT STATEMENT

SHORT GROUP WEIGHT STATEMENT
NAVAIR FORM 13060/3 (4-72) DATE

	STRUCTURE MODEL		Lbf	Kgf	% TOW		
			7,055	3,201	23.52		
1.	WING		2,062	935			
2.	ROTOR						
3.	TAIL (Vertical)		119	54			
4.	BODY		2,605	1,182			
5.	ALIGHTING GEAR		1,313	596			
6.	ENGINE SECTION		956	434			
7.	PROPULSION		5,985	2,715	19.95		
8.	ENGINE INSTALLATION		4,920	2,232			
9.	ACCESS. GR. BOXES & DRIVE	IN 8					
10.	EXHAUST SYSTEM	IN 8					
11.	ENGINE COOLING	IN 8					
12.	WATER INJECTION						
13.	ENGINE CONTROLS	IN 8					
14.	STARTING SYSTEM	IN 8					
15.	PROPELLER INSTAL.						
16.	SMOKE ABATEMENT						
17.	LUBRICATION SYSTEM	IN 18					
18.	FUEL SYSTEM		1,065	483			
19.	DRIVE SYSTEM						
20.	JET DRIVE						
21.	FLIGHT CONTROLS	IN 24					
22.	AUX. POWER PLANT	IN 8					
23.	INSTRUMENTS		120	54			
24.	HYDRAULICS & PNEUMATICS		1,640	739	5.47		
25.	ELECTRICAL	IN 24					
26.	AVIONICS		1,177	534			
27.	ARMAMENT (inc.missile launcher)		167	76			
28.	FURNISHINGS & EQUIPMENT		250	113			
29.	AIR CONDITIONING		260	118			
30.	ANTI-ICING						
31.	PHOTOGRAPHIC						
32.	LOAD & HANDLING						
33.	MANUFACTURING VARIATION						
34.	WEIGHT EMPTY		16,654	7,550	55.51		
35.	CREW (NO.)		215	98			
36.	PASSENGERS (NO)						
37.	FUEL-UNUSABLE		150	68			
38.	FUEL-INTERNAL		12,558	5,696	41.86		
39.	FUEL-EXTERNAL						
40.	OIL		50	23			
41.	FUEL TANKS. AUX.						
42.	BAGGAGE						
43.	CARGO. TROOPS						
44.	GUNS						
45.	AMMUNITION						
46.	EQUIPMENT (O_2. SURVIVAL KITS)	IN 28	13	6			
47.	WEAPONS INSTALLATION						
48.	BOMBS						
49.	ROCKETS. MISSILES		360	163			
50.							
51.							
52.							
53.	PHOTOGRAPHIC						
54.	MISCELLANEOUS						
55.	USEFUL LOAD		13,346	6,054	44.49		
56.	GROSS WEIGHT		30,000	13,604	100.0		

TABLE 5-2. BASELINE AVIONICS SUITE

	BASELINE		OPTIONS
COMMUNICATIONS NAVIGATION IDENTIFICATION	JTIDS TERMINAL UHF RADIO MMW RADIO INTERCOM INTEGRATED INERTIAL ASSEMBLY LANDING/TAKE-OFF SENSORS	68KG (150 LBS)	GPS TERMINAL TF/TA (IN RADAR)
TARGET ACQUISITION/ WEAPON DELIVERY	SYNTHETIC APERTURE MULTIMODE RADAR GUN FIRE CONTROL & DISPLAY WEAPON LAUNCH CONTROL ARMAMENT CONTROL-FIBER OPTICS TERMINAL DAMAGE ASSESSMENT SET	122KG (270 LBS)	FLIR (MULTICOLOR) TARGET DESIGNATOR LASER/MMW MMWAVE SENSOR TVSU
CONTROLS & DISPLAYS	WIDE ANGLE HEAD-UP DISPLAY MASTER MONITOR DISPLAY MULTIMODE SITUATION DISPLAY VOICE ACTUATED/SIGHT LINE ACTUATED & MANUAL CONTROLS HELMET SIGHT UNIT	45KG (100 LBS)	INTEGRATED IMAGING/MAP DISPLAY
DATA PROCESSING & DISTRIBUTION	MISSION COMPUTER AIR DATA/FLIGHT CONTROL & NAVIGATION COMPUTER FIBER OPTICS/MUX BUS CONTROL TERMINAL	23KG (50 LBS.)	
DEFENSIVE SYSTEMS (ELECTRONIC WARFARE)	THREAT WARNING RECEIVERS ECM/EOCM/IRCM OBSERVABLES REDUCTION & CONTROL INTERFERENCE & POWER MANAGEMENT EXPENDABLES	152KG (335 LBS)	
	TOTAL	410 KG (905 LBS)	

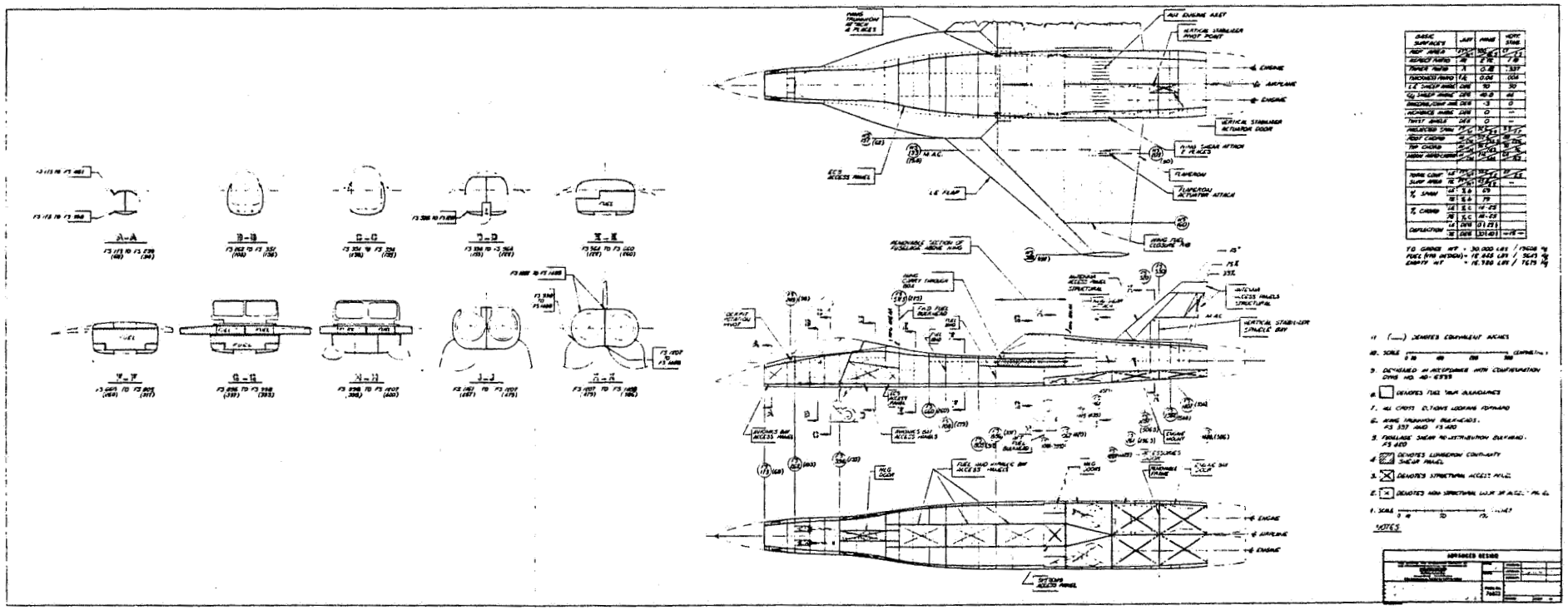

FIGURE 5-1. STRUCTURE DIAGRAM

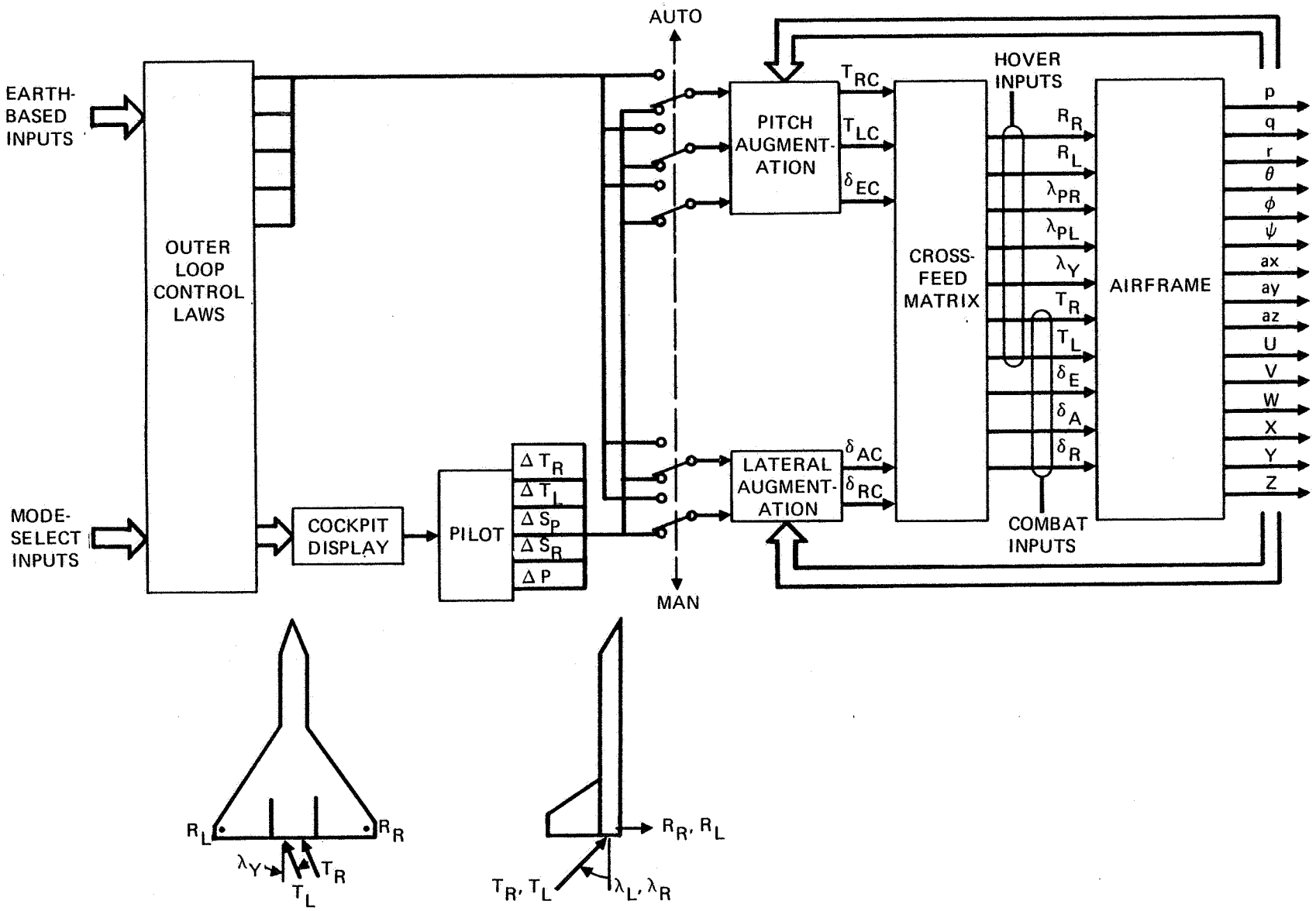

FIGURE 5-2. AIRFRAME-FLIGHT CONTROL SYSTEM CONFIGURATION

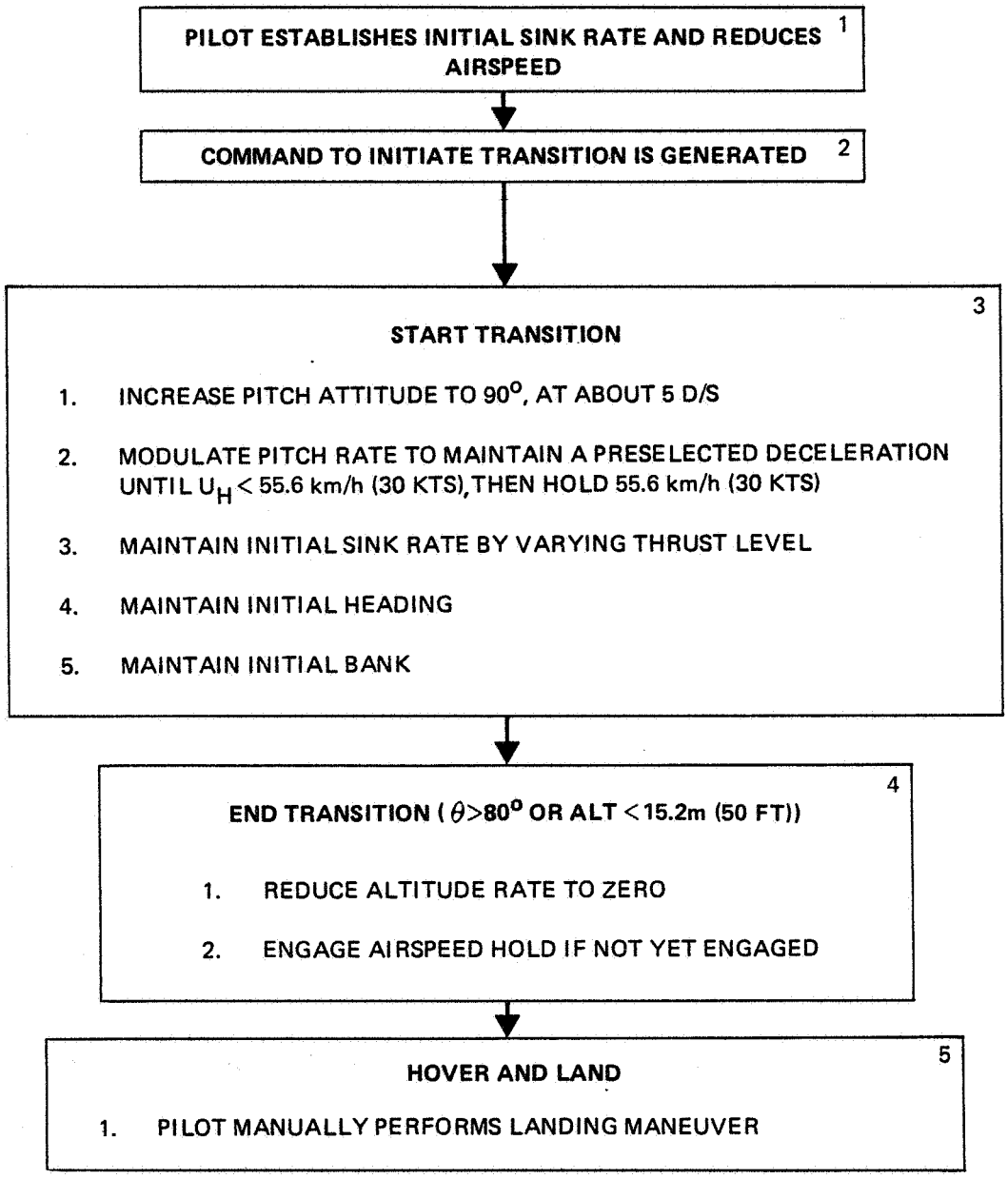

NOTE: FUNCTIONS IN BLOCKS 3 AND 4 PERFORMED AUTOMATICALLY

FIGURE 5-3. TRANSITION-LANDING SEQUENCE

ALL GAINS POSITIVE

SW 1 TO -0.1G WHEN $U_A \leq 1.1\ V_S$ AND LAND UNTIL $U_H < U_1$

SW 1 TO +0.1G WHEN ALT > 15.2 m (50 FEET) AND TAKEOFF UNTIL $U_A > 1.1 V_S$

SW 2 TO CENTER WHEN $U_A \leq 1.1\ V_S$ UNTIL $\theta > 80^o$ OR ALT $\leq$ 15.2 m (50 FEET), THEN CLOSES TO POSITION A

$a_H = a_\ell \cos\theta - a_N \sin\theta$

$a_V = a_\ell \sin\theta + a_N \cos\theta$

a_ℓ IS POSITIVE FOR ACCEL ALONG X-BODY AXIS

a_N IS NEGATIVE FOR ACCEL ALONG Z-BODY AXIS

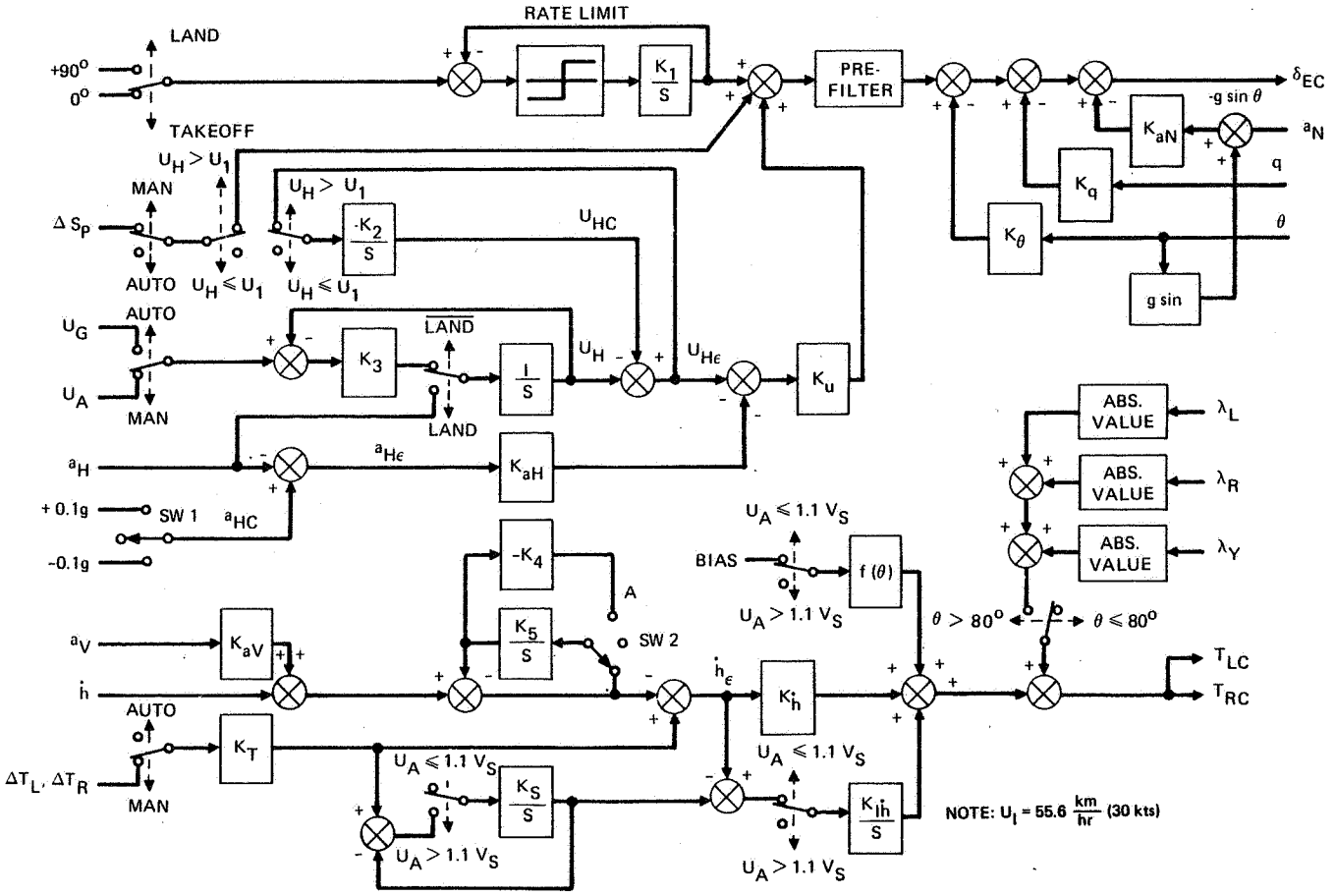

FIGURE 5-4. PITCH AUGMENTATION

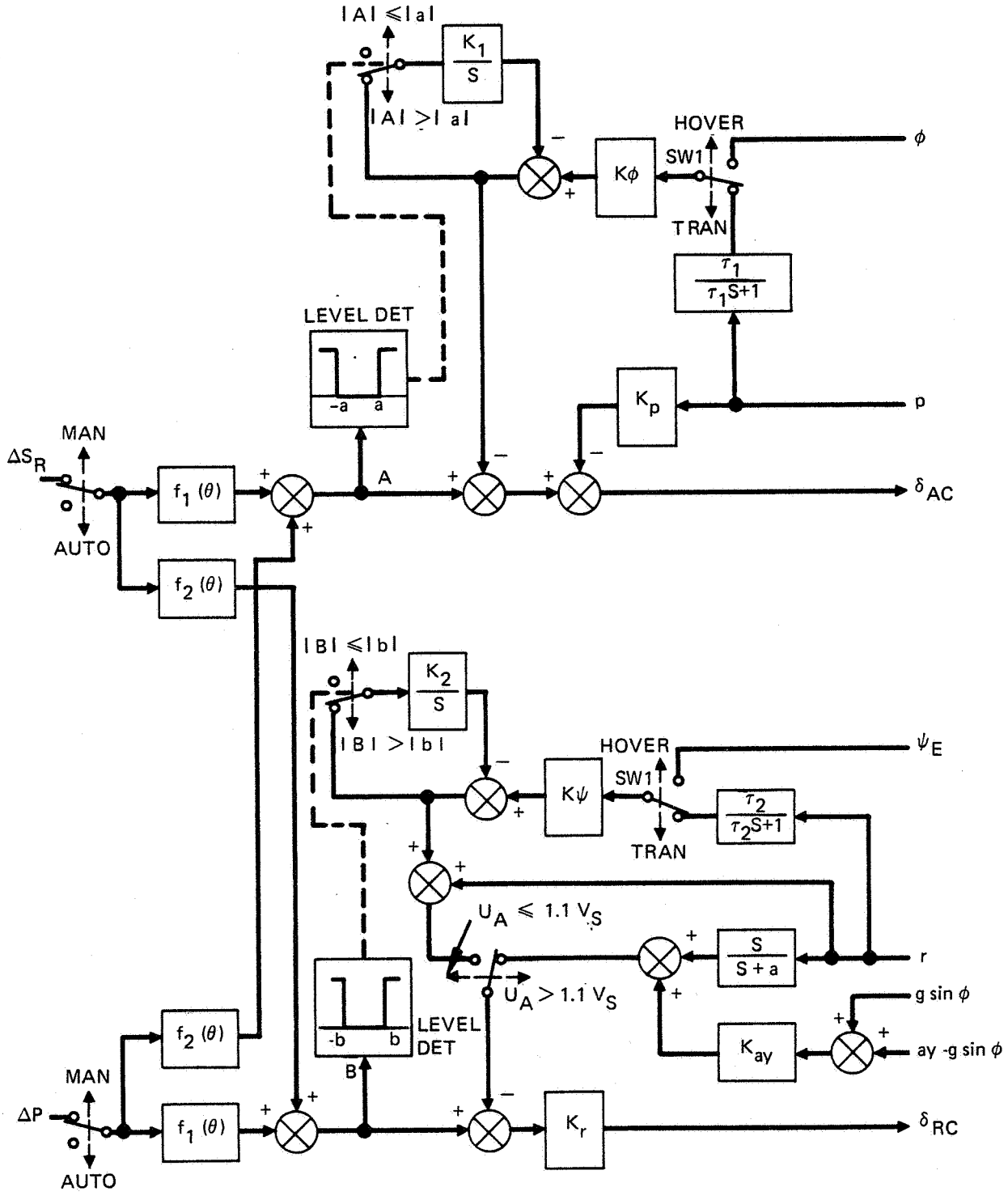

SW1 - AS SHOWN WHEN $U_A \leq 1.1\ V_S$ UNTIL $\theta > 80^o$, THEN SWITCHES TO OPPOSITE POSITION

FIGURE 5-5. LATERAL AUGMENTATION

$Y = AX$

$Y = [R_R\ R_L\ \lambda_R\ \lambda_L\ \lambda_Y\ T_R\ T_L\ \delta_E\ \delta_A\ \delta_R]^T$

$X = [T_{RC}\ T_{LC}\ \delta_{EC}\ \delta_{AC}\ \delta_{RC}]^T$

MATRIX A

Y \ X	T_{RC}	T_{LC}	δ_{EC}	δ_{AC}	δ_{RC}
R_R	0	0	0	a_{14}	0
R_L	0	0	0	a_{24}	0
λ_R	0	0	a_{33}	a_{34}^S	0
λ_L	0	0	a_{43}	a_{44}^S	0
λ_Y	0	0	0	0	a_{55}
T_R	a_{61}	0	0	0	0
T_L	0	a_{72}	0	0	0
δ_E	0	0	a_{83}	0	0
δ_A	0	0	0	a_{94}	0
δ_R	0	0	0	0	a_{105}

$a_{33} = a_{43}$

$a_{34}^S = -a_{44}^S$

ALL ELEMENTS EXCEPT THESE EQUAL ZERO IN CONVENTIONAL FLIGHT

SUPERSCRIPT S INDICATES THIS TERM IS OF SECONDARY IMPORTANCE, BUT NOT NECESSARILY NEGLIGIBLE.

FIGURE 5-6. CROSSFEED MATRIX

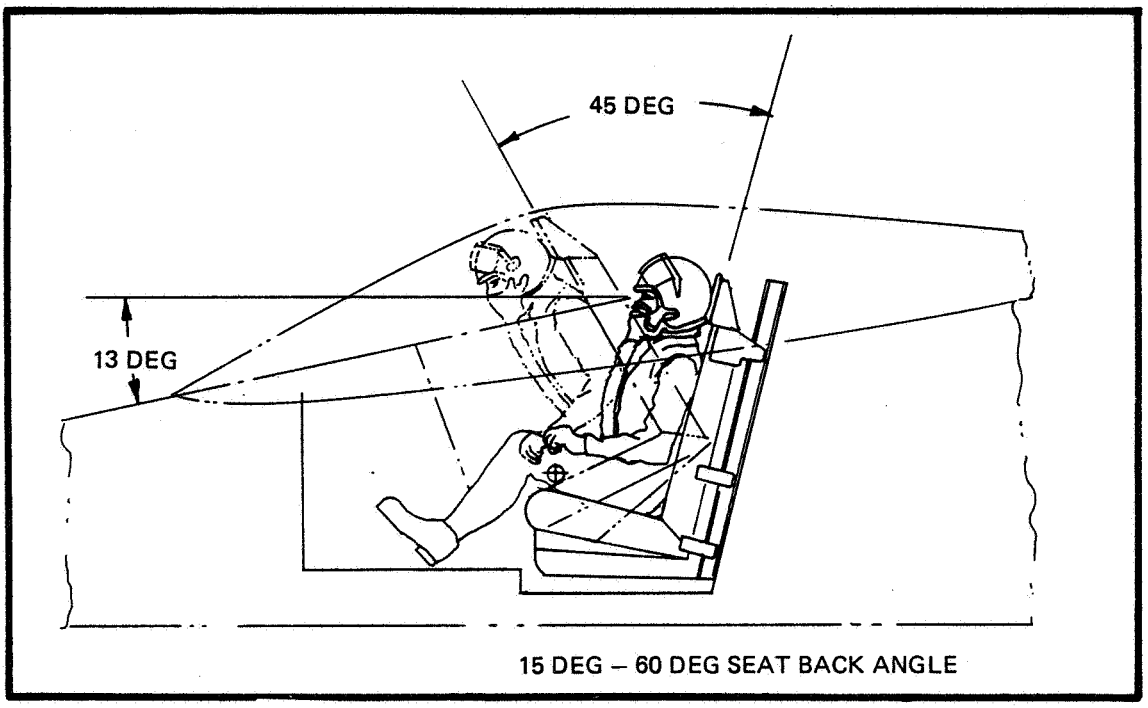

FIGURE 5-7. ARTICULATING SEAT

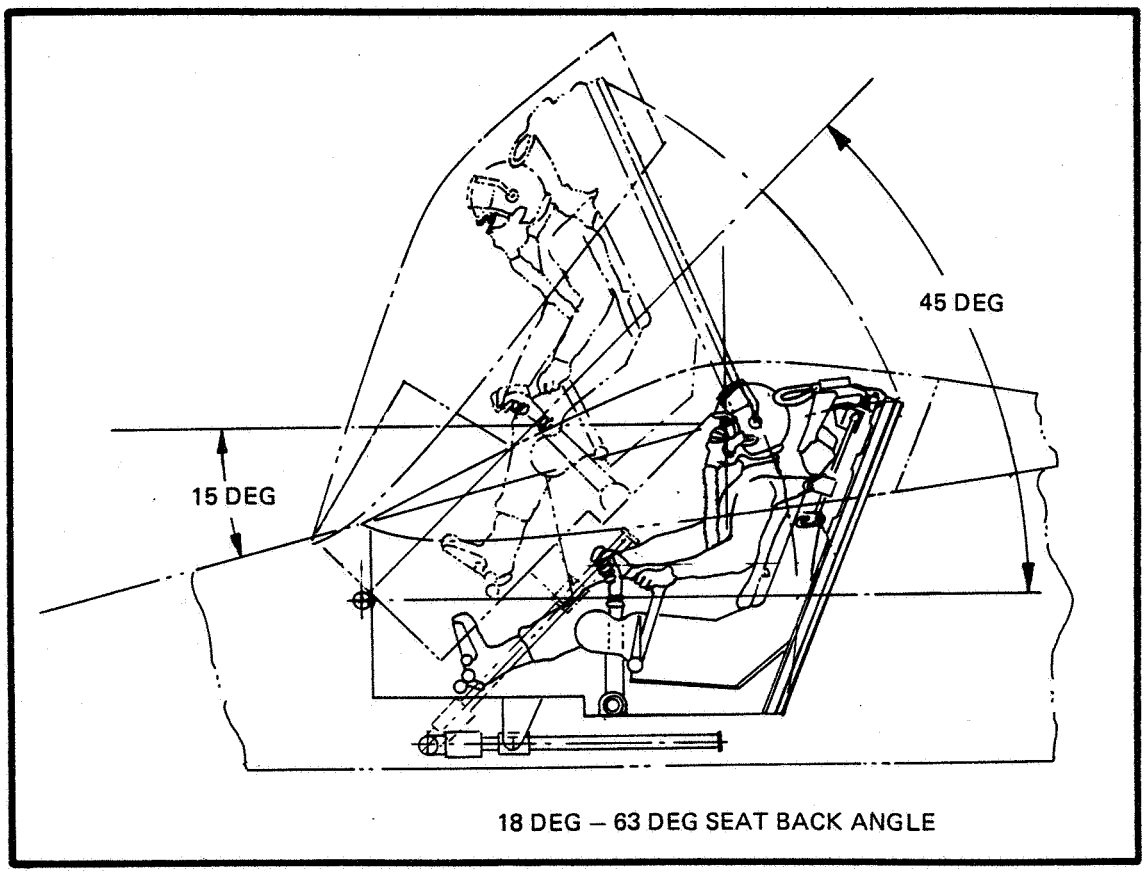

FIGURE 5-8. ARTICULATING CREW STATION

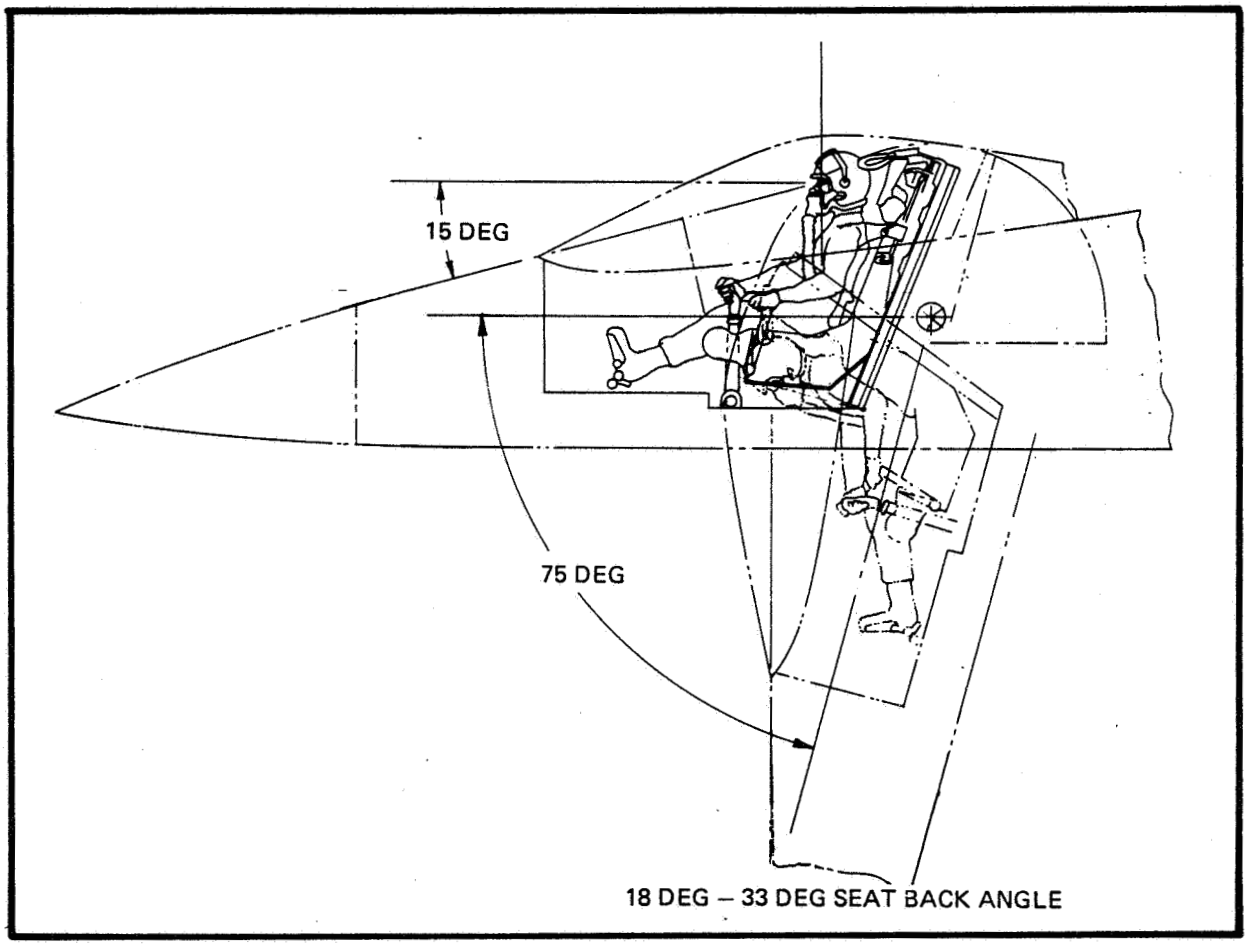

FIGURE 5-9. ARTICULATING FORWARD FUSELAGE

ARTICULATING SEAT

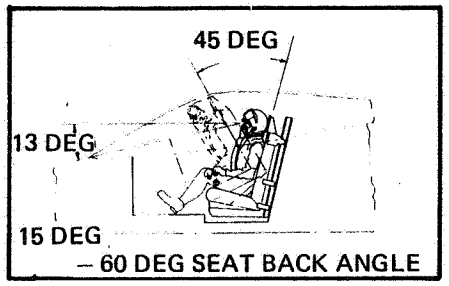

POSITIVE

- LEAST WEIGHT
- MINIMUM COMPLEXITY
- HAS ALREADY BEEN FLOWN

NEGATIVE

- HIGH CROSS--SECTIONAL AREA
- LOWEST "G" TOLERANCE
- POOREST VISIBILITY (HORIZONTAL & VERTICAL ATTITUDE)
- POOREST PILOT ORIENTATION
- COMPLEX EGRESS
- REDUCED INSTRUMENT AREA

ARTICULATING CREW STATION

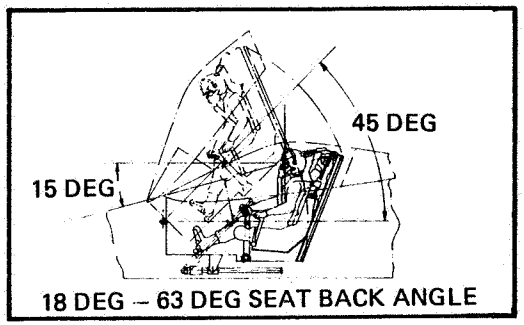

POSITIVE

- MINIMUM VOLUME
- GOOD VISIBILITY

NEGATIVE

- WEIGHT INCREASE
- MODERATE "G" TOLERANCE
- UNDEVELOPED SYSTEM

ARTICULATING FORWARD FUSELAGE

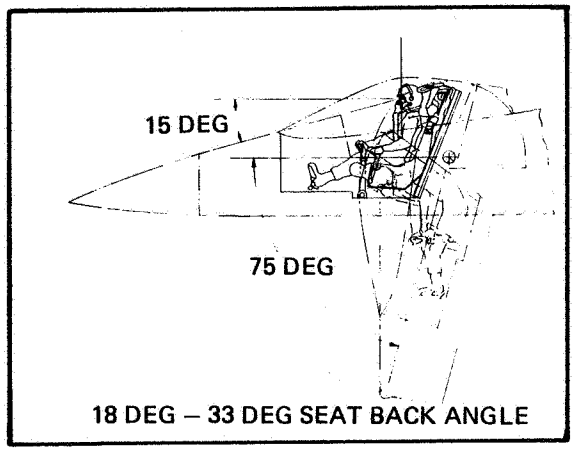

POSITIVE

- BEST VISIBILITY (HORIZONTAL & VERTICAL ATTITUDE)
- BEST PILOT ORIENTATION
- GOOD "G" TOLERANCE

NEGATIVE

- HIGHEST COMPLEXITY
- HEAVIEST WEIGHT
- HIGHEST VOLUME REQUIRED
- POSSIBLE GANTRY INTERFERENCE

FIGURE 5-10. ADVANTAGES/DISADVANTAGES - VERTICAL ATTITUDE CREW STATION CONCEPTS

SECTION 6

AIRCRAFT PERFORMANCE

Aircraft performance is presented in two sections. The first pertains to combat performance, and the second pertains to takeoff and landing performance.

6.1 FLIGHT PERFORMANCE

6.1.1 Data Summary

All combat performance data are presented at 88 percent of takeoff weight. The specific excess power performance capabilities, as a function of load factor, of the 13,608kg (30,000 lb) baseline configuration are provided in Figures 6-1 through 6-3 for 3048; 6096; and 9144 m (10,000; 20,000; and 30,000 ft), respectively. The baseline configuration has a wing loading of 2.873 kN/m^2 (60 psf) and a T/W of 1.17 installed tropical day. Data for M0.5, 0.6, 0.9, and 1.2 are presented for each altitude with M1.6 data for 6096 and 9144 m (20,000 and 30,000 ft). Sustained load factor capabilities decrease with altitude for all Mach numbers except M1.6. At each altitude, the sustained load factor capability increases with Mach number in the subsonic region (M0.9) and through the transonic region (M1.2) at 6096 and 9144 m (20,000 and 30,000 ft). The maximum instantaneous load factor available is limited by the maximum usable lift coefficient for M0.5 at all altitudes and for M0.6 at 6096 and 9144 m (20,000 and 30,000 ft.) The structural design load factor of 8g can be attained at all other Mach numbers. At 3048 m (10,000 ft), M0.9 and 1.2, the specific excess power capabilities are greater than 35 m/sec (115 fps) at 8g.

Additional flight performance data are presented in Figures 6-4 and 6-5 in terms of flight envelope contours. Figure 6-4 gives specific excess power contours of 0.91, 183, and 274 m/sec (0,300, 600 and 900 fps) for lg flight. Figure 6-5 provides lg, 3g, 6g and 8g sustained load factor contours.

The baseline configuration at 88 percent takeoff weight can accelerate from M0.8 to M1.6 at 9144 m (30,000 ft) in 63 sec with a maximum speed capability of M1.76. (See Figure 6-4). The absolute ceiling is approximately 19,500 m (64,000 ft). The lg specific excess power goal of 274 m/sec (900 fps) at M0.9 at 3048 m (10,000 ft) can be attained at 4000 m (13,000 ft). The structural design load factor level of 8g can be achieved from M0.79 to 1.21 at 3048 m (10,000 ft) and at M1.05 at 4600 m (15,000 ft). The sustained load factor goal of 6.2g at M0.6 at 3048 m (10,000 ft) can be attained at M0.606.

A representative fighter escort mission depicted and defined in Table 6-1 was selected to determine the baseline configuration radius capability and for the T/W and W/S trades sizing studies discussed below. The baseline configuration can perform the mission at 1170 km (630 nm) radius. A radius of 926 km (500 nm) was selected as a more representative Navy radius requirement for the T/W and W/S trades. The takeoff and landing allowances reflect Navy specified allowances.

6.1.2 Thrust Loading and Wing Loading/Aircraft Sizing

The effects of T/W and W/S variations on the size of aircraft capable of performing the 962 km (500 nm) mission can be seen in Figure 6-6. For this matrix of sized aircraft, specific excess power and sustained load factor matrices are presented in Figures 6-7 and 6-8 for combat weights at 88 percent of the takeoff weights of Figure 6-6. The rated T/W of 1.27 required to perform a VTO at sea level on a tropical day, a 2743 m/sec (900 fps) specific excess power line from Figure 6-7 and a 6.2g sustained load factor line from Figure 6-8 (performance goals) have been superimposed on the sizing matrix of Figure 6-6 and are shown in Figure 6-9.

The intersection of the takeoff line and the 6.2g load factor goal line indicates that a wing loading of approximately 2.750 kN/m (57 psf) is the highest that could be used to provide the performance goals. The aircraft weight would be approximately 10,500 kg (23,200 lb) with an acceleration time of 93 sec from M 0.8 to 1.6 at 9144 m (30,000 ft). A slightly lighter weight aricraft results at a wing loading of approximately 2.3 kN/m^2 (48 psf). However, the higher wing loading is required to assure an acceleration time less than 100 sec and provide the highest specific excess power capabilities. The takeoff weight of the lighter aircraft is 10,450 kg

(23,050 lb), 50 kg (100 lb) less than the aircraft just meeting the takeoff and sustained load factor goal. The minimum weight aircraft has a 6.9g and 290 m/sec (950 psf) performance level, but cannot achieve M 1.6 at 9144 m (30,000 ft).

Data shown in Figure 6-10 have been transferred from the specific excess power matrix (Figure 6-7) to the aircraft sizing matrix, Figure 6-6. The same procedure for sustained load factor levels gives the data of Figure 6-11.

Figures 6-10 and 6-11 can be used to perform additional trade studies to determine the effects of various levels of specific excess power and sustained load factor combinations on aircraft size and T/W – W/S. For example, if the performance goals were 6g and 290 m/sec (950 psf), the aircraft weight would be approximately 10,750 kg (23,700 lb) with a T/W of 1.29 and wing loading of 2.92 kN/m^2 (61 psf) with an acceleration time of about 80 seconds.

6.1.3 Sensitivity Studies

Two forms of sensitivity studies have been conducted, one at constant takeoff weight with mission radius and combat performance varying and one at constant mission radius with takeoff weight and combat performance varying. The parameter varied are empty weight, minimum drag, drag-due-to-lift, specific fuel flow, and installed thrust. For the selected sized aircraft, the effect on mission radius and combat performance as shown in Figure 6-12. The weight variation is approximately 5 percent of the empty weight, and the minimum drag variation is approximately 8 percent at M 0.8 at 9144 m (30,000 ft). For convenience, the performance parameters variations are based on 70 percent fuel rather than 88 percent takeoff weight. From Figure 6-12, we see that the empty weight change produces almost twice the change in radius capability as the specific fuel consumption. The specific fuel consumption is almost three times as significant as the other parameters. As expected, the thrust variation is the most significant for the performance parameters P_S, n_Z and radius. The effect on takeoff weight and combat performance at constant radius with T/W and W/S maintained is shown in Figures 6-13 and 6-14.

For the constant mission radius sensitivity studies, the empty weight variation produces over twice as much change in takeoff weight as the specific fuel consumption

and eight to ten times the effect of the other parameters (see Figure 6-13). The thrust variation still produces more effect on the performance parameters for sized aircraft; however, the other parameters can be as significant. As the aircraft are resized for each parameter variation, the installed thrust changes at constant T/W are greater than the minimum drag changes with wing area at constant W/S. The selected aircraft is marginal on achieving M 1.6 at 9144 m (30,000 ft). Consequently, five percent reductions of thrust, specific fuel consumption and 1,000 lb empty weight and an increase of 10 counts (0.0010) in minimum drag reduces the maximum speed below M 1.6. Direct addition of the effects of combinations of the sensitivity parameters provides reasonable accuracy.

6.2 TAKEOFF AND LANDING

6.2.1 Control Concept

For flight in the sub-aerodynamic regime, with the airplane essentially in the vertical attitude, the controllers include thrust modulation of the two engines in unison for height control and coupled gimballing deflections of the two nozzles for pitch and yaw control. Anti-symmetric pitch deflections provide roll control in conjunction with reaction nozzles at the wing tips. Motions in the horizontal plane are obtained by inclining the aircraft in the direction of the desired movement.

6.2.2 Takeoff Transition

Transitions of vertical attitude VTOL configuration are potentially more difficult than horizontal attitude VTOL configuration transitions in that, at least in the decelerating landing transition, the airplane has to rotate through a 90-degree angle of attack range. Difficulties encountered during transition by the Ryan X-13 demonstrated that poor aerodynamics in and beyond stall can interfere with the smoothness of transition. LEX-generated vortex flow is used in the study concept to increase the angle of attack for maximum lift and to cause the lift to drop gradually past the stall. These characteristics were found to produce smooth transition trajectories using simple control command schedules.

A series of accelerating transition trajectories is shown in Figure 6-15. For fuel economy and for flight safety reasons, it is advisable to complete the transition in the shortest time possible. This means holding the time in vertical ascent to a minimum and pitching over rapidly, in order to maximize kinetic energy (airspeed) as much as reasonable vertical clearance will permit. Pitch angle time histories follow closely the commanded pitch, and the pitch rate averages about 12 degrees per second. The actual control commands used in the calculations are pitch attitudes as a function of airspeed, which are shown in Figure 6-16. Angles of attack during accelerating takeoff transitions generally remain below stall, as shown in Figure 6-17. All takeoff transitions were executed with maximum thrust.

Flight safety aspects in takeoff transition in case of failure of one engine were studied to determine the extent of the initial unsafe zone in which pilot ejection is the only recourse for survival. Engine failures were programmed to occur at various points along the flight path, after which transitions continued with one engine inoperative. The boundary beyond which transitions can be completed safely is indicated in Figure 6-15. From the time marks, it is evident that there is a critical time almost independent of the initial trajectory which must be exceeded to acheve flight safety in case of an engine failure.

6.2.3 Landing Transition

During decelerating landing transitions thrust modulation is needed as a control parameter to control flight path and deceleration in conjunction with pitch angle and associated aerodynamic lift. A combination of favorable aerodynamic characteristics and an automatic electronic control system make smooth transitions possible.

Figure 6-18 shows angle of attack versus airspeed of a high weight (13,608 kg, (30,000 lb)) decelerating transition which was executed by commanding a constant flight path angle of three degrees and the deceleration schedule shown in Figure 6-19. The smoothness of the curve in Figure 6-20 and the absence of speed reversals attest to the satisfactory high angle-of-attack aerodynamic longitudinal characteristics. The associated thrust variation is shown in Figure 6-20. As the time marks on Figure 6-18 indicate, the duration of the decelerating transition is 43 seconds which is about four times as long as an accelerating takeoff transition at the same weight. A horizontal flight path instead of a sloping one would allow more deceleration and a shorter landing transition.

6.2.4 Short Takeoff (STO)

A short takeoff, necessitated by the required 4536 kg (10,000 lb) VTO overload is difficult as thrust deflection is not available to any significant degree. In addition, landing gear geometry limitations preclude the airplane reaching a high attitude while rolling along the deck so that aerodynamic lift and the lift component of the thrust remain small. Improved STO performance may be obtained with airplane rotation to a higher atttitude over the water after leaving a flight deck. During the rotation, the airplane will sink, a condition which is not inconsistent with current Navy practice for aircraft carrier catapult operations. This maneuver minimizes the required deck run by permitting the aircraft to depart the ship at sub-airborne speed at its maximum ground clearance attitude. The subsequent rotation achieves conditions for sustained flight by the higher levels of aerodynamic lift and thrust support available at angles of attack in excess of the ground clearance limit and by continued longitudinal acceleration. Figure 6-21 shows the deck run required as a function of takeoff weight and wind over deck, if a 1.524 m (5 ft) sink off the bow is permitted. The maximum angle of attack to which the airplane was permitted to rotate was 20 degrees which corresponds to $0.9\ C_{L_{max}}$, a customary safety-related launch restriction, but in some cases this limit was not reached. Nose wheel lift off (easily initiated by thrust vectoring) to a 10 degree pitch attitude occurs during the deck roll. The pitch rate for over-the-water rotation reaches 10 degrees per second.

Deck runs can be shortened further when takeoff is aided by a ramp at the end of the deck. A straight ramp was chosen instead of the curved "ski jump" ramp to facilitate calculations. The function of the ramp is to increase the initial attitude of the airplane when it leaves the deck and to impart an upward momentum which allows more time for the airplane to reach the limiting sink condition, time which the airplane utilizes to accelerate to airborne speeds. Figure 6-22 shows how the deck run is shortened as a function of ramp angle. Two conditions are indicated: (2) the airplane is allowed to sink 1.524 m (5 ft) below the lip of the ramp, and (b) the airplane is allowed to sink 1.524 m (5 ft) below the level of the main deck. The latter condition adds ramp height to the total sink permissible. Caution should be exercised in interpreting the curves, however, as the straight ramp ends at a greater height than the more realistic curved ramp of equal length and terminal angle. On the other hand, the calculations also reduced the launch kinetic energy of the aircraft by approximately the excess height of the ramp, a consideration which would shorten the deck run.

The equivalence of ramp angle and wind over deck to achieve the same deck run length as shown in Figure 6-23.

The level of STO performance attained with the over-the-water rotation maneuver is largely made possible by the favorable high angle of attack characteristics achieved through the LEX. The LEX increases aerodynamic lift by extending the linear portion of the lift curve to higher angles of attack. This in turn allows aircraft rotation to a high attitude to achieve a high thrust lift component.

6.2.5 Conventional Takeoff and Landing

Conventional takeoffs and landings can be performed on land-based runways. Landing approach speeds in the conventional attitude will be of the order of 213 km/hr (115 kn) which will require arrestment for carrier landings. The inclusion of conventional carrier suitability is considered incompatible with design for VSTOL, but some carrier landing capability is believed desirable in the event of engine failure or similar emergency. Hence, the proposed configuration includes a standard tail hook and associated backup structure, but the aircraft and alighting gear are not designed to either carrier landing or catapult design criteria.

TABLE 6-1. TYPICAL FIGHTER ESCORT MISSION

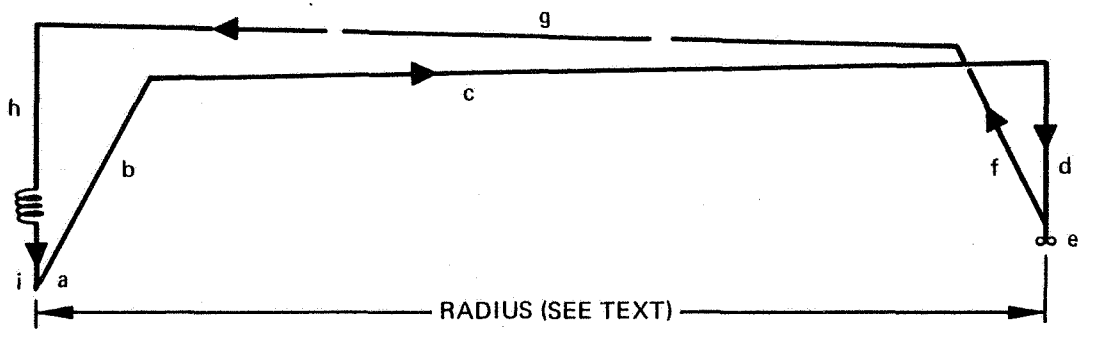

SEGMENT	MISSION EVENT	FUEL REQUIREMENT BASIS
a	START, T.O., TRANSITION AND ACCELERATE TO BEST CLIMB SPEED	2.5 MINUTES AT INTERMEDIATE POWER AT SEA LEVEL STATIC CONDITIONS 32.1°C (89.8°F), TROPICAL DAY
b	CLIMB FROM SEA LEVEL TO BEST CRUISE ALTITUDE	MAX R/C AT INTERMEDIATE POWER
c	CRUISE OUT	BEST ALTITUDE AND MACH NO.
d	DESCENT TO 9144 METERS (30,000 FEET)	NO DISTANCE OR FUEL CREDIT
e	TASK ORIENTED COMBAT	(1) ACCELERATION FROM M 0.8 TO M 1.2; 9144 METERS (30,000 FEET) AT MAXIMUM THRUST (2) 360° SUSTAINED TURNS AT M 1.2; 9144 METERS (30,000 FEET) (3) 360° SUSTAINED TURNS AT M 0.6; 3048 METERS (10,000 FEET)
f	CLIMB FROM 3048 METERS (10,000 FEET) TO BEST CRUISE ALTITUDE	MAX R/C AT INTERMEDIATE POWER
g	CRUISE BACK	BEST ALTITUDE AND MACH NO.
h	DESCENT TO SEA LEVEL	NO DISTANCE OR FUEL CREDIT
i	RESERVES AND LANDING	(1) 10 MINUTES LOITER AT SEA LEVEL AT MAXIMUM ENDURANCE SPEED – ALL ENGINES OPERATING, STANDARD DAY (2) 45 SECONDS AT INTERMEDIATE POWER AT SEA LEVEL STATIC CONDITIONS, ALL ENGINES OPERATING, 32.1°C (89.8°F), TROPICAL DAY (3) 5% OF INITIAL FUEL

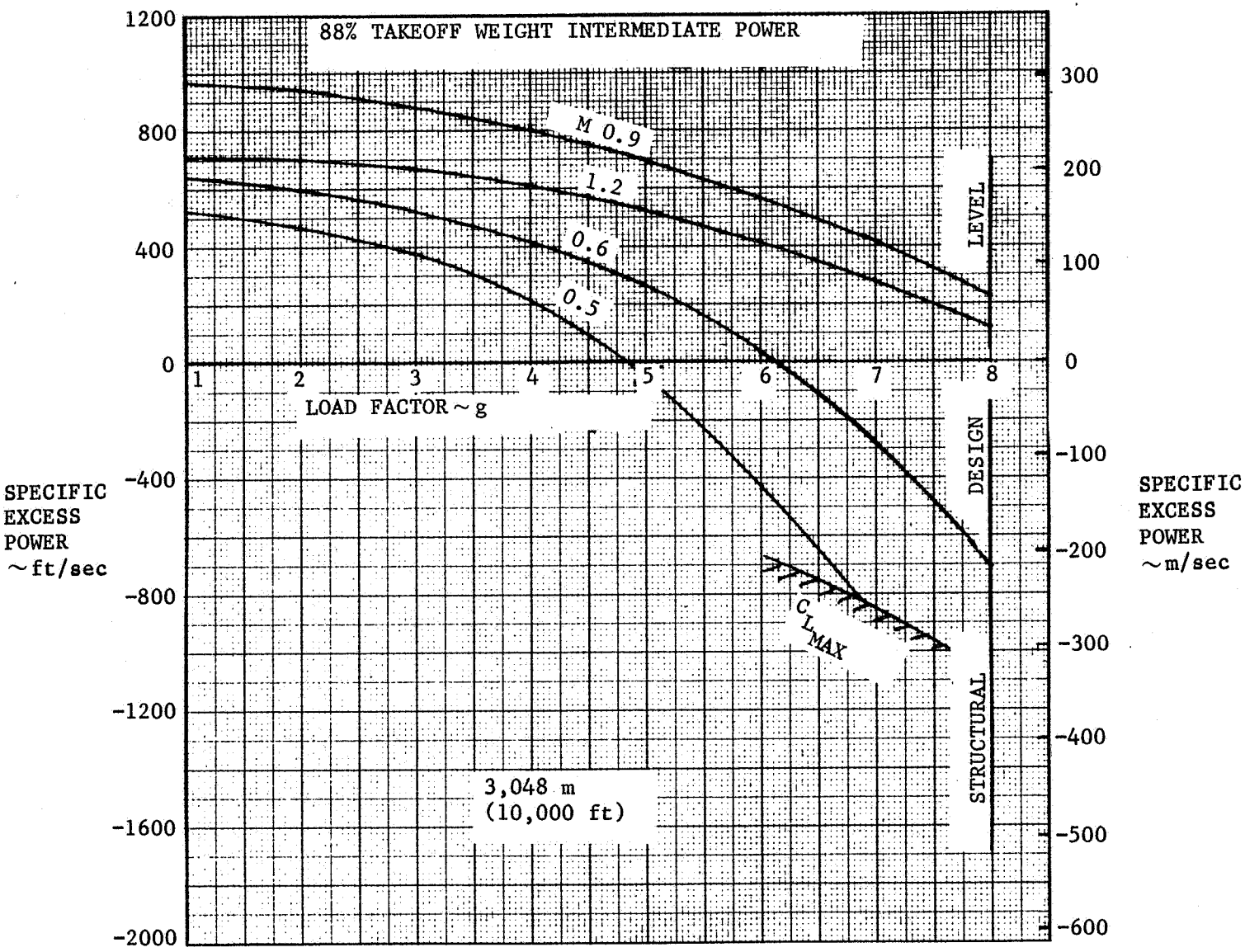

FIGURE 6-1. EFFECT OF LOAD FACTOR AND MACH NUMBER ON SPECIFIC EXCESS POWER AT 3048 m (10,000 ft)

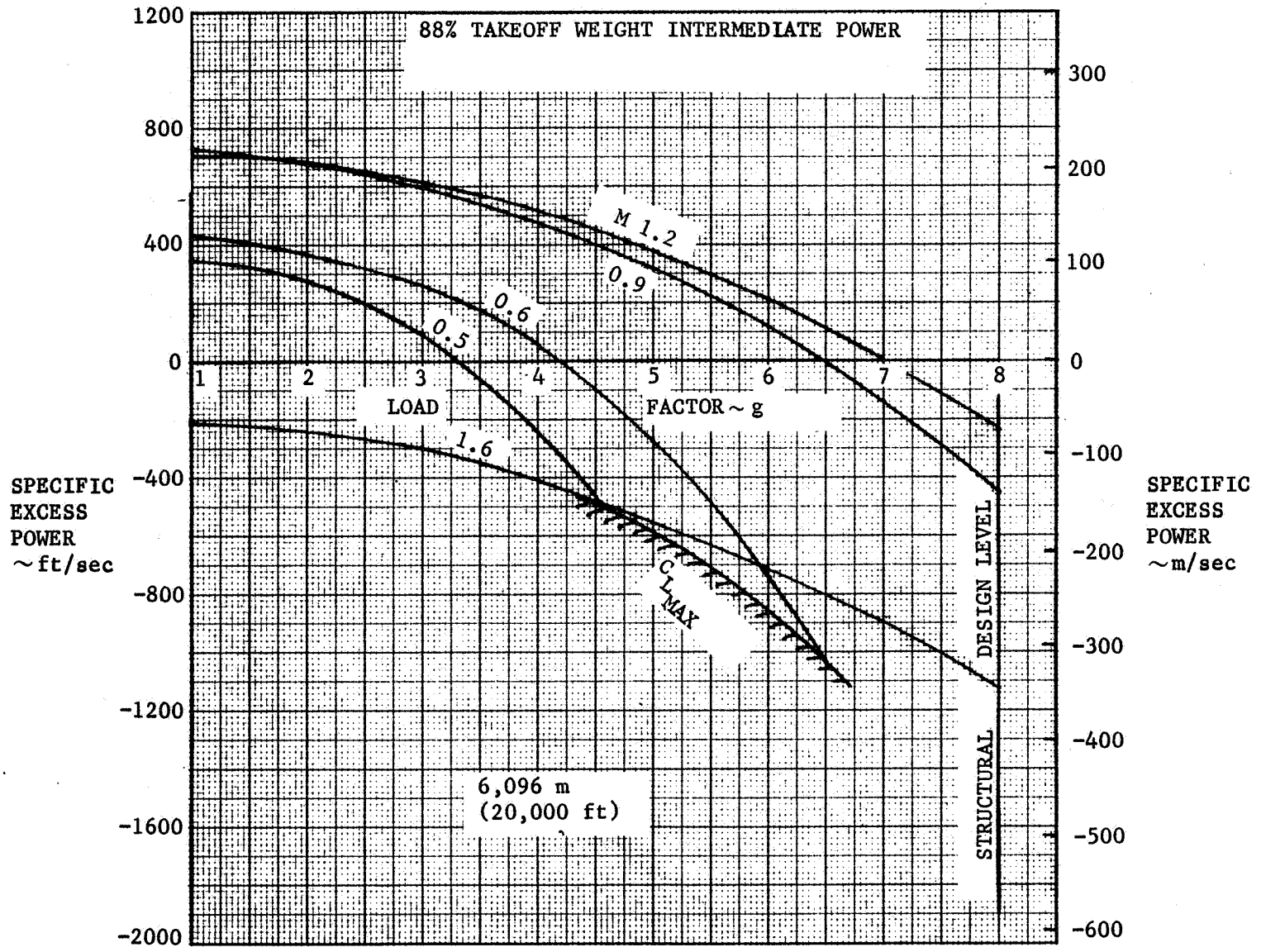

FIGURE 6-2. EFFECT OF LOAD FACTOR AND MACH NUMBER ON SPECIFIC EXCESS POWER AT 6096 m (20,000 ft)

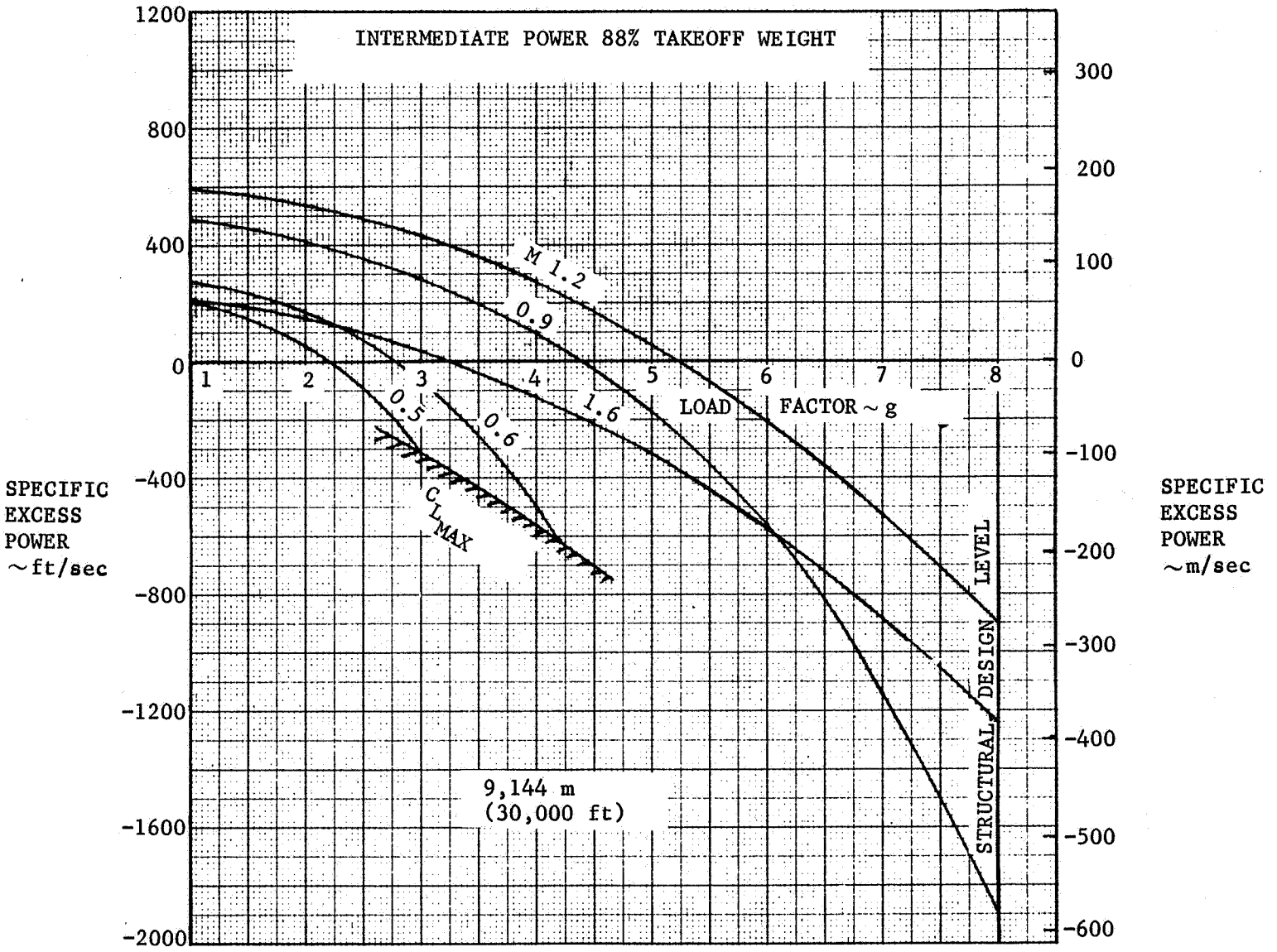

FIGURE 6-3. EFFECT OF LOAD FACTOR AND MACH NUMBER ON SPECIFIC EXCESS POWER AT 9,144 m (30,000 ft)

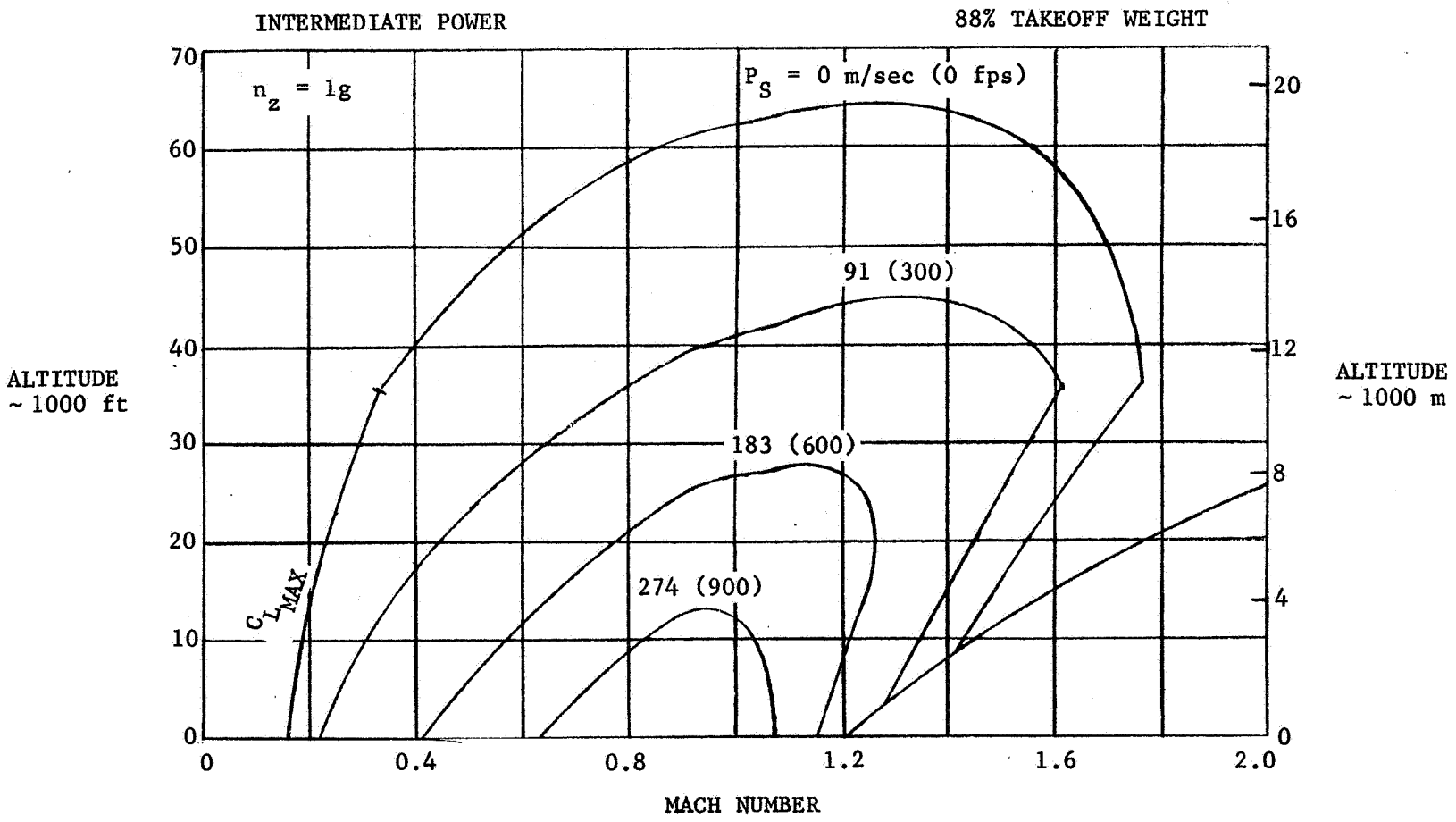

FIGURE 6-4. SPECIFIC EXCESS POWER CONTOURS

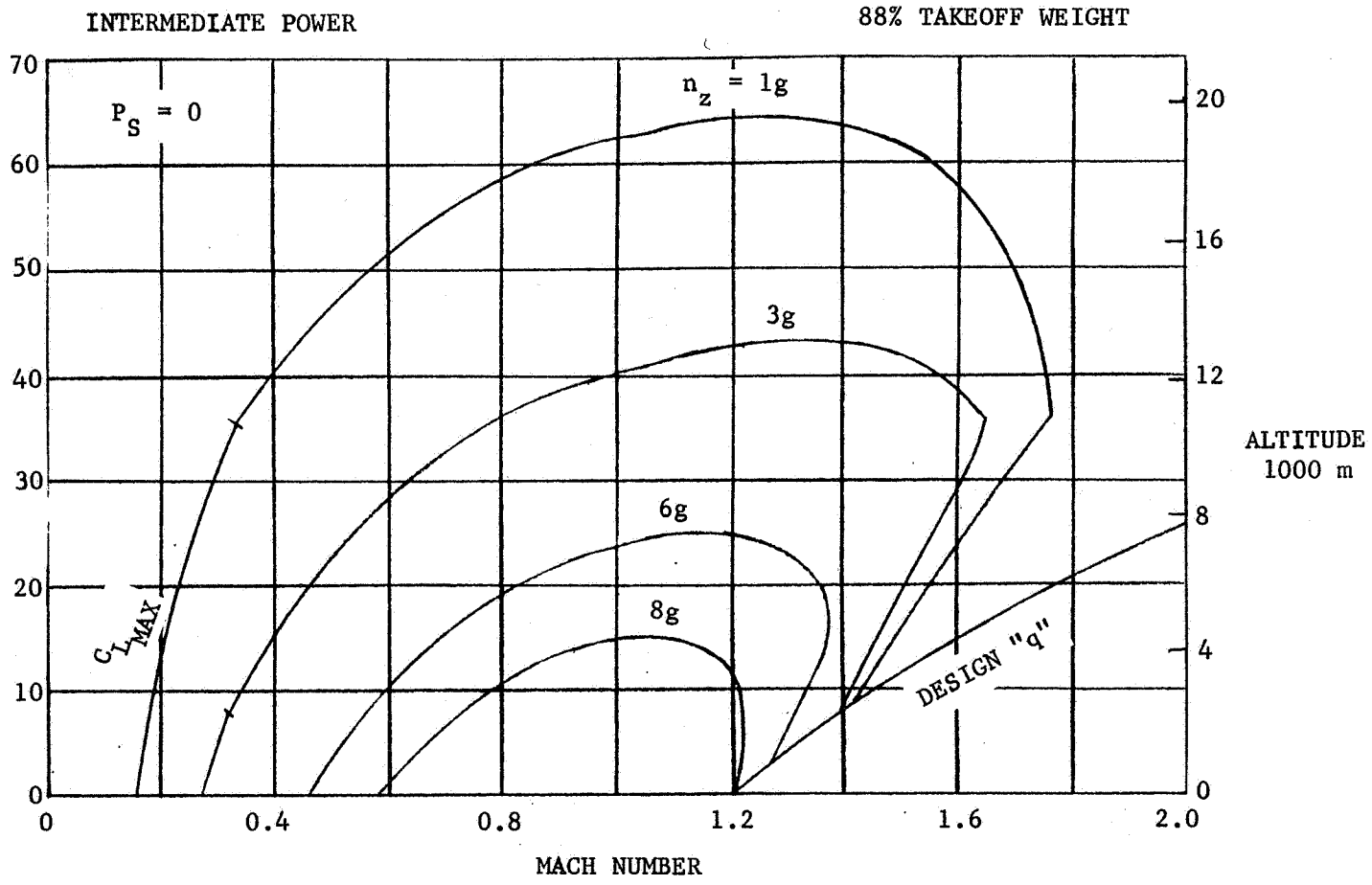

FIGURE 6-5. SUSTAINED MANEUVER CAPABILITY

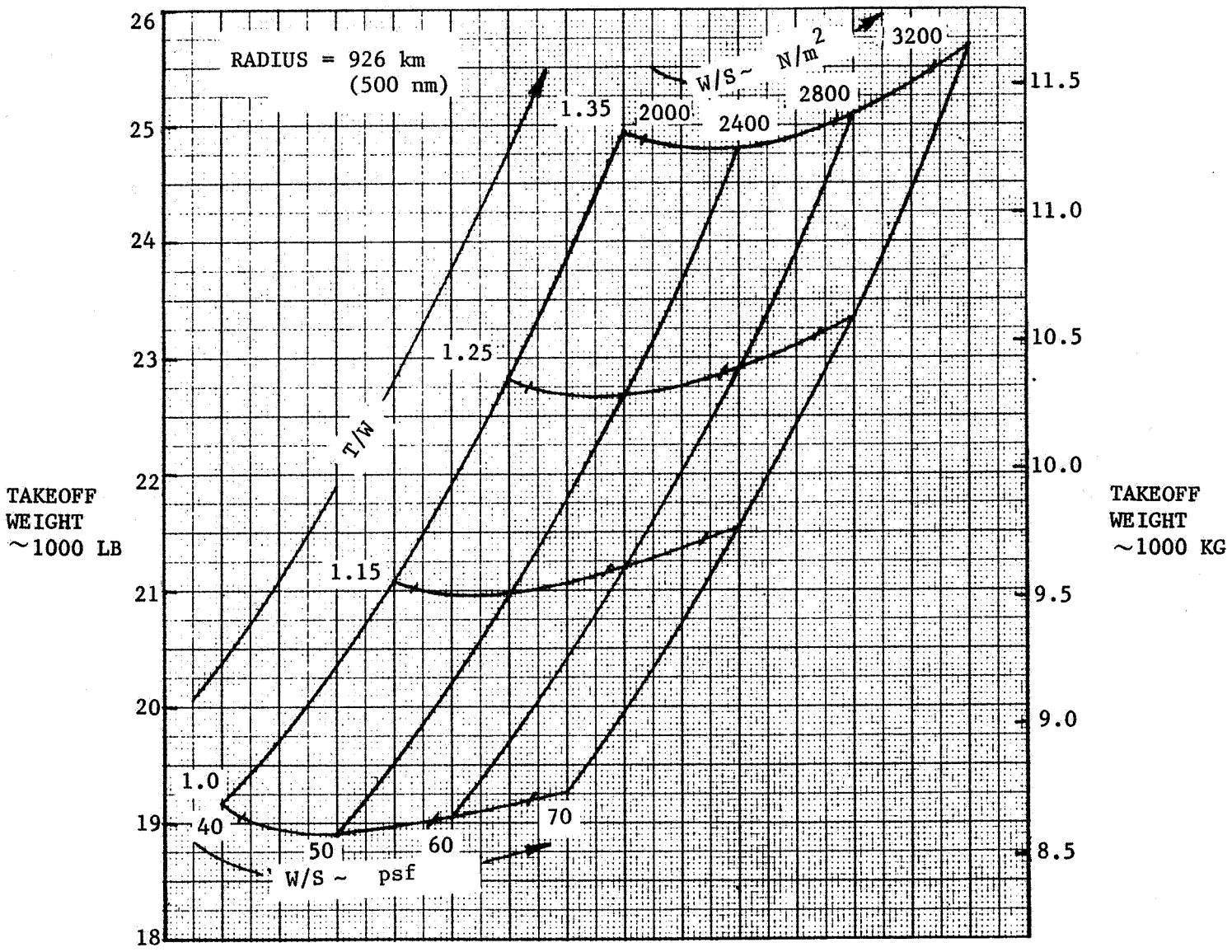

FIGURE 6-6. AIRCRAFT SIZING MATRIX

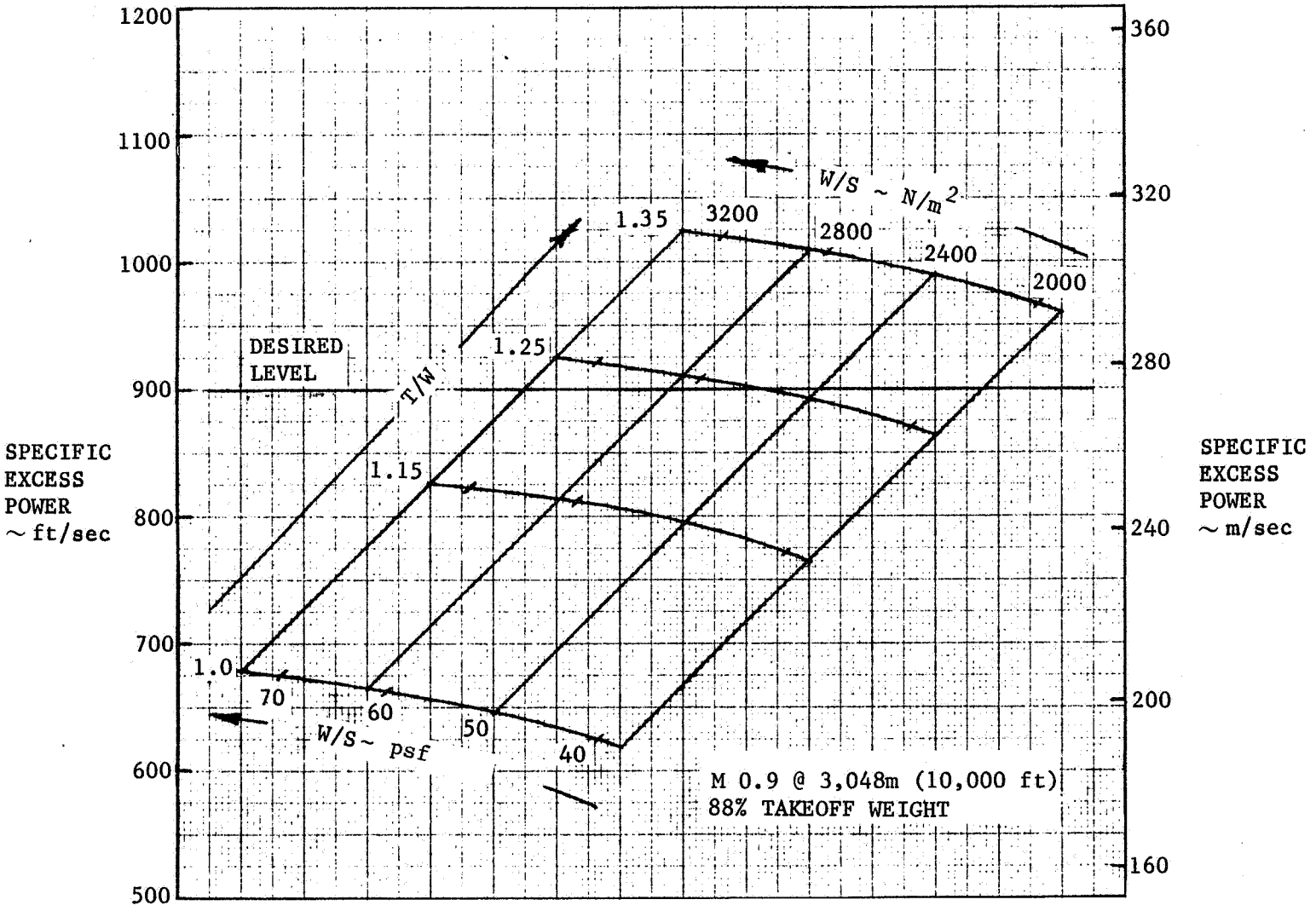

FIGURE 6-7. VARIATION OF SPECIFIC EXCESS POWER WITH T/W AND W/S FOR AIRCRAFT SIZING MATRIX

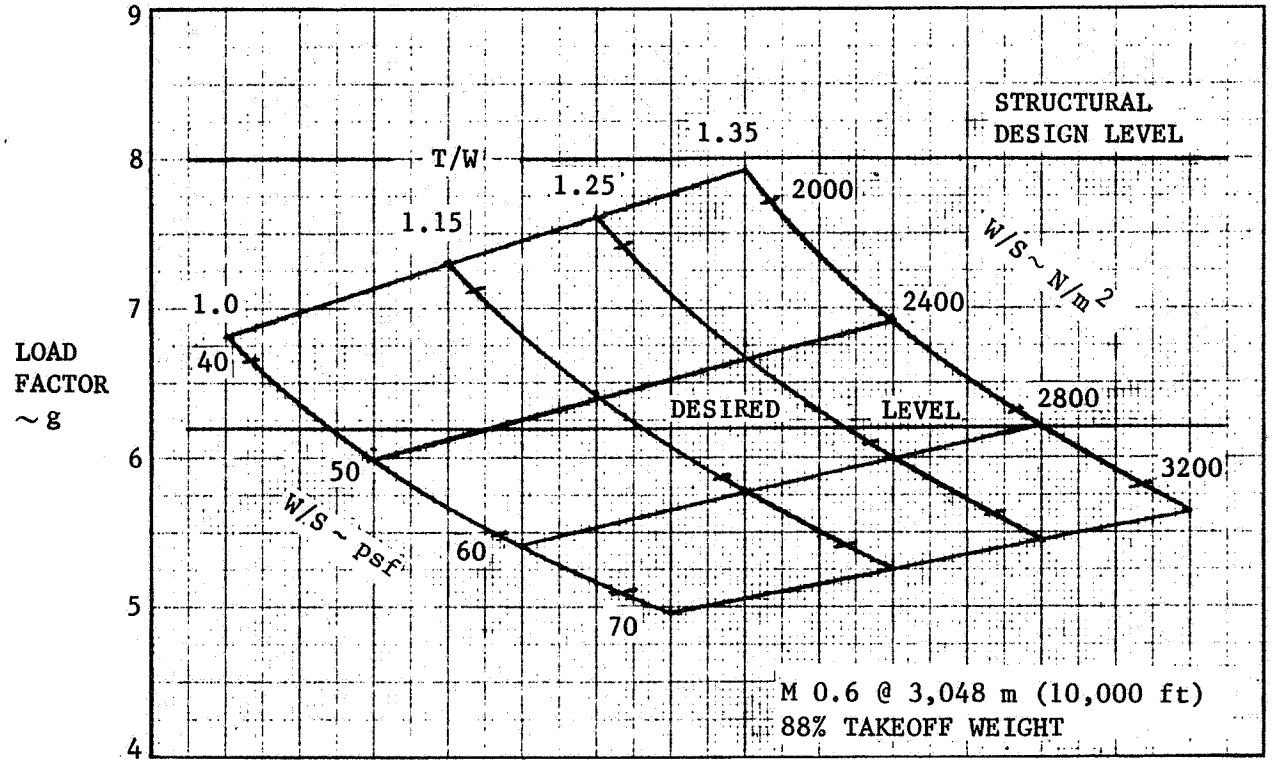

FIGURE 6-8. VARIATION OF SUSTAINED LOAD FACTOR WITH T/W AND W/S FOR AIRCRAFT SIZING MATRIX

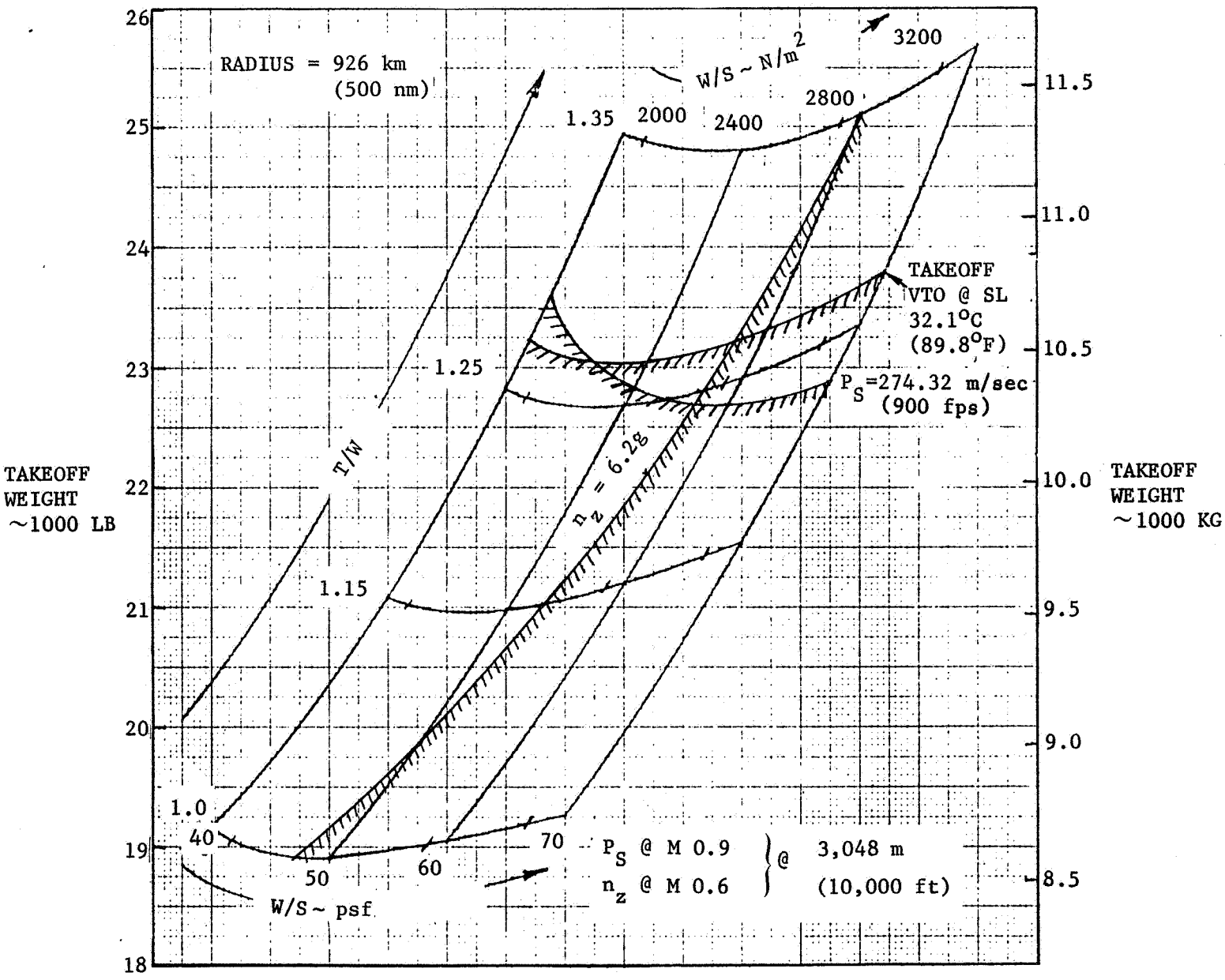

FIGURE 6-9. PERFORMANCE GOALS RELATIONSHIP WITH AIRCRAFT SIZING MATRIX

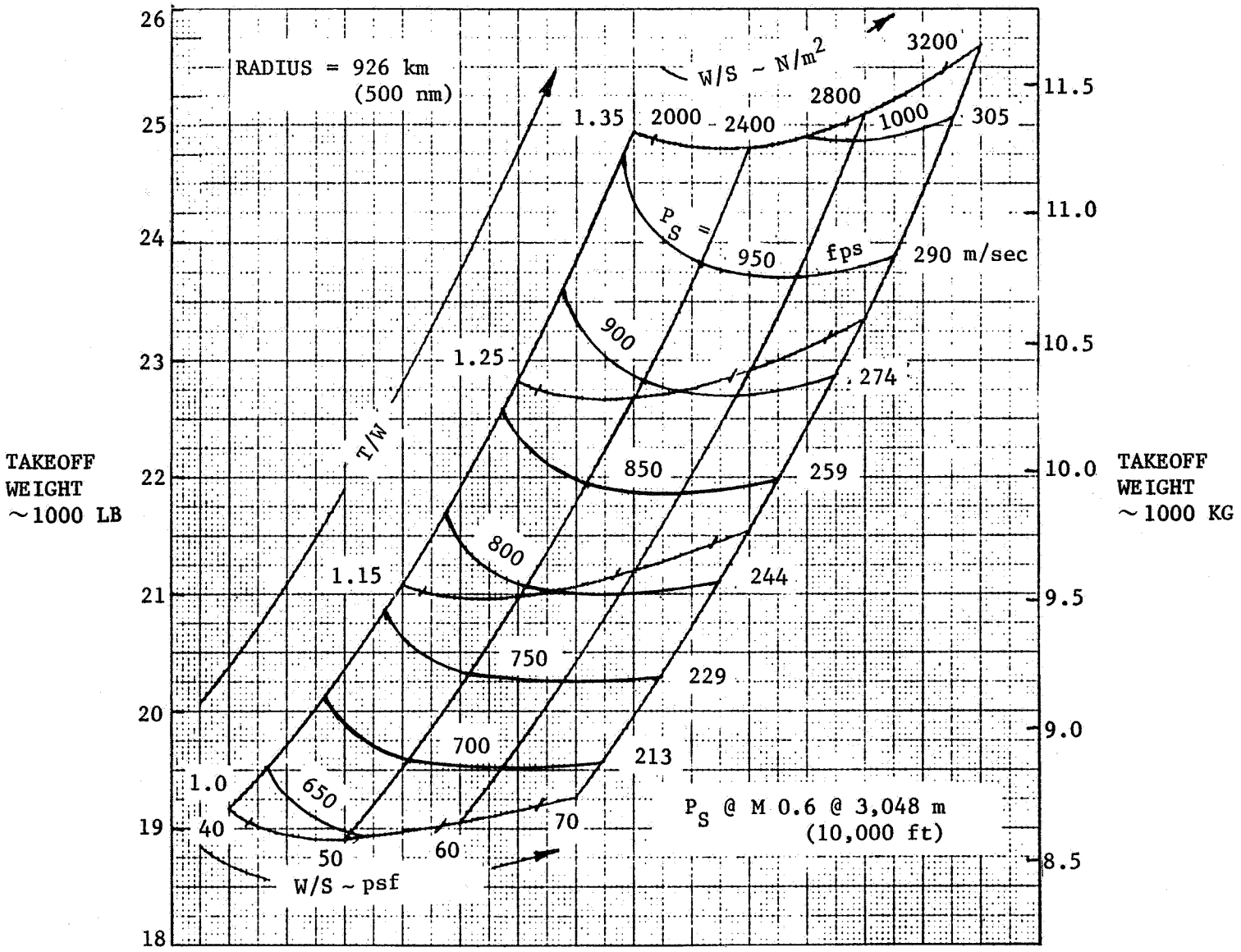

FIGURE 6-10. SPECIFIC EXCESS POWER LEVELS ON AIRCRAFT SIZING MATRIX

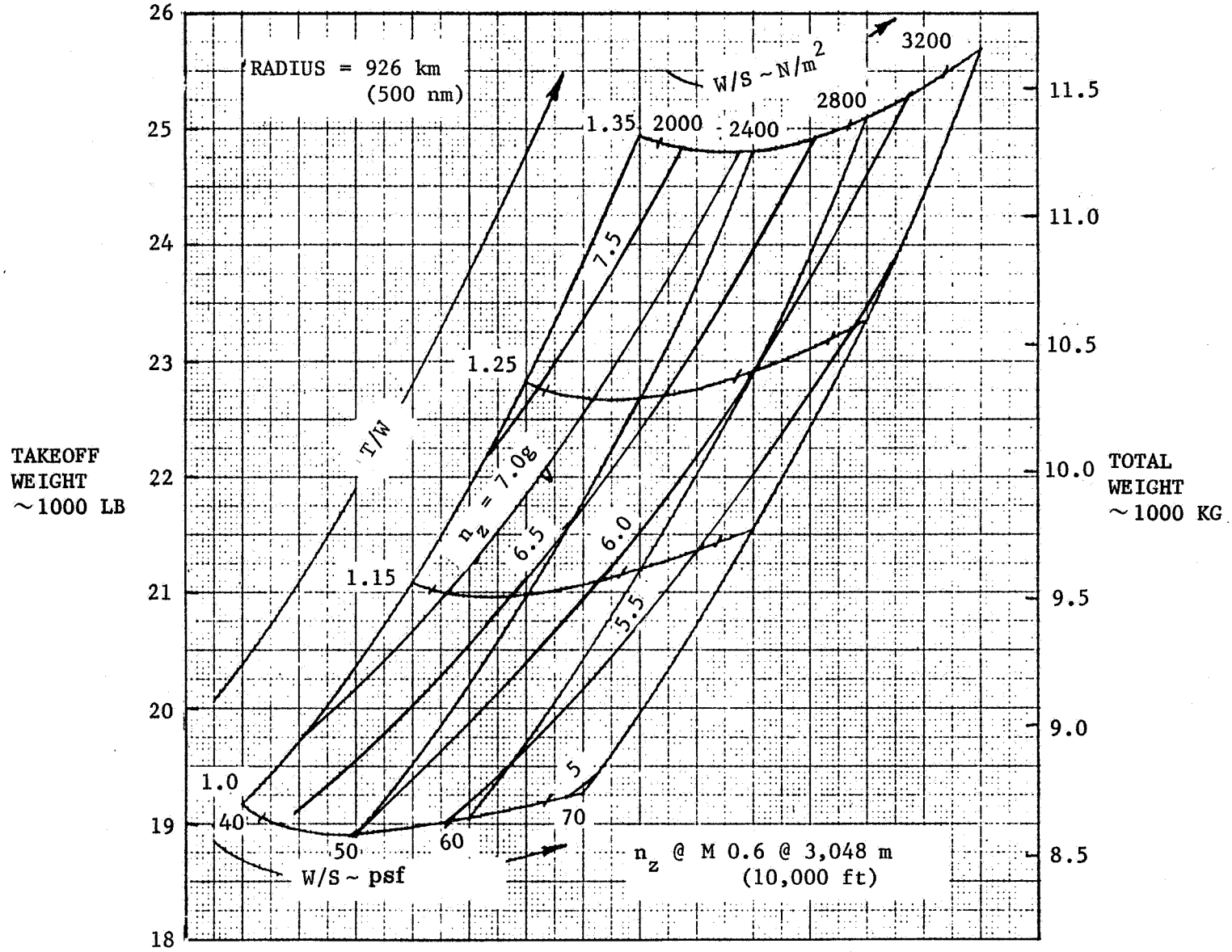

FIGURE 6-11. SUSTAINED LOAD FACTOR LEVELS ON AIRCRAFT SIZING MATRIX

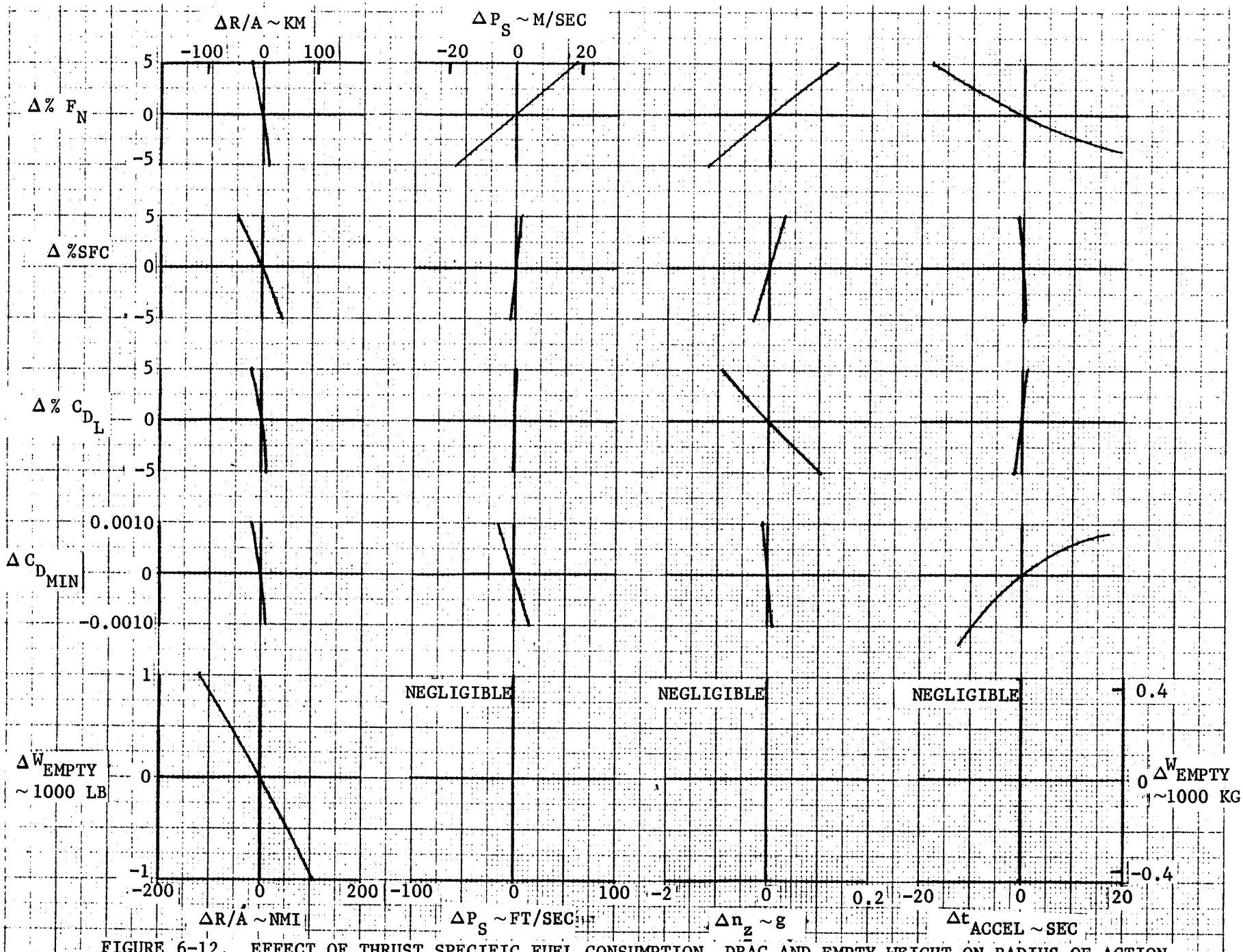

FIGURE 6-12. EFFECT OF THRUST SPECIFIC FUEL CONSUMPTION, DRAG AND EMPTY WEIGHT ON RADIUS OF ACTION, SPECIFIC EXCESS POWER, SUSTAINED LOAD FACTORS AND ACCELERATION TIME FOR THE SIZED AIRCRAFT

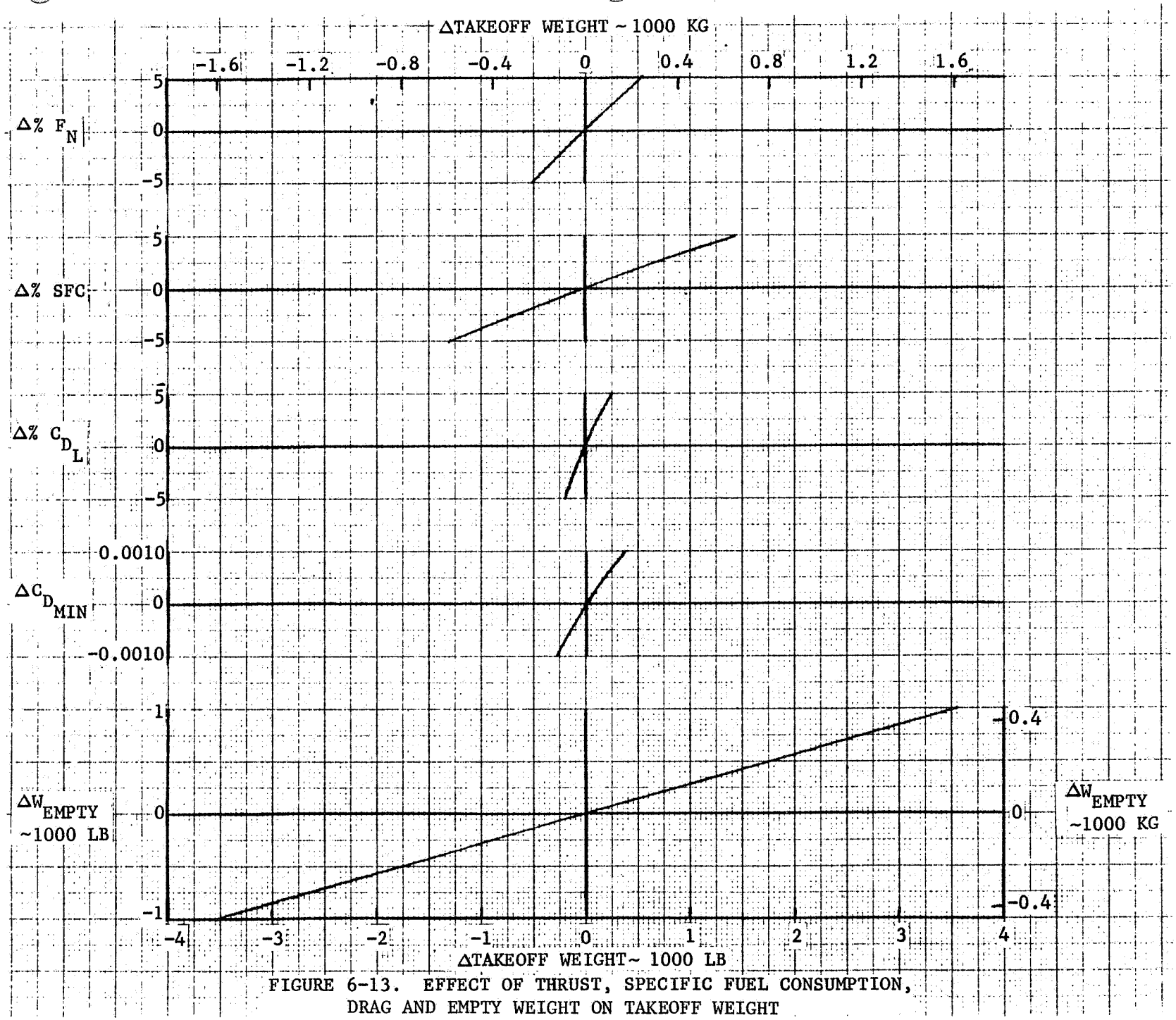

FIGURE 6-13. EFFECT OF THRUST, SPECIFIC FUEL CONSUMPTION, DRAG AND EMPTY WEIGHT ON TAKEOFF WEIGHT

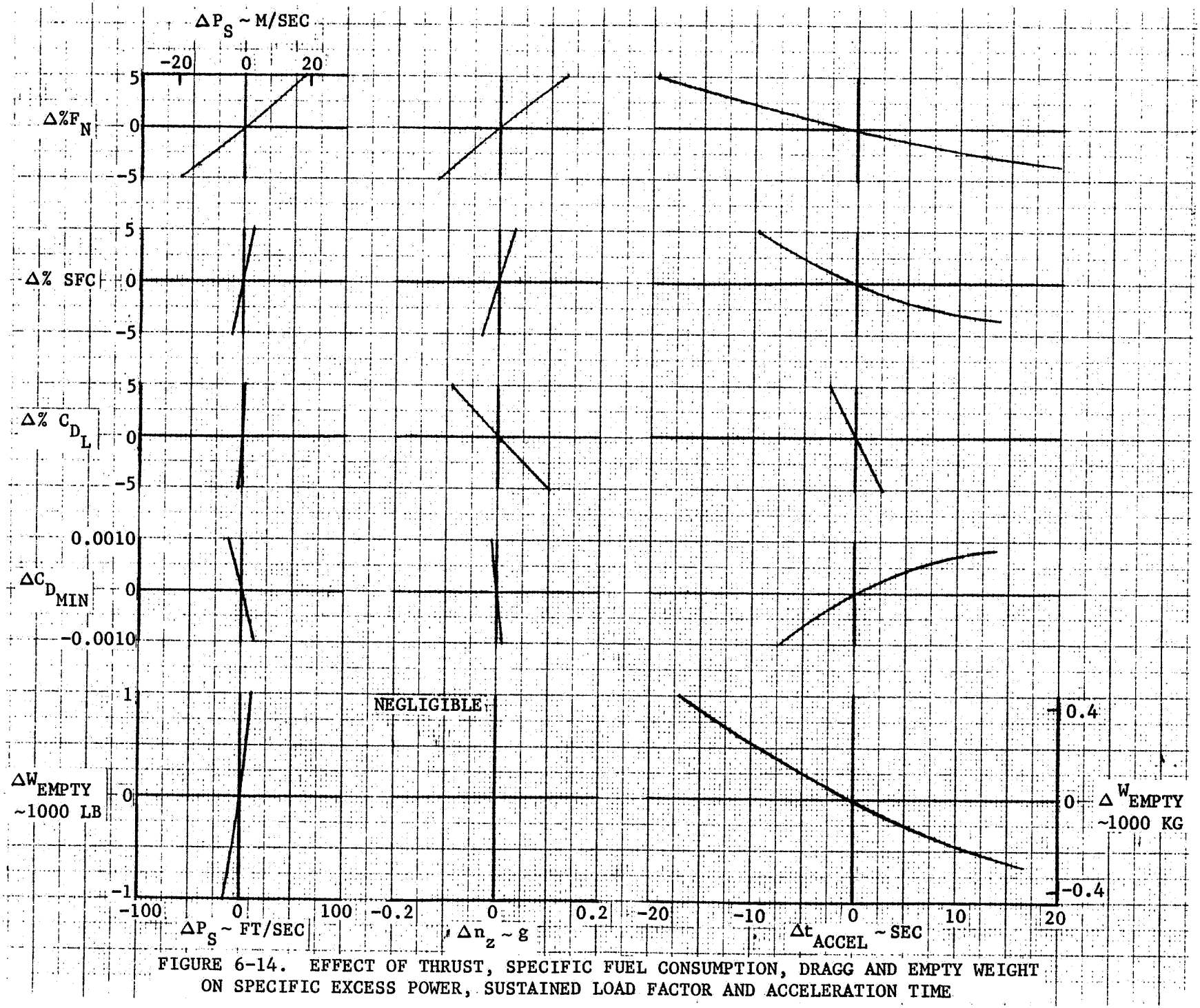

FIGURE 6-14. EFFECT OF THRUST, SPECIFIC FUEL CONSUMPTION, DRAGG AND EMPTY WEIGHT ON SPECIFIC EXCESS POWER, SUSTAINED LOAD FACTOR AND ACCELERATION TIME

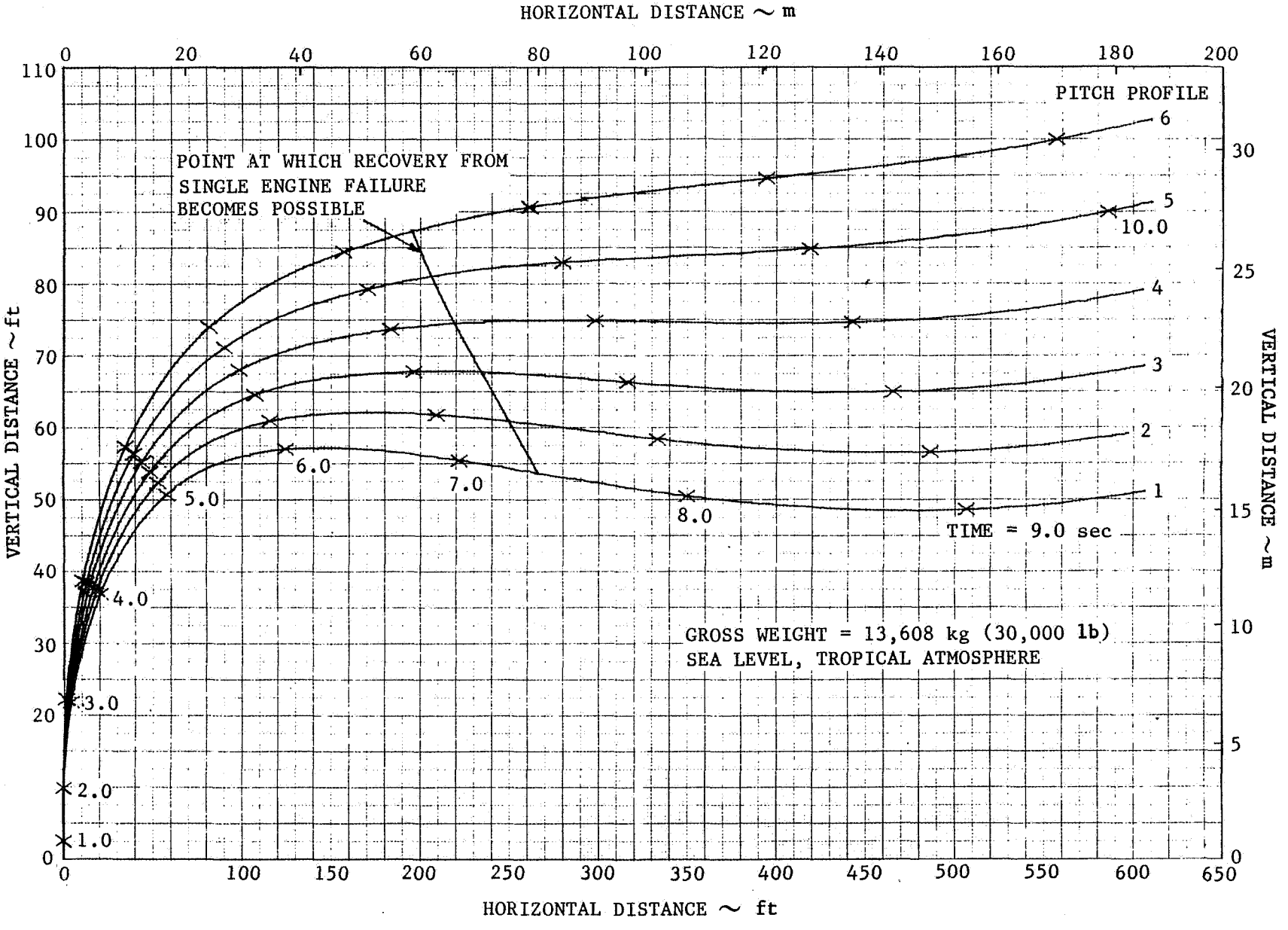

FIGURE 6-15. ACCELERATING TAKEOFF TRANSITION TRAJECTORIES

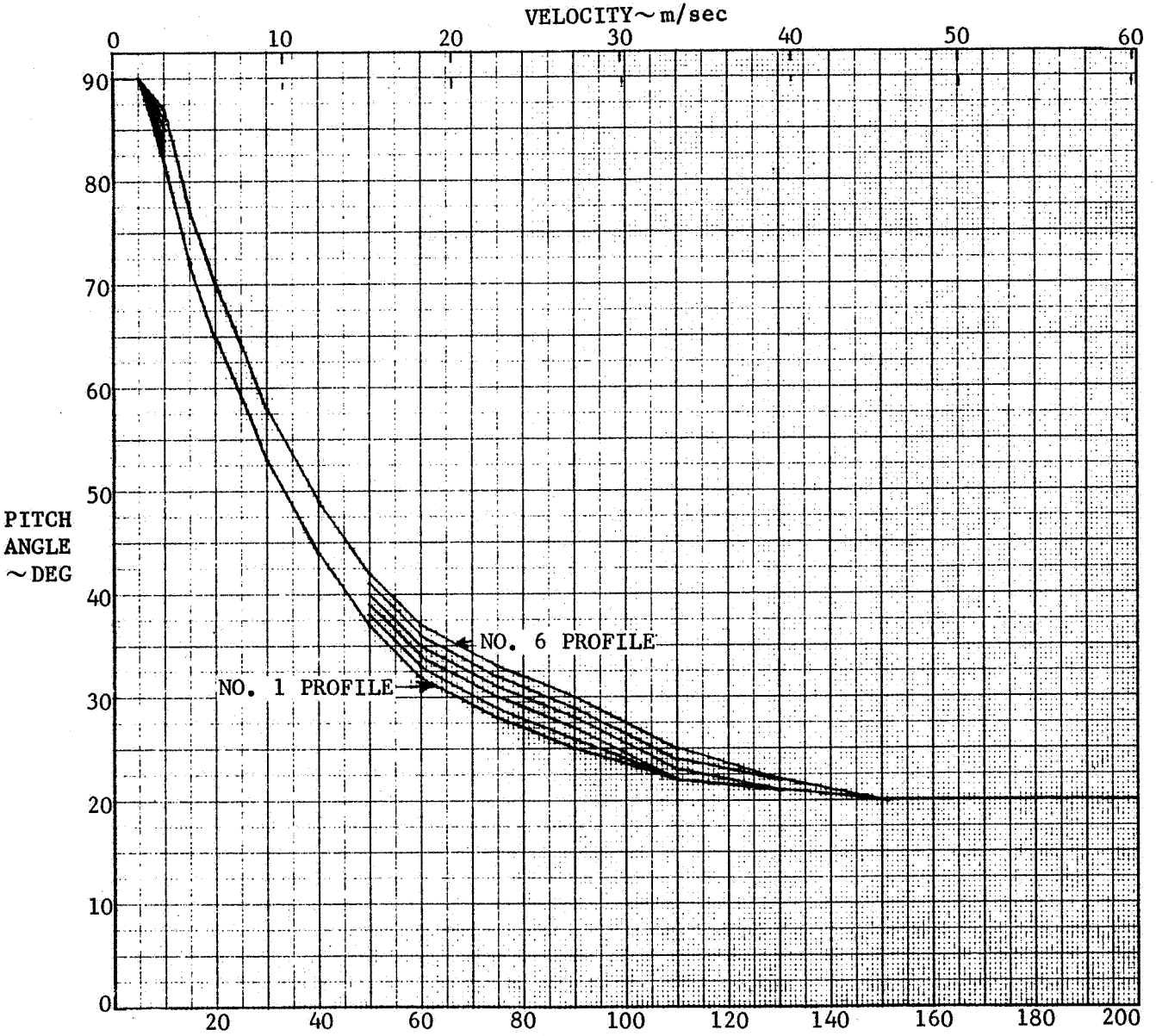

FIGURE 6-16. COMMAND PITCH SCHEDULE

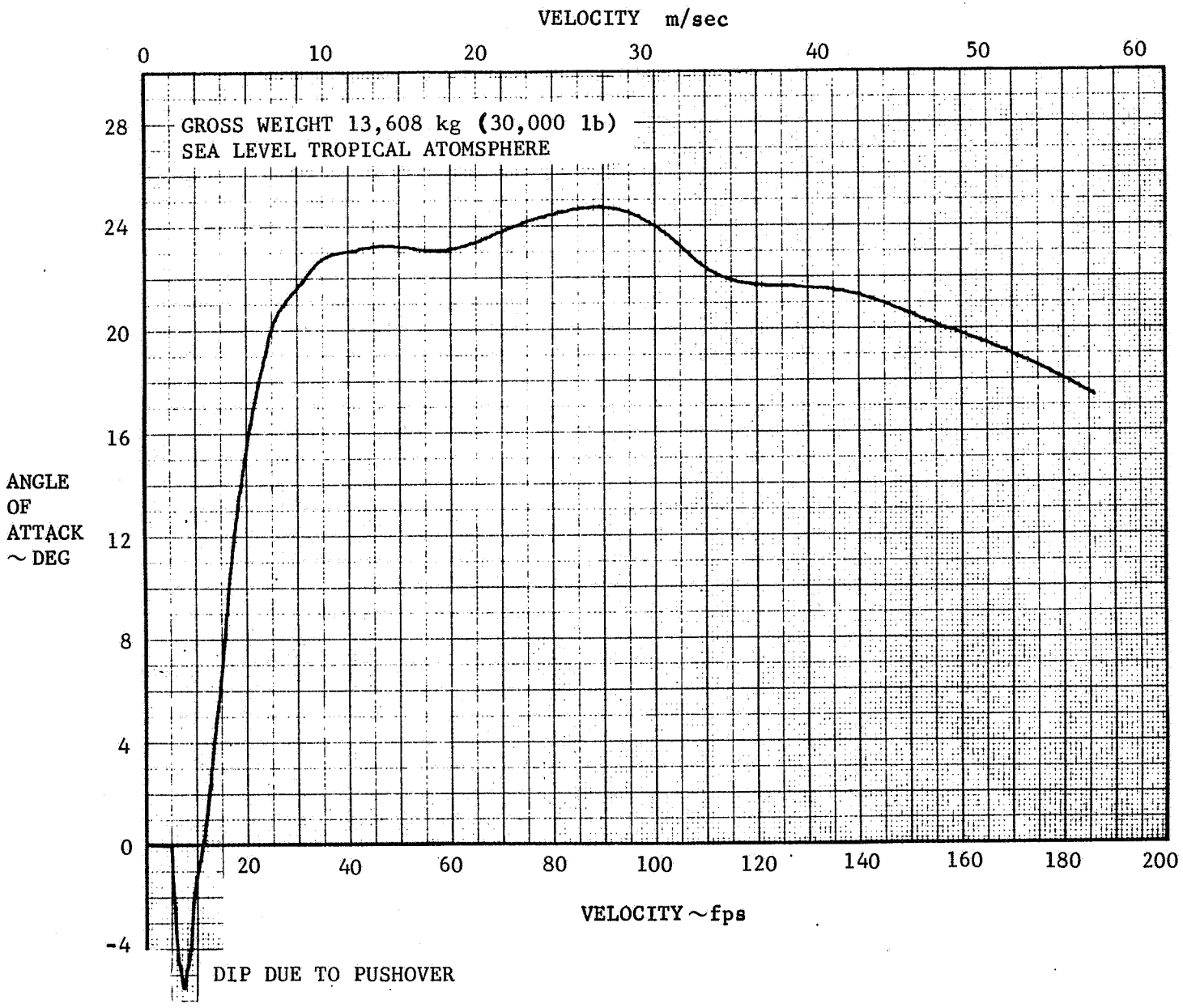

FIGURE 6-17. ACCELERATING TAKEOFF TRANSITION - ANGLE OF ATTACK PROFILE

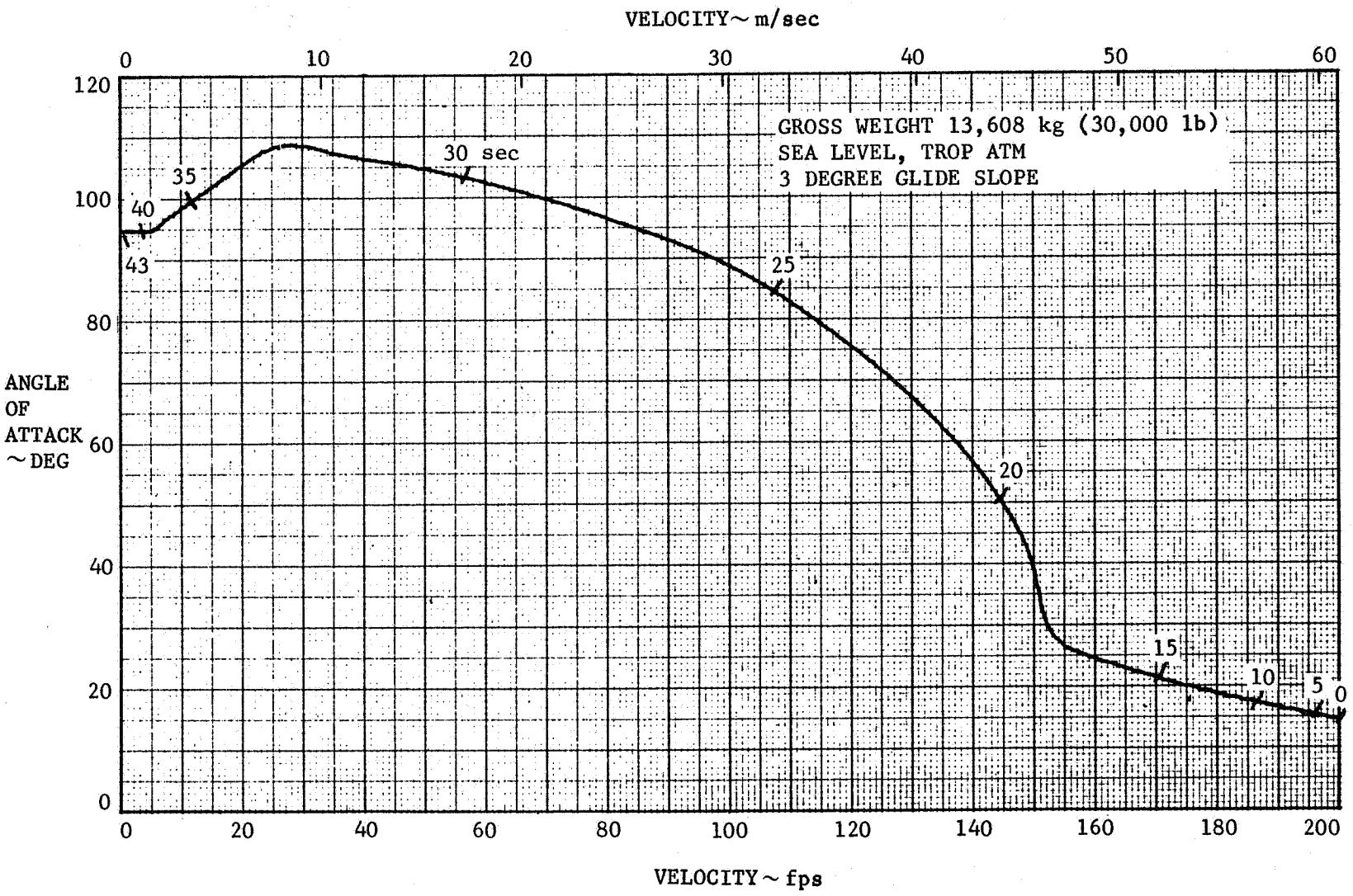

FIGURE 6-18. LANDING TRANSITION - ANGLE OF ATTACK PROFILE

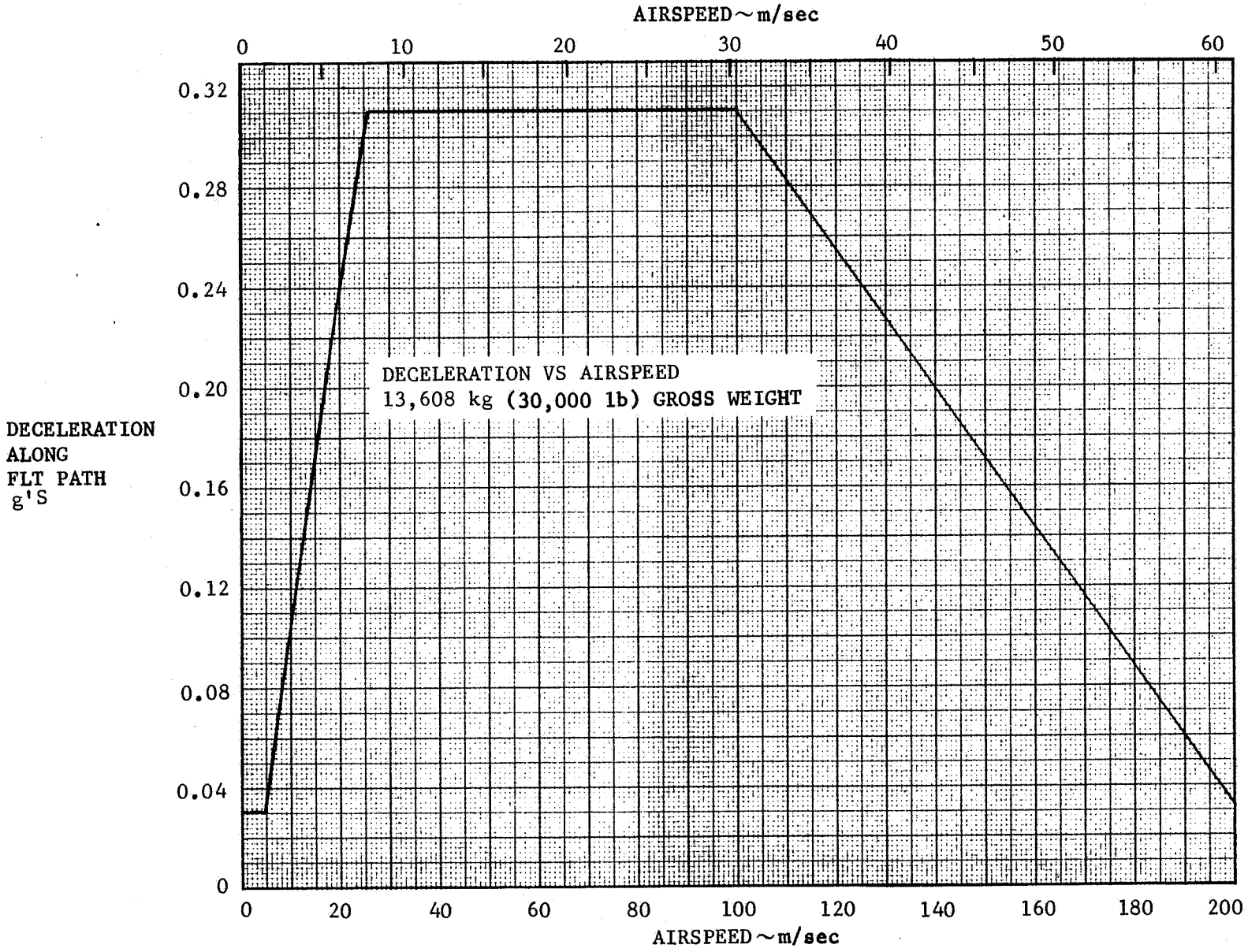

FIGURE 6-19. LANDING TRANSITION - COMMAND DECELERATION SCHEDULE

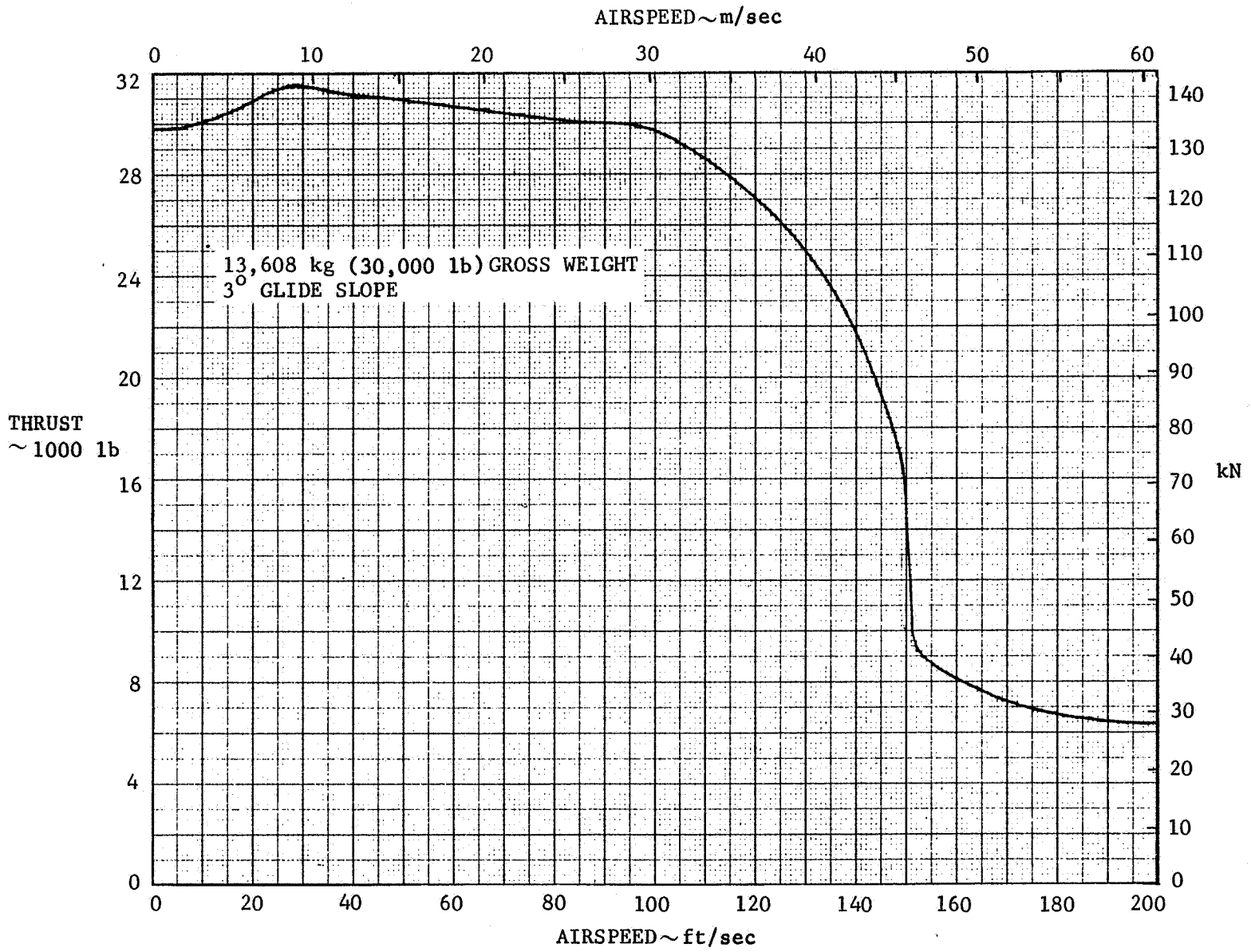

FIGURE 6-20. LANDING TRANSITION - THRUST REQUIRED VS AIRSPEED

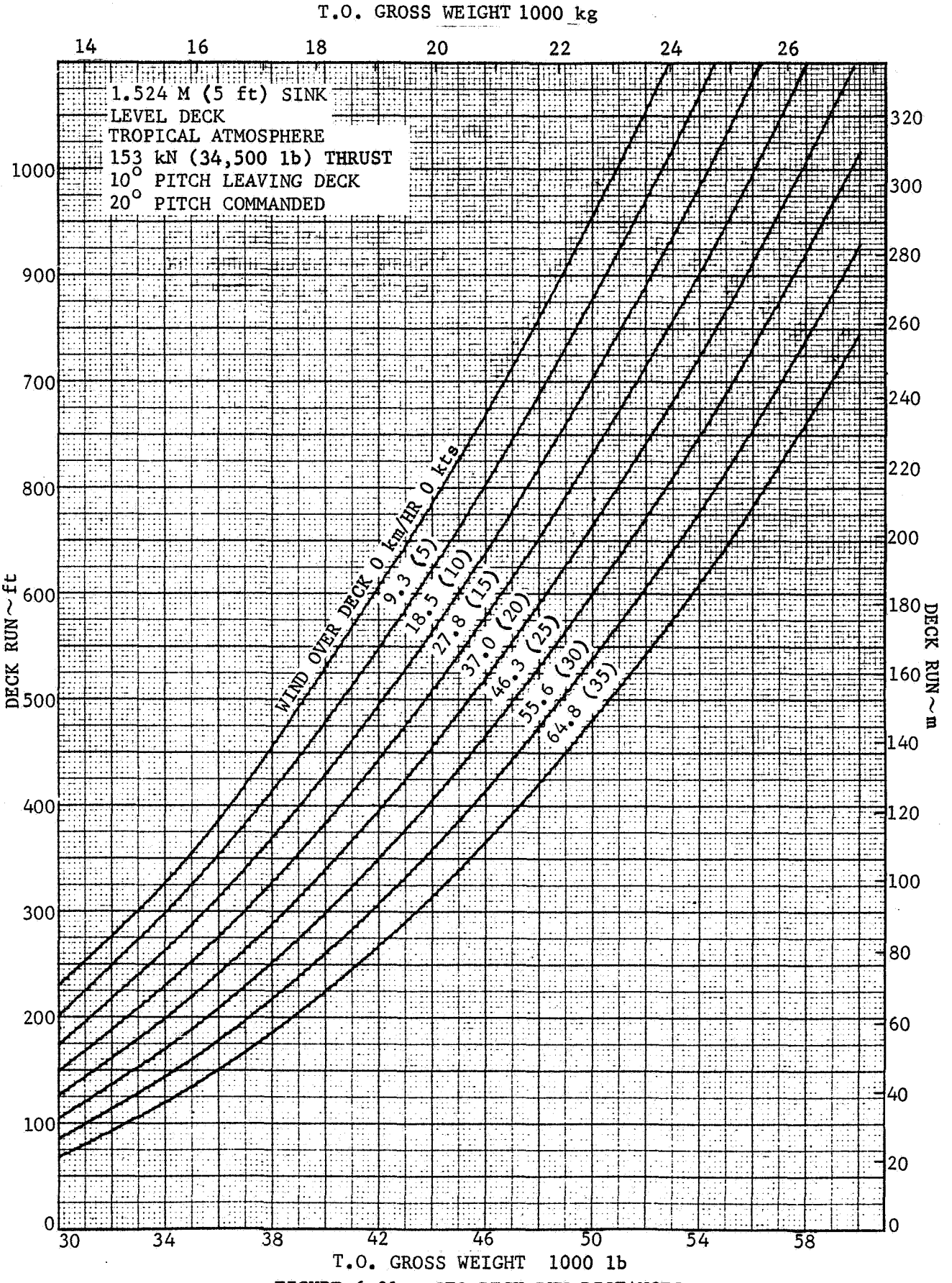

FIGURE 6-21. STO DECK RUN DISTANCES

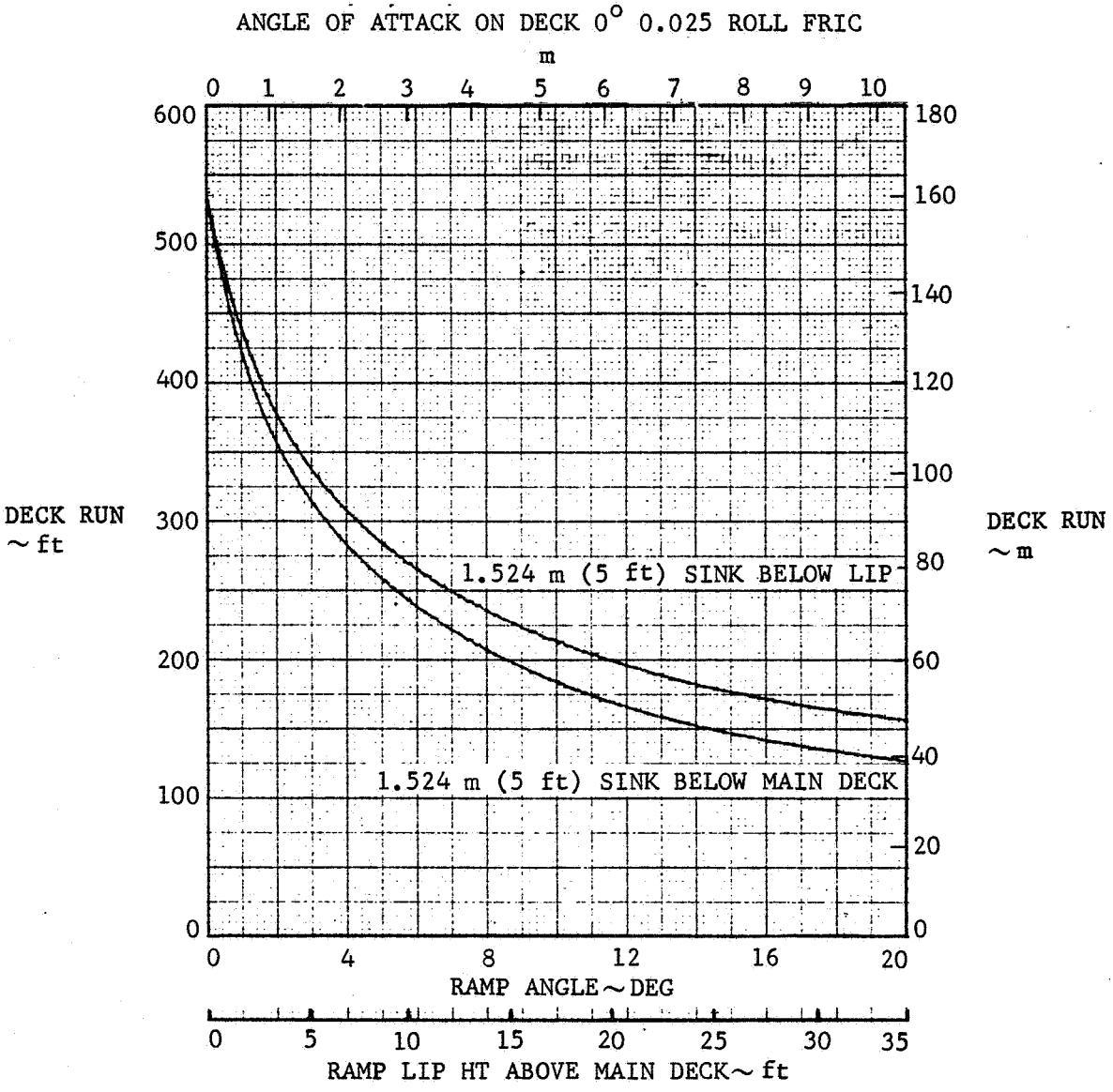

FIGURE 6-22. EFFECT OF RAMP ON STO PERFORMANCE

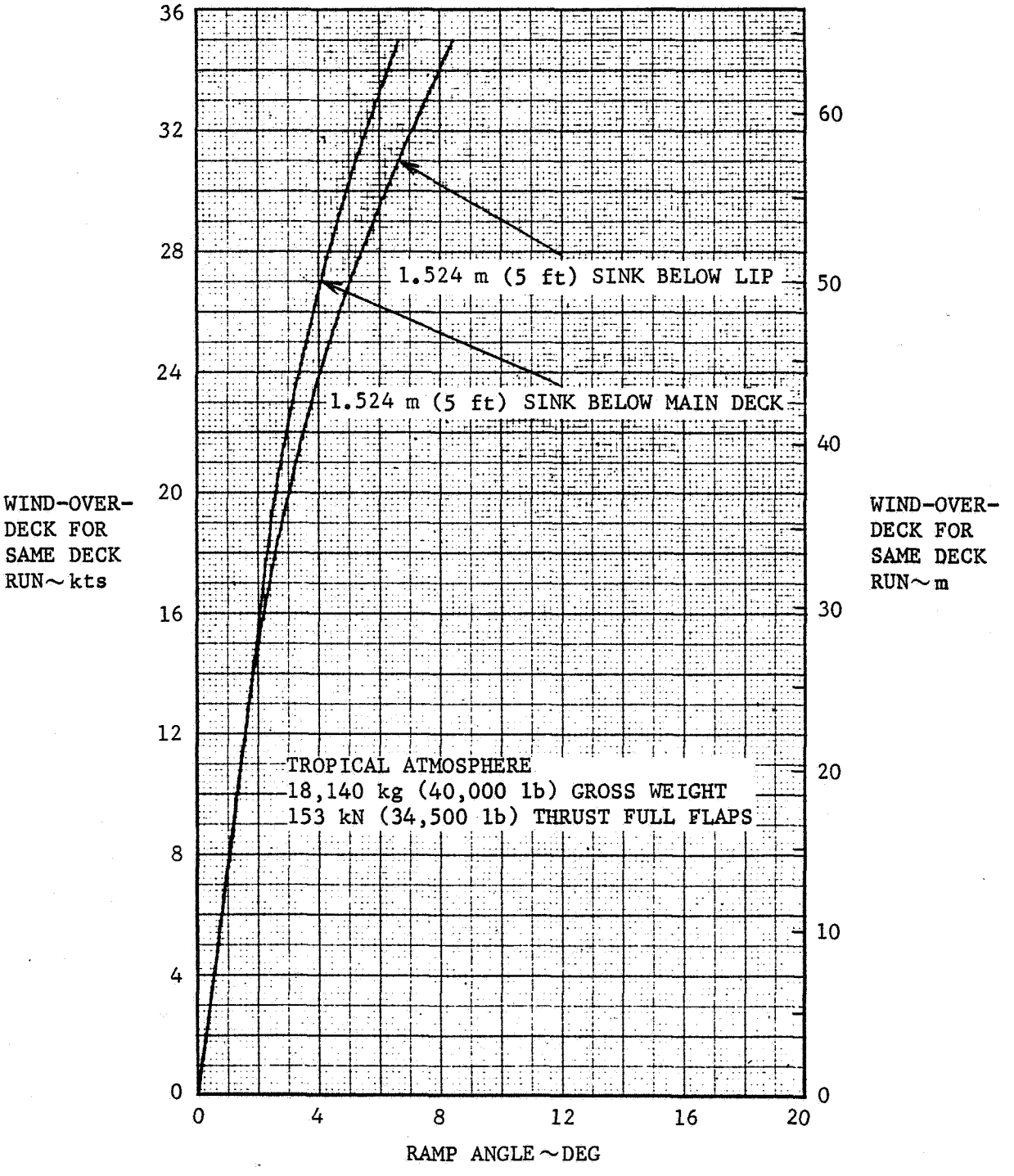

FIGURE 6-23. EQUIVALENT WIND-OVER-DECK DUE TO RAMP

SECTION 7

AERODYNAMIC UNCERTAINTIES

Aerodynamic uncertainties have been identified which are related to the VATOL concept. These include accurate estimations of supersonic wave drag, LEX effects on lift pitching moment, and flow to the top-side inlet, aerodynamic center shift, high angle-of-attack characteristics, maneuvering flap effects at supersonic speeds, and jet spray effects on takeoff and landing.

7.1 WAVE DRAG AT HIGH MACH NUMBER

Estimates show a rise in wave drag to about M 1.8 while experimental data for similar wings and others indicate that the drag is essentially constant from M 1.2. Tests should be made to verify the wave drag characteristics of the complete model.

7.2 LEADING EDGE EXTENSION RELATED

The tailless design is flown about 15 percent unstable at subsonic speeds. A wing leading edge extension (LEX) is used to provide good high angle of attack and high lift characteristics. However, the LEX causes relatively large nose up pitching moments. These moments, together with the instability, limit angle of attack to that controllable with the trailing edge flap plus thrust vectoring. The LEX is also used to provide flow control for the topside inlet and fin during combat.

Because of the large LEX pitching moment, a smaller LEX would be preferred, but not at the expense of poor high lift, inlet distortion or poor fin characteristics. It is difficult to accurately assess the effect of a LEX on the above and tests with the LEX off and two sizes of LEX are recommended. The flow field characteristics of the inlet and fin (on and off) require tests with sideslip (3 angles of attack subsonic) in addition to those in pitch. Inlet ducts should be instrumented with pressure rakes. Tests at subsonic speeds should include appropriate maneuvering flap defections. The leading edge flap contributes some help to the flow field and with the LEX off should be extended to the side of the body. The trailing edge flap for the pitch runs should be at maximum deflection (40 degrees) to determine trim capability.

7.3 AERODYNAMIC CENTER SHIFT

The correct location of the cg and the aerodynamic shift from subsonic to supersonic speeds are critical for an aircraft with relaxed static stability. The methods which are available for estimating the a.c. location are not very accurate. It is desirable to obtain subsonic and supersonic longitudinal stability data to verify the estimates of the a.c. position and to assist refinement of the prediction method.

7.4 HIGH ANGLE OF ATTACK

Only limited subsonic data are available on high angle of attack characteristics. The effects of LEX size and maneuvering flaps were extrapolated from test data at low subsonic speeds. At high subsonic speeds (M 0.9), test data were not available to correct for LEX effects, and at supersonic speeds, linear assumptions in the Carmichael – Woodward Program limit its utility. Tests, therefore, are necessary to better define the high angle-of-attack characteristics, subsonically and at transonic Mach numbers.

7.5 MANEUVERING FLAPS AT SUPERSONIC SPEEDS

The value of maneuvering flaps at subsonic speeds is well established. The use at supersonic speeds has not been clearly demonstrated. The optimum supersonic drag polar estimates indicate that there is a potential for improvement by use of deflected leading edge flaps. Wind tunnel tests at supersonic speeds are required to verify the results.

7.6 TOPSIDE INLET

Low speed wind tunnel tests have indicated that the leading edge extension produces good flow for the top inlet up to quite large angles of attack and moderate sideslip angles. The inlet characteristics which exist at angles-of-attack of 90 degrees and at transonic and supersonic speeds needs to be determined.

7.7 BUFFET ONSET

Transition from a conventional horizontal altitude to vertical altitude in the landing phase of flight must be made. It is possible that the aircraft could be subjected to intense buffet at some stage of this maneuver. Since this might have a degrading

influence on pilot performance in this critical stage of flight it is important to obtain buffet onset and intensity data at low speed and high attitude.

7.8 OTHER UNCERTAINTIES

Other, propulsion related aerodynamic uncerainties exist, but require a propulsion simulator to obtain meaningful results. Three uncertainties that have been identified follow.

7.8.1 Inlet Effect on Wing Drag

A spilling inlet can interact with the wing by the sides of the inlet producing a shock over the wing upper surface. The shock reduces lift and very probably increases drag. The side slopes of the inlets have been minimzed and the duct raked so that spill is primarily over the top. However, some interaction with the wing will exist and needs to be determined. Spillage drag may be obtained from test by varying the inlet mass flow ratio.

7.8.2 Inlet Effect on Afterbody Drag

The effect of inlet spill on afterbody drag is an uncertainty because of the close coupled inlet-nozzle relationship. Tests should be conducted to find the effect with the correct inlet mass flow and nozzle pressures.

7.8.3 Jet Spray

Another aero-hydrodynamic uncertainty exists for the concept. It is the existence and magnitude of sea spray that occur in the hover mode. Preliminary estimates indicate that this is a potential problem. However, there is a lack of data, especially larger scale data, to be able to assess the magnitude of the problem. It is recommended that tests be undertaken for different scale models to generate data so that a better assessment of the sea spray problem may be made.

SECTION 8

PROPOSED RESEARCH PROGRAM

The proposed research program defines the objectives of the research, presents a recommended wind-tunnel test program to resolve the aerodynamic uncertainties described previously and describes the wind-tunnel model to be used during the test program.

8.1 RESEARCH OBJECTIVES

The primary objectives of the wind-tunnel tests are listed in the following:

1. Verification of estimates
2. Assessment of estimation methods
3. Extension of limited test data through a more extensive angle-of-attack and Mach number range
4. Investigation of areas of aerodynamic uncertainty where analytical procedures are unavailable or inadequate.

8.2 WIND-TUNNEL TEST PLAN

The proposed wind-tunnel test plan addresses only those research tests that can be accomplished with an aerodynamic, flow-through duct model. Identified aerodynamic uncertainties requiring propulsion simulation are not included.

The proposed wind-tunnel test plans are presented in tabular form in Tables 8-1 and 8-2. Table 8-1 presents the test plan for the 11 Ft and 9 x 7 Ft tunnels and Table 8-2 presents the test plan for the 12-Ft tunnel. These tests are concerned with the variation of wave drag with Mach number and the effects of the wing leading edge extension (LEX) on the aerodynamic characteristics of the aircraft in pitch and sideslip.

Tests have been grouped and are listed numerically.

Group 1 is a Mach number series in pitch to moderate angles of attack in order to assess the variation of wave drag with Mach number for the complete configuration. Effect of leading edge flap deflection is also obtained.

Group 2 is a Mach number series in pitch to high angle of attack at subsonic speeds and moderate angles at supersonic speeds. The primary objective is to determine the effect of LEX size on the longitudinal characteristics. Besides the standard LEX, there will be a smaller LEX and LEX off configuration. All three configurations will be tested at intermediate and maximum flap deflections at subsonic speeds and zero flaps at supersonic speeds. Maximum flap deflection is used subsonically to help assess any angle of attack limits with the various LEX sizes. In addition, the standard LEX size is tested subsonically with two other flap settings in order to determine the best flap schedules for minimum trimmed drag as a function of angle of attack and Mach number. Pitch control effectiveness is automatically obtained.

Group 3 is a sideslip series of runs at three angles of attack with the standard LEX as well as LEX off and intermediate LEX. The appropriate estimated flap settings for minimum trimmed drag-due-to-lift are used. This group provides the basic data used in conjunction with groups 4 and 5 to determine the LEX effect on the vertical tail contribution to stability and the tail control effectiveness.

Group 4 is the Group 3 data repeated with vertical tail removed so that the tail contribution to stability may be assessed with various LEX sizes.

Group 5 data is for the purpose of determining vertical tail control effectiveness with various LEX sizes.

Groups 6, 7 and 8 are for the purpose of finding the LEX influence on inlet duct recovery for various angles of attack and sideslip. Duct rake measurements in these groups are made during force data measurements of Group 2. Polars at various sideslip angles are run. Maximum flap settings are used at subsonic speeds for two reasons.

1. The main interest is inlet operation at high angle of attack, and the nose flap is somewhat beneficial to inlet recovery.

2. The trailing edge flap is set at maximum as there is no effect on inlet recovery, but the data would be useful in obtaining the capability of the flap to trim at high angle of attack with sideslip.

Item 2 assumes force data can be obtained with the inlet pressure instrumentation in place. The sideslip polar force data would also be useful in cross plotting lateral directional characteristics when combined with the data of Group 3.

8.3 WIND TUNNEL TEST MODEL DESIGN

In order that the aerodynamic uncertainties of the concept may be explored and to generate an aerodynamic data base, a wind tunnel test model is required. As noted in the previous section, the configuration features significant aerodynamic/propulsion interactions which can best be studied experimentally with simultaneous simulation of inlet and exhaust flow influences. This can be achieved by the use of a propulsion simulator. However, in order that sideslip data may be obtained, and to reduce/eliminate support system interference at transonic and supersonic speeds an aft-sting mounted model with flow through inlets is also desirable.

The initial model design work was based on design of the model as a flow-through-inlet model with consideration given to later modifications to include engine simulator testing and a jet-effects model test. The impact on model size of including the propulsion simulator has been considered as well as the desirability of achieving full scale mass flow ratios and minimizing aft-end geometry changes.

The wind tunnel test model will be surface-defined by the NORLOFT computer program which represents conic shapes with parametric bi-cubic patches. This surface definition is now represented in a NORLOFT format, but the possibility exists that this data can be made suitable for the NASA/Ames analytical wind tunnel purposes. The wing, which has a 65A004-series thickness distribution on a twisted and cambered planform, is shown in Figure 8-1 with section cuts at every ten percent semi-span. This wing represents the common wing that will be used on both wind tunnel test mode configurations.

8.3.1 Powered Simulator Installation

The critical area of design which determines the size of the model is in the physical placement of the powered simulator in the model. The powered simulator to be used has a three-inch diameter compressor face with an additional 0.5-inch exterior hardware. On this basis, an 11 percent scale model is required to physically contain the powered simulator without aborting the fuselage lines (See Figure 8-2). Further study indicated that the maximum airflow of the power simulator would be approximately 25 percent under that required to simulate full scale intermediate power setting. Maximum powered simulator performance was plotted for three different model scales (Figure 8-3). The aircraft's intermediate power settings at 3,000 and 11,000 meters (10,000 and 36,000 feet) are superimposed on Figure 8-3 indicating the requirement of a 9.5 percent scale model to simulate full scale airflow. The objectives of the test are felt to be best met by aborting the fuselage lines and building a model that will simulate full scale mass flow ratios. In order to fit the powered simulator into a 9.5 percent scale model with minimum abortions, the drive and bleed manifolds will be reduced in size as determined from the chart in Figure 8-4. The approximate amount of deviation of fuselage lines from full scale lines is shown in Figure 8-5.

8.3.2 Wind Tunnel Installation

Three wind tunnels are being considered for testing the model. Those tunnels are the NASA-Ames 12-foot, 11-foot, and 9x7-foot. The sizing of the 9.5 percent model has been analyzed and the results shown in Table 8-3. The test rhombus for M 1.5 and M 1.8 in the 9x7-foot tunnel is illustrated in Figure 8-6. Models of this size and larger have been tested in these tunnels; therefore, the proposed 9.5 percent model is well within tunnel operating limits.

8.3.3 Aerodynamic Force Model

Preliminary design work on the aerodynamic force model has been completed. This model will be a conventional flow-through duct model mounted on a balance sting arrangement. A sketch of the model with commonparts to the horizontal attitude VSTOL model identified is shown in Figure 8-7. The six-component balance will measure all the forces and moments encountered. In addition, inlet rakes will be

installed at the throat to measure inlet recovery and distortion and duct exit rakes to measure air flow momentum and pressure losses through the duct. The aft end will be aborted to accommodate the sting and, if necessary, to obtain mass flow ratios approaching 1.0. The model will be capable of obtaining model build-up data. Off blocks will be provided for wing off, vertical off, etc., configurations. Control surfaces, such as leading and trailing edge flaps and rudder, will be provided.

8.3.4 Jet Effects Model

A jet effects model will be designed using the basic parts of the aero and powered simulator model. The blade sting will be used to support the model with the aft portion of the model metric. High pressure air will be provided to the internal non-metric nozzles. Numerous external surface static pressure measurements will be obtained during this phase of testing. The inlets of the model will be faired shut. The aft end abortions which were required in order to fit the powered simulator into the model and to sting mount the model will also be duplicated and tested on and off for their effects.

8.3.5 Model Support

Two methods of support will be used. One method is the use of a conventional sting entering the aft end of the model. This method will be used for the aerodynamic force model configuration incorporating flow through ducts. A blade type strut will be used for the powered simulator and the jet effects model. Figure 8-8 illustrates these two mounting arrangements. The blade support will contain air delivery/return system. It will be designed to minimize its effects on the flow over the model. This minimized effect will be tailored either for the subsonic or transonic regime.

An analysis of the maximum dynamic pressure in the Ames tunnels versus model scale is shown in Figure 8-9. The limit criteria was the maximum load capability of the respective tunnel support systems. As shown, for the 9.5 percent model, the maximum dynamic pressure is 43000 N/m^2 (900 psf) in the 11-foot tunnel, giving a Reynolds number of 19 million per meter (6 million per foot). This maximum dynamic pressure reflects the requirement to test at 28° angle-of-attack. There remains the capability of testing at higher dynamic pressures (higher Reynolds numbers) at lower

angle-of-attack. For example, at 10°, the maximum dynamic pressure, limited by the tunnel support system, is 55000 N/m^2 (1150 psf). This would give a Reynolds number approaching 25 million per meter (8 million per foot). A few runs at higher Reynolds numbers, to check Reynolds number effect, would be possible.

8.3.6 Model Balance

A two-inch diameter Task MK XXIV balance, owned by Northrop, is being considered for the subject model. This balance has a normal force limit of 2,900 kg (6,400 pounds) and an axial force limit of 160 kg (350 pounds) which corresponds to a maximum dynamic pressure of 29000 N/m^2 (600 psf). Figure 8-10 shows the balance envelope. The maximum normal force shown occurs at an angle-of-attack of approximately 28° with trailing edge flaps deflected to 40° and leading edge flaps deflected to 25°. If the dynamic pressure is held to 29000 N/m^2 (600 pfs), the maximum axial force that will be experienced by the balance will be approximately 75 percent of the gage limit. Thus, the balance is the limiting component in the system. The balance will be oriented in a reverse position when used with the blade support.

TABLE 8-1. TEST PLAN - 11 FT AND 9 X 7 FT TUNNELS

W = WING, L = LEX B = BODY-CANOPY D = DUCTS V = VERTICAL TAIL
α RANGE A = - 4° TO 20° SUBSONIC AND - 4° TO 12° SUPERSONIC
α RANGE B = - 4° TO 30°, β RANGE C = -3° TO 15°
δ_n/δ_F = NOSE FLAP DEFLECTION/T.E. FLAP DEFLECTION ~ DEG

						MACH NUMBER						
GROUP	CONFIGURATION	α	β	LEX	δ_n/δ_F	0.6	0.8	0.9	1.2	1.4	1.6	1.8
1	WLBDV	A	0°	STD	0/0	X	X	X	X	X	X	X
					5/0				X	X	X	X
2	WBDV	A	0°	OFF	0/0	X	X	X	X	X	X	X
		B			15/20	X	X	X				
		B		OFF	30/40	X	X	X				
		A		STD	0/0	X	X	X	X	X	X	X
		B			15/20	X	X	X				
		B		STD	30/40	X	X	X				
		A		ALT	0/0	X	X	X	X	X	X	X
		B			15/20	X	X	X				
		B	0°	ALT	30/40	X	X	X				
3	WBDV	0°	C	OFF	0/0				X	X	X	X
		10°			15/20	X	X	X				
		20°		OFF	30/40	X	X	X				
		0°		STD	0/0				X	X	X	X
		10°			15/20	X	X	X				
		20°		STD	30/40	X	X	X				
		0°		ALT	0/0				X	X	X	X
		10°			15/20	X	X	X				
		20°	C	ALT	30/40	X	X	X				
4	WBD	REPEAT 3 WITHOUT VERTICAL TAIL										
5	WBDV	REPEAT 3 WITH VERTICAL TAIL DEFLECTED 10°										
6	WLBDV PLUS INLET RAKES	A	5°	STD	0/0				X	X		
		B	5°		30/40	X	X	X				
		A	10°		0/0				X	X		
		B	10°	STD	30/40	X	X	X				
7	WBDV	REPEAT 6 WITH NO LEX										
8	WLBDV	REPEAT 6 WITH ALTERNATE LEX										

TABLE 8-2. TEST PLAN - 12 FT. TUNNEL

W = WING, L = LEX B = BODY CANOPY D = DUCTS V = VERTICAL TAIL
α RANGE D = 0^o TO 90^o
β RANGE C = -3^o TO 15^o
δ_F = NOSE FLAP DEFLECTION/T.E. FLAP DEFLECTION ~ DEG

GROUP	CONFIGURATION	α	β	LEX	δ_F	M 0.2
1	WLBDY	D	0	STD	0/0	X
2	WSDY	D	0^o	OFF	30/40	X
		D	0^o	STD	15/20	X
		D	0^o	STD	30/40	X
		D	0^o	ALT	30/40	X
3	WBDV	40^o	C	OFF	30/40	X
		0	C	STD	0/0	X
		20^o	C	STD	30/40	X
		40^o	C	STD	30/40	X
		40^o	C	ALT	30/40	X
4	WBD	REPEAT 3 WITHOUT VERTICAL TAIL				
5	WBDV	REPEAT 3 WITH VERTICAL TAIL DEFLECTED 10^o				
6	WLBDV Plus Inlet Rakes	D	5^o	STD	0/0	X
		D	5^o	STD	30/40	X
		D	10^o	STD	0/0	X
		D	10^o	STD	30/40	X
7	WBDV	REPEAT 6 WITH NO LEX				
8	WILBDV	REPEAT 6 WITH ALTERNATE LEX				

TABLE 8-3. COMPARISON MODEL SIZE TO TUNNEL SIZE

(9.5% VATOL MODEL)

PARAMETERS	AMES 11' TUNNEL	AMES 12' TUNNEL	AMES 9x7' TUNNEL
WING REFERENCE AREA			
FULL SCALE: m^2 (ft^2)	46.45 (500)	46.45 (500)	46.45 (500)
MODEL SCALE: cm^2 (ft^2)	4189.9 (4.51)	4189.9 (4.51)	4189.9 (4.51)
% TUNNEL CROSS-SECTION AREA:	3.7	4.5	7.2
MAXIMUM FRONTAL AREA			
FULL SCALE: m^2 (ft^2)	2.68 (28.82)	2.68 (28.82)	2.68 (28.82)
MODEL SCALE: cm^2 (ft^2)	241.5 (0.260)	241.5 (0.260)	241.5 (0.260)
% TUNNEL CROSS-SECTION AREA:	0.21	0.26	0.41
WING SPAN			
FULL SCALE: m (ft)	9.94 (32.6)	9.94 (32.6)	9.94 (32.6)
MODEL SCALE: cm (ft)	94.49 (3.10)	94.49 (3.10)	94.49 (3.10)
%TUNNEL WIDTH:	28.2	27.4	44.2
PLANFORM AREA			
FULL SCALE: m^2 (ft^2)	59.97 (645.5)	59.97 (645.5)	59.97 (645.5)
MODEL SCALE: cm^2 (ft^2)	5416.2 (5.83)	5416.2 (5.83)	5416.2 (5.83)
% TUNNEL CROSS-SECTION AREA:	4.8	5.8	9.2

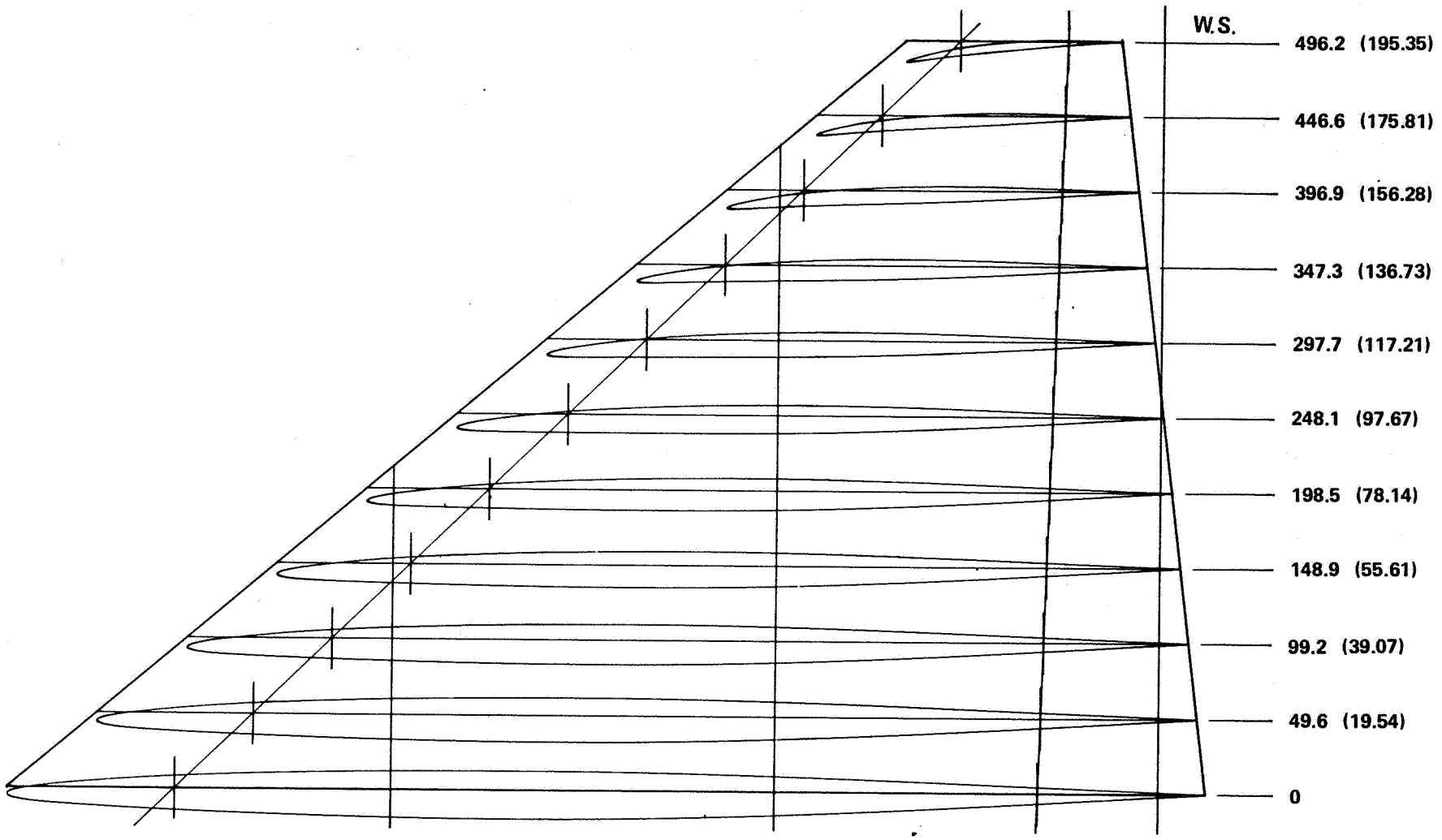

FIGURE 8-1. WIND TUNNEL MODEL WING

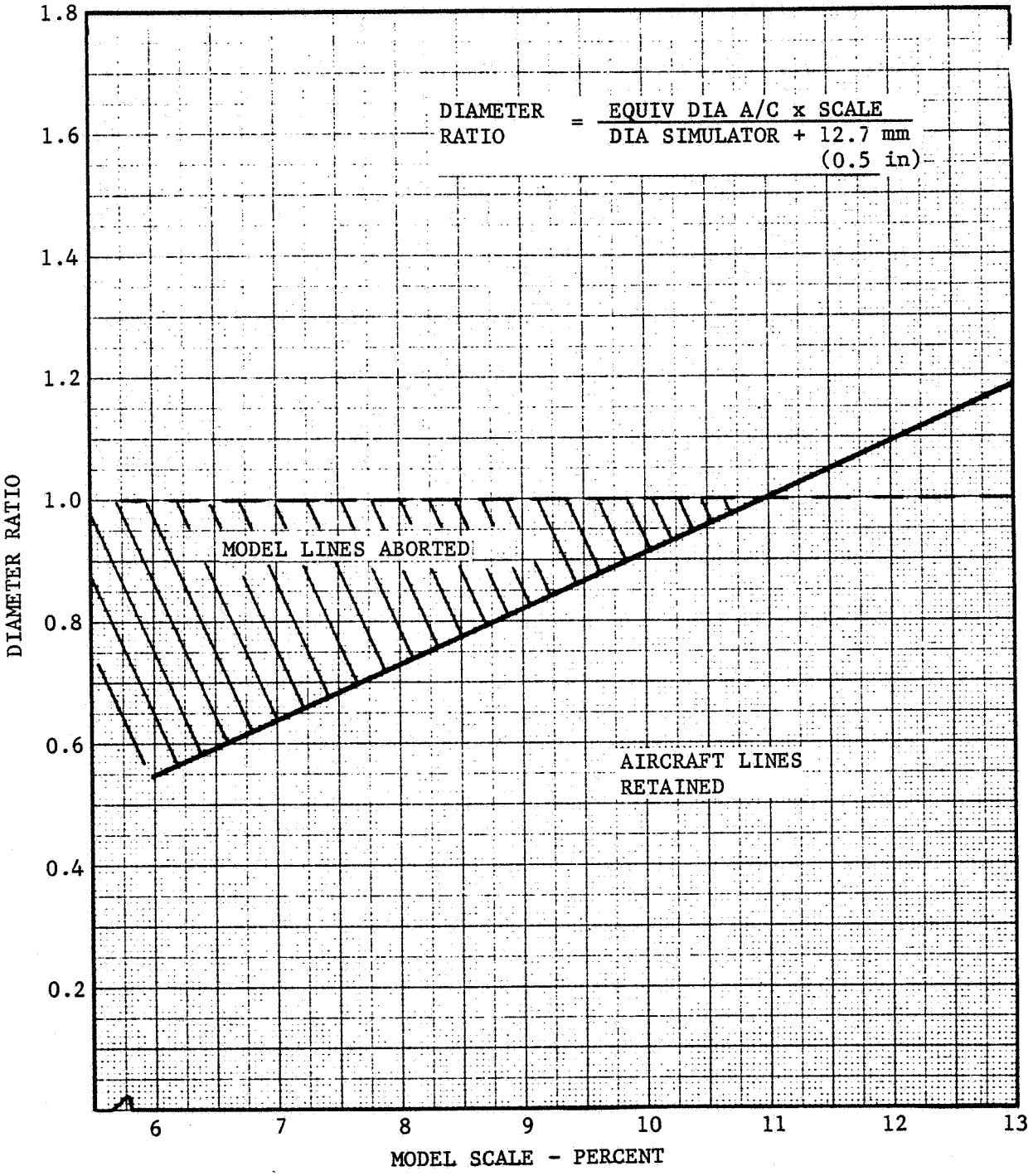

FIGURE 8-2. MODEL SCALE REQUIREMENTS FOR PROPULSION SIMULATOR SIZE

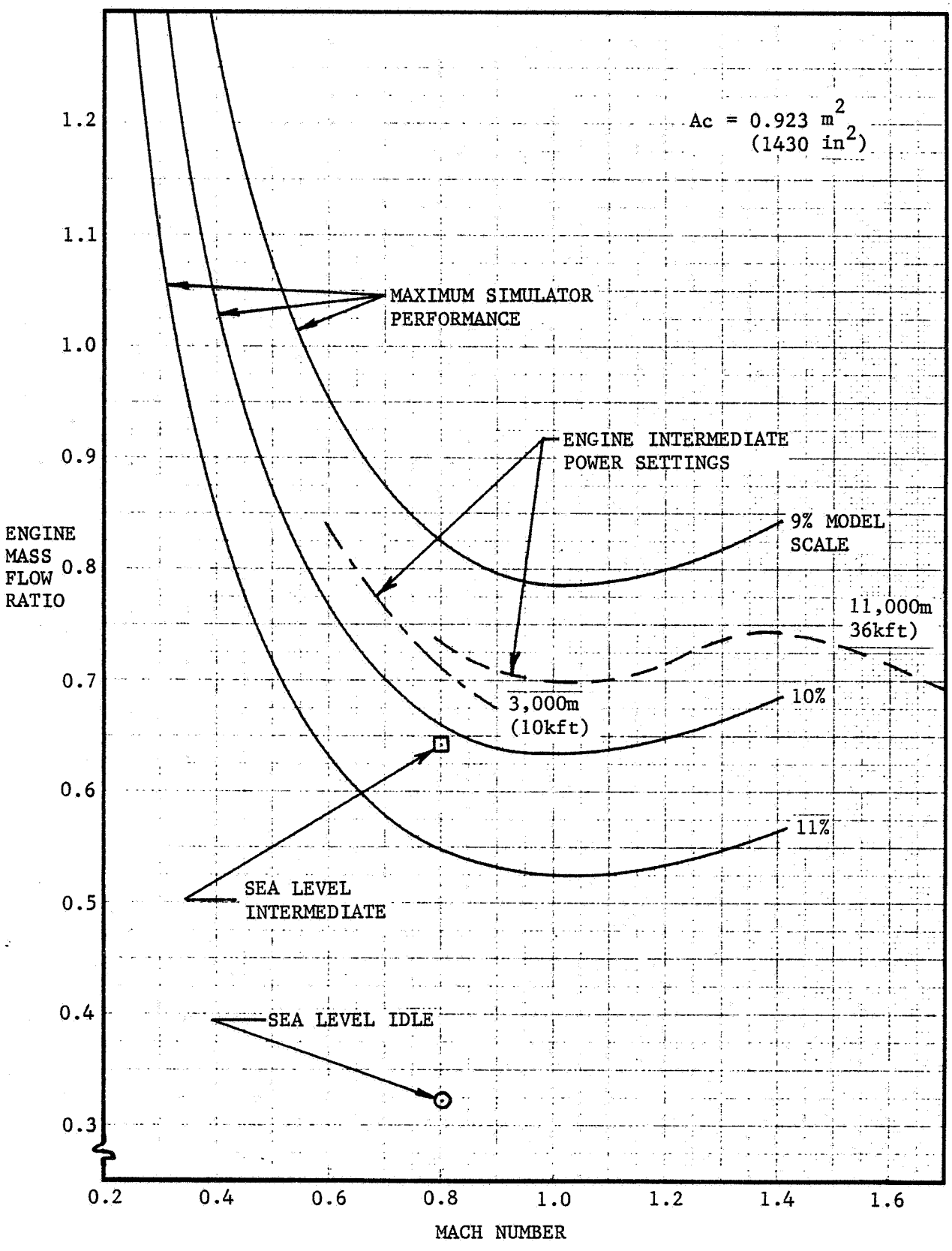

FIGURE 8-3. ENGINE SIMULATOR PERFORMANCE

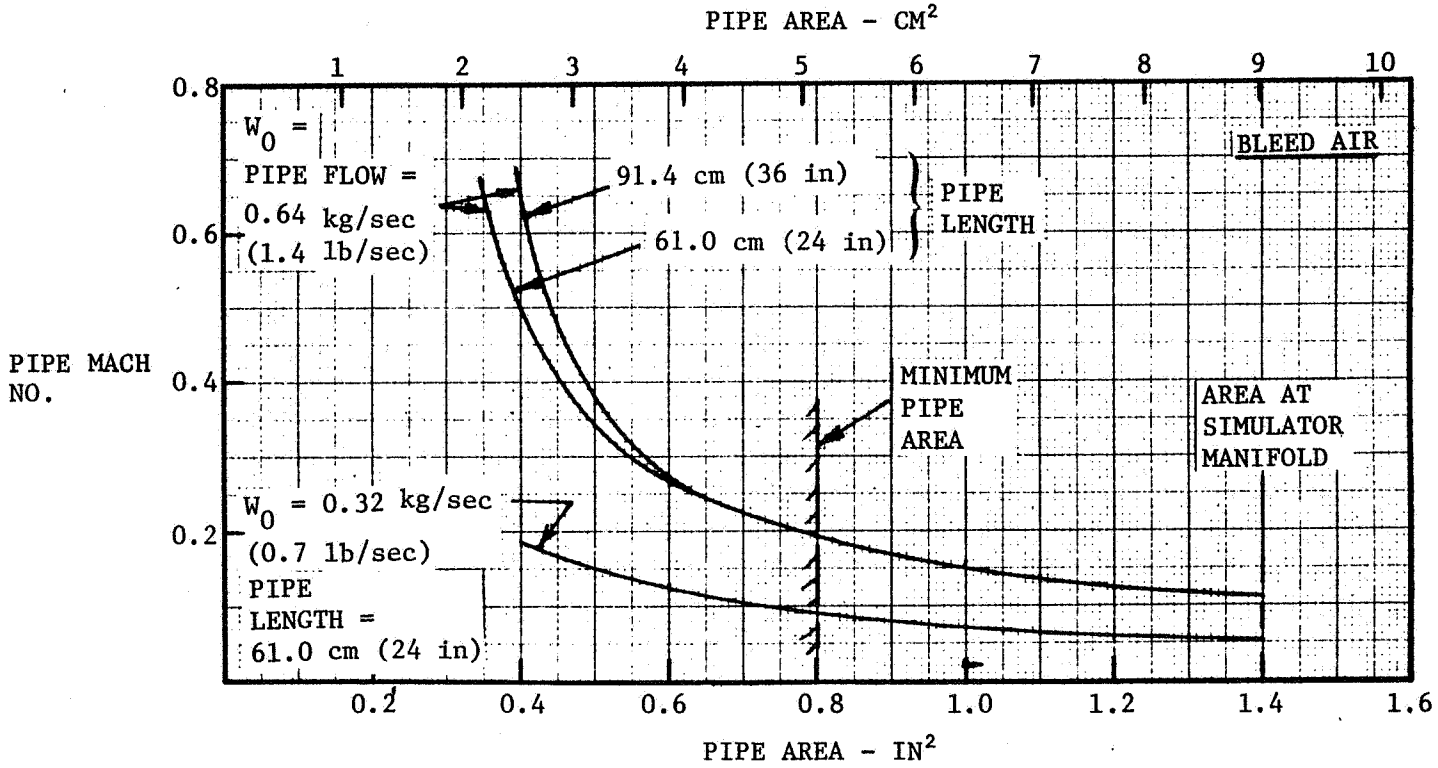

FIGURE 8-4. PIPE MACH NO. - SIMULATOR DRIVE AND BLEED LINES

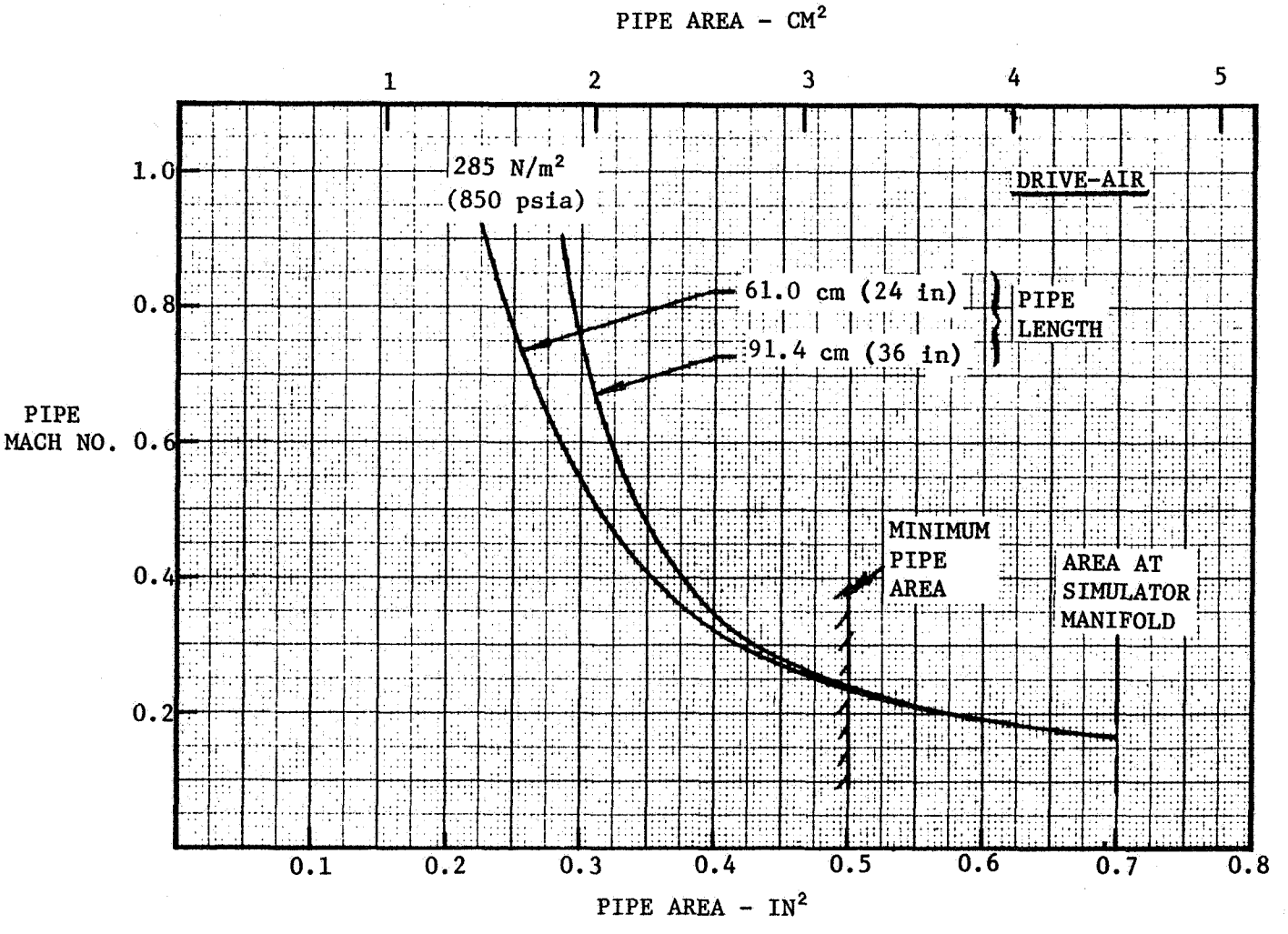

FIGURE 8-4. PIPE MACH NO. - SIMULATOR DRIVE AND BLEED LINE (CONCLUDED)

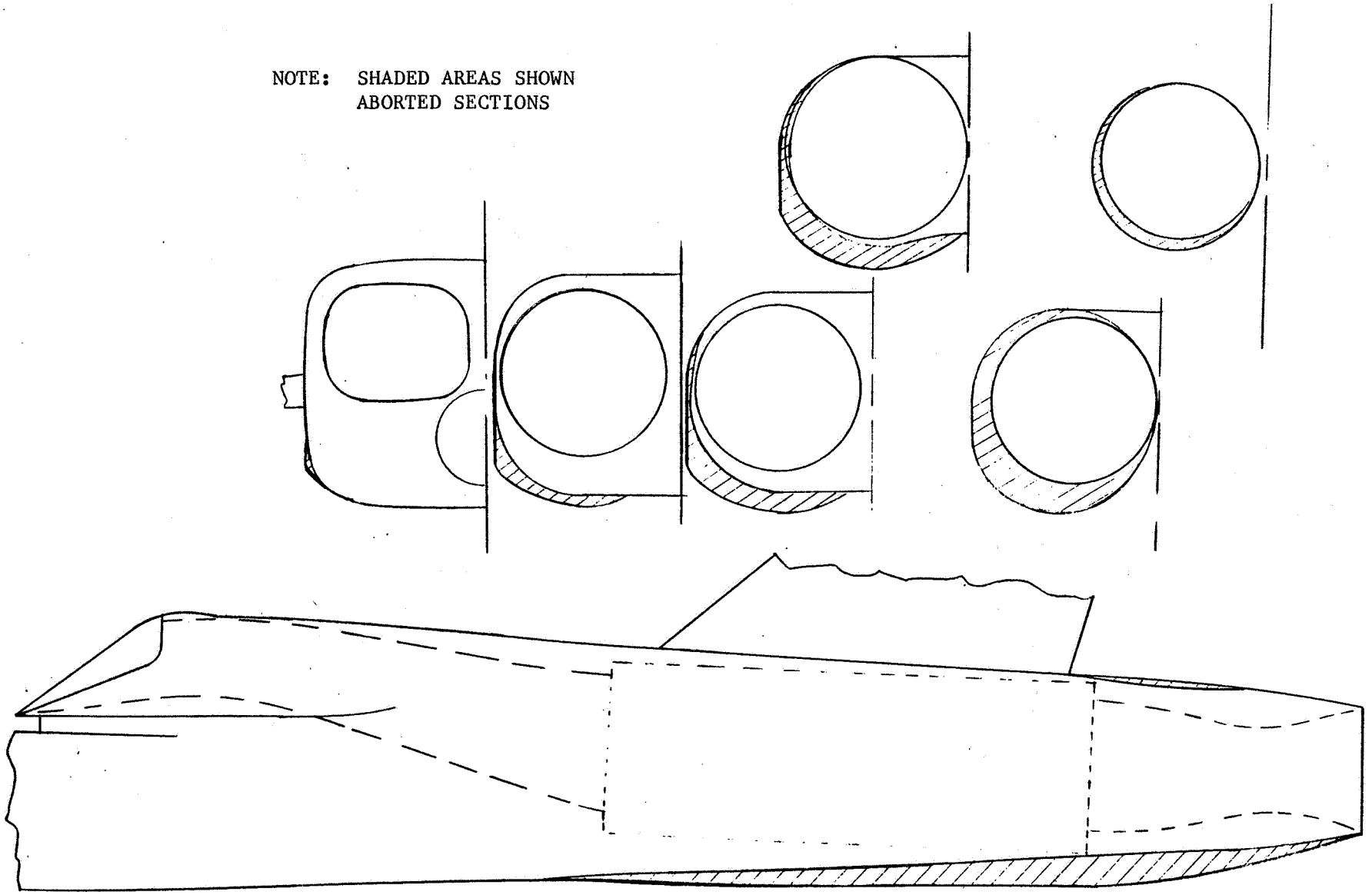

FIGURE 8-5. FUSELAGE ALTERATIONS DUE TO POWERED SIMULATOR INSTALLATION

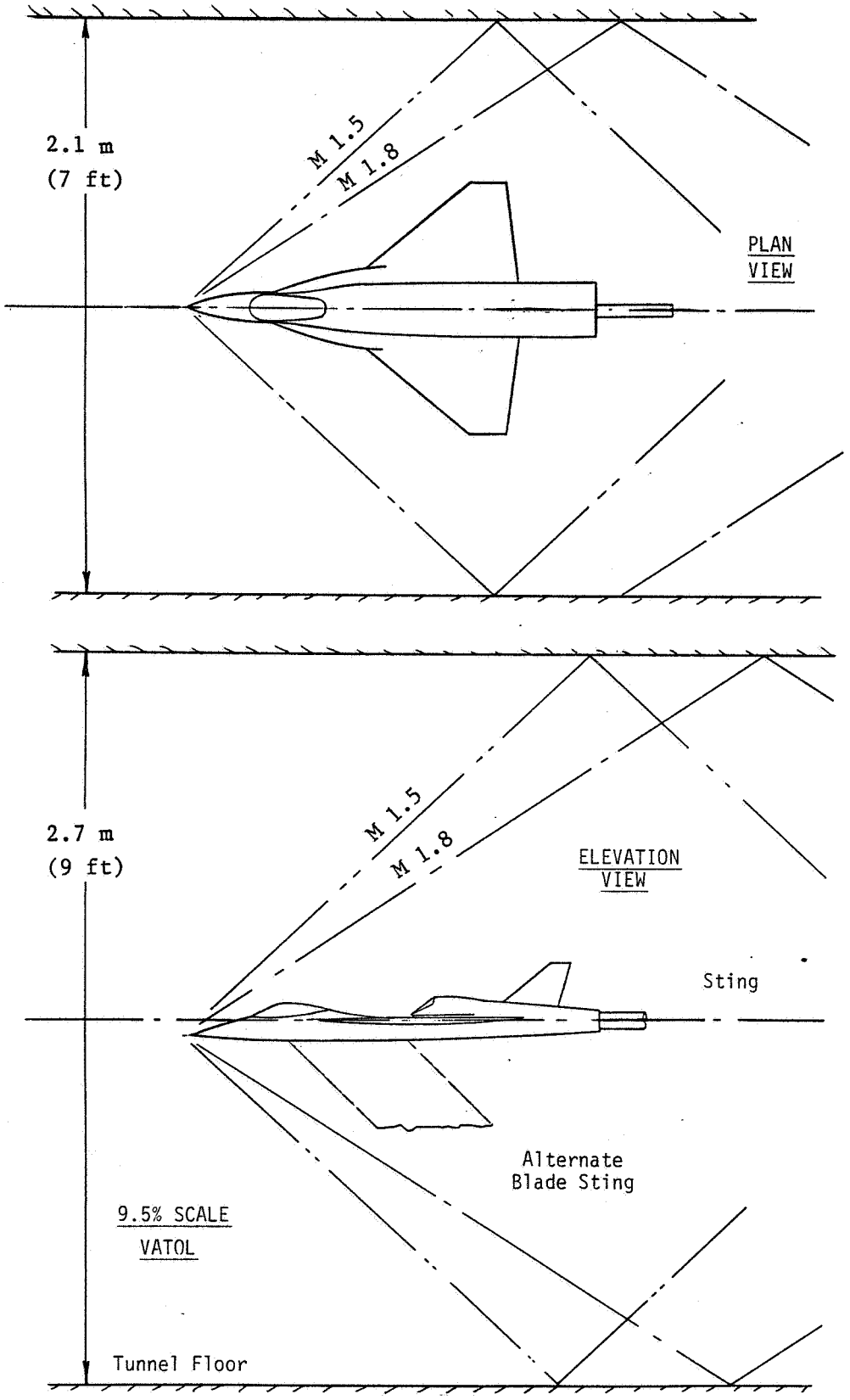

FIGURE 8-6. AMES 9x7 FT WIND TUNNEL ENVELOPE

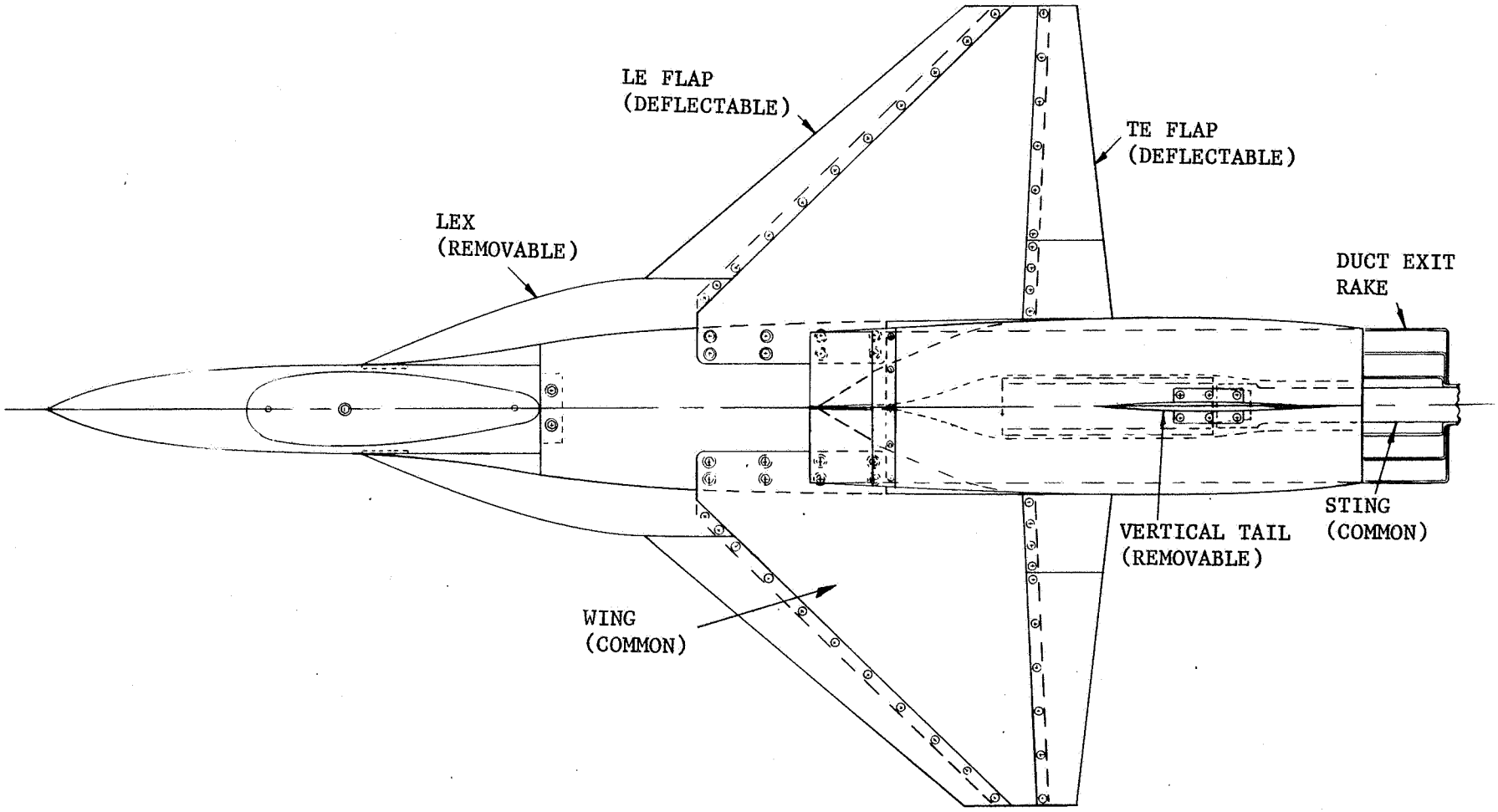

FIGURE 8-7. MODEL SKETCH

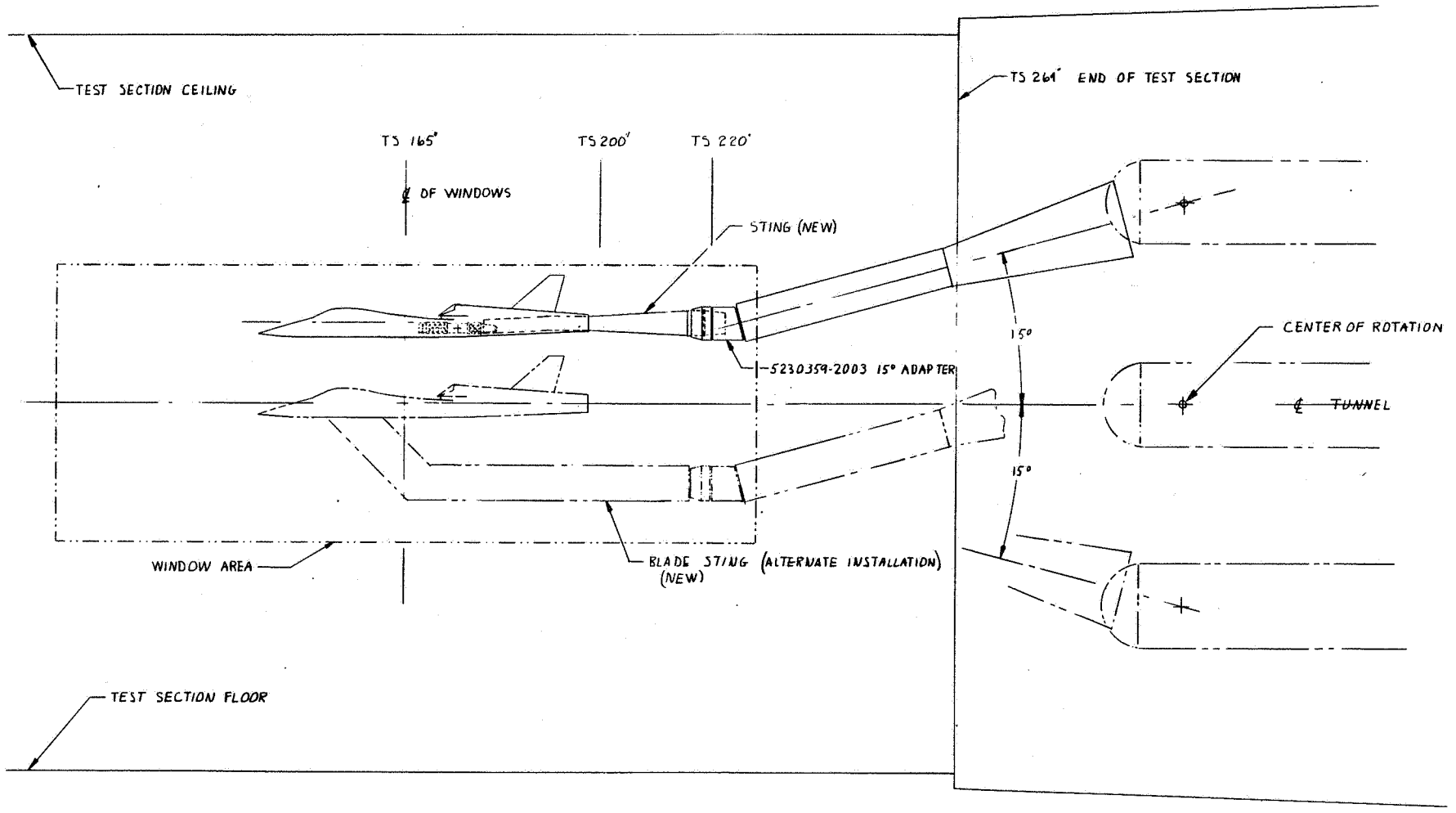

FIGURE 8-8. WIND TUNNEL MODEL SUPPORT CONCEPTS

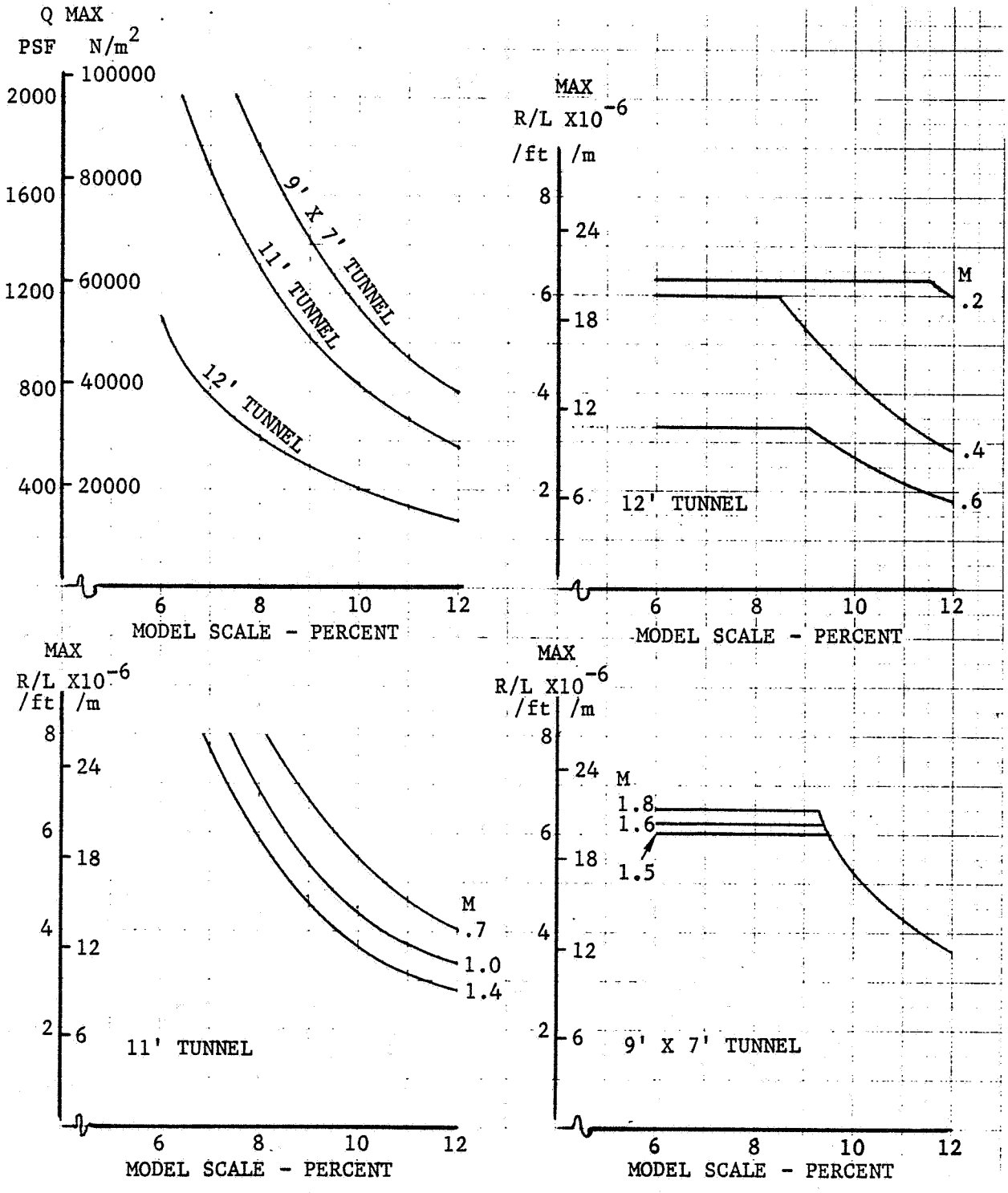

FIGURE 8-9. MAXIMUM DYNAMIC PRESSURE AND REYNOLDS NUMBER
— BASED ON STRUT LIMITS —

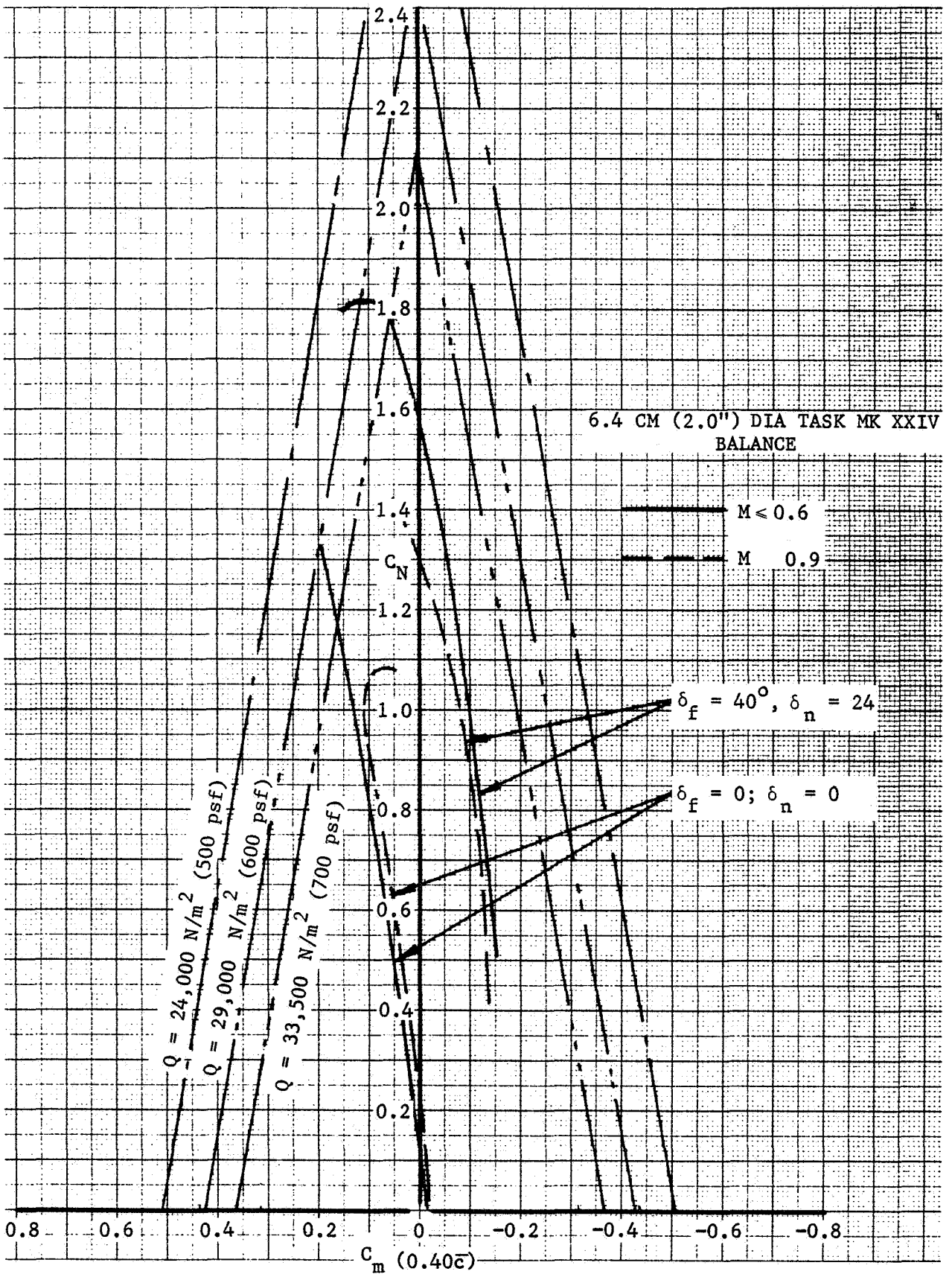

FIGURE 8-10. BALANCE ENVELOPE

SECTION 9

CONCLUSIONS

A detailed aerodynamic study has been made of a vertical attitude VSTOL (VATOL) fighter attack aircraft concept. The aircraft design was investigated to sufficient depth to ensure that the configuration was sufficiently credible to justify the aerodynamic study. As a result of this study it is concluded that:

1. The VATOL concept offers a viable solution to the shipboard supersonic VSTOL fighter/attack requirement.
2. The requirement for VTOL involves little compromise on the VATOL concept. However, it will require new equipment and techniques for ship interface.
3. The minimum drag at supersonic speeds may be increasingly conservative as Mach number is increased because of the corrections that were applied to the estimates. Test data are required to establish the correct drag levels.
4. The topside inlet appears to operate in a good flowfield due to the leading edge extension. Inlet flow characteristics at high angle of attack and sideslip needs to be determined, especially at transonic and supersonic speeds.
5. The NASA-Ames Wing-Body Aerodynamics Program is a good tool for generating wing-body fixed camber and variable camber effects. The effectiveness of supersonic variable camber needs to be verified.
6. The longitudinal aerodynamics at high angles of attack, especially the LEX effects on pitching moment need verification through wind tunnel test.
7. Sea spray generation by the VATOL engine exhaust in hover is a potential problem area requiring further study.

SECTION 10

REFERENCES

1. Douglas Report ES29074, "Charts for Determining Skin-Friction Coefficients on Smooth and on Rough Flat Plates at Mach Numbers Up to 5.0 With and Without Heat Transfer," April 1952.

2. Craig, R.R., "Drag Estimation Procedures for Preliminary Design Configuration Studies," General Dynamics' Convair Aerospace Division, Aerodynamics TN-70-AM-01, 24 March 1970.

3. Harris, Roy V., Jr., "An Analysis and Correlation of Aircraft Wave Drag," NASA TM X-947.

4. Hoerner, Fluid Dynamic Drag."

5. North American Aviation, Inc., Report NA 58-949, "Drag Penalties of Boundary Layer Removal Systems at Supersonic Speeds, June 1958.

6. Stoney, William E., Jr., "Collection of Zero-Lift Drag Data on Bodies of Revolution From Free-Flight Investigations," NASA TR-R-100.

7. Kantos, E.G., "Data Report of a 2.7 percent Scale Advanced Fighter Configuration Transonic Wind Tunnel Test," NAL-171 (NOR 77-037), February 1977.

8. Dawson, R.A., "Data Report of a 2.7 percent Scale Advanced Fighter Configuration Transonic Wind Tunnel Test, Second Entry," NAL-180 (NOR 77-52), April 1977.

9. Franco, B.G. and Kontos, E.G., "Data Report of a 2.7 percent Scale Advanced Fighter Configuration Subsonic Wind Tunnel Test, First Entry," NAL-192 (NOR 77-108), July 1977.

10. Franco, B.G., "Data Report of a 10 percent N340 Fighter Configuration, Subsonic Wind Tunnel Test, First Entry," NAL-204 (NOR 77-141), December 1977.

11. Woodward, F.A., "Analysis and Design of Wing-Body Combinations at Subsonic and Supersonic Speeds, J. of Aircraft, Vol. 5, No. 6, Nov-Dec 1968.

12. Brown, S.H., "Study of Aerodynamic Technology for VSTOL Fighter/Attack Aircraft-Horizontal Attitude Concept, NASA CR-152130, May 1978.

13. "An Investigation of the Over Water Aspects of VTOL Airplanes at High Disc Loading", Final Report No. 012-26, December 1963, Curtiss Wright Corporation.

14. Kuhn, R., "An Investigation to Determine Conditions Under Which Downwash from VTOL Aircraft will Start Surface Erosion from Various Types of Terrain", NASA TN D-56, September 1959, pp. 215-216.

15. Potter, Merle C., and Foss, John F.: "Fluid Mechanics", The Ronald Press Company, New York, 1975, pp. 215-217.